EVOLUTION OF THE WESTERLY WINDS BELT IN THE MIDDLE LATITUDES OF THE SOUTHERN HEMISPHERE SINCE THE LAST GLACIAL MAXIMUM

by

William Iván Henríquez González

A thesis

submitted to the Victoria University of Wellington

in fulfilment of the requirements for the degree of

Doctor of Philosophy

Victoria University of Wellington

2021

Abstract

The Southern Westerly Winds (SWW) are a symmetric component of the global climate system that govern the modern climate of all Southern Hemisphere landmasses south of ~30°S. Changes in the strength and latitudinal position of the SWW influence the precipitation patterns in the southern mid-latitudes, and have been postulated as fundamental drivers of ocean-atmospheric CO_2 exchange since the Last Glacial Maximum (LGM: ~34.0-18.0 ka). Despite their role in modern and past climatic dynamics, the evolution of the SWW at locations within their zone of influence is still uncertain; this is largely because of the paucity of paleoclimate records with well constrained chronology, adequate sampling resolution and an appropriate depositional setting. Resolving these issues will help understand the behaviour of the SWW in the past at different spatial (regional and hemisphere) and temporal (centennial to multi-millennial) scales. Here I present new paleoclimate data based on the examination of detailed chronologies of fossil pollen, charcoal and chironomids preserved in lake sediments from western Patagonia: Lago Emerenciana (43°S) and Lago Pintito (52°S) and New Zealand's southwestern South Island: Lake Von (45°S). These data, spanning a broad range of the SWW zone of influence, provide insights into the role of shifting SWW in environmental and climate dynamics of the middle latitudes of the Southern Hemisphere spanning the last ~24,000 years.

In the first study site, I performed detailed fossil pollen and charcoal analyses from sediment cores collected from Lago Emerenciana, a relatively small closed-basin lake located in northwestern Patagonian (43°S), to examine past vegetation, fire regime and climate change during the last ~24,000 years. I detect very low temperature and increased precipitation between ~24.0 and ~17.0 ka, followed by a warming trend and reduced precipitation between ~17.0 and ~14.3 ka. A cold reversal and increased precipitation regime occurred between ~14.3 and ~12.4 ka, followed by a return to warming and a slight decline in precipitation between ~12.4 and ~11.0 ka. I identify warmer temperatures and a major decline in precipitation at the beginning of the Holocene between ~11.0 and ~9.0 ka, conditions that persisted until ~6.2 ka. Centennial to millennial precipitation variability occurred during the last ~6200 years.

In the second study site, I developed high resolution fossil pollen and charcoal records, along with an exploratory chironomid record from sediment cores obtained from Lake Von, a small closed-basin lake located in the southwestern sector of the South Island of New Zealand (45°S), to examine vegetation, fire and climate trends spanning the last ~18,000 years. I observe a trend toward warming and relatively dry conditions between ~18.0 and ~14.8 ka with relatively wet conditions between ~18.0 and ~16.7 ka, increased precipitation between ~16.7 and ~14.8 ka, and cooling conditions and enhanced precipitation between ~14.8 and ~12.8 ka, followed by a marked drop in precipitation between ~12.6 and ~11.2 ka. I detect warmer and diminished precipitation between ~10.8 and ~7.2 ka, followed by lower temperature and enhanced precipitation between ~7.2 and ~3.7 ka. The mid-late Holocene is also characterised by alternating dry and wet oscillations of millennial- and centennial-scale phases with low precipitation between ~6.0 and ~5.2, ~4.4 and ~4.1, ~3.7 and ~2.9, and ~1.9 and ~0.56 ka, and increased precipitation in the intervening intervals.

In the third study site, I produced high resolution fossil pollen and charcoal records from sediment cores I collected from Lago Pintito, a small and shallow closed-basin lake located in southwestern Patagonia (52°S). This record allows the detection of past vegetation, fire and hydroclimatic shifts at millennial and centennial scales over the last ~17,000 years. From these data, I identify cold and dry conditions between ~17.0 and ~16.4 ka, increased precipitation between ~16.4 and ~14.2 ka and ~12.5 and ~11.4 ka, and intense precipitation but lower in magnitude than the neighbouring intervals between ~14.2 and~12.5 ka. I detect a major decline in precipitation at the beginning of the Holocene between ~11.4 and ~6.8 ka, followed by centennial-scale changes in precipitation until the present.

The comparison between precipitation variability reconstructed from the records from western Patagonia (Lago Emerenciana and Lago Pintito) and New Zealand's southwestern South Island (Lake Von) allows the inference of SWW changes at a hemispheric scale during and since the LGM, based on the premise that there is a strong and positive correlation between zonal wind speeds and local precipitation in these regions. The results of this thesis suggest: i) strong SWW influence at 43°S between ~24.0 and ~17.5 ka, ii) a southward shift of the SWW between ~17.5 and ~16.5 ka and reduced SWW influence north of 52°S, iii) strengthening and/or a northward shift of the SWW between ~16.5 and ~ 14.5 ka, with strong SWW influence between 52°S and 43°S, iv) a northward shift of the SWW between ~14.5 and

~12.6 ka which resulted in stronger SWW influence between 43°S and 46° S and weaker SWW influence at 52°S, v) a southward shift of the SWW between ~12.6 and ~11.2 ka leading to weaker SWW influence between 43°S and 46°S and stronger SWW influence at 52°S, vi) a generalized multi-millennial decline in the strength of the SWW between ~11.2 and ~7.2 ka, and vii) high variability in the SWW in Western Patagonian and New Zealand's southwestern South Island during the last ~7200 years. Based on these findings, I postulate that hemisphere-wide changes in the position and/or strength of the SWW have modulated the atmospheric CO_2 concentration through wind-driven upwelling of CO_2-rich deep waters in the high southern latitudes during and since the LGM.

Acknowledgment

First, I would like to thank to my Primary supervisor Prof. Rewi Newnham for his constant support during all these years of work and study. I also want to thank to my secondary supervisors, Dr. Gavin Dunbar and Dr. Andrew Rees for their support and assistance during the development of this thesis. I will always be grateful for all the effort you all put during these years, instructing me in New Zealand pollen, chironomid analysis, and to help me get to the end.

I also want to thank to Dr. Patricio Moreno from Universidad de Chile for his collaboration in this thesis as an international supervisor. I am thankful for the opportunity to work alongside him in Patagonia, and for giving me access to field equipment, fieldwork support, sample material, and laboratory facilities, which were all crucial for the Patagonian-based content of this thesis. I also want to thank his team from Laboratorio de Paleoecologia Quaternaria de la Universidad de Chile for their support during the collection of material and lab work, especially Maria José Kaffman and Loreto Hernández.

I would also like to thank Dr. Brent Alloway for his initial support and encouragement to come to New Zealand.

I am grateful to Dr. Chris Moy and his team for giving me the opportunity to work alongside him in southern South Island of New Zealand, and for giving me access to field equipment, fieldwork support, sample material and laboratory facilities.

I also want to thank Victoria University of Wellington and the School of Geography, Environment and Earth Sciences. Special thanks to Patricia Stein, Jane Chewings, Kosta Tashkoff, Miranda Voke, and many others. A special mention to Bill McLea, who always was willing to help me any time I needed it.

I would also like to acknowledge Victoria University and the Agencia Nacional de Investigación y Desarrollo (ANID) for PhD scholarships. I want to thank to the Chilean Fondo Nacional de Desarrollo Científico y Tecnológico grants 1191435 abd 1171773, and the Agencia Nacional de Investigación y Desarrollo Millennium Science Initiative/Millennium Nucleus Paleoclimate NCN17_079.

I thank Sara González and Sergio Henríquez for looking after me from heaven. I also want to thank to my Chilean friends, Victoria Núñez and Estrella Durán and their families for the support and love they gave me during all these years. I thank all my relatives in Chile, especially my aunt Cecilia Jara and my uncles Hugo González and Juan Carlos González. I am grateful thank to all the friends I made over the last few years in New Zealand, especially my lovely friend Anna Jane Abbey. I also want to thank Erina Masuda for her patience and support during the last year, especially during the Covid-19 pandemic. Thanks to my officemates, old and new, for their support and for making a great work environment: Kate Mauriohooho, Stephen Piva, Hannah Elms, Katie Janes, Kerstin Gruende, Valerie van den Bos, Elliot Swallow, Ignacio Jara, Leo Pure and Céline Mandon.

Finally, I want to dedicate this thesis to my family in Chile, to my mother Rosa González González, my father William Henríquez Orellana and my younger sister Nicole Henríquez González. Esta tesis es para ustedes.

Contents

List of Figures

List of Tables

Chapter 1

Introduction

1.1. Background

The current glacial-interglacial cycle (~116 ka to present, ka= 1000 calendar years before present, present= AD 1950) represents the last of a series of recurrent climate cycles that characterise the Quaternary period (the last ~2.6 million years) (e.g. Letréguilly et al., 1991; Pichon et al., 1992; Pillans and Naish, 2004). The current glacial-interglacial cycle features a sequence of global climate and environmental changes at different timing, magnitude and direction, with the key features on these timescales being explained by invoking the Milankovitch theory of orbital forcing (e.g. Chapman et al., 2000; Langgut et al., 2011). Investigations into the climatic and environmental changes within the current glacial-interglacial cycle have attempted to examine and decipher climate variability on shorter timescales, seeking clues toward a better understanding of both past and future climate scenarios. These studies have revealed that at millennial scales, climatic changes occurred in an asynchronous manner between high latitudes of the Northern and Southern Hemispheres (Buizert et al., 2015; Maslin and Smart, 2010), often referred to as the "bipolar seesaw" (Broecker, 1998; Stocker, 1998) and associated with net shifts in ocean heat flux (Alley et al., 1999; Knutti et al., 2004). This asynchronous inter-hemispheric pattern seems to be less clear over mid-latitudes (Ljung and Björck, 2007; Maslin and Smart, 2010; Newnham et al., 2012) suggesting alternative mechanisms were involved, including feedbacks between the cryosphere, biosphere and atmospheric and ocean processes (Ljung and Björck, 2007; McGlone et al., 2010; Seager and Battisti, 2005; Timmermann et al., 2003; Whittaker et al., 2011). Compared with the Northern Hemisphere, the Southern Hemisphere has a paucity of paleoclimate studies from the mid-latitudes and, consequently, our understanding of the putative drivers forcing climate fluctuations throughout the last glacial-interglacial cycle is limited.

Literature of the mid- and high-latitudes of the Southern Hemisphere has suggested that the Southern Westerly Winds (SWW) may have played a key role in the climate evolution and atmospheric CO_2 variation during the Last Glacial Maximum (LGM: ~34.0-18.0 ka) (Anderson

et al., 2009), its termination (Last Glacial Termination, T1: ~18.0-11.7 ka) (Anderson et al., 2009; Denton et al., 2010; Toggweiler, 2009; Toggweiler et al., 2006), and the subsequent, ongoing interglacial (Holocene: ~11.7 ka to present) (Fletcher and Moreno, 2011; Moreno et al., 2010). The SWW are an important component of the hemispheric and global climate systems that govern the modern climate and strongly influence precipitation patterns between ~30°S and 60°S (Garreaud, 2007) (Figure 1.1). Under modern climate regimes, SWW variability is strongly modulated by atmospheric flow shifts in subtropical (<30°S) and high-latitude (>60°S) regions (Sturman and Tapper, 2006). Empirical and modelling studies have postulated that changes in SWW strength and position have influenced ocean-atmosphere CO_2 exchange, where increased (reduced) SWW influence on the surface of the Southern Ocean resulted in enhanced (diminished) upwelling and release of CO_2 to the atmosphere (Fletcher and Moreno, 2011; Toggweiler et al., 2006). Reconstructed SWW variability linked to atmospheric CO_2 concentration changes during and since the LGM includes an equatorward displacement of the SWW (between 43°S and 30°S) during the LGM (Heusser, 1990b; Moreno et al., 2018a), implying reduced SWW influence at the latitude of the Drake Passage and sub-Antarctic region (>55°S) and lowering of atmospheric CO_2 concentration (Anderson et al., 2009). A subsequent southward shift of the SWW at the beginning of T1 (Moreno et al., 2018a; Pesce and Moreno, 2014) induced major SWW influence on the surface of the Southern Ocean (Anderson et al., 2009). This was followed by an equatorward shift of the SWW coeval with a halt in the deglacial CO_2 rise concurrent with the Antarctic Cold Reversal (ACR :~14.5 and ~12.9 ka), and a poleward shift during the Younger Dryas chron (YD: ~12.9 and ~11.5 ka) coeval with the resumption of the deglacial CO_2 rise (Anderson et al., 2009; Moreno et al., 2018a). An inferred generalized weakening of the SWW between ~11.0 and ~7.0 ka, contemporaneous with a reversal in the CO_2 rise, is followed by enhanced SWW influence between ~7.0 and ~5.5 ka, coeval with a steady multimillennial increase in CO_2 (Anderson et al., 2009; Fletcher and Moreno, 2011). These changes were followed by asymmetric behaviour and high variability of the SWW over the last ~5000 years (Fletcher and Moreno, 2012; Moreno and Videla, 2016).

Heterogeneities in timing and direction of inferred SWW changes, however, are evident among paleoclimate records from the mid-latitudes of the Southern Hemisphere, and this has led to alternative scenarios regarding the behaviour of the SWW (e.g. Dodson, 1998; Fletcher

and Moreno, 2012; Heusser, 1989; Lamy et al., 1999; Lamy et al., 2010; Markgraf, 1993; McGlone et al., 2000; Moreno et al., 2010; Moreno et al., 1999; Moros et al., 2009; Rojas et al., 2009; Shulmeister et al., 2004). Additional empirical data are needed from a broad latitudinal range of the SWW influence to validate/corroborate the postulated SWW behaviour described above spanning from the LGM to the present.

Numerous paleoecological and paleoclimate studies from all Southern Hemisphere mid-latitudinal landmasses (Australia, e.g. Fitzsimmons and Barrows, 2010; South America, e.g. Lamy et al., 2010; Africa, e.g. Meadows and Baxter, 1999; New Zealand, e.g. Vandergoes et al., 1997), have contributed to the understanding of terrestrial ecosystem dynamics, climate variability and SWW evolution during the LGM, T1 and the Holocene. Most of these studies are based on the examination of chronologies of fossilized micro- and macro-organisms preserved in multiple depositional settings. Time series of fossil records offer the opportunity to document past changes in the distribution and composition of a broad range of biological ecosystems at different temporal and spatial scales, and to infer different climatic conditions from such changes. The range of climatic interpretations of the fossil records from southern mid-latitudes include centennial, millennial and multi-millennial shifts in temperature and precipitation linked to SWW variability at local, regional and sub-continental scales (e.g. Jara et al., 2017; Moreno et al., 2018a; Rees and Cwynar, 2010a). Nevertheless, differences in degree of stratigraphic continuity, chronologic control, sampling resolution and interpretation among these various fossil records make it difficult to precisely compare inferred paleoclimate signals within and between the southern mid-latitude landmasses, and to assess whether these paleoclimate variations operated in a hemisphere-wide manner or not (Fletcher and Moreno, 2012).

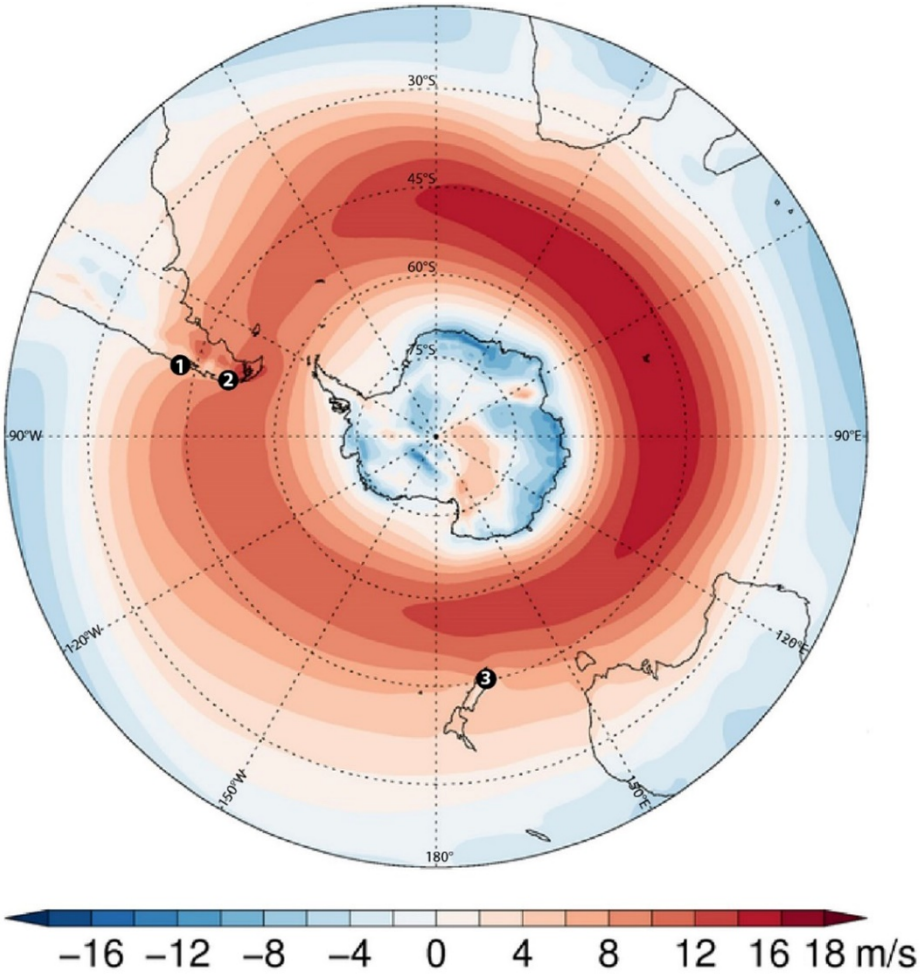

Figure 1.1. Map of the Southern Hemisphere showing the SWW zone of influence (between 30° to 60°S) and the annual average westerly wind speed at 850hPa from 1979 to 2019 defined by the ERA-Interim reanalysis (Bracegirdle, 2019), and the location of the sites from Western Patagonia (1: Lago Emerenciana, 2: Lago Pintito) and southern South Island of New Zealand (3: Lake Von).

In much the same way, there has only been limited use of paleo wildfire records in the southern mid-latitudes, and, therefore, our understanding of the link between terrestrial environments, climate, fire regimes and human perturbation is still poor. Global to local-scale studies have postulated that the generation of wildfires is limited by accumulation of dense biomass, ignition sources and fuel desiccation during distinctive climatic states (Holz and Veblen, 2012; Krawchuk et al., 2009). A regional synthesis of charcoal records from southern South America (between 34° and 54°S) show high spatial coherence in fire activity at sub-continental and regional scales following the LGM (Whitlock et al., 2007). These authors propose that fires were driven primarily by climate changes at multi-millennial timescales related to shifts in the SWW. Power et al. (2008) developed a global synthesis of charcoal records, including regional paleofire curves spanning from the LGM to the present. The South

American paleofire curve (<30°S) shows strong coherence with the patterns identified by Whitlock et al. (2007), but there is heterogeneity in the paleofire signals between other Southern Hemisphere landmasses. One explanation for this spatial divergence in paleofire trends is the presence of local human populations as a source of ignition of biomass (Power et al., 2008), supported by archaeological records of diachronous settlement of landmasses across the southern mid-latitudes spanning pre-LGM (Australia; Roberts et al., 2001), T1 (southern South America; Borrero et al., 2009) and the late Holocene (New Zealand; Wilmshurst et al., 2008). A closer examination of patterns of paleofire regimes since T1 across the middle latitudes of the Southern Hemisphere therefore should help to resolve whether they were primarily climate- or human-controlled, a question with ramifications for contemporary wildfire regimes in these regions.

Western Patagonia (40°-54°S) in southern South America and the southern South Island (44°-46°S) of New Zealand (Figure 1.1) constitute key regions for deciphering past climate and terrestrial ecosystem changes in the middle latitudes of the Southern Hemisphere, including the hemisphere-wide behaviour of the SWW since and during the LGM. On the one hand, these regions feature similarities in climate settings, topography and biological dynamics. They are the southernmost continental landmasses affected by the permanent influence of the SWW (Figure 1.1) (Bracegirdle, 2019; Garreaud, 2007; Hinojosa et al., 2017; Shulmeister et al., 2004). The SWW are intersected directly by the New Zealand Southern Alps and Patagonian Andes, inducing a marked west-east precipitation gradient. In both cases, abundant orographic precipitation, in conjunction with adiabatic cooling, controls the altitudinal, latitudinal and longitudinal distribution of biological ecosystems (e.g. vegetation, chironomids, etc) at the regional scale (Dieffenbacher-Krall et al., 2007; Dodson, 1998; Heusser et al., 1999; Paez et al., 1994; Wardle, 1991) that can provide proxies for reconstructing past environmental changes. On the other hand, these regions contrast strongly in the timing of first arrival of people. Archaeological findings indicate that the local human settlement in Western Patagonia and New Zealand started during T1 and the early stage of the last millennial (~0.75 ka), respectively (Borrero et al., 2009; Wilmshurst et al., 2008). These divergent human histories should provide good opportunity to disentangle the role of climate and humans as agents of environmental change. Therefore, sensitive biological ecosystems from Western Patagonia and New Zealand's southern South Island can provide

analogues for tracing past climate variability and SWW evolution during and since the LGM, as well as for the examination of human impacts on terrestrial environments through T1 and the Holocene.

This thesis research presents detailed fossil pollen and charcoal records from sediment cores from two small closed-basin lakes located in Western Patagonia in southern South America (Lago Emerenciana [43°8'7.55''S, 74°15'37.63''W, 44 m.a.s.l.] and Lago Pintito [52°2'39.82''S, 72°22'46.73''W, 170 m.a.s.l.]) (Figure 1.1), along with detailed fossil pollen and charcoal records and an exploratory chironomid record from sediment cores obtained from a closed-basin lake from southern South Island of New Zealand (Lake Von [45°14'27.73''S, 168°17'57.10''E, 685 m.a.s.l.]) (Figure 1.1). The examination of these multi-proxy terrestrial paleoenvironmental records will help to reconstruct vegetation, fire and climate history from the LGM to the present. Taken together, these sites represent a broad latitudinal span (~9°) of the zone of SWW influence at the western and eastern margins of the South Pacific Ocean. As such, the high-resolution records from these sites offer good opportunity to evaluate the alternative postulated histories of SWW evolution described earlier. The development of new detailed records from sites located in sensitive regions to changes in the position and intensity of the SWW is crucial to better understand past SWW variability and their implications for current and future climate scenarios

1.2. Thesis aims, objectives and hypotheses

This thesis aims to reconstruct vegetation, fire regime and climate change, as well as the behaviour of the SWW during and since the LGM in Western Patagonia in southern South America and southern South Island of New Zealand. In addition, this thesis aims to explore multi-millennial and sub-millennial hemisphere-wide trends in climate and SWW in the southern mid-latitudes, and examine their link with terrestrial environmental dynamics, fire occurrence, and atmospheric-ocean processes from the LGM to the present.

The aims of this thesis will be addressed using five objectives:

i) Generate high-resolution pollen and macroscopic charcoal records from sediment cores obtained from Lago Emerenciana, located in northwestern Patagonia in southern South America.

ii) Generate high-resolution pollen and macroscopic charcoal records from sediment cores obtained from Lago Pintito, located in southwestern Patagonia in southern South America.

iii) Generate high-resolution pollen and macroscopic charcoal records and a preliminary chironomid record from sediment cores obtained from Lake Von located in southwestern South Island, New Zealand.

iv) Produce a preliminary summer air temperature reconstruction (SmT) from the chironomid record from Lake Von.

v) Compare and integrate fossil pollen- and charcoal-based climate reconstructions from Lago Emerenciana, Lago Pintito and Lake Von records, along with an exploratory SmT from a chironomid record from Lake Von with relevant and pertinent published paleoclimate records from mid- and high-latitudes in the Southern Hemisphere (Western Patagonia, New Zealand, Antarctica). This will help to improve our understanding of climate change at regional and hemispheric scales and test the putative role of the SWW as driver of variations of atmospheric CO_2 concentration from the LGM to the present.

vi) Compare inferred fire and climate trends from Lago Emerenciana, Lago Pintito and Lake Von with published chronologies of paleoclimate, fire regimes and archaeological findings from western Patagonia and New Zealand to examine the role of climate change and humans as drivers of paleofires in southern mid-latitudes through T1 and the Holocene.

This research will also enable me to test the following hypotheses:

i) Climate variability

Hypothesis 1: If hemisphere-wide climate changes have been the main drivers of terrestrial environmental transformations in landmasses across the southern mid-latitudes during and

since the LGM, then fossil pollen and macroscopic charcoal records from Western Patagonia (at 43° and at 52°S) and New Zealand's southern South Island (at 46°S) should show:

a) Coherence in the timing and direction of vegetation change;
b) Coherence in the timing and direction of fire-regime change

Hypothesis 2: If sub-continental climatic and/or non-climatic (human activity) regimes have been the main drivers of terrestrial environmental transformations in landmasses across the southern mid-latitudes during and since the LGM, then fossil pollen and macroscopic charcoal records from Western Patagonia (at 43°S and at 52°S) and New Zealand's southern South Island (at 46°S) should show:

a) Divergence in the timing and direction of vegetation change;
b) Divergence in the timing and direction of fire-regime change.

ii) SWW and atmospheric CO_2 co-variability

Hypothesis 1: If shifts in the position and/or strength of the SWW modulated the atmospheric CO_2 concentration through wind-driven upwelling of CO_2-rich deep waters in the high southern latitudes during and since the LGM, then inferred SWW changes from paleoecological records from Western Patagonia and New Zealand's southern South Island should show:

a) Poleward shifts and/or enhanced SWW influence concurrent with increases in atmospheric CO_2 concentration;
b) Equatorward shifts and/or reduced SWW influence concurrent with declining atmospheric CO_2 concentration.

Hypothesis 2: If shifts in the position and/or strength of the SWW do not modulated the atmospheric CO_2 concentration through wind-driven upwelling of CO_2-rich deep waters in the high southern latitudes during and since the LGM, then inferred SWW changes from paleoecological records from Western Patagonia and New Zealand's southern South Island should show:

a) Poleward shifts and/or enhanced SWW influence concurrent with declining in atmospheric CO_2 concentration;
b) Equatorward shifts and/or reduced SWW influence concurrent with increases atmospheric CO_2 concentration.

1.3. Thesis structure

This thesis consists of six chapters. The current chapter introduces the research problems and presents the temporal and spatial context to the thesis, culminating in the aims, objectives and hypotheses of this thesis. Chapter 2-Methods includes the rationale for study area, site setting and proxy selection, and a detailed description of each method involved in this thesis. Chapters 3 to 5 present original results and conclusions from three selected sites (Lago Emerenciana, Lake Von and Lago Pintito). These chapters are written as journal articles, and include Introduction, Study area, Material and Methods, Results, Discussion and Conclusion section. It should be noted that, with this thesis structure, some repetition between these 3 results chapters and chapters 1 and 2 is inevitable but will be kept to a minimum. For example, the Material and Methods sections for each results chapter (3 to 5) describes the material collected from and methods applied to the relevant study site with cross-reference to more detailed generic methods descriptions in Chapter 2. Finally, Chapter 6 summarizes, compares and integrates multiproxy-based reconstructions of paleoclimate reported in chapters 3 to 5 to produce a chronology of past climate, fire regimes and SWW change across a broad latitudinal range (between 43° and 52° S) in the Southern Hemisphere from the LGM to the present. This chapter also addresses the research hypotheses in light of these findings and considers their contribution to understanding the evolution of terrestrial environments, fire regimes and atmospheric-ocean processes in the Southern Hemisphere since the last glaciation.

1.4. Contributions and authorships

I, William Iván Henríquez González, am the primary author of this thesis, the sole author of chapters 1, 2 and 6 and the first author of chapters 3, 4 and 5. My contributions to this thesis include i) collection of sediment cores, ii) sampling and preparation for pollen, macroscopic

charcoal and chironomid analyses, and radiocarbon dates, iii) development of high-resolution pollen, macroscopic charcoal and chironomid records, and iv) writing and editing of all chapters. My New Zealand supervisors Dr. Rewi Newnham, Dr. Gavin Dunbar and Dr. Andrew Rees contributed with the reviewing and editing of all chapters, the guidance for data interpretation and the suggestion of reference literature. In particular, Dr. Rewi Newnham (primary supervisor) contributed financial support to field work, laboratory research and support for international conference attendance. Dr Gavin Dunbar contributed with the logistics of sediment cores transportation. Dr. Andrew Rees contributed with his knowledge and expertise on chironomid analysis.

This thesis also benefits from the collaboration of Dr. Patricio Moreno from Universidad de Chile, Chile. He was involved in this thesis as an international co-supervisor, collaborating with the reviewing and editing of Chapters 3 and 5, and providing financial support for field work assistance and laboratory research work carried out in Chile.

I am planning to submit three papers for publication that draw upon this thesis. These papers will be closely aligned to the three 'results' chapters of the thesis which are formatted as journal articles. The following presents the titles and the target journals of Chapters 3 to 5.

Chapter-3. *Environmental and climate changes near the Pacific coast of southwestern Isla Grande de Chiloé, northwestern Patagonia, spanning the last ~24,000 years*.

Paper in preparation to be submitted to *Quaternary Science Reviews*.

Chapter-4. *Multi-proxy-climate reconstruction from southwestern South Island (45°S), New Zealand, spanning the last ~18,000 years.*

Paper in preparation to be submitted to *Quaternary Science Reviews*.

Chapter-5. *Vegetation, fire and paleoclimate history in Southwestern Patagonia (52°S) during the last 17,000 years*.

Paper in preparation to be submitted to *Quaternary Science Reviews*.

Chapter 2

Study area and Methodology

2.1 Structure of the chapter

This chapter provides general information about the study areas and methods used in this thesis. The first section gives an overview of the modern climate of the Southern Hemisphere and describes the main climate and physiographic elements of Western Patagonia and Southern New Zealand. The second section describes the rationale for setting and proxy selection. The third and last section describes the techniques used in this research, which include Loss on Ignition (LOI), radiocarbon chronology, pollen, chironomid, and charcoal analysis.

2.2. Settings

2.2.1. Modern climate of the Southern Hemisphere

Unlike the Northern Hemisphere, the Southern Hemisphere is mostly oceanic, allowing the development of strongly zonal atmospheric and oceanic circulation patterns, e.g. the Southern Hemisphere Westerly Winds (SWW) (Karoly et al., 1998). The SWW are a symmetric atmospheric component that impact on the climate of the middle- to high-latitude Southern Hemisphere landmasses south of ~30°S (Figure 2.1) (Garreaud, 2007). Changes in the strength of the SWW over these regions control the amount of orographic precipitation, mirrored in the strong and positive correlation between local precipitation and zonal wind speeds across the Andes and Southern Alps in South America and New Zealand, respectively (Figure 2.2) (Garreaud, 2007). Similarly, it is expected that latitudinal variations in the SWW also contribute to shifts in precipitation regimes, where its southward displacement results in reduced SWW influence and decreased precipitation over Southern Hemisphere landmasses north of its modern core (~50°S). Northward displacement of the SWW generates enhanced precipitation over the sector north of its modern core (Figure 2.3).

Interannual variability in precipitation is predominantly modulated by two climate modes: the El Niño-Southern Oscillation (ENSO) (Kidson and Renwick, 2002; Quintana and Aceituno, 2012) and the Southern Annular Mode (SAM) (Thompson and Wallace, 2000). ENSO is described as variations in the air pressure and sea-surface temperature (SST) gradient across the tropical Pacific (Diaz et al., 2001; Philander, 1983). During El Niño years there are positive SST anomalies in the eastern and central Pacific Ocean and weaker easterly trade winds. During its negative phase, referred to as La Niña, there are negative SST anomalies in the eastern Pacific and stronger easterly trade winds at tropical latitudes (Kidson and Renwick, 2002; Quintana and Aceituno, 2012). The SAM is defined as the mean zonal sea level pressure (SLP) difference between southern middle- (~40°S) and high-latitudes (~65°S). During positive phases of SAM (+SAM), SLP are higher than normal over the middle latitudes, the SWW contract poleward and, consequently, there is enhanced SWW influence over the Southern Ocean. In the negative phase of SAM (-SAM) SLP are higher than normal over Antarctica, the SWW migrate equatorward and, as result, the SSW are stronger than normal over middle latitudes (Thompson and Wallace, 2000).

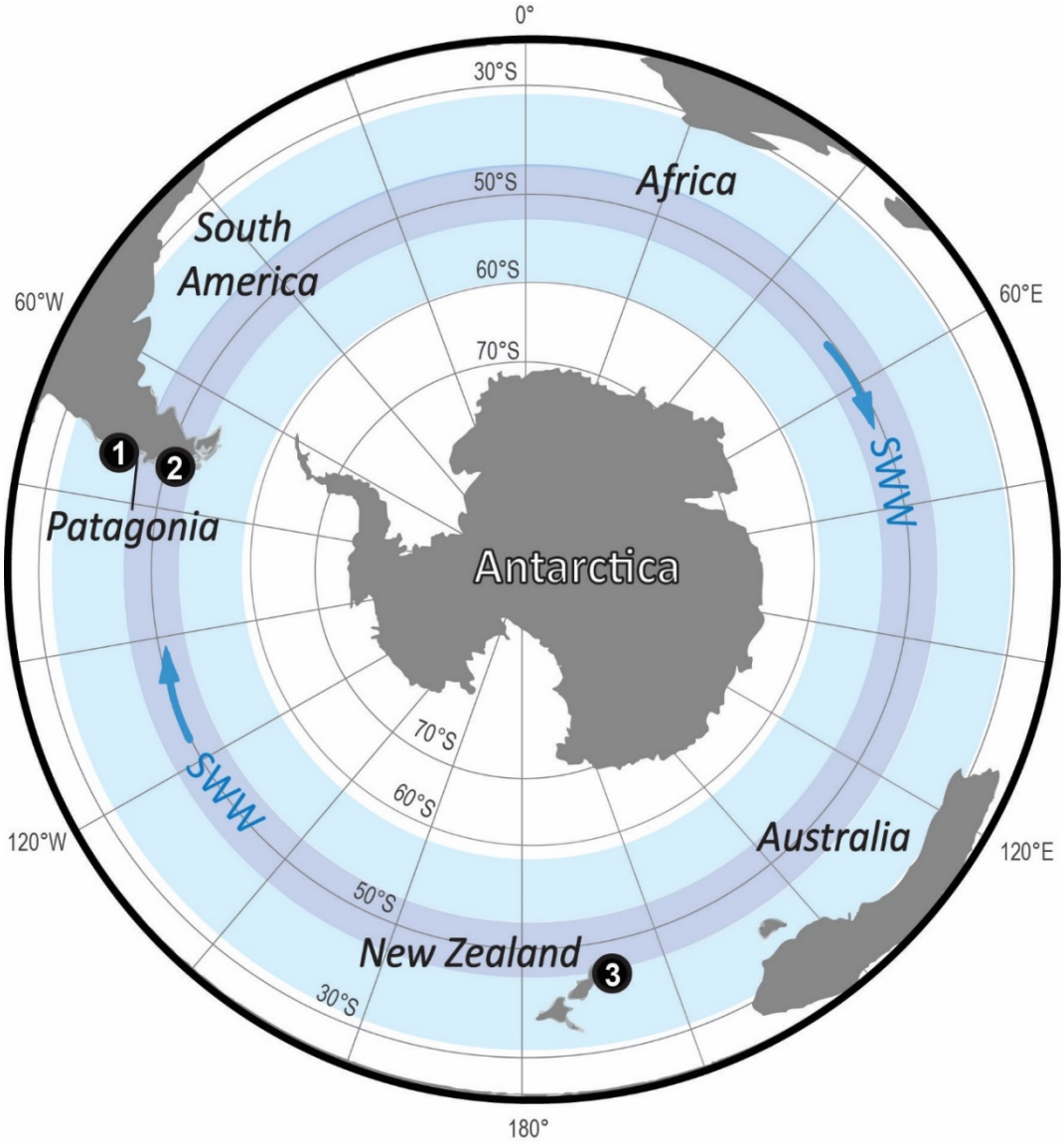

Figure 2.1. Schematic map of the Southern Hemisphere showing the main landmasses and the SWW zone of influence in the Southern Hemisphere including the current zone of maximum SWW influence (dark blue, core at~50°S) and its northern and southern edges (light blue). The blue arrows show the direction of the SWW flow. Cores sites are Lago Emerenciana (1), Lago Pintito (2) and Lake Von (3).

As the only substantial landmasses that intercept the SWW flow, Western Patagonia and the southern South Island of New Zealand represent key regions for monitoring past hydrologic and climate changes. Precipitation over these sectors is strongly and positively correlated with the intensity of the westerly flow (Figure 2.2) (Garreaud, 2007). This correlation is stronger west of the axial ranges due to orographic enhancement of precipitation. The Patagonian Andes in Western Patagonia and the Southern Alps in the South Island of New Zealand intersect the SWW and form an effective barrier to the westward advection of moisture-laden air masses originating from the Atlantic and western Pacific, respectively.

When the SWW flow is stronger (weaker), precipitation over western sectors increases (decreases). In eastern regions stronger SWW flow inhibits the penetration of easterly sourced precipitation from the oceans to the east and intensifies the evaporative potential of foehn winds resulting in reduced precipitation (Garreaud, 2007; McGlone et al., 1993).

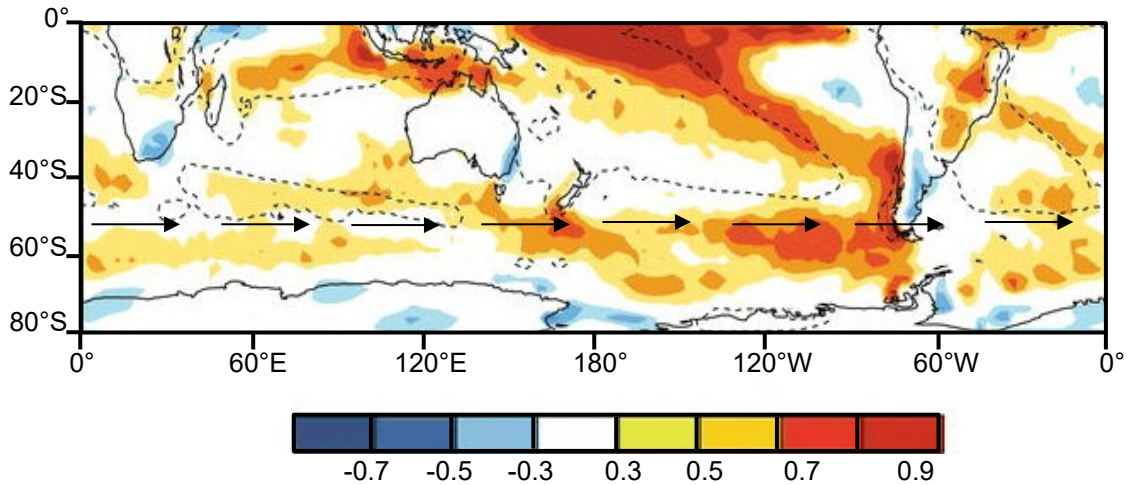

Figure 2.2. Map of the Southern Hemisphere and correlation between mean monthly zonal wind strength and local precipitation at 850-hPa. The black arrows indicate the approximate latitude of maximum westerly wind speed (core ~50°S). Dashed lines outline regions where mean annual precipitation exceeds 1000 mm. Modified from Garreaud (2007).

This study develops three terrestrial proxy records to reconstruct past SWW changes at different spatial and temporal scales. Paleohydrological reconstructions from Western Patagonia and South Island of New Zealand, both regions located within the SWW zone of influence, can be used to infer changes in the strength and latitudinal position of the SWW, based on the premise that these regions show a strong and positive correction between local precipitation and zonal wind speeds (Garreaud, 2007) (Figure 2.2). In the following sections I will describe the regional climate patterns of western Patagonia and New Zealand's southern South Island.

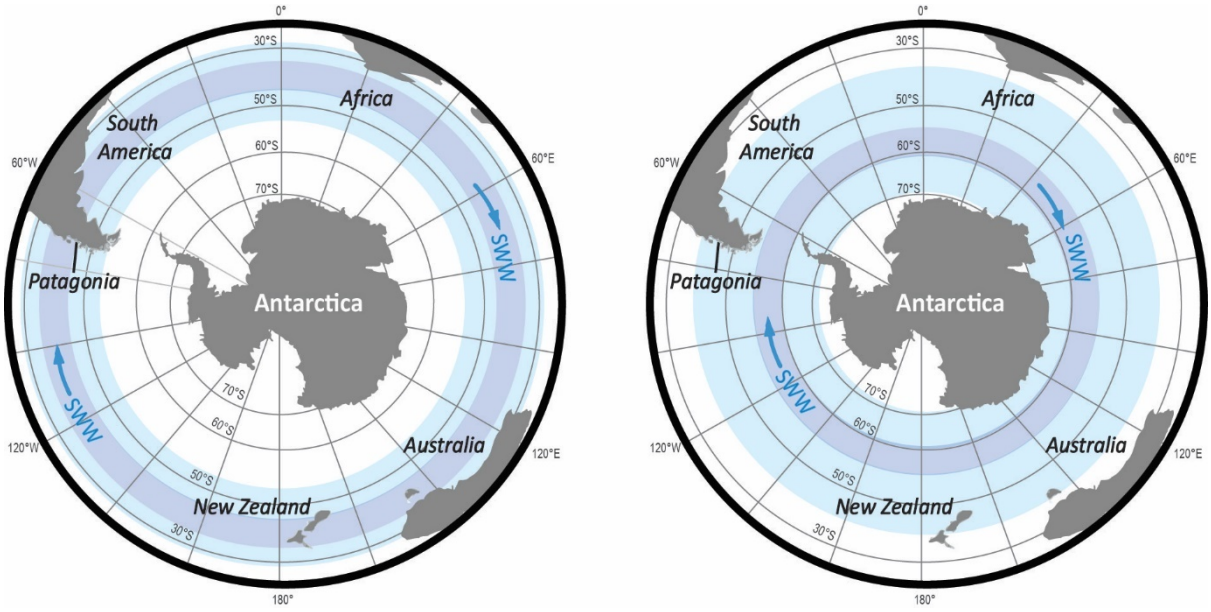

Figure 2.3. Schematic representation of the location of the SWW in two scenarios (dark blue: maximum zone of influence, core; light blue: northern and southern edges of the SWW). Left panel shows a northward displacement of the maximum influence of SWW (black blue). Right panel shows a southward shift of the maximum influence of the SWW.

2.2.2. New Zealand

New Zealand is a long (about 1900 km) and narrow (about 400 km at its widest point) series of islands located in the southwestern Pacific Ocean between 34 and 45°S (Figure 2.4). New Zealand's landscape is dominated by numerous active volcanoes and the presence of high axial ranges aligned from southwest to northeast (the Southern Alps). The southern two-thirds of the country has a nearly continuous mountain barrier, reaching altitudes above 3000 m in central South Island, whilst the northern half of North Island has no high mountains.

The climate of New Zealand is influenced by subtropical (easterly) and subantarctic (westerly) atmospheric circulation patterns (Ummenhofer and England, 2007). The North Island and northern sector of South Island protrude into the subtropical ridge, whereas southern sectors of the South Island of New Zealand are embedded in the SWW (McGlone et al., 1993; Sturman and Tapper, 2006). The presence of the north-south trending Southern Alps generates a marked west-east precipitation gradient across both islands, but it is less pronounced toward northern sectors as the elevation of the alps decreases. The southern South Island shows the most pronounced west-east gradient, recording mean annual precipitation in excess of 6000

mm yr^{-1} along the mountainous west coast and 600-1500 mm yr^{-1} over eastern sectors (Macara, 2014; Ummenhofer and England, 2007). These precipitation patterns are less evident in the North Island, in both east-west and north-south gradients (Ummenhofer and England, 2007). Whilst lake Von lies east of the main divide, there is sufficient 'spill over' orographic rainfall into the region that it still exhibits a strong correlation with westerly wind flow (Hinojosa et al., 2017; Sinclair et al., 1997). Thus, the marked precipitation gradient and the predominant influence of the SWW over southern sectors of the South Island offer the opportunity to reconstruct SWW-derived precipitation from terrestrial records.

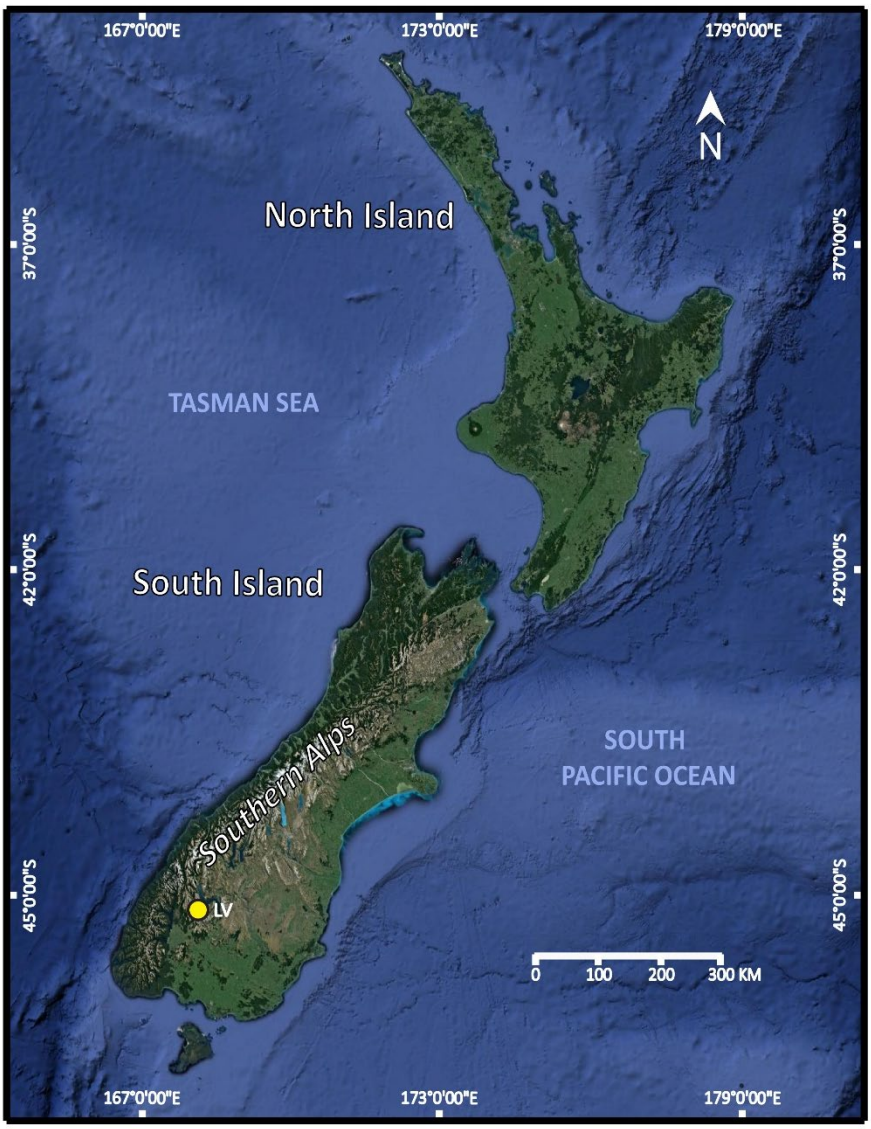

Figure 2.4. Map of New Zealand showing North Island, South Island and the Southern Alps. The yellow dot represents the location of the study site: Lake Von (LV, 45°14'27.73''S, 168°17'57.10''E).

Inter-annual and multi-decadal-scale climate modes such as ENSO and the SAM modulate precipitation variability (Lorrey and Bostock, 2017). During ENSO years, New Zealand experiences stronger than normal westerly flow and increased precipitation, lower seasonal temperature and drier conditions in the northeast of the country. During La Niña phase, New Zealand experiences more northeasterly flows, higher temperatures and wetter conditions in the north and east of the North Island. The positive (negative) phase of the SAM is manifested as anomalous negative (positive) rainfall across the southern South Island and the North Island, while the northern edges of the North Island are out of phase with these changes (Turney et al., 2003; Ummenhofer and England, 2007).

2.2.3. Western Patagonia

Western Patagonia (40° and 54°S, Figure 2.5) features numerous channels, fjords, islands and archipelagos, ice fields, and the Patagonian Andes. The northern sector, known as northwestern Patagonia (40° and 44°S), is characterized by the Valle Longitudinal, a north-to-south trending tectonic depression bounded by the Cordillera de las Costa and Cordillera de los Andes. The southernmost Patagonian sector, known as southwestern Patagonia (50° and 54°S), features the subsidence of the southern Patagonian Andes into the Pacific Ocean, and includes several glacier lobes such as the northern (NPI) and southern (SPI) Patagonian ice fields sourced from the massive southern Patagonian Ice Field (SPI)(Figure 2.5).

Western Patagonia is the only continuous continental landmass spanning subtropical to subantarctic regions that intersects the SWW (Figure 2.2). Regional precipitation is modulated by shifts in the strength and latitudinal position of the SWW. This relation between SWW and precipitation is revealed by the positive correlation between mean monthly zonal wind speeds at 850 hPa and local precipitation measured in weather stations throughout Western Patagonia (Garreaud, 2007; Moy et al., 2008). Interannual precipitation variability in western Patagonia is related to ENSO and SAM. In northwestern Patagonia, negative anomalies in summer precipitation are correlated with positive anomalies in ENSO and SAM (+SAM). Summer temperature anomalies are positively correlated with SAM at the regional scale (Villalba et al., 2012). In southwestern Patagonia, positive (negative) phases of SAM are

correlated with negative (positive) anomalies in precipitation and temperature during the summer months (Moreno et al., 2014).

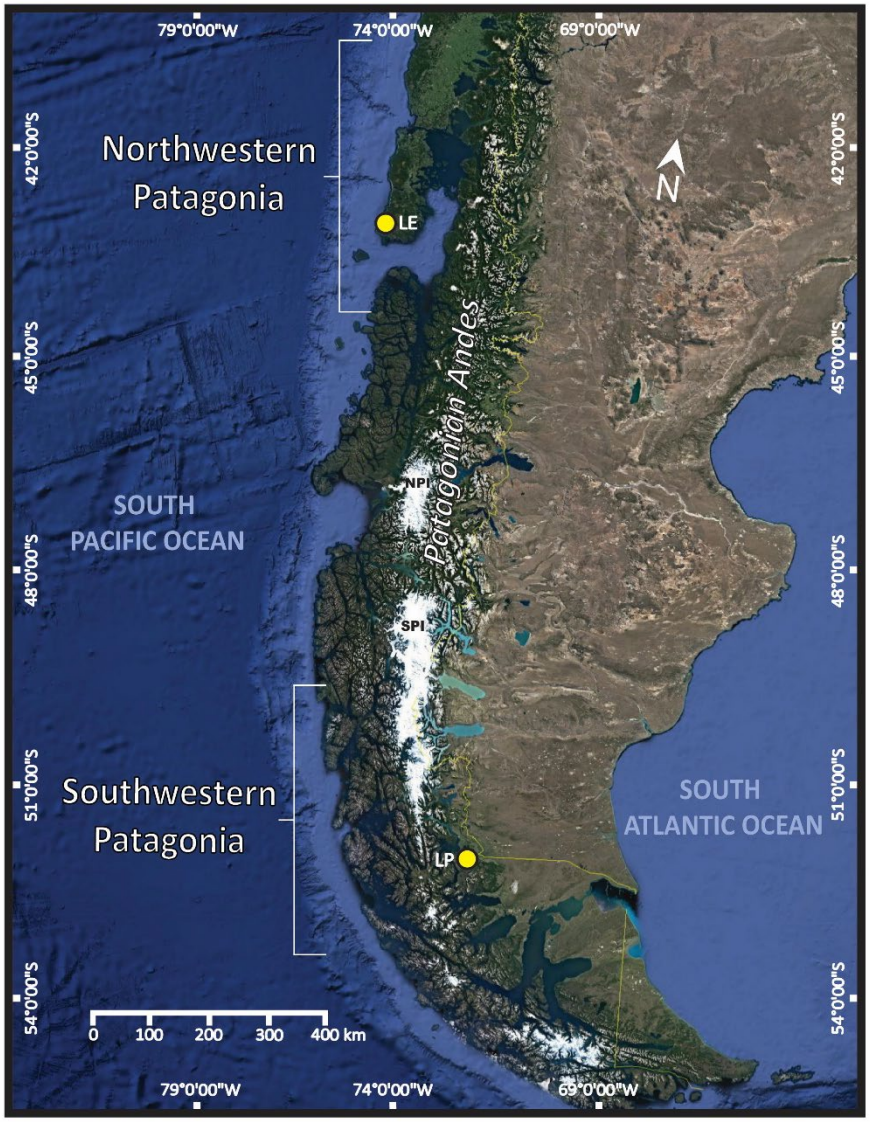

Figure 2.5. Map of southern South America indicating northwestern Patagonia (40°-44°S) and southwestern Patagonia (50°-54°S), along with the Patagonian Andes and the northern (NPI) and southern (SPI) Patagonian ice fields. The yellow dots represent the location of the study sites: Lago Emerenciana (LE, 43°8'7.55''S, 74°15'37.63''W) and Lago Pintitio (LP, 52°2'39.82''S, 72°22'46.73''W).

2.3. Rationale

2.3.1. Rationale for setting selection

Western Patagonia and the southern South Island of New Zealand have experienced repeated expansion and retreat of large ice-masses under different climate conditions during and since the LGM (Denton et al., 1999; Fitzsimons, 1997; Lorrey and Bostock, 2017; Lorrey and Bostock, 2014; Sutherland et al., 2019). This glacial dynamic allowed the development of numerous depositional settings across the landscape, which constitute natural archives that are characterized by the accumulation and preservation of material as discrete sedimentary layers through time, incorporating aquatic, terrestrial and atmospheric signals or proxies (e.g. pollen, spores, insects, isotopes, etc.) into sediments (Bradley, 2015). Thus, depositional environments can provide insights into the evolution of these different ecosystems under the superimposed influence of climate change beyond the instrumental records.

Among terrestrial depositional environments, bogs and lakes have been preferentially used in the Quaternary paleoclimate literature of Western Patagonia and the southern South Island of New Zealand because of their high capability to continuously monitor changes in terrestrial and aquatic ecosystems and climate variability at different temporal (decade, centennial, millennial) and geographic (local, regional) scales (e.g. Barrell et al., 2013). However, heterogeneities in stratigraphic continuity, chronologic control, and spatial sensitivity to the climate modes of interest between bog and lake records can result in differences in their reliability, applicability, and precision for reconstructing past environmental and climate changes. Peat bogs commonly feature alternation of subaquatic and subaerial phases, exposing sediments to erosional processes driven by natural (e.g. climate change, wildfires, volcanic eruptions, etc.) and anthropogenic (e.g. grazing, burning, artificial drainage, afforestation, infrastructure, etc.) pressures (Fenner and Freeman, 2011; Noble et al., 2018; Parry et al., 2014). Consequently, their stratigraphic continuity (e.g. the occurrence of hiatuses) and chronologic precision of the records is often compromised. In addition, ecological processes (e.g. vegetation growth, wildfires, etc.) occurring on the surfaces or the peripheries of bogs can impose a biased signal in sedimentary records that may override extra-local or regional ones (Moreno et al., 2009a; Moreno et al., 2018c). In contrast, lakes are usually characterized by stable subaquatic settings. These environments are less susceptible to perturbances and hyperlocal biases, ensuring the temporal continuity of

sediment records and the detection of local and/or regional environmental changes (Moreno et al., 2009a). Thus, lacustrine depositional environments have the potential to provide pertinent sedimentary records to develop detailed and continuous time series of past environmental and climate changes at adequate spatial (a few km^2) and temporal (decadal to millennial) scales.

In this thesis, therefore, I use sediment cores obtained exclusively from lakes situated in Western Patagonia and South Island of New Zealand. The nature of these records allows the development of continuous time series of environmental changes at different spatial and temporal scales. In the following section I will describe the rationale for the proxy selection used in my study for reconstructing environmental and climate changes.

2.3.2. Rationale for proxy selection

2.3.2.1. Pollen analysis

The topographically induced precipitation gradients (section 2.2.1), in association with adiabatic cooling and enhanced continentality east of the Patagonian Andes and Southern Alps, control altitudinal, latitudinal and longitudinal zonation of vegetation at the regional scale (Dieffenbacher-Krall et al., 2007; Dodson, 1998; Heusser et al., 1999; Paez et al., 1994; Wardle, 1991). This relationship between climate and plant communities provides the modern analogue for interpreting paleovegetation reconstructions in terms of past changes in climate, with particular emphasis on precipitation regimes. Several paleovegetation records from these regions have previously been developed using plant micro- and macro-fossils accumulated in lacustrine environments (Anderson et al., 2018; e.g. Villa-Martínez et al., 2012). Among these, fossil pollen and spores (palynomorphs), hereafter grouped as 'pollen' for simplicity, have been widely used for examining and documenting past vegetation shifts (Moreno et al., 2018b; e.g. Vandergoes et al., 2005), and specific taxa interpreted in multiproxy frameworks to examine regional atmospheric circulation changes (Lorrey et al., 2008). Pollen grains are small structures (from 10 to 150 µm) produced and released into the atmosphere by all seed-bearing plants. Depending on the dispersal mechanism (wind, insects or birds), pollen grains can travel long or short distances from their original source, providing either local or extra-local signals of vegetation communities. The most striking feature of the

pollen grains is the exine made of sporopollenin, a polymer highly resistant to chemical degradation over long periods of time (millions of years) (Zetzsche et al., 1937). Varieties of shapes, sizes, sculptures, and number of apertures in pollen grains are useful taxonomic characters (Punt et al., 2007) as they allow the identification of plant communities mostly at genus and family levels and, in some cases, at species level (Faegri et al., 1989). Therefore, fossil pollen records can provide important sources of information for understanding the evolution of vegetation and climate changes at local and regional scales.

This thesis principally uses the analysis of fossil pollen and spores (i.e. palynology) preserved in lake sediments from Western Patagonia and the southern South Island of New Zealand as the main approach to reconstruct past environmental and climate changes. Palynological records from Western Patagonian have been largely used for reconstructing hydrological and climate variability and from these to infer SWW shifts (e.g. Heusser, 2003). The applicability of this approach, however, is less well established in the literature from New Zealand's southern South Island, despite the similar climatic and physiographic setting to that of Western Patagonia, as described above. Thus, the challenge in this thesis is to attempt to utilize pollen records from both regions for reconstructing hydrological balance and climate trends. In addition to pollen-based climate inferences, this study attempts to deconvolute the climate signals (temperature and precipitation) from terrestrial records from the southern South Island of New Zealand using an alternative proxy (following section).

2.3.2.2. Chironomid analysis

Chironomids (nonbiting midges; Order Diptera) are the most widely distributed group of insects that inhabit freshwaters (Armitage et al., 2012) and are a particularly useful environmental and climate indicator (Walker, 1987, 2001) . These insects have an aquatic larval stage in their life cycle. The head capsule of the larvae is composed of chitin, a biopolymer that preserves well (Muzzarelli, 2011) and potentially for thousands of years in lake sediments (e.g. Massaferro et al., 2014). The different morphologies of the head capsules enable chironomids to be identified at the genus and species levels (Brooks et al., 2007). Ecological studies indicate that the chironomid life cycle is controlled by changes in pH (Rees and Cwynar, 2010b), salinity (Henrichs et al., 2001), lake productivity (Brodersen and Quinlan, 2006) and, above all, summer temperature (of the air and/or water) (Brodersen and Lindegaard, 1999; Dieffenbacher-Krall et al., 2007; Rossaro, 1991).

A growing number of paleoclimate studies from across Southern Hemisphere landmasses have validated the potential of using chironomids for reconstructing and quantifying summer temperature (SmT) through transfer functions (Africa, e.g. Eggermont et al., 2008; South America, e.g. Massaferro and Larocque-Tobler, 2013; Australia, e.g. Rees et al., 2008; New Zealand, e.g. van den Bos et al., 2018). Thus, in this thesis I perform a SmT reconstruction from a new and preliminary chironomid record from Lake Von.

2.3.2.3. Charcoal analysis

Western Patagonia and New Zealand are interesting regions to explore the linkages between fire regimes, vegetation, climate, and human disturbance because they possess similar ecology but have very different human occupation histories (see chapter 1, subsections 1.1). Charcoal analysis of lake sediment cores is a widely used approach in paleoecological studies to reconstruct past fire activity beyond instrumental records (Whitlock and Larsen, 2001). Charcoal particles are produced by the incomplete combustion of organic matter at temperatures between 280°C and 500°C, generating ash at higher temperatures (Chandler et al., 1983; Whitlock and Larsen, 2001). Charcoal particles can be classified into two categories with different dispersal characteristics, microscopic (<125µm) and macroscopic (>125µm) particles. Samples for microscopic charcoal analysis are prepared and analysed as part of pollen analysis (see sections 2.3.3.1.). Because of its small size, microscopic charcoal can be carried long distances by wind, implying that the source of microscopic charcoal is generally poorly defined. Conversely, macroscopic charcoal particles generally deposit closer to the source fire and, therefore, are a better indicator of local fires (Whitlock and Larsen, 2001).

In this thesis I perform macroscopic charcoal analysis from lacustrine sediment cores. These new records will allow the reconstruction of fire history from and the detection of local fire events in Western Patagonia and the southern South Island of New Zealand.

2.4 Methodology

2.4.1. Site selection and field sampling

For this thesis, three lake sites were used for pollen, charcoal and chironomid analyses. The sediment cores were obtained from two lakes from Western Patagonia (Lago Emerenciana and Lago Pintito) and one from southern South Island of New Zealand (Lake Von) (Table 2.1, Figures 2.4 and 2.5).

Table 2.1. Synthesis of study sites for this thesis. The sites are arranged in order of increasing latitude.

Site name	Latitude	Longitude	Elevation (m.a.s.l.)	Lake area (km^2)	Water depth (m)	Core length (cm)
Lago Emerenciana	43°8'7.55''S	74°15'37.63''W,	44	1.13	15	951
Lake Von	45°14'27.73''S	168°17'57.10''E	685	0.11	14	577
Lago Pintito	52°2'39.82''S	72°22'46.73''W	170	0.03	1.5	440

All sites are closed-basin lakes (i.e. without inflowing or outflowing rivers/creeks) and relatively small. The sites were expected to provide continuous records although a gap was eventually detected in the stratigraphy of Lago Emerenciana (more details in chapter 3). All sediment cores were collected using an anchored platform. For cores retrieved from Lago Emerenciana, this platform was equipped with a 7.5-cm diameter water interface piston core and Uwitec coring equipment. The cores were split using a Geotek core splitter. Coring at Lago Pintito used 10-cm diameter aluminium casing tubes, a 5-cm-diameter Wright square-rod piston corer and a 7.5-cm diameter water-sediment interface piston corer equipped with a 1-m-long clear plexiglass chamber. All sediment cores from Lago Emerenciana and Lago Pintito were stored at 4°C at the Quaternary Paleoecology Laboratory of Universidad de Chile. At Lake Von, the New Zealand site, a 5-cm diameter Wright square rod piston-corer was used for coring, along with 7-cm diameter plastic tubes and a 7-cm diameter sediment-interface gravity core. Thus, the lake Von record is a composite of a number of overlapping cores (Figure A2.1 in Appendix 2). The cores were stored at the University of Otago, Geology Department, also at 4°C.

2.4.2. Loss on Ignition (LOI) procedure

I performed LOI analysis by obtaining continuous/contiguous 1-cc samples from 1-cm-thick intervals throughout the sediment core. The LOI results are expressed as percent weight (See figures in chapters 3-5).

LOI is a well-established method for determining the organic and carbonate contents of sediments (e.g. Dean, 1974). Sequential combustion leads first to the oxidation of organic matter at 550°C to carbon dioxide and ash. This is followed by burning off carbonate ($CaCO_3$) at 950°C, generating carbon dioxide and leaving Ca oxide (Heiri et al., 2001). The detailed procedure is described in the following paragraphs based on Heiri et al. (2001) and involves three steps:

i) Empty crucibles were dried at 105°C overnight in an electric oven. Then, all crucibles were cooled to room temperature (18-25°C) in a desiccator to avoid moisture absorption and weighed on electronic balance. Subsequently, continuous/contiguous wet sediment samples (1 cc) were taken from all cores, deposited in pre-weighed crucibles, and then weighed. All crucibles with wet sediment samples were dried at 105°C overnight, cooled and weighed again. The dry weight of the sediment samples was calculated using the following equation:

$$DW_{105} = CDW_{105} – CW$$

where CW represents the weight of the empty crucibles, CDW_{105} corresponds to the dry weight of the samples contained in the crucibles, and DW_{105} the dry weight of the samples (all in g).

ii) The crucibles with the dry sediment samples were transferred to a muffle furnace to be combusted at a temperature of 550°C for 2 hours. Then, the crucibles were cooled to room temperature and weighted. The LOI_{550} was calculated using the following equation:

$$LOI_{550} = (DW_{105} – DW_{550})/DW_{105}*100$$

where LOI_{550} represents LOI at 550°C (as a percentage) and DW_{550} the dry weight of the sample after burning to 550°C (measured in g).

iii) The residual sediment (and crucible) after combustion at 550°C was further combusted at a temperature of 950°C for 4 hours. The crucibles then were cooled to room temperature and weighed. LOI_{950} was calculated as:

$$LOI_{950} = (DW_{550} - DW_{950})/DW_{105}*100$$

where LOI_{950} corresponds to LOI at 950°C (as a percentage) and DW_{950} represents the dry weight of the samples after burning to 950°C (measured in g).

2.4.3. Radiocarbon chronology

2.4.3.1. Sample selection

The chronology of all the sedimentary records in this thesis is constrained by multiple Accelerator Mass Spectrometry (AMS) radiocarbon dates. Selection of individual samples was based on the main pollen transitions observed in the assemblages and the chance occurrence macro fossils (wood, leaves, chironomid, charcoal) found throughout the sediment cores. For the Western Patagonia samples (Lago Emerenciana and Lago Pintito), 1-cc to 3-cc bulk organic samples were taken from sediment cores (details are provided in chapter 3 and 5) for radiocarbon analysis. For the southern South Island New Zealand samples (Lake Von), 1-cc bulk organic samples, along with plant material, charcoal and chironomids picked from 1-cc to 5-cc sediment samples from 1-cm sections throughout the cores were used for radiocarbon dating (more details in chapter 4).

2.4.3.2. Calibration and age model

All radiocarbon dates were calibrated using the SHCal13 calibration dataset (Hogg et al., 2013) included in CALIB 7.0.1 (Reimer et al., 2013) (see radiocarbon age tables in chapters 3-5) I point out that at the time this thesis was being developed, SHCal20 was not yet released (Hogg et al., 2020). Bayesian age models were developed using ages from each site from Western Patagonia (Lago Emerenciana and Lago Pintito) and southern South Island of New Zealand (Lake Von) using the 'Bacon' package for R (Blaauw and Christen, 2011). All age models are presented as plots showing the probability distribution of the radiocarbon dates

once calibrated into calendar years before present (present being 1950 by convention) and the calculated confidence interval of the Bayesian age models (see chapters 3-5). The thickness of all tephra present in the profiles from Western Patagonia was subtracted from the age models, on the assumption that these were deposited instantaneously.

2.4.4. Pollen analysis

2.4.4.1. Pollen processing

I performed pollen analysis on 1-cc or 3-cc sediment samples obtained from 1-cm thick sections through all selected sediment cores. Sampling intervals vary among records, with contiguous and contiguous sediment samples for the Lago Pintito record, spaced every 1 cm for the Lake Von record, and ranging from 1 t o3 cm for the Lago Emerenciana record. Isolating pollen grains and spores from the matrix of organic or inorganic sediments requires a sequence of chemical treatments. For this thesis, the pollen samples were processed following a modified version of a standard procedure (Faegri et al., 1989), as described here:

i) Potassium hydroxide (KOH). Individual samples were soaked in a 5-mL solution of 10% KOH in a water bath at 80°C for 15 minutes at to neutralise humic acids and release the palynomorphs from organic matrix material (deflocculation). Then the samples were washed twice with distilled water, centrifuging at 3500 rpm for 5 minutes and decanting the supernatant liquid each time .

ii) Hydrochloric acid (HCl). The samples were soaked in 5-mL solution of 10% HCl. This treatment is used to dissolve calcium carbonate in the sediment and the binder in the exotic *Lycopodium* spore tablets that allows calculation of pollen concentration (pollen grains cm^{-3}) and pollen accumulation rates (or pollen influx=pollen grains cm^{-2} yr^{-1}) for pollen and spores (Stockmarr, 1971). The samples were heated in a water bath at 80°C for 5 minutes and washed once by adding distilled water and centrifuging at 3500 rpm for 5 minutes.

iii) Sieving. The samples were sieved through a 150µm nylon mesh and washed once by adding distilled water and centrifuging at 3500 rpm for 5 minutes.

iv) Sodium polytungstate (SPT) and Hydrofluoric acid (HF). At this step, the samples were treated using either a) STP or b) HF depending of the sample source. Samples obtained from

Western Patagonia (Lago Emerenciana and Lago Pintito) were treated with HF, whilst samples from southern South Island, New Zealand (Lake Von) were treated with a solution of SPT. STP and HF treatments are used to separate the organic material (including pollen) from the minerogenic fraction by floating organic matter and dissolving silicates respectively. The two treatments have been shown to yield comparable results (e.g. Campbell et al., 2016) and both methods are conventionally used for preparing pollen samples. The different methods were employed in this study to observe the protocols operating in the two pollen laboratories.

a) 5-mL of SPT with a density of 2.0 g/cm^3 were added to float the organic fractions and centrifuged at 2000 rpm for 10 minutes. The organic material was sieved through a 6µm nylon mesh and transferred into new tubes. The inorganic fraction was discarded. The organic material was washed once by adding distilled water and centrifuging at 3500 rpm for 5 minutes.

b) a 5-mL solution of 30-40% HF was added to the samples. The samples were heated in an 80°C water bath for 20 minutes to accelerate the dissolution process. Then the samples were centrifuged at 3500 rpm for 5 minutes. The precipitate was conserved and the supernatant discarded.

v) Acetolysis. The samples were first dehydrated by adding 5-mL of a solution of glacial acetic acid ($C_2H_4O_2$), followed by centrifuging at 3500 rpm for 5 minutes. A solution of 0.5-mL of sulphuric acid (H_2SO_4) and 4.5-mL acetic anhydride ($(CH_3CO)_2O$) were then added to the samples to remove the cellulose matrix of the organic fraction. These samples were heated in an 80°C water bath for 2 minutes, followed by centrifuging at 3500 rpm for 5 minutes. A 5-mL solution of glacial acetic acid ($C_2H_4O_2$) was added to the samples and centrifuged at 3500 rpm for 5 minutes. Sequential washes in distilled water were made with centrifuging after each wash. The supernatant was discarded after each wash.

vi) Mounting. Each sample was dehydrated by adding 5-mL of tert-Butyl alcohol and centrifuging at 3500 rpm for 5 minutes. The samples were transferred to Eppendorf tubes using ~1.5 mL of tert-Butyl alcohol, followed by centrifuging at 3500 rpm for 5 minutes. The mounting medium (silicon oil) was added to the sample residue in a ratio of 3:1. One to two drops of the silicon oil solution were placed onto microscopic slides, and the coverslips were sealed with nail varnish.

2.4.4.2. Pollen identification and counting

Identification of fossil pollen and spores was conducted at 400X and 1000X magnification using a light microscope. Pollen grains in fossil samples were compared with reference samples or published pollen catalogues. Fossil pollen samples from New Zealand were identified with the aid of published catalogues (Moar, 1993) and unpublished reference material (Newnham's personal collection). Fossil pollen samples from Western Patagonia were identified based on a modern reference collection housed at the laboratory of Quaternary Paleoecology of Universidad de Chile, along with published descriptions and keys (Heusser, 1971; Villagrán, 1980). For each sample, a minimum of 300 pollen grains from trees, shrubs and herbs (terrestrial pollen) was identified. The percent abundance of each terrestrial taxon was calculated relative to this terrestrial sum (terrestrial pollen). The percent abundance of aquatic plants and pteridophytes was calculated in reference to the sum pollen total (terrestrial pollen + aquatics) and pollen total + pteridophytes (terrestrial pollen + aquatics + spores), respectively. The abundance of the green microalgae *Pediastrum* was calculated on the basis of the sum pollen total, spores and microalgae.

2.4.4.3. Pollen diagrams and zonation

The pollen records are presented as pollen percentage diagrams (X axis), including composite depth and age model (Y axes). The pollen records were divided in pollen assemblage zones with the aid of a stratigraphically constrained cluster analysis applied to all terrestrial taxa with abundance values ≥2%. Sum and percentage of all terrestrial taxa were recalculated and converted to square root values using CONISS for Tilia 2.0.41 (Grimm, 1987).

2.4.4.4. Rate of change (ROC)

The rate of change parameter is a critical variable used for identifying the magnitude and rapidity of changes in terrestrial vegetation (Grimm and Jacobson, 1992). I performed ROC analysis for the Lago Pintito pollen record to evaluate the sensitivity of arboreal vegetation through time. I only used ROC analysis in this record because the palynology shows the dominance (>95%) of forest composed exclusively by one taxon (more detailed in chapter 5), impeding the visualization of changes in the vegetation.

2.4.5. Chironomid analysis

2.4.5.1. Chironomid sample preparation

I sampled 0.5 to 1cc of sediment for chironomids analysis, in order to retrieve at least 50 whole head capsules per level (Heiri and Lotter, 2001). The samples were prepared following a standard procedure (Walker et al., 1991). Sediment samples were deposited into an empty beaker and filled with 10%KOH for deflocculating. The KOH/pollen mix was then placed on a hot plate for 15 minutes and stirred before sieving over a 90µm nylon mesh. After sieving and drying of the >90µm fraction, head capsules were picked in a Bogorov tray under 50X magnification. Chironomid samples were mounted onto slides and fixed with Entellan. Identification of chironomid taxa was conducted at 400X magnification using a light microscope and based on published literature (Dieffenbacher-Krall et al., 2008).

2.4.5.2. Chironomid diagram and zonation

The chironomid record is presented as a percentage diagram (X axis), including composite depth and age model (Y axes). The chironomid record was divided in chironomid assemblage zones with the aid of a stratigraphically constrained cluster analysis applied to all taxa. Sum and percentage of all taxa were calculated and converted to square root values using CONISS for Tilia 2.0.41 (Grimm, 1987).

2.4.5.3. Summer temperature reconstruction (SmT)

Summer temperature reconstructions (SmT) were developed using models adapted from Dieffenbacher-Krall et al. (2007), where “short” and “long” variants of *Tanystarsus funebris* types went undistinguished. I opted to use the WA-PLS model, which has a root mean square error of prediction ($RMSEP_{jack}$) of 1.27 and a coefficient of determination ($r2_{jack}$) of 0.80.

To test the reliability of the temperature reconstruction, the goodness of fit of the samples to the training sets was performed for SmT (Birks et al., 1990), as well as the abundance of rare taxa. I determined goodness of fit comparing the squared residual distance of the training set samples (Dieffenbacher-Krall et al., 2007) from an ordination axis constrained by temperature to the squared residual distance of the fossil samples that were passively fitted to the same

axis using the R package “analogue” (Simpson, 2007).It is considered a poor fit if the squared residual distance of a sample is greater than the 90th percentile of the squared residual distances of the training set samples. The fit is considered very poor if it is greater than the 90th percentile (Birks et al., 1990). In the case of Rare taxa, they are defined as taxa that have a Hill’s N2 (Hill, 1973) of 5 or less in the training set samples (Dieffenbacher-Krall et al., 2007). In addition, I tested the dissimilarity between chironomid assemblage from Lake Von and the closest modern analogue in the training set. Samples with dissimilarity greater than the 5th percentile of the distribution of dissimilarities between training set samples are considered to have no close modern analogue (Simpson, 2007) (Figure A3.4 in Appendix 2).

2.4.6. Macroscopic charcoal analysis

2.4.6.1. Macroscopic charcoal processing

I sampled and processed 2-cc sediment samples along continuous/contiguous 1-cm thick sections throughout all sediment cores for macroscopic charcoal analysis. The samples were prepared and analysed using a standard procedure that involves:

i) Deflocculation: 2-cc sediment samples were deposited in empty plastic beakers. Then, all plastic beakers with wet samples were filled with 10% KOH and left overnight.

ii) Sieving: The sediment samples were then careful sieved to avoid rupture of individual particles. Charcoal samples derived from sediment cores retrieved from Western Patagonia (Lago Emerenciana and Lago Pintito) were sieved through 106 and 212-µm meshes. Charcoal samples derived from sediment cores obtained from Lake Von (New Zealand site) were sieved through 125 and 225-µm meshes; the nearest available sizes to those used for the Patagonian samples. Then, charcoal particles remaining on each sieve were transferred into separate petri dishes using water.

iii) Counting: Macroscopic charcoal particles were counted by visual inspection on a stereoscope at 10X magnification. The counts were recorded manually and then transferred to a spreadsheet.

Charcoal data are presented as charcoal accumulation rates (CHAR= particles cm^{-2} year^{-1}) and concentration (particles cm^{-3}) when is required.

2.4.6.2. CHAR Analysis

I performed time-series analysis of macroscopic charcoal to detect local fire events, and their frequency and magnitude using the software CharAnalysis (Higuera et al., 2009). All charcoal data were resampled/interpolated to consistent time intervals based on the median time resolution of each charcoal record (described in chapter 3-5). The background charcoal signal (charcoal accumulation not associated with local fires) was defined by using a Lowess robust-to-outliers and smoothing windows between 500 and 1,000 years. A locally defined threshold was used to identify charcoal peaks exceeding the 99th percentile distribution of positive residuals, utilizing a Gaussian mixture model (figures in chapter 3- 5).

Chapter 3

Environmental and climate changes near the Pacific coast of southwestern Isla Grande de Chiloé, northwestern Patagonia, spanning the last ~24,000 years

3.1. Abstract

Isla Grande de Chiloé (IGC, 40-43°S) is the southernmost terrestrial sector of northwestern Patagonia that remained ice-free during the late Quaternary, offering the opportunity to examine paleoenvironmental and paleoclimate changes during and since the LGM. Here, I present detailed pollen and charcoal records from sediment cores collected in Lago Emerenciana (43°8'7.55''S, 74°15'37.63''W, 44 m.a.s.l.), a closed-basin lake located in southwestern IGC. The record shows abundant presence of arboreal pollen (*Nothofagus*), accompanied by other trees, shrubs and alpine herbs between ~24.0 and ~17.5 ka. These results suggest scattered *Nothofagus*-dominated subantarctic woodlands and alpine vegetation under cold and hyperhumid conditions, with major cooling and enhanced precipitation between ~19.7 and ~17.5 ka under strong SWW influence. A sustained increase in Myrtaceae started at ~17.5 ka, along with declines in cold-resistant hygrophilous herbs, shrubs, ferns and *Nothofagus* suggesting a shift from cold-hyperhumid to temperate/humid conditions, associated with a southward shift of the SWW. This interval coincided with an increase in fire activity associated with extensive arboreal cover and less humidity. This was followed by cold-temperate conditions and increased precipitation with high seasonality between ~16.3 and ~14.5 ka, revealed by an increase in the conifers *Fitzroya*/*Pilgerodendron*, a rise in the *Tepualia*+*Raukaua* parameter and a decline in macrophytes (Cyperaceae and *Isoetes*), reflecting a northward shift or strengthening of the SWW following the onset of T1. Subsequent increases in cold-tolerant hygrophilous trees between ~14.5 and ~12.5 ka indicates spread of cold-tolerant and opportunistic taxa in a relatively open-canopy Subantarctic Patagonian rainforest, implying a shift to colder temperatures and enhanced precipitation during the Antarctic Cold Reversal, consistent with a northwards shift in, or stronger, SWW. A major increase in Myrtaceae, the disappearance of cold-tolerant conifers and a rise in the *Tepualia*+*Raukaua* parameter between ~12.5 and ~11.1 ka suggest persistent cold conditions and a decline in precipitation. This was followed by dominance of Myrtaceae,

along with an increase in *Nothofagus*, the appearance of the Valdivian rainforest trees *Eucryphia*/*Caldcluvia* and high *Tepualia*+*Raukaua* values between ~11.1 and ~7.6 ka, suggesting a warming and reduction in precipitation. These findings suggest reduced SWW influence between ~12.5 and ~11.1 ka, interpreted as a southward shift during the Younger Dryas chron, followed by minor SWW influence between ~11.1 and ~7.6 ka, suggesting weakening of the SWW during the early Holocene. A prominent increase with low-magnitude variability of species characteristic of modern Valdivian evergreen rainforest communities (*Eucryphia/Caldcluvia*) between ~7.6 and ~2.4 ka, occurred in a context of increased precipitation between ~7.6 and ~4.6 ka suggesting major SWW influence, and reduced precipitation between ~4.6 and ~2.4 ka in response to minor SWW influence. I posit that that high climate variability with major seasonality in precipitation at ~43°S (wetter winters, drier summers) were ideal conditions for the expansion of *Eucryphia/Caldcluvia* in this sector of IGC between ~7.6 and ~2.6 ka, considering that these trees are highly resistant to summer-drought. The palynological record reveals that changes in the structure and composition of rainforest communities at the southwestern IGC were driven by shifts in temperature, with precipitation variability linked to SWW shifts. Beyond SWW behaviour, these findings constitute the first empirical data from these sectors that show ice-free conditions during the LGM, suggesting that southwestern IGC constituted a source area or corridor for the colonization of recently deglaciated areas east of Lago Emerenciana.

3.2. Introduction

As outlined in Chapter 1, there is particular interest in deciphering shifts in the strength and latitudinal position of the Southern Westerly Winds (SWW) during the last glacial-interglacial cycle. SWW variability influences local and regional climate of landmasses south of ~30°S (Garreaud, 2007) and has been proposed as a driver of past atmospheric CO_2 variations through ventilation of CO_2-rich deep water in the Southern Ocean (SO) (Anderson et al., 2009; Denton et al., 2010; Moreno et al., 2010; Toggweiler, 2005; Toggweiler et al., 2006). Nevertheless, our current understanding of the timing, direction and magnitude of multi-millennial variations of the SWW during and since the LGM is still limited.

Isla Grande de Chiloé (IGC, 40-43°S, 71-74°W, Figure 3.1), in northwestern Patagonia, constitutes a key region in the paleoenvironmental and paleoclimate discussion of the

southern mid-latitudes. The intense glacial activity during the last ice age in IGC (Marine Isotope Stages 2-4) (Denton et al., 1999) led to a diverse topography, including a myriad of potential depositional environments to develop time series of ecological proxies of climatic significance before, during and following the LGM. In fact, several palynological studies from bogs and lakes located in north and southeastern IGC have documented, with varying degrees of detail and continuity, the vegetation, fire and climate history throughout the last glacial-interglacial cycle (Abarzúa and Moreno, 2008; Abarzúa et al., 2004; Fercovic, 2020; Godley and Moar, 1973; Gonzalorena, 2015; Heusser, 1994; Heusser, 1990a; Heusser et al., 1995; Heusser and Flint, 1977; Heusser and Heusser, 2006; Heusser et al., 1999; Heusser et al., 1981; Pesce and Moreno, 2014; Ugalde, 2016; Villagrán, 1985, 1988a, 1988b). These studies have reported valuable information on the timing and magnitude of climate trends, the response of plant communities to climatic (fire events) and non-climatic disturbance regimes (in particular human induced fires, explosive volcanism), shifts in the composition and distribution of the vegetation from extreme glacial to extreme interglacial climate, and the SWW variability in northwestern Patagonia. Despite considerable advances made in the northern and southeastern sectors of IGC, there are no records from the southwestern sector of IGC and, consequently, the paleovegetation and paleoclimate evolution in this sector during and since the LGM remains largely unknown.

The lack of paleoecological records from the Pacific coast of southwestern IGC has also limited our understanding of the regional deglacial history, and plant biogeography, in particular the spatial and temporal patterns of plant colonization during the last glacial-interglacial transition. An entrenched assumption in the literature of the last five decades has been that nearly three quarters of IGC were covered by Andean piedmont glaciers at their most extensive position during the LGM (Figure 3.1) (Hollin and Schilling, 1981; Mercer, 1965). Radiocarbon-dated stratigraphic and geomorphic records show that glaciers extended into northeastern IGC during the LGM (Denton et al., 1999; Moreno et al., 2015), whereas the glacier margins south of ~42°40’S are hypothesized/modelled to have reached the Pacific coast of IGC (Davies et al., 2020; Hollin and Schilling, 1981; Mercer, 1965), albeit with no empirical support. This LGM glaciation pattern across and along IGC has led some authors to postulate the existence of glacial vegetation refugia in the vicinity of ice margins located in the northwestern portion of IGC during the LGM (Heusser, 1990a; Villagran, 2001), potentially

acting as a source area or corridor for the colonization of newly exposed ice-free sectors farther east and south during the Last Glacial Termination (Termination 1: T1, between ~18.0 and ~11.7 ka) (Heusser, 1990a; Villagran, 2001). Ice withdrawal was triggered by an abrupt warm pulse at the beginning of T1 (Denton et al., 1999; Moreno et al., 2015). Recently, Moreno et al. (2015) reported a synthesis of minimum-limiting radiocarbon dates for ice recession obtained from several pertinent sites located in the northeastern and central sectors of IGC (Figure 3.1). Based on nearly identical minimum-limiting dates of ice recession these authors suggested that ice lobes had retreated from these sectors prior to ~17.8 ka, consistent with the recessional chronology from the mainland in northwestern Patagonia (Moreno et al., 2015). Farther south in southeastern IGC, minimum limiting radiocarbon dates for ice recession obtained from four sites yielded nearly identical ages of ~15.3 ka (Laguna Soledad, Laguna Chaiguata, Puerto Carmen, Lago Oqueldán) (Fercovic, 2020; Villagrán, 1988b) (Figure 3.1). The lag of ~2300 years for the onset of ice-free conditions between the northern and southern portion of IGC could be attributed to heterogeneous responses of the Golfo de Ancud and Golfo de Corcovado ice lobes to climate forcing at different latitudes (Fercovic, 2020; Pesce and Moreno, 2014). Unfortunately, the Pacific sector of southwestern IGC has remained largely unexplored and, consequently, glacial, ecological and biogeographic processes have not been addressed. New data from this sector would offer insights into the environmental evolution following the LGM, the timing and direction of plant colonization of a newly deglaciated landscape, and help to resolve the location of the LGM ice margins and related questions concerning putative refugia along the Pacific coast of IGC.

Here I report detailed fossil pollen and macroscopic charcoal records from sediment cores obtained from Lago Emerenciana (43°8’7.55’’S, 74°15’37.63’’W, ~24 m depth, 44 m.a.s.l., Figure 3.1), a small (~1000 m^2) lake, to examine millennial and multi-millennial vegetation, climate and fire-regime changes over the last ~24,000 years in the southwestern sector of IGC. These data allow the assessment of the following questions: i) Was the extreme southwestern IGC ice-free during the LGM? Did this sector of the island harbour floral refugia during the LGM? What was the timing for the colonization and expansion of terrestrial vegetation in newly deglaciated landscape? How did the vegetation and fire-regime change during and since the LGM? Was the deglacial warming an uninterrupted/unidirectional process? or were there any climate reversals? These questions will be addressed within the

overall context of my overarching research goal: understanding SWW variability across the southern mid-latitudes during and since the LGM.

3.2.1. Study area

IGC is located in the southwestern portion of the Chilean Lake District, in northwestern Patagonia (Figure 3.1). This island is the largest and westernmost of the Chilotan archipelago, which features several small islands distributed from Golfo de Ancud on its northern limits to Golfo de Corcovado along its eastern and southern shores. The northern limit of IGC faces the Canal de Chacao, which establishes a narrow and shallow seaway with the mainland. Western sectors of the island feature the Coastal Range (Cordillera de la Costa), with elevations that reach up to ~800 m in its northern half and ~500 m in its southern portion.

The present-day climate of western Patagonia is temperate and wet, with north-south and west-east precipitation gradients, and maritime influence toward southwestern sectors including the periphery of IGC (Moreno et al., 2018a; Quintana and Aceituno, 2012). The SWW are the sole source of precipitation along the Pacific slopes of the Andes Cordillera and local precipitation shows a strong positive correlation with zonal wind speeds (Garreaud, 2007). Thus, precipitation amount in this region is a good diagnostic for past shifts in the strength and position of the SWW at zonal scale. Interannual precipitation variability is modulated by El Niño-Southern Oscillation (ENSO) and the Southern Annular Mode (SAM). Positive anomalies in these indices are correlated with negative anomalies in summer precipitation in northwestern Patagonia (Montecinos and Aceituno, 2003). Summer temperature anomalies, on the other hand, are positively correlated with SAM at regional scale (Villalba et al., 2012). The positive phase of SAM generates favourable conditions (e.g. warm and dry summers) for the occurrence of wildfires along western Patagonia (Holz and Veblen, 2012). Precipitation in IGC occurs year-round, reaching maximum values during the winter and minimum recorded during the summer. Mean annual precipitation measured in Puerto Montt (41°43’S, 73°09’W, 85 m.a.s.l) is 1857 mm (summer mean precipitation 156 mm; winter mean precipitation 1215 mm). Equivalent observations for other weather stations are: Ancud (41°54’S, 73°48’W, 20 m.a.s.l) 2118 mm (179-1456 mm); Castro (42°29’S, 73°46’W, 50 m.a.s.l.), 1800 mm (156-1284 mm); and Quellón (43°08’S, 73°37’W, 50 m.a.s.l.), 1663 mm (139-1096 mm). Mean annual

temperature measured in Puerto Montt is 10.3°C (summer mean temperature 13.7°C, winter summer temperature 6.6°C), in Ancud is 11.1°C (15°-7.5°C), Castro is 10.5°C (14°-6.8°C) and Quellón is 11.3°C (15.1°-7.7°C) (Figure 3.1) (Climatic explorer CR2 2020, http://explorador.cr2.cl/). The presence of the Coastal Range generates a marked orographic effect on precipitation amount, with the highest annual values along its western slopes (>4000 mm) and a decline along the eastern sectors (~2000 mm) (Dirección General de Aguas,1987). Further to the east, annual rainfall on the western slopes of the Andes reaches values of ~3620 mm (182-447 mm summer-winter means) near sea level (Chaitén meteorological station) (Figure 3.1).

Temperate broad-leaved rainforests dominated the regional vegetation prior to the Chilean-European settlement. The agrarian and forestry industries have impacted on the native vegetation at least during the last three centuries (Jara and Moreno, 2012; Moreno and Videla, 2016). Currently, most plant communities are mostly confined to the Coastal Range and the western Andean flanks and foothills. Several studies have analysed the distribution and composition of the regional vegetation along latitudinal and altitudinal gradients in temperature and precipitation (Heusser, 1990a; Heusser et al., 1999; Schmithusen, 1956; Villagrán, 1985). This zonation can be used as a modern analogue for interpreting palynological records and inferring past climate changes. Continental sectors feature remnants of the three main forest communities occurring in northwestern Patagonia: the evergreen Valdivian and North Patagonian rainforests, and Subantarctic forests; and High Andean vegetation along the Pacific slopes of the Andes Cordillera. IGC is dominated by these rainforest communities at mid- and low elevations, with scattered occurrences of cold-tolerant and hygrophilous herbs and shrubs at higher elevations (Poaceae, Asteraceae, Apiaceae, Ericaceae). The main plant communities distributed throughout IGC include key diagnostic taxa that enable the changing vegetation patterns to be reconstructed from palynological records (Heusser, 1990a; Villagrán, 1985) (Table 3.1). The Valdivian rainforest is distributed in the warm lowland of northern and central IGC (<250 m.a.s.l.) with its southern limit at Lago Huillinco (Figure 3.1). It is characterized by the summer-drought tolerant *Eucryphia cordifolia*, along with *Gevuina avellana* and *Aextoxicon punctatum*. The North Patagonian rainforest occurs between 250 and 450 m.a.s.l. throughout IGC. This plant community is distinguished by the absence of *Eucryphia cordifolia*, dominance of *Nothofagus*

dombeyi and *Laureliopsis phillipiana*, and includes several species of Myrtaceae and *Weinmannia trichosperma*. Its presence at higher elevation denotes the capability of North Patagonian rainforests to tolerate higher precipitation regimes and lower temperature than the Valdivian rainforest. The Subantarctic rainforest is distributed above 450 m.a.s.l. in the Coastal Range of IGC, and features the replacement of Myrtaceae species by the trees *Nothofagus dombeyi*, *N. betuloides* and *N. nitida*, associated with the cold-resistant hygrophilous conifers of the family Podocarpaceae (*Saxegothaea conspicua*, *Podocarpus nubigena*), and Cupressaceae (*Fitzroya cupressoides* and *Pilgerodendron uviferum*), often associated with *Drimys winteri* and the clubmoss *Lycopodium magellanicum*. Magellanic Moorland vegetation occurs at the summits of the Coastal Range, as well as in low-elevation Pacific sectors of central and south IGC with high precipitation regimes. This vegetation community is dominated by cushion-forming plants such as *Donatia fascicularis*, *Astelia pumila* and *Tetroncium magallanicum* (Table 3.1).

Table 3.1. Modern plant communities in Isla Grande de Chiloé, indicating dominant species and altitudinal distribution (Heusser, 1990a; Heusser et al., 1999; Schmithusen, 1956; Villagrán, 1985).

Plant communities	**Dominant species**	**Altitude (m.a.s.l.)**
Valdivian Rainforest	*Eucryphia cordifolia-Gevuina avellane-Aextoxicon punctatum*	<250
North Patagonian Rainforest	Myrtaceae-*Nothofagus dombeyi-Laureliopsis phillipiana*	250-450
Subantarctic Rainforest	*Nothofagus dombeyi-Podocarpus nubigena-Fitzroya/Pilgerodendron*	>450-650
Magellanic Moorland	*Donatia fascicularis-Astelia pumila-Tetroncium magallanicum*	>650 and at sea level

Lago Emerenciana is a small closed-basin lake located ~3 km from the Pacific coast of southwestern IGC (Figure 3.1). The vegetation surrounding the lake consists of trees characteristic of North Patagonian rainforest, dominated by the trees of the myrtle (Myrtaceae) and Nothofagaceae families (*Nothofagus*). The periphery of the lake is dominated by the trees *Raukaua laetevirens* and *Tepualia stupularis*, and scarce presence of

Cyperaceae. I also noted the occurrence of Magellanic Moorland in a bog located south of the lake.

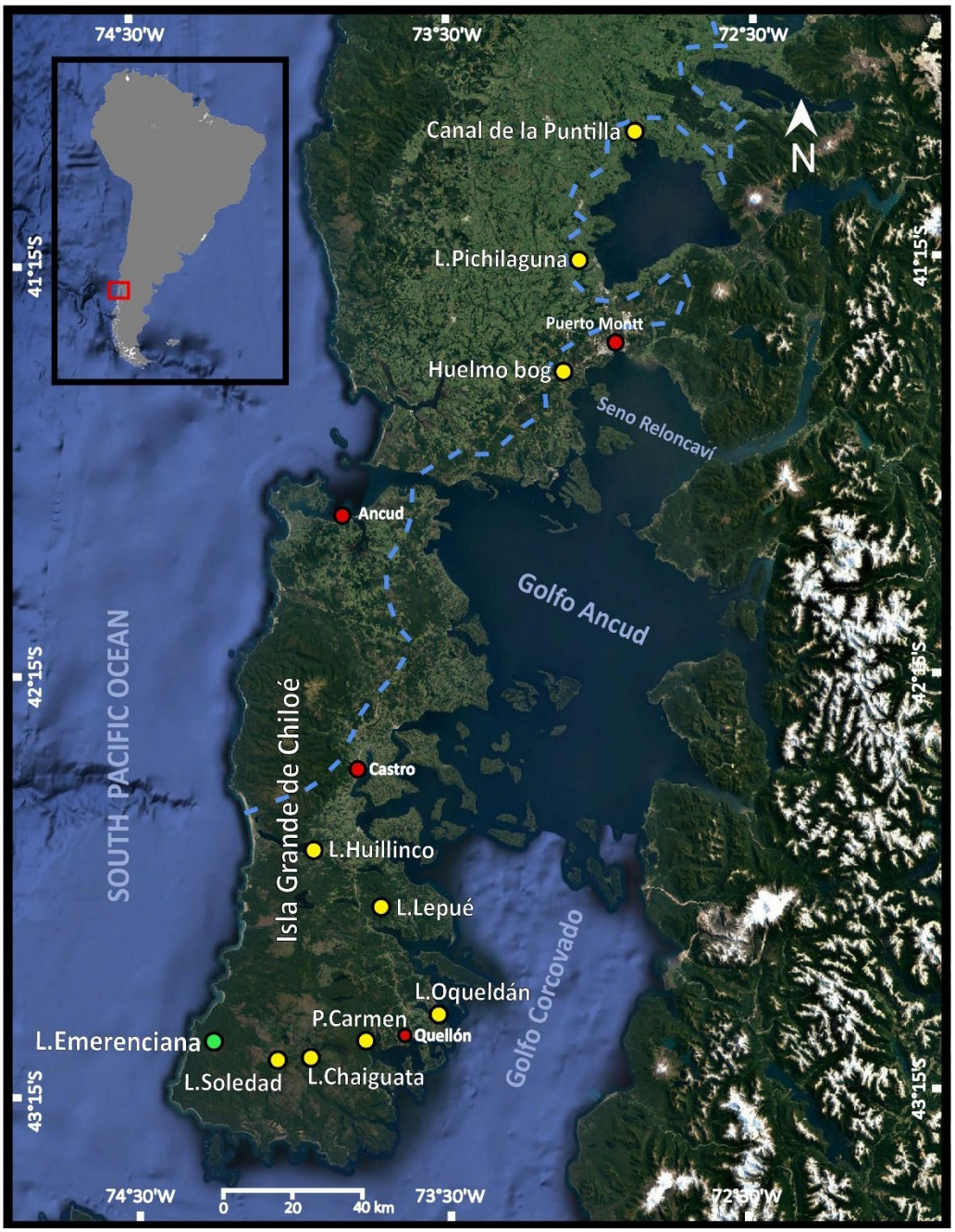

Figure 3.1. Map of the study area showing the location of Lago Emerenciana (L. n: Lago n) (green dot), sites (yellow dots) and places (red dots) mentioned throughout the text. Also shown is the reconstructed extent of Andean piedmont glacier lobes during the last glacial maximum (dashed blue horizontal lines) (Denton et al., 1999; Hollin and Schilling, 1981; Mercer, 1965; Moreno et al., 2015).

3.3. Materials and methods

3.3.1. Stratigraphy and chronology

Sediment cores were retrieved from Lago Emerenciana during 2016 and 2017. I sub-sampled the organic section of the sedimentary sequence for pollen and macroscopic charcoal analyses. For pollen samples, I sampled and processed 1-cc sediment samples obtained from 1-cm thick sections at different intervals that range from 1 to 3 cm. I tallied macroscopic charcoal particles (>125µm) from 2-cc sediment samples along continuous/contiguous 1-cm thick sections. The abundance of macroscopic charcoal is expressed as concentration (particles cm^{-3}) and accumulation rate (particles cm^{-2} $year^{-1}$). All procedures involved in the extraction and sampling of sediment cores, the development of the age model, the processing of pollen and charcoal samples, and the time-series analysis applied to the charcoal record (CharAnalysis) are described in chapter 2.

I identified palynomorphs based on reference samples stored in the laboratory of Quaternary Paleoecology of Universidad de Chile, along with published descriptions and keys (Heusser, 1971; Villagrán, 1980). The majority of palynomorphs were identified to family or genus level, but some palynomorphs were identified to the species level (*Podocarpus nubigena*, *Drimys winteri*, *Tepualia stipularis*, *Weinmannia trichosperma*, *Raukaua laetevirens*). The palynomorph *Nothofagus dombeyi* type includes the species *Nothofagus dombeyi*, *Nothofagus alessandri*, *Nothofagus leonii* and *Nothofagus nitida*, *Fitzroya/Pilgerodendron* includes the cupressaceaous conifers *Fitzroya cupressoides* and *Pilgerodendron uviferum*, and *Eucryphia/Caldcluvia* includes the species *Eucryphia cordifolia* and *Caldcluvia paniculata*.

3.4. Results

3.4.1. Stratigraphy and chronology

The sedimentary record from Lago Emerenciana combines cores from the series GC1705A (segment 1 to 5), GC1705B (segment 2B) and the water-sediment interface core GC1602SC (Figure 3.2). The sediment cores were correlated by overlapping different cores with the aid of LOI and the pollen record. I noted that the stratigraphy of the water-sediment interface core GC1602SC and the long core GC1705AT1 do not overlap, indicating a gap in the stratigraphy (Figure A1.1 in Appendix 1). Visual inspection of all cores, along with LOI analysis, the radiocarbon chronology and pollen stratigraphy (Figures 3.2, 3.3 and 3.4) suggest

continuous organic sedimentation in the Lago Emerenciana basin. Originally, the core GC1705AT1 was expected to overlap the water-sediment interface core at~60 cm. I conclude that this gap reflects incomplete sampling during the coring operation rather than a halt in the sedimentation process. Further field work is needed to resolve this stratigraphic issue. Assuming a stratigraphic gap of 30 cm, the Lago Emerenciana record has an estimated length of 951 cm (including gap) and consists of a basal unit of silt/clay between 951 and 579 cm, overlain by an organic silt unit with an increasing trend in the percentage of organic matter between 579 and 495 cm. This trend toward increasing organic matter continues with organic-rich lake mud between 495 and 0 cm, with fluctuations between 495 and 314 cm, a plateau between 314 and 64 cm and a modest rise between 64 and 0 cm. I detected a 4-cm thick clastic layer at 370-373 cm depth, and a <1-cm thick clastic layer at 309 cm depth that are likely to be tephra layers.

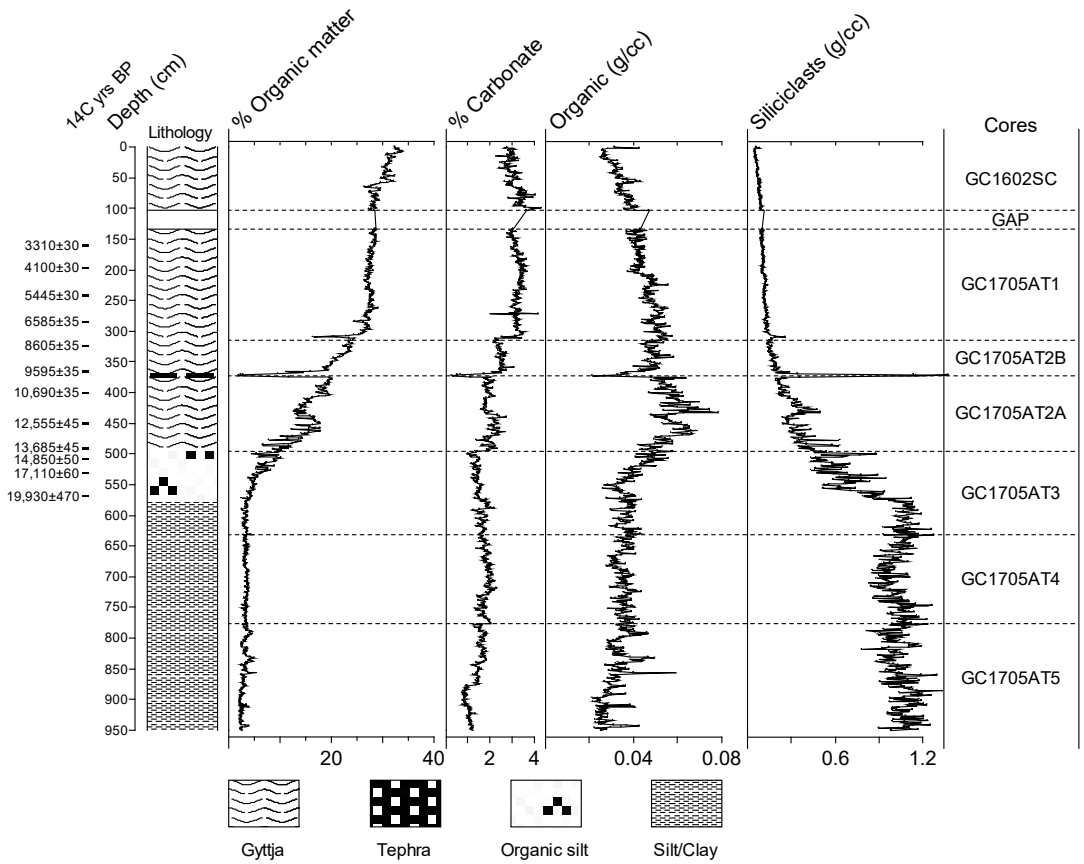

Figure 3.2. Radiocarbon dates, composite depth, stratigraphic column and loss-on-ignition parameters form the Lago Emerenciana record. The black rectangles on the left represent the stratigraphic position of radiocarbon-dated levels. The column on the right shows the identity and boundary (dashed horizontal lines) of each core segment. The white horizontal rectangle in the stratigraphic column indicates the position and estimated thickness of the stratigraphic gap.

The chronology of the Lago Emerenciana record is constrained by 12 AMS radiocarbon dates obtained from bulk organic lake sediment due to absence of suitable plant macrofossil material (Table 3.2, Figure 3.3). The lowermost radiocarbon date yielded an age of 19,930 ± 470 ^{14}C yr BP, followed by progressively younger ages toward the top of the record.

Table 3.2. Radiocarbon dates obtained from the Lago Emerenciana record. These dates were calibrated to calendar years before present using the southern hemisphere datasets (SHCal13) included in CALIB 7.0.1 (Reimer et al., 2013). All dates were obtained from bulk sediment samples.

Laboratory code	**Core code and length**	**Original depth (cm)**	**Tephra-free depth (cm)**	**^{14}C yr BP**	**± 1σ error**	**2σ age range cal yr BP**	**Median probability cal yr BP**
CAMS-182721	GC1705AT1_27	160	160	3310	30	3399-3575	3498
CAMS-182722	GC1705AT1_63	196	196	4100	30	4424-4799	4540
CAMS-182723	GC1705AT1_109	242	242	5445	30	6024-6292	6225
CAMS-182724	GC1705AT1_151	284	284	6585	35	7334-7563	7456
CAMS-182918	GC1705AT2B_19	324	324	8605	35	9477-9594	9533
CAMS-182746	GC1705AT2B_60	365	365	9595	35	10,716-11,089	10,926
CAMS-182747	GC1705AT2A_28	400	396	10,690	35	12,557-12,693	12,632
CAMS-182748	GC1705AT2A_83	450	446	12,555	45	14,359-15,085	14,772
CAMS-182749	GC1705CT2_102	490	486	13,685	45	16,231-16,675	16,441
CAMS-179791	GC1705AT3_16	507	503	14,850	50	17,838-18,197	18,010
CAMS-179792	GC1705AT3_40	531	527	17,110	60	20,372-20,804	20,586
CAMS-179793	GC1705AT3_78	569	565	19,930	470	22,838-25,172	23,941

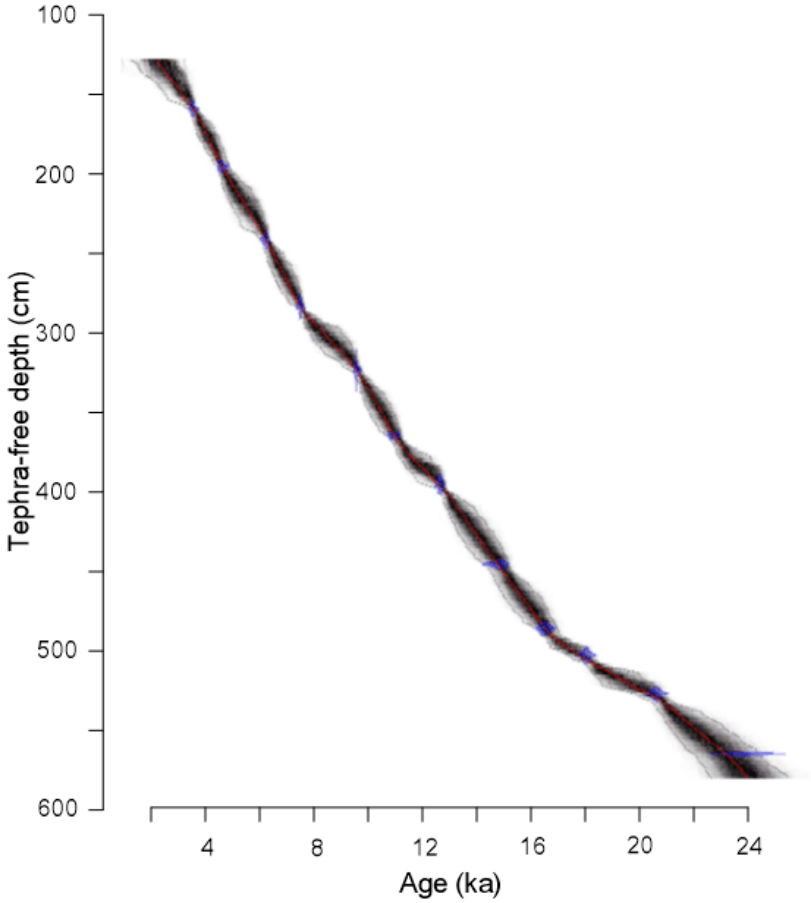

Figure 3.3. Bayesian age model from Lago Emerenciana. The blue zone represents the probability distribution of the calibrated ages, the grey zone shows the calculated confidence interval of the age model, and the red line represents the median probability age of the age model.

3.4.2. Pollen record

The pollen record from Lago Emerenciana comprises 300 samples that span the last ~24,000 years with a mean time resolution between pollen samples of ~330 years between ~24.0 and ~16.6 ka and ~80 years between ~16.6 and ~2.4 ka. I divided the record into 11 local pollen assemblage zones considering the major changes in the pollen stratigraphy with the aid of a stratigraphically constrained cluster analysis. In the following paragraphs I describe each zone, highlighting the three most abundant terrestrial taxa in decreasing order of abundance, indicating their tephra-free depths and age ranges and their mean and peak abundance in parenthesis whenever pertinent (Figures 3.4 and 3.5).

Zone EME-1 (575-530 cm, ~24.0-20.6 ka) is characterized by the dominance of *Nothofagus* (48%), Poaceae (32%), and Asteraceae Asteroideae (4%), accompanied by low abundance of

Myrtaceae (3%) and the herbs *Gunnera* (3%) and Apiaceae (3%), along with traces of *Misodendrum* (<1%), *Empetrum* (<1%), and Solanaceae (<1%). Poaceae exhibits a rapid increase at the beginning of this zone, reaching its peak abundance of the record (peak ~49%), followed by sustained decrease. Arboreal pollen (54%) shows relatively low values through this zone. The ferns *Blechnum* (7%) and Hymenophyllaceae (4%), as well as the aquatic *Isoetes* (8%) and Cyperaceae (2%) show low abundance during the first half of this zone, followed by prominent increases.

Zone EME-2 (530-494 cm, ~20.6-17.0 ka) features dominance of *Nothofagus* (33%), Apiaceae (19%), and Poaceae (17%). *Nothofagus* shows a declining trend, Poaceae continues the decline from the previous zone, Apiaceae (peak: ~31%) and *Drimys* (6%, peak: 13%) exhibit rapid increases and achieve their peak abundances at the end of this zone. Myrtaceae (3%) and total arboreal pollen (47%) show their lowest abundance, *Embothrium coccineum* (2%) appears in the record, while *Blechnum* (27%, peak: 30%), *Isoetes* (20%, peak: 26%) and Cyperaceae (11%, peak: 26%) reach their maximum abundances of the entire record.

Zone EME-3 (494-441 cm, ~17.0-14.6 ka) is dominated by the assemblage Myrtaceae (44%)-*Raukaua laetevirens* (12%)-*Fitzroya/Pilgerodendron* (9%), along with a prominent increase in Myrtaceae from 24% to 64% that culminates at the end of this zone, forcing a substantial rise in arboreal pollen from a mean of 60% to 98%. *Fitzroya/Pilgerodendron* increases at ~16.3 ka, attains its peak abundance at ~15.4 ka, and declines thereafter. *Nothofagus* (6%) and Poaceae (3%) continue their decreasing trends observed in the previous zone, achieving their lowest abundances of the record. Other herbs also exhibit persistent declines. *Drimys* (5%), Apiaceae (9%), *Blechnum* (14%) and *Isoetes* (8%) drop from their peak abundances, *Lomatia/Gevuina* (3%) appears in the record, Cyperaceae (2%) shows a steady decrease.

Zone EME-4 (441-394 cm, ~14.6-12.5 ka) is characterized by a Myrtaceae (35%)-*Raukaua* (11%)-*Podocarpus nubigena* (10%) assemblage, exhibiting a conspicuous drop in Myrtaceae from 58% to 22%, a rapid rise in *Podocarpus nubigena* which attains its maximum abundance (peak: 24%) at the end of this zone, and declining trends in *Raukaua* and arboreal pollen (85%). *Fitzroya/Pilgerodendron* (2%) *Drimys* (5%), *Nothofagus* (10%), *Misodendrum* (<1%) and *Tepualia stipularis* (2%) show modest increments, *Lomatia/Gevuina* (3%) features a slight decline, Poaceae (10%) exhibits an important increase from 2% to 17%, *Blechnum* (10%),

Isoetes (5%), Cyperaceae (2%) and *Pediastrum* (1.5%) show slight rises, while the rest of herbs and ferns remain in trace abundances.

Zone EME-5 (394-370 cm, ~12.5-11.1 ka) features dominance of Myrtaceae (39%), Poaceae (13%), and *Nothofagus* (10%), with a steady increase in Myrtaceae from 30% to 45%, a prominent decline in *Podocarpus nubigena* (8%) from its peak abundance (24%) to 3%, and modest declines in *Drimys* (2%), *Nothofagus* (10%), *Misodendrum* (<1%) and Poaceae (13%). *Tepualia stipularis* (9%) and *Hydrangea* (7%) feature prominent increases, along with a moderate rise in arboreal pollen, while *Raukaua* (5%), *Lomatia/Gevuina* (2%) and the fern *Blechnum* (7%) show little variation. The rest of ferns and aquatics remain in low abundance.

Zone EME-6 (370-320 cm, ~11.1-9.4 ka) is dominated by the assemblage Myrtaceae (47%)-*Hydrangea* (15%)-*Nothofagus* (10%). Myrtaceae remains relatively invariant in high plateau (~45%), *Hydrangea* rises abruptly, while *Fitzroya/Pilgerodendron*, *Podocarpus nubigena*, *Drimys* and *Misodendrum* decline to trace abundance (<1%). *Nothofagus* and Poaceae (8%) feature slight increments, *Lophosoria quadripinnata* (1.9%) shows a rapid increase, while *Blechnum* (5%) exhibits the opposite behaviour. *Tepualia stipularis* (8%) increases abruptly at the beginning of this zone, followed by modest decreases. *Raukaua* (5%), *Lomatia/Gevuina* (2%) and *Embothrium coccineum* (1%) show little change.

Zone EME-7 (320-286 cm, ~9.4-7.5 ka) features the pollen assemblage *Nothofagus* (29%)-Myrtaceae (27%)-Poaceae (11%), a prominent decline in Myrtaceae from 47% to 12%, a steady increase in *Nothofagus*, the appearance and rapid increase of *Weinmannia trichosperma* (6%), and traces in *Eucryphia/Caldcluvia* (<1%). *Tepualia stipularis* (9%) and Poaceae (11%) exhibit modest rising trends, while *Raukaua* (4%), *Hydrangea* (8%), *Lomatia/Gevuina* (1%) and arboreal pollen (88%) show slight declining trends throughout this zone. Ferns and aquatic taxa persist with little variation.

Zone EME-8 (286-244 cm, ~7.5-6.3 ka) is characterized by abundant *Nothofagus* (36%), *Eucryphia/Caldcluvia* (17%), and *Weinmannia trichosperma* (10%), along with a rapid and conspicuous increase in *Eucryphia/Caldcluvia* from 5% to 33% accompanied by declining trends in *Nothofagus*, *Weinmannia trichosperma*, *Tepualia stipularis* (7%), *Raukaua* (2%), *Hydrangea* (6%), and Poaceae (8%), and a modest rise in arboreal pollen (91%).

Zone EME-9 (244-196 cm, ~6.3-4.6 ka) features dominance of *Nothofagus* (29%), *Eucryphia/Caldcluvia* (27%), and *Weinmannia trichosperma* (12%). *Nothofagus*, *Eucryphia/Caldcluvia,* and Myrtaceae (6%) exhibit declining trends throughout this zone, while *Weinmannia trichosperma* shows a moderate increase. Other trees and vines persist with little variation. Poaceae levels remain stable while the rest of herbs and shrubs disappear.

Zone EME-10 (196-134 cm, ~4.6-2.4 ka) is dominated by the assemblage *Nothofagus* (28%)-*Eucryphia/Caldcluvia* (24%)-*Weinmannia trichosperma* (11%), all of which taxa exhibit declines with fluctuations throughout this zone. *Hydrangea* (6%) and *Misodendrum* (4%) increase slightly, while all other plants persist in low abundance.

Zone EME-11 (103-0 cm) is characterized by the pollen assemblage *Nothofagus* (38%)-Myrtaceae (13%)-*Tepualia stipularis* (9%). *Eucryphia/Caldcluvia* (4%) and *Weinmannia trichosperma* (4%) exhibit lower abundance, contemporaneous with higher abundance in *Drimys winteri* (3%) than the previous zone. The exotic herb *Rumex* (*Rumex acetosella*) appears in trace abundance (<0.3%). These substantial variations occurred across the stratigraphic gap between 134 and 103 cm.

3.4.3. Macroscopic charcoal

The macroscopic charcoal accumulation rate (CHAR) record from Lago Emerenciana shows relatively high values between ~17.0 and ~10.6 ka, ~8.0 and ~6.0 ka, ~5.0 and ~4.0 ka, and ~2.8 and ~2.4 ka (Figure 3.6). Time series analysis of the macroscopic charcoal data using CharAnalysis reveals 5 fire episodes (statistically significant peaks), interpreted as local fire events (Figure 3.6). I note clustering of events between ~13.7 and ~12.9 ka (three events), and isolated events at ~10.7 and ~7.3 ka. Fire frequency shows maximum values at ~13.2 ka, and minimum values at ~10.6 and ~7.3 ka. The largest-magnitude fires occurred at ~12.8, ~10.7, and ~7.3 ka (Figure 3.6).

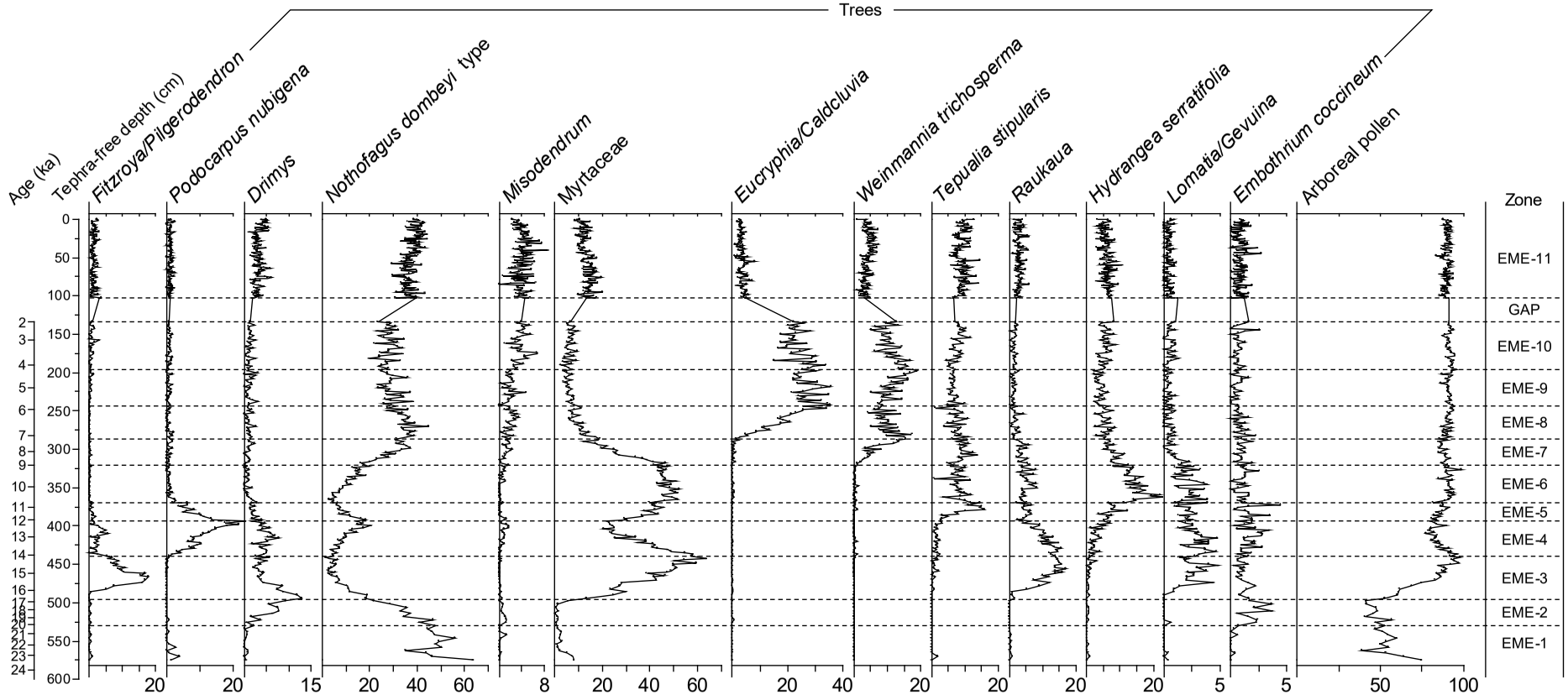

Figure 3.4. Pollen percentage record from Lago Emerenciana, showing rainforest tree taxa. The primary y axis shows the depth scale without tephra, the secondary y axis indicates the age scale. Note the difference in scale between taxa.

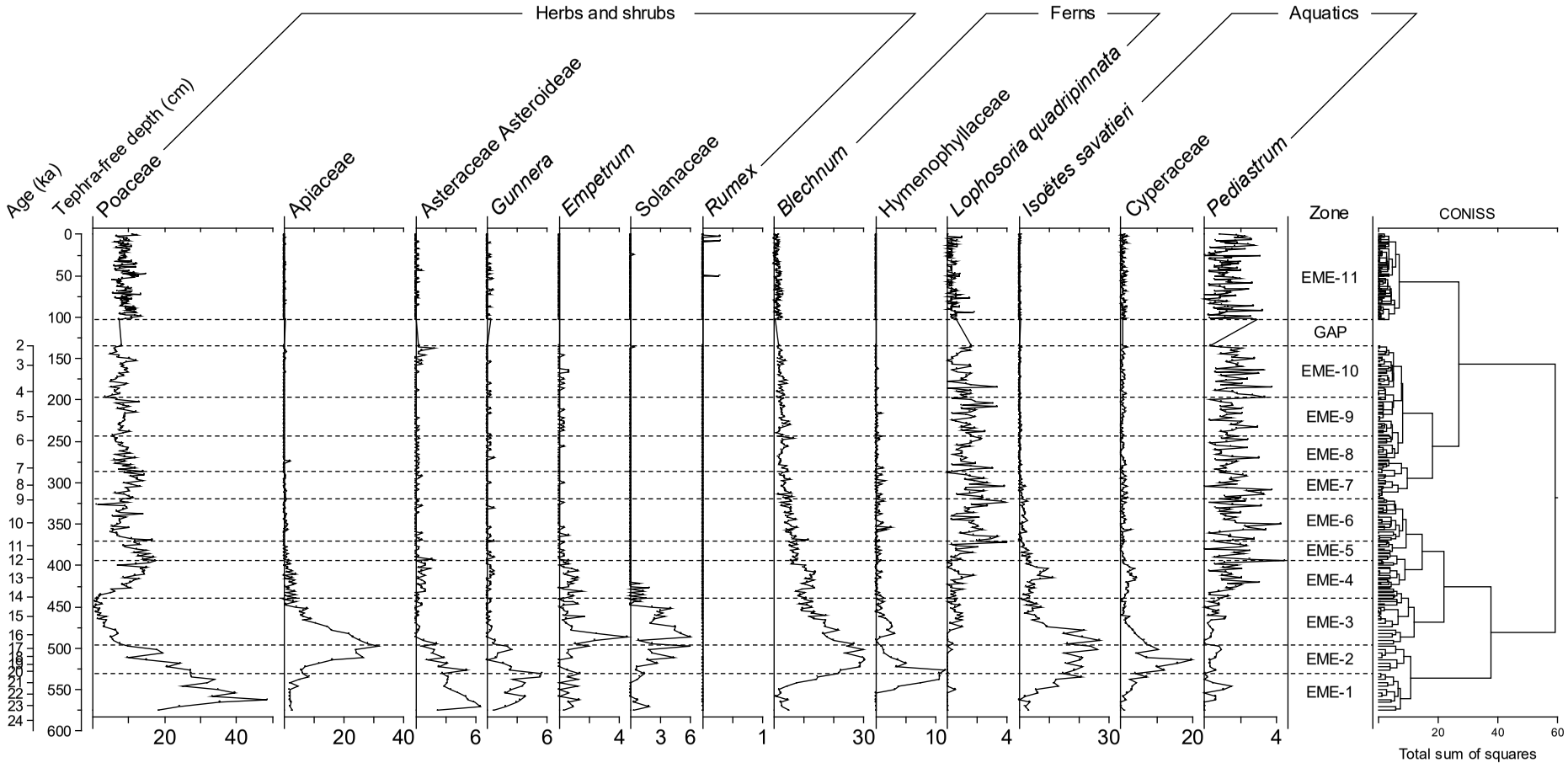

Figure 3.5. Pollen percentage record from Lago Emerenciana, showing herbs, shrubs, ferns and aquatic taxa. The primary y axis shows the depth scale without tephra, the secondary y axis indicates the age scale. Note the difference in scale between taxa.

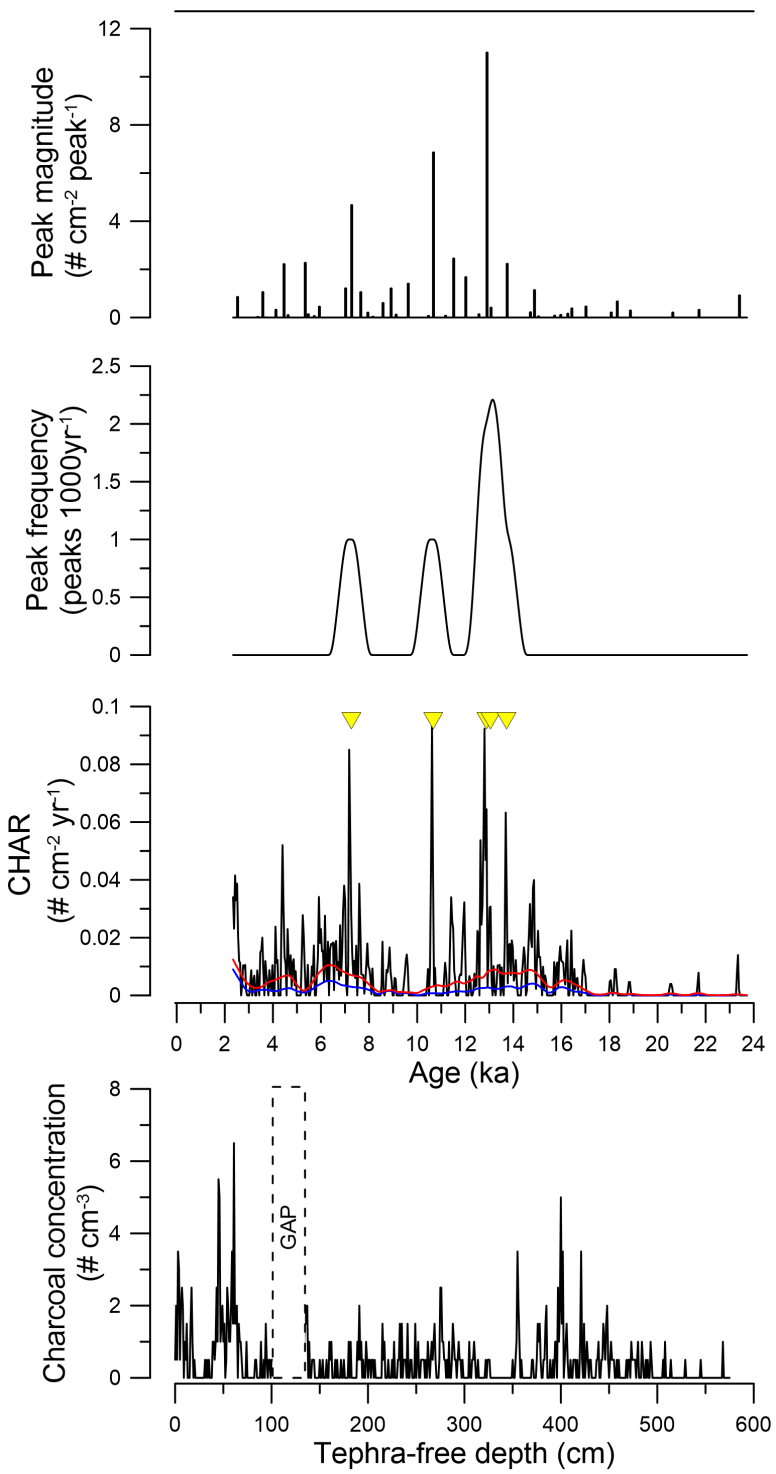

Figure 3.6. Macroscopic charcoal concentration and accumulation rate record from Lago Emerenciana and time series analysis using CharAnalysis, showing the calculated background (blue line) using a lowess robust to outliers, the local defined threshold (red line), and the statistically significant charcoal peaks (yellow triangles). Also shown are the fire frequency curve and the peak magnitude. The white vertical rectangle indicates the position of the stratigraphic gap.

3.5. Discussion

3.5.1. Vegetation and fire history

The palynological record reveals the continuous presence of plant communities with changes in their structure and composition in the vicinity of Lago Emerenciana over the last ~24,000 years. Arboreal vegetation is a notable feature of the earliest parts of the record. *Nothofagus* dominates between ~24.0 and ~20.0 ka, accompanied by traces of its hemiparasite *Misodendrum*, low percentages of the conifer *Podocarpus nubigena,* along with abundant herbs (Poaceae, Apiaceae) and shrubs (*Empetrum*) commonly found in open landscapes from near sea levels to above the modern Andean treeline and the Patagonian steppe (Figure 3.7). I also note low percentages of the shade-tolerant thermophilous Myrtaceae taxa characteristic of modern mid-elevation North Patagonian rainforests (Heusser, 1990b; Villagrán, 1985). This was contemporaneous with low abundance of the understory and water-demanding fern *Blechnum*, possibly *Blechnum penna-marina*, and high abundance of the hygrophilous herb *Gunnera,* both species currently absent from the Patagonian Steppe but present in wet sectors of the western Andes. Considering that species of the genus *Nothofagus* produce large quantities of pollen grains susceptible to long-distance transport, I interpret this early assemblage as an open landscape consisting of cold-tolerant and hygrophilous herbs and shrubs with scattered tree populations. The co-occurrence of key diagnostic taxa during this early interval (e.g. *Podocarpus nubigena*, *Blechnum*, *Gunnera*) suggests an initial stage with scattered, species-poor *Nothofagus*-dominated woodlands and probably High-Andean vegetation.

Within this interval, the Lago Emerenciana record shows a persistent decline in Poaceae, contemporaneous with a slight decline in *Nothofagus* between ~22.8 and ~19.7 ka, along with a rapid increase in the shade-intolerant cold-resistant shrub/tree *Embothrium coccineum*, a modest rise in the cold-resistant herbs of the Apiaceae family, maximum values in the hygrophilous herb *Gunnera,* prominent increases in the epiphytic fern Hymenophyllaceae and the understory fern *Blechnum*. These changes were followed by a prominent increase in Apiaceae between ~19.7 and ~17.5 ka, maximum values in *Embothrium coccineum* and the fern *Blechnum*, a major decline in *Nothofagus*, the virtual disappearance of the thermophilous Myrtaceae and the lowest abundance of arboreal pollen in the entire record (47%) (Figure 3.7). These data suggest a shift toward major openness of the landscape which led to the

spread of shade-intolerant shrubs/trees and understory herbs and ferns near Lago Emerenciana. Because this pollen assemblage shows a large increase in herbs commonly found in High Andean sectors (Apiaceae), I interpret these changes as a treeline lowering between ~19.7 and ~17.5 ka.

Myrtaceae starts rising at ~17.5 ka, coincident with declines in the shade-intolerant tree *Embothrium coccineum*, the understory fern *Blechnum* and herbs associated with high Andean environments such as Apiaceae and Poaceae, and the practical disappearance of the hygrophilous herb *Gunnera*. The fact that arboreal pollen increased, and opportunistic cold-resistant trees, herbs and ferns declined, suggests a rise in the treeline in the vicinity of Lago Emerenciana at the commencement of T1. The increase of Myrtaceae at ~17.5 ka marks the transition from an open landscape co-dominated by cold-resistant and hygrophilous taxa commonly found in Subantarctic forests and alpine environments toward a closed-forest landscape dominated by thermophilous trees characteristic of North Patagonian rainforests (Figure 3.7). This vegetation turnover was preceded by an increase in the tree *Drimys* between ~19.7 and ~16.3 ka, shade-intolerant and moisture-demanding tree species that commonly grow in large forest gaps following disturbances (Figueroa and Lusk, 2001), indicative of a transitional phase that preceded the establishment of forested conditions. This was followed by the culmination of the rising trend in Myrtaceae between ~16.3 and ~14.6 ka, contemporaneous with rapid increases in the cold-resistant hygrophilous conifers *Fitzroya/Pilgerodendron* and the tree *Lomatia/Gevuina*, a gradual rise in the vine *Hydrangea*, a rapid decline in the shade-intolerant tree *Drimys*, and a major drop in herbs (Apiaceae, Poaceae, Asteraceae Asteroideae) (Figure 3.7). These findings suggest the expansion and establishment of closed-canopy forests dominated by tree taxa (Myrtaceae and *Fitzroya/Pilgerodendron*) commonly found in waterlogged and upland environments characteristic of North Patagonian rainforests.

I note a macroscopic charcoal rise at ~17.0 ka, preceded by virtual absence between ~24.0 and ~17.0 ka (Figure 3.6). This increase in macroscopic charcoal coincided with a floristic turnover from an open landscape dominated by herbs, shrubs and scattered trees toward a Myrtaceae forest after ~17.5 ka. Because wildfires in these rainforest communities are limited by ignition sources and fuel desiccation (Holz and Veblen, 2012), I suggest that climate conditions and scarce biomass were limiting factors for the occurrence of fires between ~24.0

and ~17.0 ka. Higher spatial continuity of coarse fuels and climate conditions conducive to desiccation of fuels after ~17.5 ka might have triggered the generation of wildfires in the vicinity of Lago Emerenciana.

The cold-tolerant hygrophilous conifer *Podocarpus nubigena* increased between ~14.5 and ~12.5 ka at the expense of the thermophilous Myrtaceae, coeval with rises in the trees *Drimys* and *Embothrium*, herbs and ferns (Poaceae, Asteraceae Asteroideae, *Blechnum*), along with a decline in arboreal pollen (Figure 3.7). *Podocarpus nubigena* is abundant in the modern cold tolerant Subantarctic forests above ~450 m.a.s.l. in the Coastal Range of IGC and above the North Patagonian rainforest communities. Hence, I interpret these data as the spread of cold-tolerant and opportunistic taxa in a relatively open-canopy Subantarctic Patagonian rainforest in response to deteriorating climate conditions. This interval also features peak fire activity between ~13.7 and ~12.9 ka (three statistically significant events) (Figure 3.6). Ignition sources in these broad-leaved evergreen temperate rainforest ecosystems may also involve the effect of volcanic ash deposition, lightning strikes and/or human activity. I will discuss these changes in the subsection 3.6.3. Paleoclimate inferences.

The cold-tolerant hygrophilous trees *Podocarpus nubigena* and *Drimys* declined after ~12.5 ka, both showing a pronounced drop at ~11.1 ka. These changes were contemporaneous with increasing trends in the thermophilous trees Myrtaceae and the vine *Hydrangea*, along with arboreal pollen, exhibiting major rises between ~11.1 and ~9.2 ka (Figure 3.7), followed by their persistent decline. I note that *Nothofagus* shows a steady increase that started at ~11.1 ka and reached its maximum at ~7.6 ka, concomitant with two isolated fire events at ~10.7 and ~7.3 ka. This increase in *Nothofagus* was coeval with the appearance of intermittent low values of the opportunistic shade-intolerant tree *Weinmannia trichosperma* and the thermophilous summer-drought resistant trees characteristic of Valdivian rainforests *Eucryphia/Caldcluvia*, leading to their rapid increases at ~9.2 and ~7.6 ka, respectively (Figures 3.4 and 3.5). Altogether, I interpret these results as the reestablishment of closed-canopy Myrtaceae-dominated North Patagonian rainforests near Lago Emerenciana between ~12.5 and ~11.1 ka, followed by a transitional interval toward a mixed forest dominated by *Nothofagus* with trees diagnostic of Valdivian rainforests between ~11.1 and ~7.6 ka. Fire activity and relatively major openness of the landscape drove an increase in plants favoured by disturbance (*Weinmannia trichosperma*) between ~9.2 and ~7.6 ka.

A prominent increase in *Eucryphia/Caldcluvia* at ~7.6 ka led to its highest abundance between ~6.2 and ~4.4 ka with centennial-scale variations, followed by a decline. These shifts were contemporaneous with declines in *Weinmannia trichosperma* between ~7.6 and ~6.2 ka and ~4.6 and ~2.4 ka, and a marked increase between ~6.2 and ~4.6 ka (Figure 3.7). I also note sustained declines in the trees *Nothofagus*, Myrtaceae and the vine *Hydrangea*, followed by slight increases between ~4.2 and ~2.4 ka. These vegetation changes indicate high variability in the structure and composition of the vegetation that featured elements characteristic of Valdivian and North Patagonian rainforests between ~7.6 and ~2.4 ka. This point marks the beginning of the estimated ~30-cm gap in the stratigraphy (section 3.5.1. Stratigraphy and chronology) (Figure 3.2).

The most recent ~2400 years of the pollen record shows *Nothofagus*-dominated North Patagonian rainforests, with low abundance in *Eucryphia/Caldcluvia* and *Weinmannia trichosperma*, and the appearance of the non-native *Rumex* (probably *Rumex acetosella*) in trace abundance, in a context of dense temperate North Patagonian rainforest and increased charcoal concentration (Figures 3.4 and 3.5).

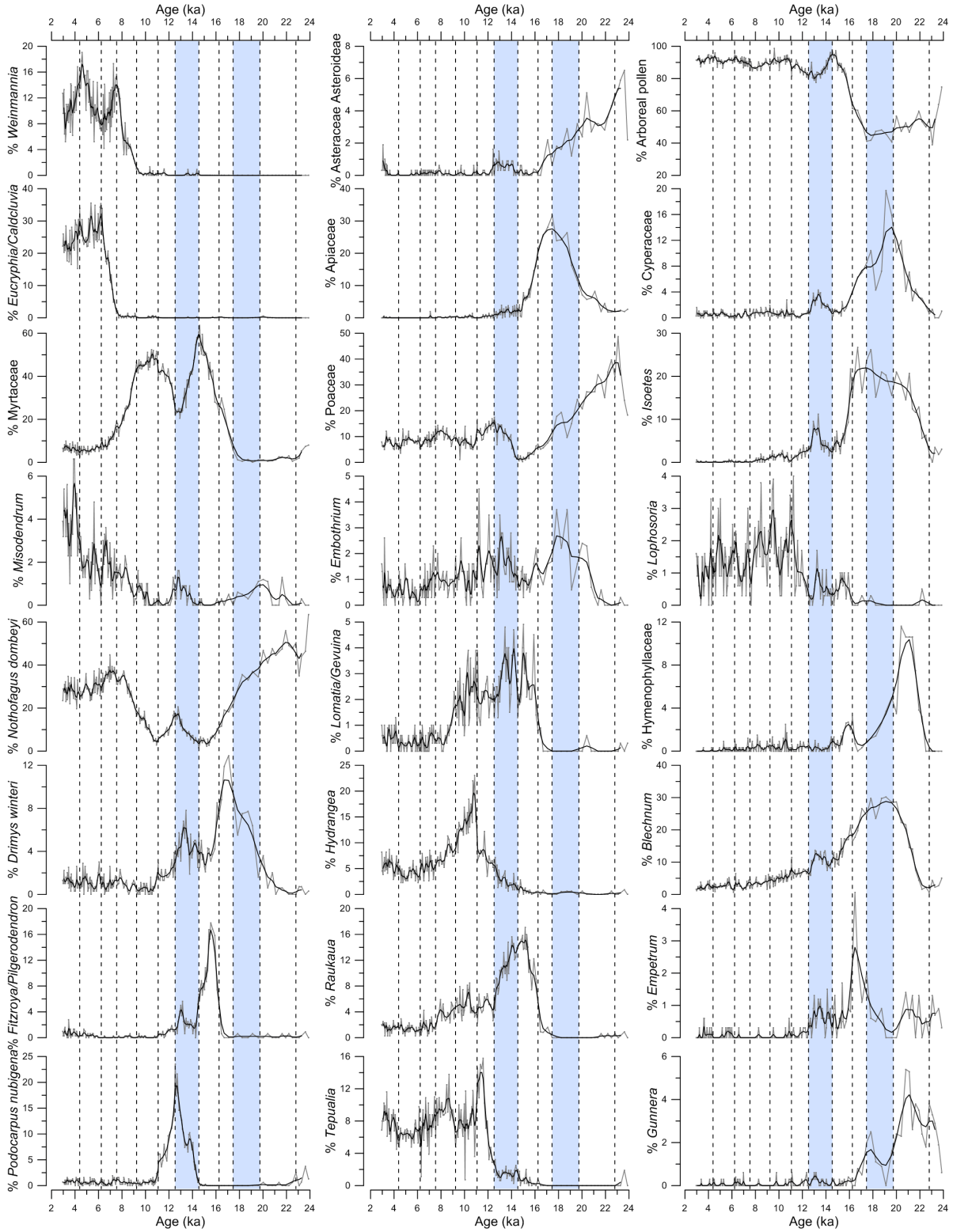

Figure 3.7. Selected pollen taxa from the Lago Emerenciana record. The dashed vertical lines indicate major transitions in the pollen stratigraphy described and discussed through the text. The blue vertical rectangles highlight conspicuous cold/wet intervals.

3.5.2. Inferences on past changes in hydrologic balance

The palynology of Lago Emerenciana records important changes in the paludal/aquatic taxa Cyperaceae and *Isoetes*. These taxa commonly inhabit shallow environments, normally growing in the periphery of northwestern Patagonian lakes. Thus, variations in Cyperaceae and *Isoetes* in the pollen record from sediment cores collected from the deep portions of closed-basin lakes can be indicative of changes in the extent and/or proximity of shallow littoral environments to the coring site through time. The Lago Emerenciana pollen record shows low abundance of Cyperaceae and *Isoetes* between ~24.0 and ~22.8 ka, followed by steady increases toward maximum abundance between ~22.8 and ~19.7 ka and ~22.8 and ~16.3 ka, respectively (Figures 3.7 and 3.8). Possible explanations for the rise of these taxa include a) the inundation of extensive flatlands in the periphery of Lago Emerenciana driven by a lake level rise or b) the littoral habitat shifted centripetally to the core site in response to lake level lowering. I note that low values in Cyperaceae and *Isoetes* between ~24.0 and ~22.8 ka were contemporaneous with relatively low abundance in hygrophilous cold-tolerant herbs and ferns. I observe covariation with *Blechnum* and Apiaceae between ~22.8 and ~16.3 ka (Figure 3.8), which I interpret as a transgressive lake-level phase that inundated the extensive flatlands in the periphery of Lago Emerenciana, increasing the area suitable for the establishment of the macrophytes under analysis. From this discussion I interpret positive hydrologic balance between ~22.8 and ~16.3 ka.

An apparent divergence in hydroclimate signals emerges when comparing the increased abundance of macrophytes between ~17.5 and ~16.3 ka and the LGM to T1 dryland vegetation transition discussed in the previous subsection which suggests a shift from hyperhumid to humid conditions at ~17.5 ka (Figure 3.8). One explanation for this apparent incongruence is the occurrence of a low-magnitude moisture decline between ~17.5 and ~16.3 ka, triggering irreversible declines in hygrophilous cold-tolerant herbs and ferns, and allowing the maintenance of extensive low-lying marginal areas formerly inundated above a critical threshold for the growth of Cyperaceae and *Isoetes*. Thus, these data suggest a negative hydrologic balance between ~17.5 and ~16.3 ka.

Then, Cyperaceae and *Isoetes* declined rapidly between ~16.3 and ~14.5 ka, contemporaneous with an increase in the cold-tolerant and hygrophilous conifers *Fitzroya/Pilgerodendron* indicative of a moisture rising. This was synchronous with

conspicuous increases in the trees *Raukaua* and *Tepualia stipularis* (Figure 3.8). These trees commonly inhabit environments with poor drainage and grow partially submerged along the periphery of northwestern Patagonian lakes, including Lago Emerenciana today. In view of these considerations, I combined their abundance for inferring past shifts of littoral environments relative to the coring location. Hence, I interpret increases in the *Tepualia*+*Raukaua* parameter as a centripetal shift of the littoral zone that enabled the habitat of these plants to develop closer to the core site during the post ~16.3 ka forested phase in the Lago Emerenciana record (Figure 3.8). The fact that pollen percentage of macrophytes decreased and *Tepualia*+*Raukaua* parameter increased in a context of more annual moisture, suggests lower lake levels and probably terrestrelization of flatlands in the periphery of Lago Emerenciana as a result of strong desiccating winds during summer, with wetter winters and higher hydrologic balance.

These changes were followed by a slight increase in Cyperaceae and *Isoetes* between ~14.5 and ~12.4 ka, coeval with a decline in *Tepualia*+*Raukaua*, suggesting a lake-level rise and an increase in hydrologic balance. The parameter *Tepualia*+*Raukaua* rose rapidly at ~12.4 ka exhibiting high abundance until ~7.8 ka, while the paludal/aquatic Cyperacea and *Isoetes* show very low values. This period was followed by a declining trend in *Tepualia*+*Raukaua* between ~7.8 and ~4.8 ka, and a persistent increase between ~4.8 and ~2.4 ka (Figure 3.8). I interpret these changes as low lake levels and decreased hydrologic balance between ~12.4 and ~7.8 ka and ~4.8 and ~2.4 ka, along with higher lake level and hydrologic balance between ~7.8 and ~4.8 ka. Therefore, coherent changes between the abundance of the macrophytes Cyperaceae and *Isoetes* and variations in dryland vegetation in the Lago Emerenciana record suggest that changes in terrestrial and aquatic ecosystems were trigger by a common driver, i.e. changes in precipitation.

3.5.3. Paleoclimate inferences

Past changes in the structure and composition in terrestrial and aquatic vegetation revealed by the Lago Emerenciana record allow assessment of paleoclimate changes in southwestern IGC during the last ~24,000 years. The pollen record shows scattered woodlands featuring high-elevation species-poor *Nothofagus*-dominated Subantarctic and High-Andean

vegetation between ~24.0 and ~17.5 ka, and absence of fires. Within this interval I observe a sustained increase in cold-resistant herbs of the Apiaceae family and the water-demanding fern *Blechnum* that started at ~22.8 ka, showing peak abundance between ~19.7 and ~17.5 ka. These results suggest an initial phase with relatively cold conditions and persistent precipitation between ~24.0 and ~22.8 ka, followed by a decline in temperature and a marked increase in precipitation between ~19.7 and ~17.5 ka.

Myrtaceae rose at ~17.5 ka, at the expense of vegetation indicative of Subantarctic forests and High-Andean environments (*Nothofagus*, Apiaceae, *Gunnera*, Poaceae, Asteraceae Asteroideae, *Empetrum*), and accompanied by an increase in CHAR. Because the present-day transition between these vegetation communities reflects responses to shifts in temperature and moisture (Heusser, 2003; Villagrán, 1980) and wildfires in these rainforest communities are limited by ignition sources and fuel desiccation (Holz and Veblen, 2012), I interpret these changes as a floristic turnover with a transition from glacial cold conditions and high precipitation toward temperate conditions and less precipitation at the onset of T1. Cold-temperate conditions along with strong desiccation winds during summer with increased annual precipitation and seasonality ensued between ~16.3 and ~14.5 ka, mirrored by increases in the cold-resistant hygrophilous conifers *Fitzroya/Pilgerodendron* and the *Tepualia*+*Raukaua* parameter and a decline in macrophytes (Cyperaceae and *Isoetes*).

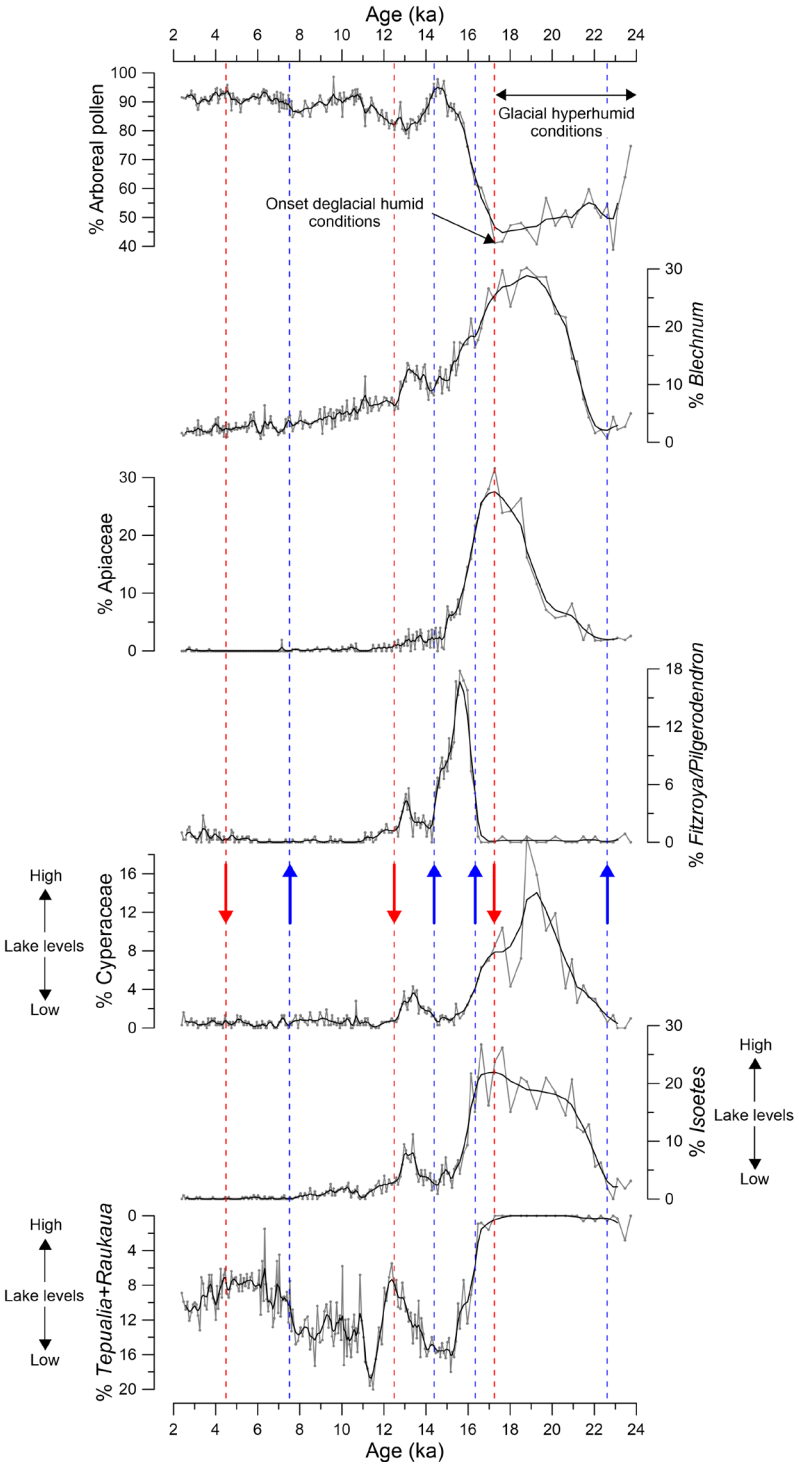

Figure 3.8 Comparison of selected pollen taxa from Lago Emerenciana. From bottom to top, are shown the percent abundance of *Tepualia+Raukaua,* indicative of low lake level following the onset of T1; *Isoetes* and Cyperaceae, indicative of high lake level during LGM and early T1; percent abundance of *Fitzroya*/*Pilgerodendron,* indicative of high moisture; Apiaceae, indicative of Andean environment probably under cold and wet conditions; the water demanding fern *Blechum* and the percent abundance of arboreal pollen. The vertical red and blue dashed lines/arrows constrain the timing of the main climate transitions toward dry and wet conditions, respectively.

The increase and persistence of the cold-tolerant hygrophilous conifer *Podocarpus nubigena* between ~14.5 and ~11.1 ka suggests a decline in temperature. Within this interval I identify an initial cold phase between ~14.5 and ~12.4 ka with higher hydrologic balance suggesting enhanced precipitation. This was followed by a relatively cold phase with lower hydrologic balance between ~12.5 and ~11.1 ka, suggesting a decline in precipitation. The virtual disappearance of *Podocarpus nubigena* at ~11.1 ka was coeval with a major increase in Myrtaceae, and contemporaneous with a rising trend in *Nothofagus*, the appearance of the thermophilous, summer-drought resistant trees *Eucryphia*/*Caldcluvia*, major openness of the landscape revealed by a rise in *Weinmannia trichosperma* and persistence of low hydrologic balance between ~11.1 and ~7.6 ka, all of which suggest warm conditions and persistent low precipitation at the beginning of the Holocene.

Within this multi-millennial interval, I observe peak fire activity between ~13.7 and ~12.9 ka (three statistically significant events) (Figure 3.6). As stated in previously (subsection 3.6.1. Vegetation and fire history), possible explanations for the generation of paleofires in these broad-leaved evergreen temperate rainforest ecosystems may involve the effect of volcanic ash deposition, lightning strikes and/or human activity. I rule out volcanic disturbance as a trigger of paleofires in this sector of IGC, because there is no stratigraphic correspondence between volcanic deposits (1 tephra) in Lago Emerenciana at ~11.4 ka and local fire events, as well as the fact that Lago Emerenciana is located ~150 km west and upwind from the nearest eruptive center in the Andes. Attribution of fire events to human activity during T1 is uncertain, considering that the only archaeological site in the entire region attesting for human occupation during the Pleistocene is located ~200 km northeast of Lago Emerenciana (Dillehay et al., 2015). The more likely explanation for the generation of wildfires is lightning associated with synoptic weather systems linked to climate variability such as the SAM, even under the cool-temperate and wet conditions of IGC (Holz and Veblen, 2012).

Eucryphia/*Caldcluvia* increased rapidly at ~7.6 ka and achieved a plateau with centennial-scale variations between ~6.2 and ~4.6 ka, followed by marked decline between ~4.6 and ~2.4 ka. This interval also shows the lack of local fire events between ~7.6 and ~2.4 ka. I note that high abundance of the thermophilous summer drought-resistant trees *Eucryphia*/*Caldcluvia* occurred in a context of high hydrologic balance suggesting increased precipitation regime, while the decline in *Eucryphia*/*Caldcluvia* was contemporaneous with lower hydrologic

balance suggesting reduced precipitation. I interpret these data as indicating major climatic variability and likely an increase in seasonality between ~7.6 and ~2.4 ka.

3.5.4. Regional and hemispheric implications

3.5.4.1. Paleoclimate changes

The palynological record from Lago Emerenciana suggests glacial cold conditions and abundant precipitation between ~24.0 and ~17.5 ka. Within this LGM interval I identify a rise in cold-tolerant hygrophilous trees, herbs and ferns that started at ~22.8 ka, achieving maximum abundance between ~19.7 and ~17.5 ka. Because local precipitation exhibits a strong positive correlation with zonal SWW speeds in this part of western Patagonia (Garreaud, 2007), these results suggest persistent SWW influence during the LGM, with maximum SWW influence between ~19.7 and ~17.5 ka. These findings replicate pollen-inferred glacial conditions reported from sites located in the mainland of northwestern Patagonia, indicating cooler conditions and an increased precipitation regime during the final portion of the LGM (Heusser et al., 1995; Heusser et al., 1999; Moreno et al., 2015; Moreno et al., 1999; Moreno et al., 2018a), and contemporaneous with the youngest advance of Andean ice lobes in the same region (Denton et al., 1999).

Lago Emerenciana record indicates a deglacial warming and transition from hyperhumid to humid conditions at the beginning of T1. This climate transition is also detected in palynological studies from northwestern Patagonia (Moreno et al., 2015; Moreno et al., 2018a; Pesce and Moreno, 2014) interpreted as a reduction in SWW influence brought about by a southward shift of the SWW at the onset of T1. This shift is coeval with glacier recession in the southern Alps of New Zealand (Putnam et al., 2013), and a sustained rise in temperature and atmospheric CO_2 concentration revealed by Antarctic ice cores (Monnin et al., 2001) (Figure 3.9). A poleward shift of the SWW may have enhanced the ventilation of CO_2-enriched deep waters to the atmosphere via upwelling, establishing a positive feedback on deglacial warming (Anderson et al., 2009).

Following this initial T1 phase, strong winds during summer time and, thus, increased precipitation seasonality occurred between ~16.3 and ~14.5 ka at Lago Emerenciana,

suggesting an increased influence of the SWW at this latitude (~43°S). These results are in agreement with paleoclimate inferences from records from northwestern (41°-43°S) (Moreno, 2020; Moreno et al., 2015; Moreno et al., 2018a; Pesce and Moreno, 2014) and central-west Patagonia (Henríquez et al., 2017; Vilanova et al., 2019) reflecting a northward shift or strengthening of the SWW following the onset of T1.

I identify a reversal in warming that featured enhanced precipitation, given by the rise in the cold-tolerant hygrophilous *Podocarpus nubigena* at the expense of thermophilous trees between ~14.5 and ~12.5 ka, conditions I interpret as enhanced SWW influence and contemporaneous with the Antarctic Cold Reversal (ACR), a halt in the deglacial CO_2 rise, and a southern mid-latitude trans-Pacific glacier readvance (Sagredo et al., 2018). Similar climate conditions have been reported from records from central-eastern IGC and the Longitudinal Valley in northwestern Patagonia (Moreno, 2020; Moreno et al., 2015; Moreno et al., 2018a; Pesce and Moreno, 2014). Persistent SWW influence is also reported from central (Vilanova et al., 2019) and southwestern Patagonia (Moreno et al., 2018b; Moreno et al., 2012) during the ACR, consistent with enhanced SWW influence. Recently, Moreno (2020) discussed similarities in timing of this ACR vegetation signal in northwestern Patagonia, including sites located in the Longitudinal Valley (Lago Proschle, Huelmo bog; Lago Pichilaguna) and IGC (Lago Lepué). Moreno detected equivalent ages for the beginning of the ACR signal in sites located in the Longitudinal Valley and significant differences with the Chilotan site. He postulated that residual Andean ice masses during this interval may have imposed a cooling signal in the down valley sectors of the northwestern Patagonian Andes, with a westward fading of this influence. My results from Lago Emerenciana record replicate the ACR signal recorded in the Lago Lepué pollen record, also located in IGC (Figure 3.1) and ~57 km northeast from Lago Emerenciana, which shows an increase in *Podocarpus nubigena* at ~14.5 ka, achieving its maximum at ~12.5 ka (Pesce and Moreno, 2014). The Lago Emerenciana record therefore lends support to Moreno's (2020) interpretation, establishing the southern- and westernmost recorded ACR signal in northwestern Patagonia (40°-43°S).

The Lago Emerenciana record indicates relatively cold conditions and decline in precipitation between ~12.5 and ~11.1 ka, suggesting less SWW influence. This signal was coeval with the Younger Dryas chron (YD) chron of the Northern Hemisphere, renewed warming and CO_2 rise in Antarctic ice cores (Monnin et al., 2001), glacial recession in southwestern Patagonia

(García et al., 2018a; Mendelova et al., 2017; Moreno et al., 2009b; Sagredo et al., 2011) and in the Southern Alps of New Zealand (Kaplan et al., 2010; Strelin et al., 2011), and increased precipitation in central (Vilanova et al., 2019) and southwestern Patagonia (Moreno et al., 2010; Moreno et al., 2012), suggesting a poleward shift of the SWW. An early Holocene warming pulse and persistence of low precipitation between~11.1 and ~7.6 ka revealed by the decline in *Podocarpus nubigena*, major increase in Myrtaceae, rising *Nothofagus*, and the appearance in trace abundance of the summer-drought tolerant trees *Eucryphia*/*Caldcluvia*. These developments signal a decline in the SWW influence, coherent with previous studies from northwestern Patagonia (Abarzúa et al., 2004; Moreno, 2004, 2020; Moreno et al., 2015; Moreno and Videla, 2016; Moreno et al., 2018a; Pesce and Moreno, 2014). Warm and low precipitation in Lago Emerenciana record between ~11.1 and ~7.6 ka have also been reported from central-west (Vilanova et al., 2019; Villa-Martínez et al., 2012) and southwestern Patagonia (Moreno et al., 2010; Moreno et al., 2018b; Moreno et al., 2012), concurrent with peak fire activity in South America south of 30°S (Power et al., 2008; Whitlock et al., 2007) and diminished SWW influence throughout Southern Hemisphere landmasses, suggesting a zonally symmetric decline in the SWW strength during the early Holocene (Fletcher and Moreno, 2012).

The Lago Emerenciana record then shows an increase in precipitation between ~7.6 and ~4.6 ka suggesting major SWW influence, following by a decline in precipitation between ~4.6 and ~2.4 ka in response to minor SWW influence. Major increase and low-magnitude variability of species characteristic of modern Valdivian evergreen rainforest communities (*Eucryphia/Caldcluvia*) started at ~7.6 ka, contemporaneous with centennial-scale alternation between warm/dry and cold/wet states reported from sites located in the mainland of northwestern Patagonia (Moreno, 2020; Moreno and Videla, 2016). I propose that high climate variability with major seasonality in precipitation at 43°S (wetter winters, drier summers) were ideal conditions for the expansion of *Eucryphia/Caldcluvia* in this sector of IGC between ~7.6 and ~2.6 ka, considering that these trees are highly resistant to summer-drought.

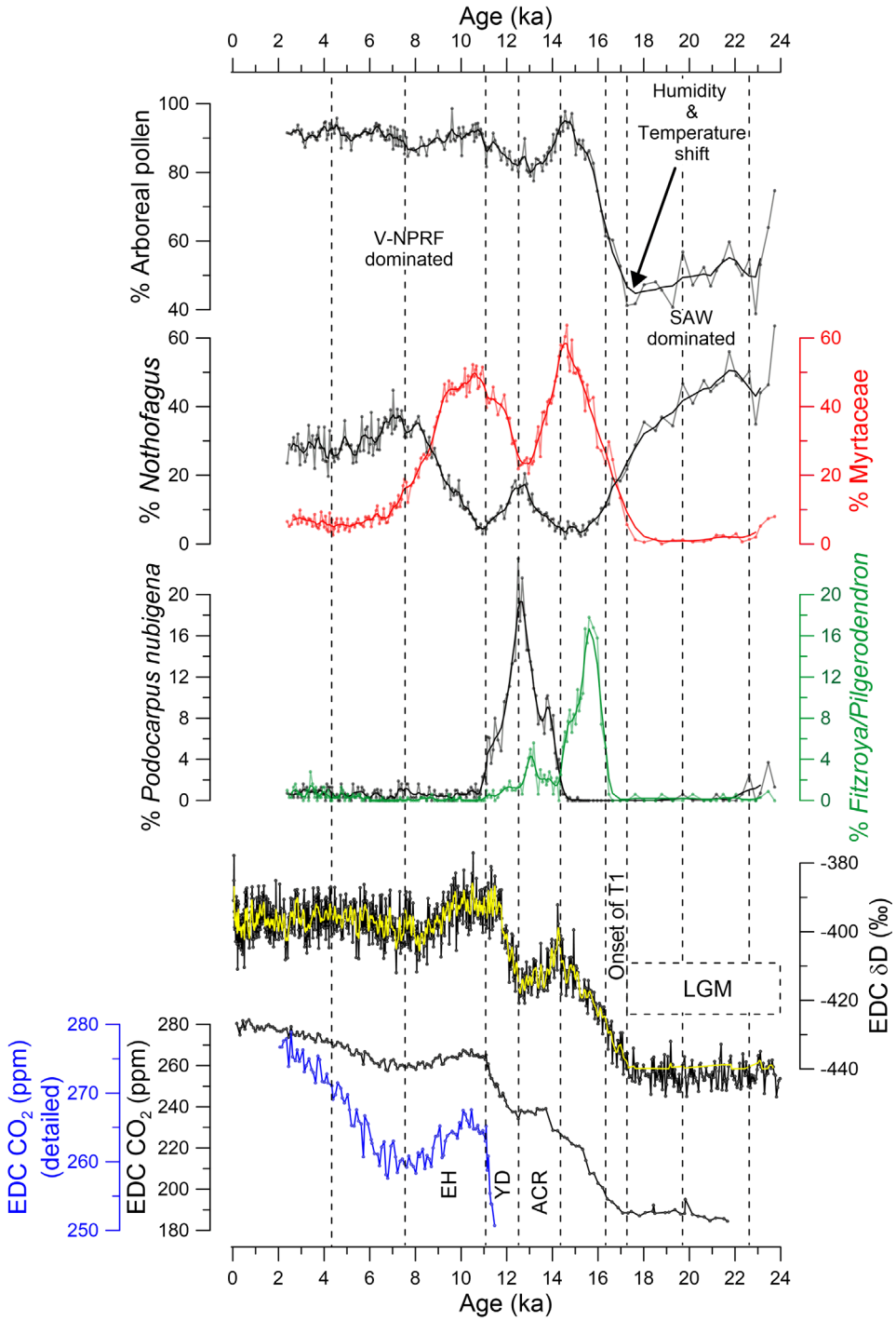

Figure 3.9. Comparison of selected taxa from Lago Emerenciana record with ice data from Antarctica over the last ~24,000 years. The dashed vertical lines constrain the timing of the main pollen-inferred climate changes from the Lago Emerenciana record, indicating the Last Glacial Maximum (LGM), onset of the T1, Antarctic Cold Reversal (ACR), Younger Dryas chron (YD) and the early Holocene (EH). The uppermost curve represents the arboreal pollen from Lago Emerenciana, pointing with an arrow the begining of the transition from glacial cool/hyperhumid to deglacial temperate/humid conditions, and indicating the period of dominance of species-poor Subantarctic-dominated woodland (SAW) and dominance of species characteristic of Valdivian and North Patagonian rainforests (V-NPRF).

3.5.4.2. Deglaciation and biogeography

Stratigraphic, chronologic, and palynologic data from Lago Emerenciana are key for deciphering and constraining vegetation evolution in the western- and southernmost sector of northwestern Patagonia during and following the LGM. The basal portion of Lago Emerenciana cores shows a ~370 cm thick unit (between 951 and 579 cm) of inorganic glacial silts and clays (Figure 3.2), followed by organic-rich lacustrine sediment starting at ~24.0 ka at least since then. Although no detailed local studies have been carried out in the west-central and southern sectors of IGC, some researchers have proposed that glacial margins overrode the coastal Range during the LGM, reaching the west Pacific coast south of 42°40'S (Davies et al., 2020; Hollin and Schilling, 1981; Mercer, 1965). The results from Lago Emerenciana constitute the first report from this largely unstudied sector, and demonstrate that the southwestern sector of IGC was ice-free during the final portion of LGM, implying that the glacier margin of the Golfo Corcovado lobe must have been east of Lago Emerenciana during the earliest advances of the LGM. Further mapping, chronologic and stratigraphic studies are necessary to establish the position and behaviour of the putative ice lobe that covered the southernmost portion of IGC during the final portion of the LGM.

Vegetation colonized and expanded in the vicinity of Lago Emerenciana at ~24.0 ka under relatively cold and wet conditions. Previous paleoecological studies have proposed that ice-free areas in the northwestern portion of the island harbored refugia of land biota during the LGM (Heusser, 1990a; Villagran, 2001). Those studies also postulated plant expansion and colonization from that sector into newly exposed ice-free sectors further east and south since T1 (Heusser, 1990a; Villagran, 2001). The results from the Lago Emerenciana record, however, reveal that the establishment of flora in southwestern areas of IGC occurred during the LGM. Because available minimum-limiting ages for ice recession from sites located in central and central-east sectors of IGC indicate the abandonment of the ice from these sectors during the onset of T1, I posit that plant colonization and expansion into southwestern sectors of IGC must have occurred through the west coast of IGC prior to ~24.0 ka. I propose that the western coast of the island must have constituted a corridor for the migration of terrestrial biota during the LGM. The formation, continuity and stability of this postulated corridor must have been dependent upon glacier extent, past sea-level fluctuation, and climate variability. I posit that glacial withdrawal provided a route for the dispersal of rainforest trees and herbs,

contributing to the afforestation of the newly deglaciated landscape of the southernmost portion of IGC, beginning from its southwestern sector and continuing toward its southeastern sector.

3.6. Conclusions

1. Local ice-free conditions persisted in southwestern IGC at least since ~24.0 ka. The Lago Emerenciana record suggests that the western margin of the Patagonian ice sheet must have been located in an unknown location east of this site.
2. Cold-resistant hygrophilous herbs, shrubs, ferns and patches of *Nothofagus* populations developed in sectors close to Lago Emerenciana between ~24.0 and ~17.5 ka. These findings suggest that southwestern IGC constituted a source area for the colonization of ice-free areas during T1 east of Lago Emerenciana.
3. A sustained increase in cold-resistant hygrophilous trees, herbs and ferns from ~22.8 ka suggests cooler and wetter conditions, with extreme cold conditions and increased precipitation regime between ~19.7 and ~17.5 ka, suggesting enhanced SWW influence at 43°S during the final portion of the LGM.
4. The appearance of Myrtaceae at ~17.5 ka marks the transition from a landscape co-dominated by taxa commonly found in Subantarctic vegetation and high-elevation environments to a forested landscape dominated by thermophilous trees characteristic of North Patagonian rainforests.
5. Because the modern transition between North Patagonian vegetation communities and Subantarctic vegetation occurs along gradients in temperature and precipitation, I interpret this floristic turnover as a transition from cold/hyperhumid to temperate/humid conditions at the onset of T1, consistent with warming and a decline in SWW influence in the region, arising most likely from a southwards shift of the SWW.
6. The establishment of the conifers *Fitzroya*/*Pilgerodendron* between ~16.3 and ~14.5 ka, along with an increase in the *Tepualia*+*Raukaua* parameter and a decline in macrophytes (Cyperaceae and *Isoetes*) suggest strong dissecting summer winds and increased precipitation seasonality. I interpret this event as an increase in SWW

influence, likely reflecting a northward shift or strengthening of the SWW following the onset of T1.

7. A reversal to cold conditions and increased precipitation occurred between ~14.5 and ~12.5 ka, suggesting enhanced SWW influence during the Antarctic Cold Reversal as a result of a northward shift of the SWW.
8. Relatively cool conditions ensued between ~12.5 and ~11.1 ka under reduced precipitation revealed by high abundance of the *Tepualia*+*Raukaua* parameter. A warming phase started at ~11.1 ka revealed by the virtual disappearance of *Podocarpus nubigena,* a major increase in Myrtaceae and the appearance of the summer-drought tolerant trees *Eucryphia*/*Caldcluvia* characteristic of Valdivian evergreen rainforests. The reduced precipitation regime lasted until ~7.6 ka, represented by high abundance of *Tepualia*+*Raukaua*. These finding suggest a decline in the SWW influence interpreted as a southward shift during the Younger Dryas chron, followed by minor SWW influence between ~11.1 and ~7.6 ka coeval with an observed zonally symmetric weakening of the SWW during the early Holocene.
9. The Lago Emerenciana records then shows a multi-millennial rise in precipitation between ~7.6 and ~4.4 ka suggesting high SWW influence, implying a strengthening of the SWW. This was followed by a decline precipitation between ~4.4 and ~2.4 ka, suggesting minor SWW influence. These shifts occurred in a context of major increase and low-magnitude variability of the modern Valdivian evergreen thermophilous drought-resistant trees *Eucryphia/Caldcluvia.* I propose that high climate variability with major seasonality in precipitation at 43°S (wetter winters, drier summers) were ideal conditions for the expansion of *Eucryphia/Caldcluvia* in this sector of IGC.

Chapter 4

Multi-proxy-climate reconstruction from southwestern South Island (45°S), New Zealand, spanning the last ~18,000 years.

4.1. Abstract

I report pollen, spore and charcoal records, along with a preliminary chironomid record from Lake Von (45°14'S; 168°17'E, 685 m.a.s.l), a small closed-basin lake located in southwestern South Island of New Zealand. These records allow the examination of past vegetation and climate changes, along with an exploratory chironomid-based summer temperature reconstruction (SmT) during and since the Last Glacial Termination (T1). The record indicates dominance of alpine vegetation with cold-tolerant shrubs, herbs and ferns between ~18.0 and ~16.7 ka, followed by a gradual transition toward *Coprosma*-dominated subalpine vegetation with the local presence of subalpine/montane hygrophilous trees between ~16.7 and ~14.8 ka and a rise in SmT. These data suggest an early stage with cold and relatively wet conditions between ~18.0 and ~16.7 ka under moderate SWW influence, followed by cold-temperate conditions with warmer summer and a slight increase in precipitation between ~16.7 and ~14.8 ka under strong SWW influence. I observe a rise in vegetation characteristic of alpine environments between ~14.8 and ~12.6 ka at the expense of *Coprosma*, accompanied by increases in cold-tolerant hygrophilous species and lake levels. This was followed by the increase and dominance of *Coprosma* between ~12.6 and ~10.8 ka, along with decline in alpine vegetation, cold-tolerant hygrophilous trees, lake levels and SmT. I interpret these data as indicating decline in temperatures with high seasonality and enhanced precipitation between ~14.8 and ~12.6 ka under stronger SWW influence, followed by warming with likely milder winter temperatures and reduced precipitation between ~12.6 and ~10.8 ka under weak SWW influence. Conspicuous increases in *Halocarpus* and *Phyllocladus* between ~10.8 and ~7.2 ka, along with increases in drought-resistant conifers, fire activity and SmT, suggest a further warming pulse and reduced precipitation under weaker SWW influence. The record shows an increase in the cool-temperate silver beech (*Lophozonia menziesii*) between ~7.2 and ~3.7 ka, along with the hygrophilous conifer *Dacrydium cupressinum*, relatively low abundance but with high variability in the warm-temperate tall conifers and a declining trend in SmT. Within this multi-millennial-scale

interval, I detect low-magnitude centennial-scale decline in *Lophozonia menziesii* and *Dacrydium cupressinum* between ~6.0 and ~5.2 ka and ~4.4 and ~4.1 ka, concurrent with increase in the drought-tolerant *Prumnopitys taxifolia*. These changes were followed by decline in *Lophozonia menziesii* and *Dacrydium cupressinum* between ~3.7 and ~2.9 ka, sustained increase in *Lophozonia menziesii*, *Dacrydium cupressinum* and drought-intolerant species between ~2.9 and ~1.9 ka, and a rapid and prominent rise in *Fuscospora* between ~1.9 and ~0.56 ka. I interpret these data as a decline in temperature, especially during summer, and a sustained rise in precipitation between ~7.2 and ~3.7 ka under increased SWW influence. Superimposed upon, and following this multi-millennial climate trend, I detect alternating dry and wet oscillations of millennial- and centennial-scale with low precipitation between ~6.0 and ~5.2, ~4.4 and ~4.1, ~3.7 and ~2.9, and ~1.9 and ~0.56 ka under decreased SWW influence, and wet periods in the intervening intervals suggesting increased precipitation under strong SWW influence. Finally, the records show increased fire activity during the last ~600 years, coeval with a decline in arboreal pollen and rise in vegetation indicative of human disturbance (Māori). The climate trends detected from Lake Von record are coherent with variations of the SWW identified in other terrestrial mid-latitude records, suggesting synchronic and symmetric changes in the SWW during and since T1.

4.2. Introduction

A limited number of proxy records across New Zealand are providing valuable insights into past climate dynamics, their evolution and driving mechanisms during and since the Last Glacial Termination (T1: ~18.0-11.7 ka, ka= 1000 calendar years before present, present= AD 1950) (e.g. Barrell et al., 2013; Jara et al., 2017; van den Bos et al., 2018). This thesis highlights the key role of the Southern Westerly Winds (SWW) as a driver for the initiation and/or propagation of climate and environmental changes in the Southern Hemisphere. Empirical and modeling studies have hypothesized that past shifts in the position and intensity of the SWW drove variations in Southern Ocean upwelling, ocean productivity, ventilation of deep-water CO_2 and, consequently, a rise in atmospheric CO_2 concentrations during the last glacial-interglacial period (Anderson et al., 2009; Denton et al., 2010; Fletcher and Moreno, 2011; Moreno et al., 2010; Toggweiler, 2009; Toggweiler et al., 2006). Despite their importance, our understanding of past variations of the SWW and their role as a critical paleoclimate

component in the middle latitudes of the Southern Hemisphere since the T1 is still not well documented.

The South Island of New Zealand (40°-47°S, 174°-166°E, Figure 4.1) belongs to a small group of landmasses located in the Southern Hemisphere that extend into the SWW zone of influence (Chapter 1, Figure 1.2). This southern landmass intersects the northern margin of the SWW belt, offering the potential for examining and reconstructing past changes in the SWW and their impacts on land biota and high-latitude coupled ocean-atmosphere processes. The southwestern sector of the South Island is under the permanent influence of the SWW (Garreaud, 2007), exhibiting a positive strong correlation between zonal wind strength and precipitation (Garreaud, 2007; Hinojosa et al., 2017) (Chapter 2, Figure 2.2). This correlation declines east of the SW-NE trending Southern Alps, generating a marked west-east precipitation gradient (McGlone et al., 1993) that, in conjunction with adiabatic cooling, induces regional altitudinal, latitudinal and longitudinal zonation of vegetation (Wardle, 1991). Thus, changes in the distribution and abundance of plant taxa can be used to infer past shifts in temperature and precipitation in the middle latitudes of the Southern Hemisphere, including the behavior of the SWW, based on fossil pollen records.

Paleoecological studies from the southwestern South Island of New Zealand (44-46°S), primarily using palynology, have attempted to reconstruct vegetation, fire and more broadly environmental change during T1 and through the Holocene (McGlone, 1983; McWethy et al., 2010; Ogden et al., 1998; Turney et al., 2017; Vandergoes et al., 1997; Wilmshurst et al., 2002). Following ice recession, the vegetation consisted of Alpine grassland-shrubland (*Coprosma*, Asteraceae, *Myrsine*), that shifted toward low broadleaf bushland (*Griselinia littoralis*) accompanied by understory species (*Rubus*, *Aristotelia*, *Dicksonia squarrosa*) under cold and relatively wet conditions during T1. This vegetation assemblage was followed by increases in tall podocarp forests (*Prumnopitys taxifolia*, *Prumnopitys ferruginea*, *Dacrycarpus*, *Dacrydium*, *Podocarpus*) and small conifers (*Halocarpus*, *Phyllocladus*), along with a modest increase in charcoal during the early/middle Holocene (between ~11.4 and ~4.7 ka) under relatively warmer and drier conditions than the previous interval. The last ~4700 years were characterized by a rapid increase in beech forests dominated by *Lophozonia menziesii* (silver beech), followed by a rise in *Fuscospora spp.* (predominantly mountain beech, but may also include red beech, black beech and hard beech). A subsequent marked

decline in arboreal pollen at ~0.7 ka, was accompanied by increases in non-arboreal pollen, spores of the fern *Pteridium* and fire activity, marking the onset of Polynesian influences that are detectable on the landscape (McWethy et al., 2010; Ogden et al., 1998). To what extent these changes in vegetation were driven by temperature and/or precipitation fluctuations and, consequently, their implications for understanding regional and hemisphere SWW change remains an open question. To date, there have been few attempts to deconvolute the temperature and precipitation signals from southwestern South Island of New Zealand.

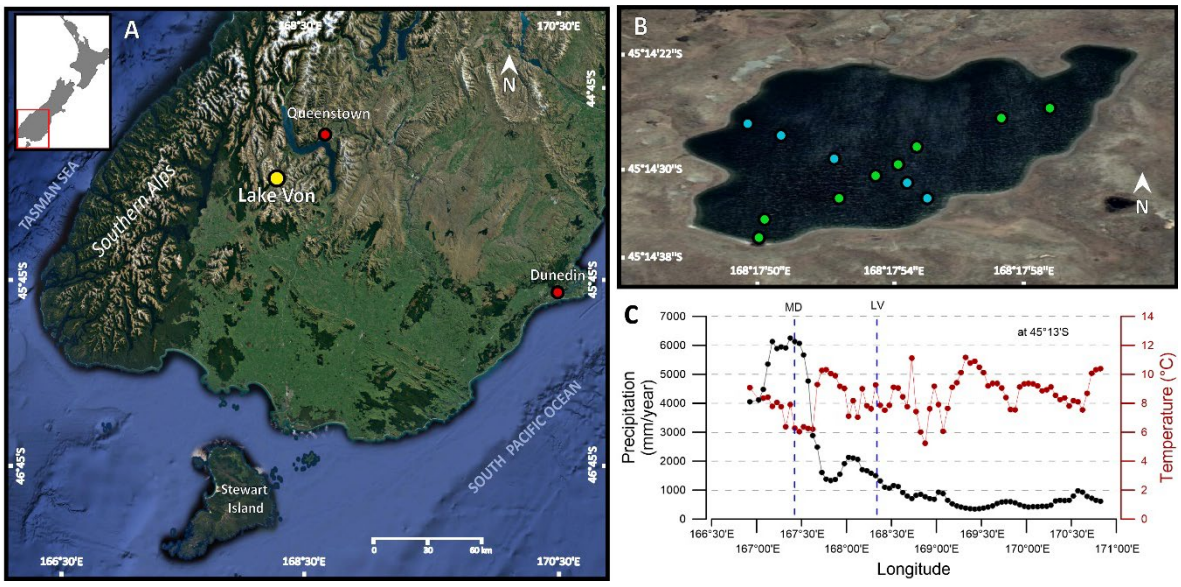

Figure 4.1. (A) Map of the study area indicating the location of Lake Von (LV) (yellow dot), and places (red dots) mentioned throughout the text. (B) Map of Lake Von showing the location of the southwest-northeast transect (green dotes) and the northwest-southeast transect (light blue dots). (C) Mean annual precipitation and temperature across a west-east transect at ~45°13'S (Macara, 2014, NIWA unpublished data). The vertical dashed lines denote the position of the main divide (MD) and Lake Von (LV).

Recently, Anderson et al. (2018) reported stratigraphic and geochemical data from Lake Von, a small lake located in the southwest of New Zealand's South Island (Figure 4.1). Based on these data, the authors attempted to reconstruct the deglacial and postglacial climate history of this region at the northern margin of the SWW. This study postulated that i) the SWW shifted southward between ~15.5 and ~14.2 ka, and ~13.0 and ~10.5 ka, the latter concurrent with the Younger Dryas chron (YD), ii) the SWW might have migrated northward between ~14.2 and ~13.0 ka broadly contemporaneous with the Antarctic Cold Reversal (ACR), iii) SWW reduced their strength during the early Holocene (between ~10.5 and 8.0 ka), and iv) the

SWW influence was enhanced after ~5.5 ka. This attempt to reconstruct SWW activity for the region, offers an important challenge for further work to test these assertions using independent multi-proxy records controlled with stratigraphic continuity, robust chronologies and detailed sampling resolution.

Here, I present high-resolution, well dated and continuously deposited fossil pollen and charcoal records from sediment cores obtained from the Lake Von site of Anderson's et al. (2018) study (Figure 4.1). These records are supplemented by a preliminary chironomid analysis from the same cores to provide exploratory chironomid-based summer temperature reconstruction (SmT). Together, these data allow examination of the timing and structure of vegetation, fire, and climate change in the context of SWW variability spanning the last ~18,000 years, and assessment of key questions: How did vegetation and fire regime evolve following local ice-free conditions? What was the timing and direction of paleoclimate conditions during T1? How did the SWW change through the Holocene? How did SmT vary during T1 and the Holocene?

4.2.1. Study area and study site

The South Island is the largest of the two major islands of New Zealand, extending ~850 km in length, facing the southern Pacific Ocean along its eastern shores and the Tasman Sea along its western shores. The South Island is separated from the North Island by the Cook Strait, a ~70 km stretch of ocean connecting the Tasman Sea to the northwest with the south Pacific Ocean to the southeast. The South Island features the Southern Alps, with deep valleys and lakes of glacial origin attesting to intense glacial erosion during the Quaternary.

The climate of the southern South Island is cool temperate (Meurk, 1984) and under the permanent influence of the SWW (Sturman and Tapper, 2006). The presence of the Southern Alps results in a marked rain shadow effect, with a hyper-humid west and a humid to sub-humid east (McGlone et al., 1993). Annual precipitation on the west coast reaches values that range between ~12000-6000 mm; precipitation declines abruptly, exhibiting values between 1200-1000 mm on the eastern slopes of the Alps. Farther to the east precipitation reaches values between 700-500 mm. Mean annual temperature measured at sea levels ranges between 10-12°C, decreasing to 0-2°C at the mountain summits (Macara, 2014).

Paleovegetation and paleoecological records indicate that the South Island was extensively forested prior to human occupation (Cumberland, 1971; Mark and McLennan, 2005; McGlone, 1983; McGlone et al., 2017). The dominant vegetation consisted of the southern beech forest species *Fuscospora* spp. and *Lophozonia menziesii* (McGlone and Bathgate, 1983; Vandergoes et al., 1997; Wardle, 1984; Wilmshurst et al., 2002). The arrival of Polynesians (Maori) at ~0.75 ka led to large-scale vegetation disturbance (Wilmshurst et al., 2008), causing reduction of nearly 50% of New Zealand's forests before European settlement (~0.35 ka) (McGlone and Wilmshurst, 1999; McWethy et al., 2010). Currently, most native vegetation in the southern South Island is confined to mountain slopes in the Southern Alps and/or patches on the lowlands. Beech forests dominate the upland areas to the tree line (~1200 m.a.s.l), with *Lophozonia menziesii* and *Fuscospora cliffortioidies* as the most common species. Along the west coast, in hyper humid environments and temperate conditions, mixed forests constitute the dominant plant community with beech, podocarp, and broad-leaved hardwood species (Holloway, 1954; Wardle, 1991). The dominant species is *Dacrydium cupressinum* (rimu), accompanied by *Prumnopitys ferruginea*, *Prumnopitys taxifolia*, *Podocarpus hallii* and *Dacrycarpus dacrydioides*. Further to the east, where rainfall declines to <700 mm/yr and human forest clearances are more extensive, the vegetation is dominated mostly by grass and shrubs, along with remnant trees such as *Phylllocladus alpinus* (Wardle, 1991).

The main plant communities occurring throughout the South Island include key taxa that enable past vegetation changes to be reconstructed from palynological records (e.g. McGlone et al., 2017). Lowland podocarp forests dominate the landscape up to 400 m.a.s.l, characterized by tall trees such as *Dacrydium cupressinum*, *Prumnopitys ferruginea* and *Dacrycarpus dacrydioides*, accompanied by the understory species *Ascarina lucida*, *Pseudopanax*, *Coprosma*, *Myrsine* and tree ferns *Cyathea smithii*, *Cyathea colensoi* and *Dicksonia squarrosa*. Montane podocarp-hardwood forest dominates higher altitude (~400-800 m.a.s.l.) and is characterized by *Metrosideros umbellata*, *Weinmannia racemosa*, *Griselinia littoralis*, *Podocarpus hallii*, along with sub canopy taxa *Myrsine divaricata*, *Pseudopanax simplex*, *Pseudowintera colorata* and *Coprosma foetidissima*. An important number of these species also occur in the subalpine zone between 800-1200 m.a.s.l., along with *Phyllocladus alpinus* and *Libocedrus bidwillii* that in conjunction form dense shrubland ~800 m.a.s.l. to the modern treeline at ~1200 m.a.s.l. Above 1200 m.a.s.l., the landscape is

dominate by alpine vegetation, characterized by shrub grassland including low shrubs of *Coprosma*, *Hebe* and *Dracophyllum*, grasses (Poaceae) and numerous species of Asteraceae (Wardle, 1991).

Regional vegetation also features beech forests occurring across much of the South Island. A notable exception is the 'beech gap' between the latitudes 42°40'S and 43°30'S (Wardle, 1991). These beech forest communities feature four species: *Lophozonia menziesii*, and *Fuscospora* type species including *Fuscospora cliffortioides*, *Fuscospora solandri*, *Fuscospora fusca* and *Fuscospora truncata*. *Lophozonia menziesii* is generally found from sea level up to the tree line, occupying hyperhumid environments in northernmost and southernmost sectors of the South Island. *Fuscospora fusca* and *F. truncata* are both less tolerant of cool conditions than *Lophozonia menziesii*, while *F. cliffortioides* occurs in poorly drained and low fertilized sites (Wardle, 1991).

Lake Von (45°14'S; 168°17'E, 685 m.a.s.l) is a small (max. depth: ~15 m, area: 0.11 km^2) closed-basin lake located ~50 km east of the Southern Alps divide in southwestern South Island of New Zealand (Figure 4.1). The lake is situated in the upper Oreti River Valley in southwestern Otago, within a glacially formed depression <5 km north of terminal moraines of Last Glacial Maximum age (LGM; ~18 ka) (Barrell, 2011). The site lies at a transition between extremely wet climate of the mountainous west and the drier east (Macara, 2014, NIWA unpublished data) (Figure 4.1) . Mean annual precipitation in the vicinity of Lake Von is 690 mm, and mean annual temperature is 9.3°C (Figure 4.1) (NIWA unpublished data). The bathymetry of the lake consists of a simple central basin that reaches 15-m deep, with a relatively large littoral zone populated by submerged macrophytes such as *Potamogeton cheesemanii* and *Nitella hookeri*. Although no more aquatic plants were seen in the lake, *Isoetes* seems to be present as suggested by *Isoetes* spores found in sediment-water sediment samples (see section Results 4.5). The vegetation presently surrounding the lake is dominated by small tussock grasses (*Chionochloa rigida*, *Festuca novae zelandiae*) and shrubs (*Discaria toumatou*, *Coprosma* spp, *Dracophyllum longifolium*) (Anderson et al., 2018).

4.3. Material and methods

Multiple sediment cores were obtained from the deepest sector of Lake Von (15 m water depth) during 2016 and 2018. I sub-sampled the composite stratigraphy of Lake Von record for pollen, macroscopic charcoal and chironomid analyses. I took 1-cc sediment samples obtained from 1-cm thick sections spaced at 2-cm intervals for pollen analysis. I analyzed the macroscopic charcoal content of 2-cc sediment samples taken at contiguous 1-cm thick intervals. For chironomid analysis, I took 0.5 to 1-cc sediment samples from 1-cm thick sections spaced at 24-cm intervals to obtain a minimum of 50 whole head capsules per level. The chronology of the record is constrained by AMS radiocarbon dates obtained from bulk organic samples retrieved from 1-cm-thick sections, along with plant material and macro-fossils found throughout the cores (Table 4.1). All procedures involved in the extraction and sampling of sediment cores, the development of the age model, the processing of pollen, charcoal and chironomid samples, the time-series analysis applied to the charcoal record (CharAnalysis) and the chironomid-based summer temperature reconstruction (SmT) are described in chapter 2.

I identified palynomorphs based on published catalogues (Moar, 1993) and unpublished reference material (Newnham's personal collection at VUW palynology laboratory). The majority of the palynomorphs were identified to family or genus levels, but some palynomorphs were identified to the specie level (*Dacrydium cupressinum*, *Prumnopitys taxifolia*, *Prumnopitys ferruginea*, *Lophozonia menziesii*). The palynomorph *Fuscospora* includes the species *Fuscospora fusca*, *Fuscospora truncata*, *Fuscospora cliffortioides* and *Fuscospora solandri*.

In addition to downcore palynology, I performed pollen analysis on sediment-water interface samples that were collected from an inflatable boat using a bottom sampling dredge across two transects at Lake Von, from the northwest to southeast coast and from the southwest to northeast coast (Figure 4.1, and Table A2.1 in Appendix 2). I prepared pollen slides from 1-cc samples following the procedure described in chapter 2. I calculated the percentage and concentration of each terrestrial and aquatic taxon following the procedure described in chapter 2 (Figures A2.2 and A2.3 in Appendix 2).

4.4. Results

4.4.1. Stratigraphy and chronology

The Lake Von sedimentary record has a total composite length of 577 cm and combines cores from the series HDC3 (segment 1), HAC1 (segments 1 and 2), HAC2 (segments 1 and 2), HD (segments 3 and 4), and the water-sediment interface core HFSC (Figure 4.2). I correlated the sediment cores by identifying overlapping sections of LOI (Figure A2.1 in Appendix 2). The record comprises a basal 41-cm thick sandy silt unit, overlain by a 35-cm inorganic silt unit, followed by 501-cm thick organic mud with varying degrees of lightness. Within this organic unit I identify 5 gray silt horizons between 380-381, 316-318, 285-286, 282-283 and 230-231 cm, defined as mottled sedimentary units (Anderson et al., 2018).

The LOI data indicate abundant organic matter content with variations throughout the sedimentary record, and relatively low carbonate and siliclastic content (Figure 4.2). Between 577 and 534 cm, the record shows very low organic matter (~1.5-4.0%) in the basal portion of the record, followed by a rising trend with variability between 534 and 259 cm. A rapid drop in organic matter occurred between 229 and 250 cm, followed by the resumption of the organic matter increase between 250 and 120 cm, reaching a ~35% plateau with variations that range between ~30% and ~40% until the top of the record (Figure 4.2).

The chronology of the Lake Von record is constrained by 17 AMS radiocarbon dates, with a calibrated basal age of ~18.6 ka (18.4-18.7 ka) (Table 4.1). This chronology, along with stratigraphic and LOI data, point to continuous lacustrine sedimentation during the last ~18,000 years (Figure 4.3). I excluded a date from the age model (7003±29) considering that this age is out of the calculated confidence interval of the age model (Figure4.3), suggesting that this age is anomalously old within an interval in the core with no stratigraphic indications of unconformity or hiatus.

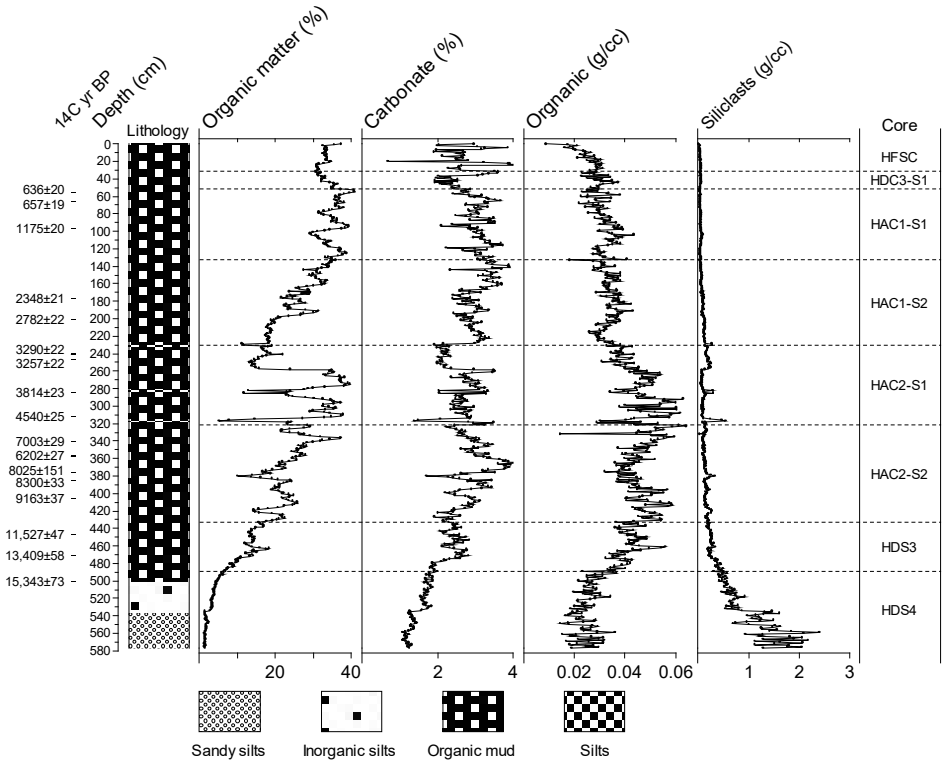

Figure 4.2. Stratigraphic column of the Lake Von record, showing the position of radiocarbon dates, lithology, selected parameters of loss-on-ignition analysis, and the identity of the individual sediment cores segments. Dashed horizontal lines represent core segment boundaries.

Table 4.1. Summary of radiocarbon dates obtained from Lake Von. The dates were calibrated to calendar years before present using CALIB 7.0.1. (Reimer et al., 2013). * I consider the age of this date as anomalously old and excluded from the age model.

Laboratory code	Core	Fraction dated	Composite depth (cm)	14C yr BP±1σ	Median probability (cal. yr BP)	2σ intercepts (cal. yr BP)
41024/1	Von HDC3	Plant material	55	636±20	609	545-635
41024/9	Von HAC1-S1	Plant material	65.5	657±19	608	552-647
41024/8	Von HAC1-S1	Plant material	97	1175±20	1016	969-1064
41024/12	Von HAC1-S2	Plant material	176	2348±21	2336	2206-2358
41024/3	Von HAC1-S2	Plant material	200	2782±22	2827	2764-2920
41024/6	Von HAC2-S1	Plant material	240	3290±22	3470	3398-3560
41024/5	Von HAC2-S1	Plant material	246	3257±22	3428	3366-3551
41024/14	Von HAC1-S3	Plant material	284	3814±23	4139	3997-4240
41341/1	Von HDS2	Plant material	311	4540±25	5166	4989-5301
41341/2*	Von HDS2	Plant material	340	7003±29	7846	7760-7932
41024/7	Von HAC2-S2	Bulk organic	357	6202±27	7069	6958-7163
41341/3	Von HES2	Plant material	376	8025±151	8849	8456-9271
41024/4	Von HAC2-S2	Plant material	385	8300±33	9240	9092-9405
41402/1	Von HDS3	Plant material	405	9163±37	10267	10207-10401
41402/7	Von HES3	Bulk organic	446	11,527±47	13,335	13,215-13,447
41402/8	Von HES3	Bulk organic	470	13,409±58	16,083	15,856-16,277
41402/6	Von HES3	Macrofossil	500	15,343±73	18,573	18,377-18,746

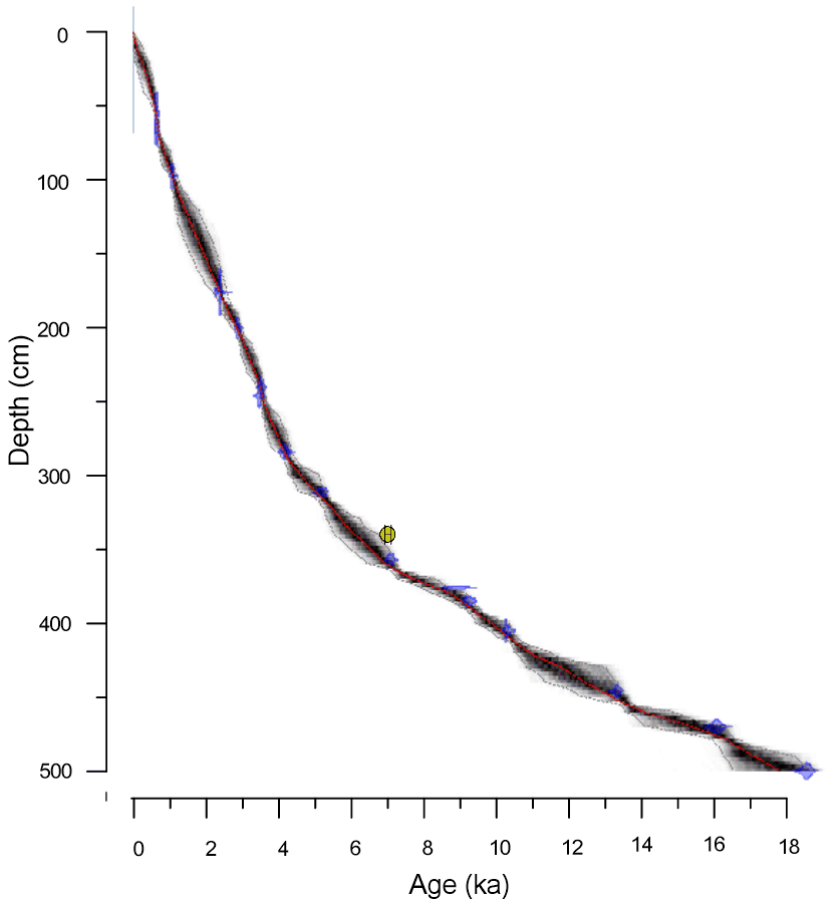

Figure 4.3. Bayesian age-model from Lake Von. The blue zone represents the probability distribution of the calibrated ages, the grey zone shows the calculated confidence interval of the age model, and the red line represents the median probability age of the age model. The yellow dot marks the position of the excluded date from the age model.

4.4.2. Pollen record

I analyzed the pollen and spore content of 251 samples from Lake Von, presumed to continuously span the last ~18,000 years with a median temporal resolution of 39 years between palynological samples (Figures 4.4 and 4.5). To facilitate the description of the pollen record I divided it into 11 palynological zones based on the most conspicuous changes in the pollen stratigraphy as determined with the aid of a stratigraphically constrained cluster analysis (CONISS) (Figures 4.4 and 4.5). In the following paragraphs I describe each zone highlighting the three most abundant terrestrial taxa in decreasing order of mean abundance, accompanied by less-abundant taxa with average percent abundances given.

Zone Von-P1 (500-484 cm; ~18.0-16.7 ka) is characterized by the assemblage *Coprosma* (46%)-Poaceae (30%)-Asteraceae Asteroideae (6%), accompanied by low abundance of *Myrsine* (3%), the herbs Caryopyllaceae (1%), Chenopodiaceae (2%), the ferns *Hypolepis* (3%), *Asplenium* (2%), *Histiopteris* type (5%), *Lycopodium* type (2%), *Lycopodium varium* (3%), the podocarp trees *Podocarpus* (4%), *Dacrydium cupressinum* (1%), *Prumnopitys taxifolia* (<1%), *Prumnopitys ferruginea* (<1%), *Metrosideros* (<1%), the conifer *Phyllocladus* (3%), and relatively low arboreal pollen overall (16%). *Coprosma* shows an increasing trend, *Isoetes* (6%) exhibits a slight increase, while *Blechnum* type (48%) and Cyperaceae (9%) feature their highest percentage, followed by their rapid decline until the end of this zone. The green microalgae *Pediastrum* (94%) shows its highest abundance of the entire record at the beginning of this zone, subsequently decreasing slightly.

Zone Von-P2 (484-442 cm; ~16.7-12.6 ka) features the dominance of *Coprosma* (61%), Poaceae (21%) and Asteraceae Asteroideae (9%), with declines in *Coprosma*, *Myrsine* (3%) and Poaceae, increases in *Metrosideros* (1%), Asteraceae Asteroideae and *Histiopteris* (2%), and the lowest abundance of arboreal pollen (7%) of the entire record. *Blechnum* type (15%) and *Pediastrum* (94%) decline abruptly at the beginning of this zone from 36% to 10% and 83% to 30%, respectively. *Cyathea* (2%) and *Asplenium* (4%) show slight rising trends, while the aquatic *Isoetes* (32%) increases rapidly from 4% to 80% exhibiting its peak abundance at ~12.9 ka.

Zone Von-P3 (442-418 cm; ~12.6-10.8 ka) is dominated by *Coprosma* (76%), Poaceae (9%) and *Myrsine* (5%), featuring increases in *Coprosma*, *Myrsine* and *Cyathea* (6%), abrupt declines in *Metrosideros* (<2%) and Asteraceae Asteroideae (3%), and a slight increase in arboreal pollen (12%). *Isoetes* (6%) shows a prominent decline from 80% to 1%, while Poaceae, Cyperaceae (1%) and *Pediastrum* (12%) exhibit decreasing trends. The remaining fern taxa decline.

Zone Von-P4 (418-404 cm; ~10.8-10.1 ka) features dominance of the assemblage *Halocarpus* (74%)-*Coprosma* (13%)-*Phyllocladus* (2%). This zone starts with an abrupt increase in *Halocarpus* from 2% to 84% at the expense of *Coprosma* which declines from 79% to 9% between ~10.8 and ~10.4 ka, mirrored in an abrupt rise in arboreal pollen (86%). *Podocarpus* (2%), *Podocarpus*/*Prumnopitys* (2%), *Prumnopitys taxifolia* (1%), *Prumnopitys ferruginea* (1%) and *Dacrycarpus* (1%) increase during this zone, while ferns and aquatic plants virtually disappear.

Zone Von-P5 (404-366 cm; ~10.1-7.4 ka) is characterized by *Phyllocladus* (74%), *Halocarpus* (14%) and *Podocarpus* (2%), an abrupt decline in *Halocarpus* from 60% to 2% and a compensatory increase in *Phyllocladus* from 8% to 92% between ~10.0 and ~8.8ka. Arboreal pollen (98%) rises reaching a plateau at ~97%, the arboreal taxa *Podocarpus*, *Podocarpus/Prumnopitys* (2%), *Prumnopitys taxifolia* (1%) and *Prumnopitys ferruginea* (1%) show slight increasing trends, while *Coprosma* (2%) achieves its minimum abundance of the record.

Zone Von-P6 (366-231 cm; ~7.4-3.3 ka) exhibits dominance of *Phyllocladus* (43%), *Lophozonia menziessi* (17%) and *Halocarpus* (14%), with a persistent decline in *Phyllocladus*, increasing trends in *Lophozonia menziessi* and *Dacrydium cupressinum* (2.5%), along with slight rises in *Podocarpus* (6%), *Podocarpus*/*Prumnopitys* (5%), *Prumnopitys taxifolia* (3%), *Prumnopitys ferruginea* (3%) and *Dacrycarpus* (<1%). *Halocarpus* shows little variation throughout this interval, while arboreal pollen (~96%) maintains the level reached in the previous zone. The aquatic plant *Isoetes* (2%) exhibits a conspicuous increase between 5.3 and 4.4 ka, and the microgreen algae *Pediastrum* (2%) increases by the end of this zone.

Zone Von-P7 (231-203 cm; ~3.3-2.9 ka) is characterized by the pre-eminence of *Phyllocladus* (56%), *Halocarpus* (14%) and *Lophozonia menziesii* (8%) with a prominent rise in *Phyllocladus* from 40% to 68% between ~3.3 and ~3.1 ka, and a conspicuous decline in *Lophozonia menziesii*. *Halocarpus* and arboreal pollen persist at 14% and 97%, respectively, while *Pediastrum* (2%) declines. *Podocarpus* (7%), *Dacrydium cupressinum* (1%), *Prumnopitys taxifolia* (~2%), *Prumnopitys ferruginea* (~2%) and *Dacrycarpus* (<1%) exhibit a decline through this zone.

Zone Von-P8 (203-155 cm; ~2.9-2.0 ka) features the assemblage *Phyllocladus* (34%)-*Lophozonia menziesii* (22%)-*Halocarpus* (14%), with a rapid decline in *Phyllocladus* followed by its steady decline, along with *Halocarpus*, an increasing trend in *Fuscospora* (4%), while arboreal pollen (96%) remains in a plateau at 97%. *Lophozonia menziesii* shows an increasing trend with high magnitude oscillations (~10%) superimposed, achieving its maximum at ~2.0 ka at the end of this zone, and *Dacrydium cupressinum* (2%) and *Metrosideros* (<1%) exhibit slight rises. *Podocarpus* (7%) shows an abrupt increase at the beginning of this zone followed by its sustained decline, along with a declining trend in *Podocarpus/Prumnopitys* (5%), and

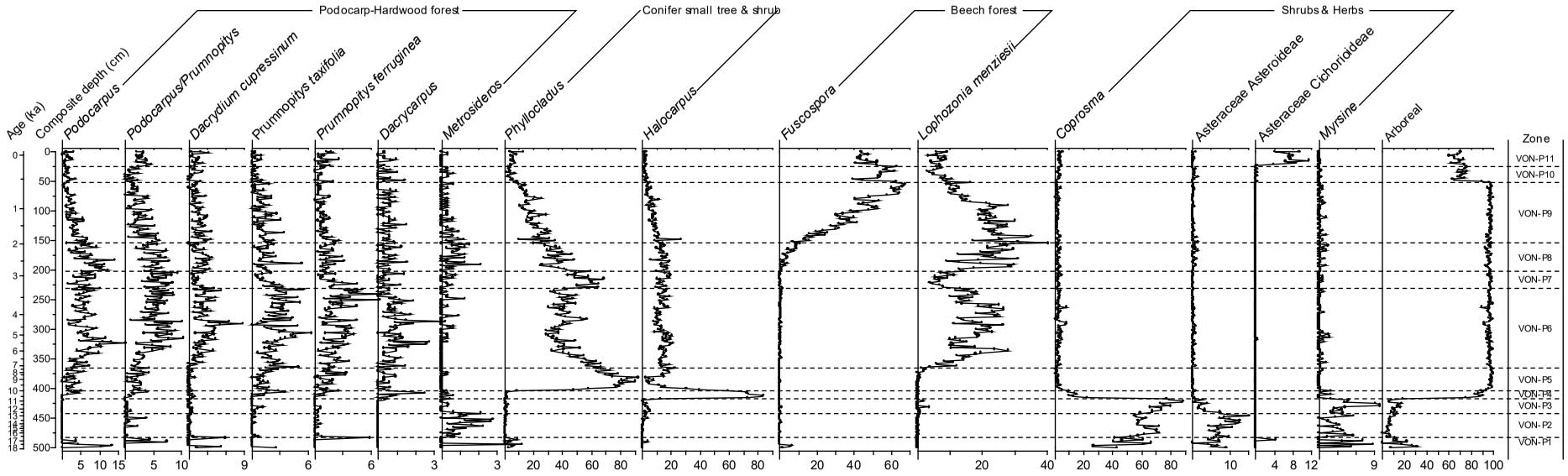

Figure 4.4. Percentage pollen diagram of arboreal, shrub and herb taxa from the Lake Von site. The primary y axis expresses the composite depth of the record, the secondary y scale expresses the age model. The labels on the right indicate the identity and stratigraphic span (black dashed horizontal lines) of each pollen assemblage zone.

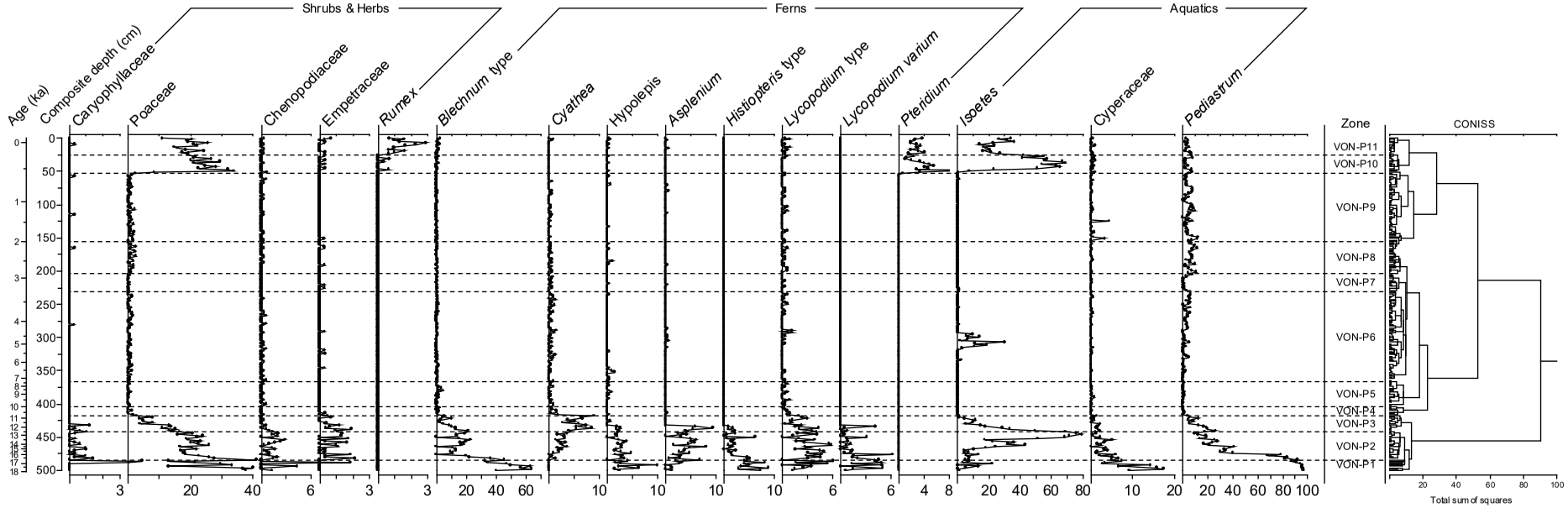

Figure 4.5. Percentage pollen diagram of shrub, herb, fern and aquatic taxa from the Lake Von site, along with results of the CONISS ordination. The primary y axis expresses the composite depth of the record, the secondary y scale expresses the age model. The labels on the right indicate the identity and stratigraphic span (black dashed horizontal lines) of each pollen assemblage zone.

relatively low abundance in *Prumnopitys taxifolia* (~1.5%) and *Prumnopitys ferruginea* (~1%). *Pediastrum* (8%) rises, exhibiting low magnitude variation throughout this interval.

Zone Vone-P9 (155-53 cm; ~2.0-0.55 ka) is dominated by *Fuscospora* (40%), *Lophozonia menziesii* (20%) and *Phyllocladus* (19%), with a declining trend in *Lophozonia menziessi* which shows a rapid decline at 0.9 ka. *Halocarpus* (7%), *Podocarpus* (3%) and *Podocarpus/Prumnopitys* (~3%) exhibit declining trends through this zone, while *Fuscospora* (40%) shows a sustained increase until the end of this zone. *Dacrydium cupressinum* (~1.5%), *Prumnopitys taxifolia* (1%), *Prumnopitys ferruginea* (<1%), *Dacrycarpus* (<1%) and *Metrosideros* (<1%) remain with low abundance, while *Pediastrum* (5%) shows high variability with values that range between ~1% and 12%.

Zone Von-P10 (53-25 cm; ~0.55-0.23 ka) indicates dominance of the assemblage *Fuscospora* (55%)-Poaceae (24%)-*Lophozonia menziesii* (7%), along with a prominent increase in Poaceae from ~2% to 32%, and abrupt declines in *Fuscospora*, *Lophozonia menziesii*, arboreal pollen (73%) and a rapid rise in *Pteridium* (4.5%). *Cyathea* (~3%) and *Isoetes* (47%) show rapid increases from 3% to 11 % and 1% to 68 %, respectively, followed by their steady decline until the end of this zone. *Pediastrum* (~5%) shows a decline at the beginning of this zone, increasing toward the end of this zone.

Zone Von-P11 (25-0 cm; ~0.23 ka-present) features the assemblage *Fuscospora* (46%)-Poaceae (19%)-Asteraceae Cichorioideae (7%). *Fuscospora* shows a rapid decline at the beginning of this zone, along with a rapid increase in Asteraceae Cichorioidea, and slight rises in *Podocarpus/Prumnopitys* (3%), *Phyllocladus* (6%), *Halocarpus* (2%), *Lophozonia menziesii* (6%) and Coprosma (~4%). Poaceae (%) exhibits a sustained decline through this zone, accompanied by an increase in the exotic *Rumex* (~1%), a slight decline in arboreal pollen (68%), relatively high values in *Pteridium* (~3%), and a prominent decline in *Isoetes* (~28%).

4.4.3. Macroscopic charcoal record

The macroscopic Charcoal Accumulation Rates (CHAR) record from Lake Von (Figure 4.6) comprises 501 samples that continuously span the last ~18,000 years, with a median temporal resolution of 20 years. The record shows an absence of charcoal accumulation prior to ~10.0 ka, followed by a rise between ~10.0 and ~8.0 ka, null values between ~8.0 and 6.9 ka, very low values between ~6.9 and ~0.8 ka, and a prominent rise in CHAR during the last ~600 years.

Time series analysis of the macroscopic charcoal data reveals 11 statistically significant charcoal peaks (Figure 4.6). Fire episodes are completely absent between ~18.0 and ~10.0 ka, followed by low- but large-magnitude events at ~9.4 and ~9.0 ka, respectively. Between ~6.4 and ~2.4 ka, I identified a conspicuous cluster of 6 events with low magnitudes at ~6.4, ~5.8, ~5.0, ~4.6, ~3.2 and ~2.4 ka, followed by a cluster of 3 events during the last ~600 years including one large-magnitude event at ~0.53 ka and two short-magnitude events at ~0.30 and ~0.18 ka (Figure 4.6).

4.4.4. Water-sediment interface samples

I analyzed the abundance of *Isoetes* spores from 13 sediment-water interface samples obtained across 2 transects from Lake Von (Figure 4.1, Figures A2.2 and A2.3 in Appendix 2). The rationale for this particular is explained further in the next section (subsection 4.6.2) but essentially this was to investigate the viability of using *Isoetes* spore abundance as a proxy for water depth at this site. I applied a linear regression to examine the relationship between the modern spore abundance of the aquatic lycopsid *Isoetes* (in concentrations) and water depths (Figure 4.7). Transect 1 (8 samples) shows percentages and concentration that vary between 2922 and 84074 spores/cm^3. Transect 2 (5 samples) shows concentrations that vary between and 4296 and 53342 spores/cm^3. I note that Transect 1 and 2 exhibit similar trends, with relatively lower abundance of *Isoetes* in shallow environments and higher abundance in deeper water depths (Figure 4.7).

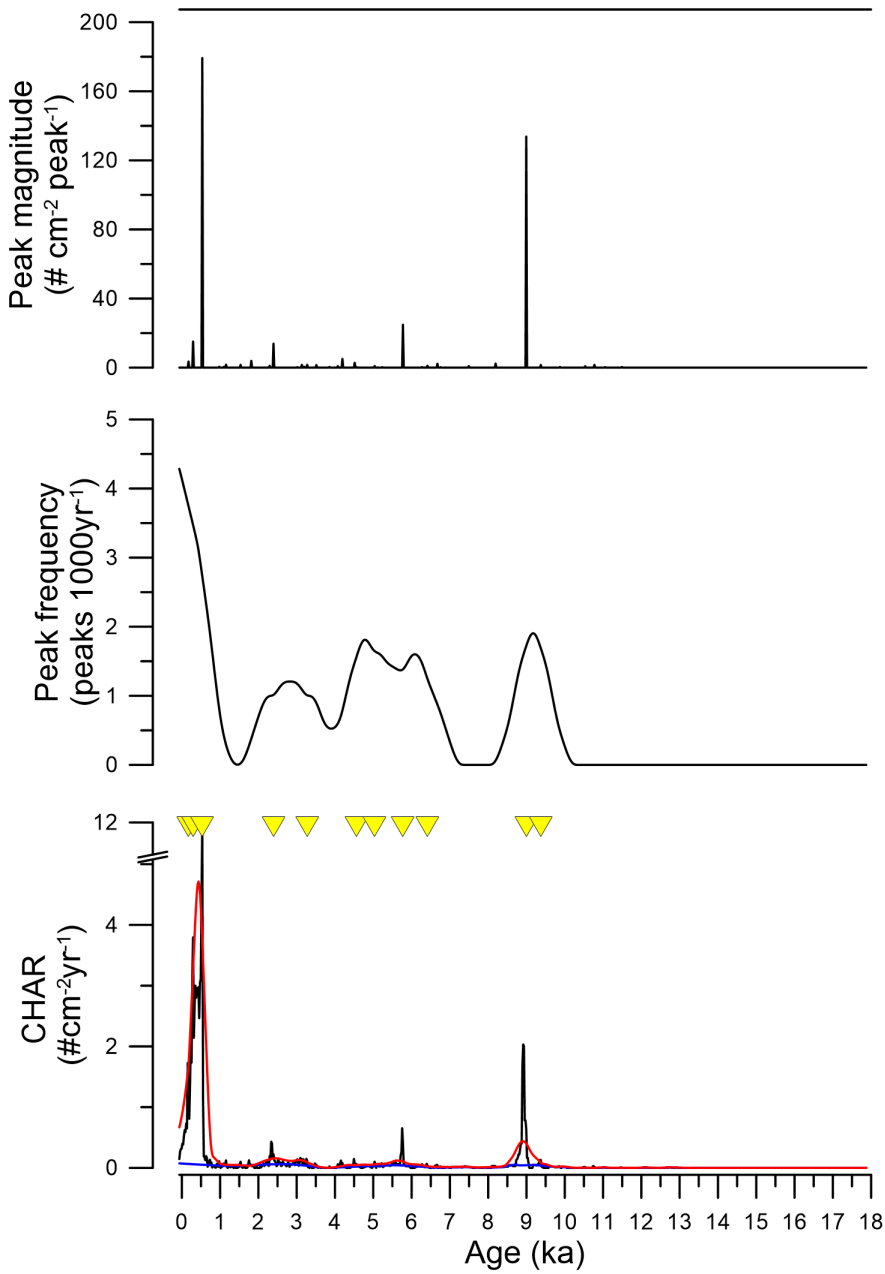

Figure 4.6. Macroscopic charcoal accumulation rate (CHAR) from Lake Von and the results of Char-Analysis, indicating the background component (blue line), locally defined threshold (red line), statistically significant charcoal peaks (yellow triangles), peak frequency and magnitude.

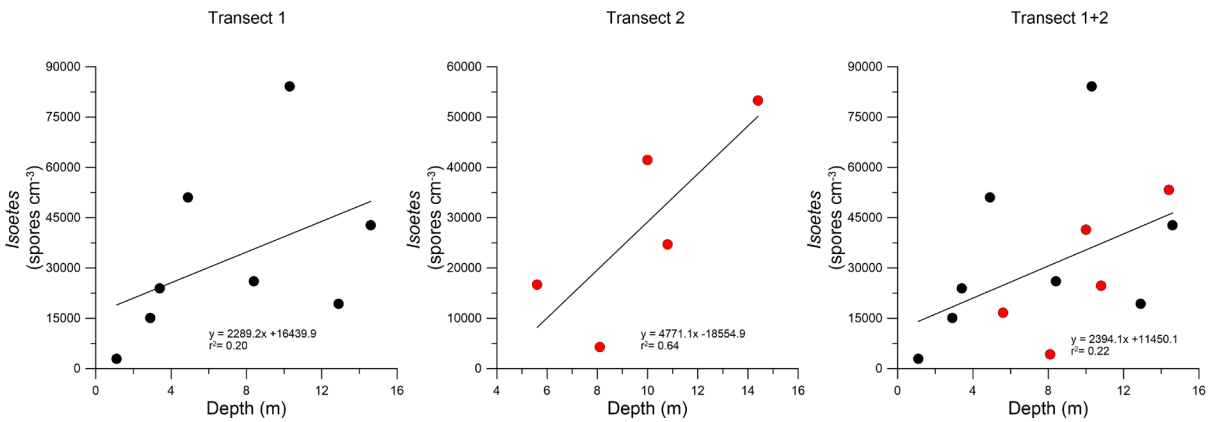

Figure 4.7. Concentration abundance of *Isoetes* from sediment-water interface samples from Lake Von, showing abundance from transect 1 (left panel, black dots) and transect 2 (middle panel, red dots) and combined transects (right panel).

4.4.5. Chironomid record

I analyzed the head capsule content of 23 samples from Lake Von, continuously spanning the last ~18,000 years with a median temporal resolution of 470 years between samples. I divided the chironomid record into 7 zones based on the most conspicuous changes in the chironomid stratigraphy with the aid of a stratigraphically constrained cluster analysis CONISS (Figures 4.8). In the following paragraphs I describe each zone indicating the average percent abundance of the main taxa in parentheses.

Zone Von-C1 (500-422 cm; ~18.0-11.1 ka) is dominated by warm associated taxa (64%) with a high abundance of *Corynocera* (58%), along with minor abundance of *Chironomus* (14%), *Tanytarsus funebris*-type A (5%) and *Tanytarsus funebris*-type C (5%), and low abundance of *Paucispinigera* (2%), *Paratanytarsus* (1.6%) and *Naonella kimihia* (1.6%).

Zone Von-C2 (422-350 cm; ~11.1-6.5 ka) is characterized by declines in *Corynocera* (20%) and *Chironomus* (7%), and an increase in *Paucispinigera* (19%), along with increases in cold associated taxa (36%) such as *Tanytarsus funebris*-type A (13%), *Tanytarsus funebris*-type C (11%) and Macropelopini 3 (1.4%).

Zone Von-C3 (350-229 cm; ~6.5-3.3 ka) features increases in *Corynocera* (38%) and *Polypedilum* (3.5%), along with the disappearance in *Paucispinogera*. *Chironomus* (16%) shows a sustained increase until ~4.6 ka, followed by its decline until the end of this zone,

contemporaneous with an increase in *Naonella forsythi* (3%). *Tanytarsus funebris*-type A (13%) and *Tanytarsus funebris*-type C (9%) maintain values exhibited in the previous zone.

Zone Von-C4 (229-157 cm; ~3.3-2.0 ka) shows a major rise in *Corynocera* (63%), a decrease in *Polypedilum* (3.5%), and declines in cold associated taxa (25%) including *Tanytarsus funebris*-type A (7%), *Tanytarsus funebris*-type C (3%), *Chironomus* (8%) and *Naonella forsythi* (2%).

Zone Von-C5 (157-109 cm; ~2.0-1.2 ka) exhibits a decline in warm associated taxa (47%) including *Corynocera* (42%) and *Polypedilum* (2.5%). Cold associated taxa (27%), such as *Chironomus* (11%) and *Tanytarsus funebris*-type C (6%), show slight increases.

Zone Von-C6 (109-37 cm; ~1.2-0.4 ka) features an increase in *Corynocera* (52%), along with rises in cold associated taxa (26%) including *Tanytarsus funebris*-type C (6%), *Naonella forsythi* (2%), Macropelopini 3 (1%) and *Tanytarsus vespertinus* (<1%).

Zone Von-C7 (37-0 cm; ~0.4 ka-present) is characterized by an increase in the warm associated taxon *Corynocera* (20.1%), and rises in cold associated taxa (57%) including Chironomini early instar (17%), *Tanytarsus funebris*-type A (13%), *Tanytarsus funebris*-type C (11%), *Naonella forsythi* (6%) and Macropelopini 2 (3%).

4.4.6. Chironomid inferred SmT reconstruction

Most of chironomid samples from Lake Von are beyond the 10% quantile, indicate that this assemblage has no close modern analogue in the training set, suggesting that the WAPLS model is the most appropriate for Lake Von record (Figure A3.4 in Appendix 2). Goodness of fit show most of fossil samples plot below the 90th and 95th percentile of the squared residual distances of training set, thus the fossil samples from Lake Von have a good fit to SmT, and finally most samples have less than 5% abundance of suspect taxa (Figure A3.4 in Appendix 2).

The reconstructed SmT based on the preliminary Lake Von chironomid record (Figure 4.8) shows increasing warmth between ~18.0 and ~8.1 ka (7 data points) reaching its highest temperature at the end of the interval. Within this multi-millennial period, I note a conspicuous but short-lived reversal centered at ~11.1 ka, although it is represented by only one data point (Figure 4.8). The beginning of this warming seems to be driven by high abundance in the intermediate-to-warm taxon *Corynocera* (Dieffenbacher-Krall et al., 2007)

between ~18.0 and ~12.8 ka, interrupted by the increase of the cold-type *Tanytarsus funebris* type A between ~12.8 and ~11.1 ka, followed by the recovery of the deglacial warming probably driven by a rapid increase in the warm-type *Paucispinigera* between ~11.1 and ~8.1 ka. Subsequently, the record shows a cooling trend between ~8.1 and ~4.6 ka (3 data points) primarily triggered by an increase in *Chironomus*, along with relatively high abundance in other cold-associated taxa such as *Tanytarsus funebris* type A, *Tanytarsus funebris* type C, *Naonella forsythi*. This was followed by a modest increase in temperature between ~4.6 and ~2.0 ka (6 data points) given by a rise in *Corynocera*, coeval with declines in *Tanytarsus funebris* type A, *Tanytarsus funebris* type C, *Naonella forsythi*. A decline in temperature between ~2.0 and ~0.6 ka (4 data points) seems to be driven by an increase in *Chironomus*, contemporaneous with a slight decline in *Corynocera.* Finally, I observe a rise in temperature during the last ~600 years (3 data points), likely representing increases in the warm-type *Parachironomus* and *Cladopelma* (Dieffenbacher-Krall et al., 2007) (Figure 4.8).

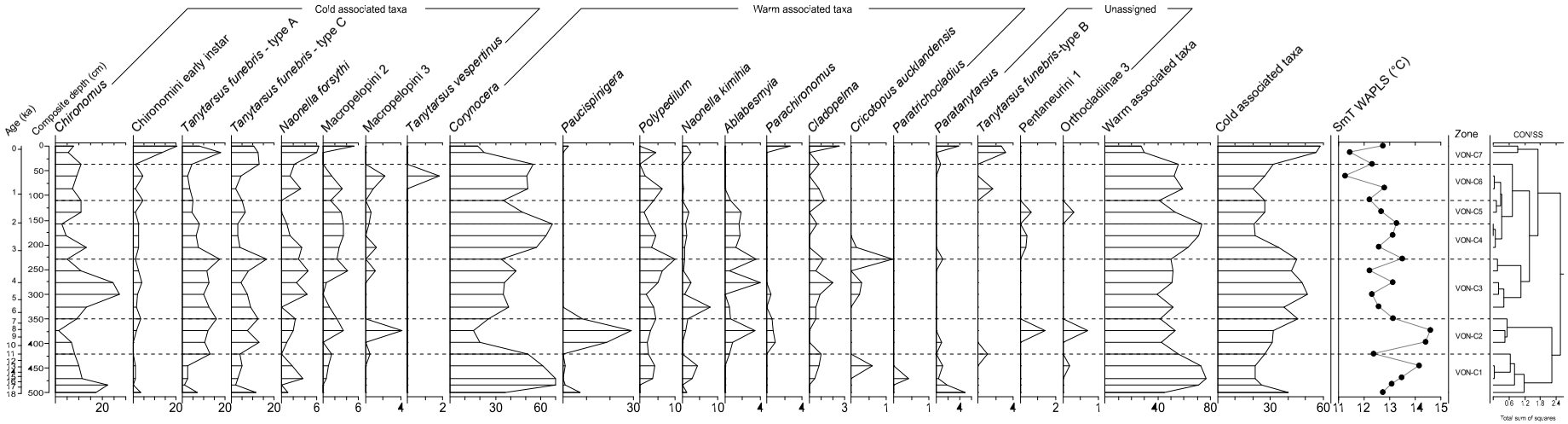

Figure 4.8. Percentage chironomid diagram from the Lake von site. The primary y axis expresses the composite depth of the record, the secondary y scale expresses the age model. The labels on the right indicate the identity and stratigraphic span (black dashed horizontal lines) of each chironomid assemblage zone. Also shown is the reconstructed mean summer temperature (SmT) using the weighted averaging partial least squares model (WAPLS).

4.5. Discussion

4.5.1. Vegetation and fire history

The Lake Von pollen and charcoal records allow examination of vegetation and fire-regime change in the southwestern South Island during the last ~18,000 years. Between ~18.0 and ~10.8 ka, the palynology of Lake Von is dominated by small shrubs (*Coprosma*, Asteraceae Asteroideae), accompanied by herbs (Poaceae), ferns (*Blechnum* type, *Cyathea*, *Hypolepis*, *Asplenium*, *Histiopteris* type, *Lycopodium* type), low abundance of arboreal pollen (*Metrosideros*, *Myrsine*, conifers) and lack of macroscopic CHAR with variability in the structure and composition of the vegetation at millennial-time scales (Figures 4.4 and 4.9). The initial millennia of this deglacial interval features a gradual and persistent increase in the low-growing small shrubs *Coprosma* and a sustained decline in Poaceae, which started at ~18.0 ka. Both taxa are abundant in modern alpine environments and grasslands located on the eastern flank of the Southern Alps in the southern South Island (Wardle, 1991). During the initial stages of the *Coprosma* rise between ~18.0 and 16.7 ka, I observe the highest abundance of ferns dominated by species of the water-demanding *Blechnum* (mean: ~48%) and very low organic matter content (<7%) (Figure 4.2) suggesting low aquatic biological productivity. Species of the genus *Blechnum* (e.g. *Blechnum penna-marina*, *Blechnum discolor*) commonly are found in sub-canopy gaps, forest margins and alpine environments in the southern South Island (Mark and Bliss, 1970; Wardle, 1964, 1991). I also note low abundance of arboreal pollen with the presence in relatively low/trace abundances of the conifers *Podocarpus*, *Prumnopitys taxifolia*, *Prumnopitys ferruginea*, *Dacrydium cupressinum* and *Phyllocladus* (Figure 4.9). Because these conifer species generally produce large amounts of pollen that can be dispersed long-distances from their source, their presence in comparatively low amounts likely represents an extra-local signal. In sum, I interpret these data as the colonization of the recently deglaciated landscape by communities dominated by *Coprosma* with cold-resistant herbs and ferns probably from alpine environments between ~18.0 and ~16.7 ka.

Between ~16.7 and 14.8 ka, *Coprosma* and Poaceae show the culmination of their increasing and declining trends respectively, that had begun in the previous interval (Figure 4.9). At the same time, the record shows a rapid decline in *Blechnum*, relatively low and stable abundances in Asteraceae Asteroideae and *Myrsine*, the disappearance of conifers and an

increasing trend in organic matter content (Figures 4.2 and 4.9). Taken together, these trends point to an expanded vegetation cover and increased biomass as *Coprosma*-dominated communities expanded along with low abundance of other shrubs, herbs and ferns taxa characteristic of alpine environments. A notable feature in this interval is the appearance and rise of the tree *Metrosideros* (probably *Metrosideros umbellata*) and the tree-fern *Cyathea* (probably *Cyathea smithii* type) (Figure 4.9). Interpretation of *Metrosideros* and *Cyathea* rises requires understanding the ecology and predominant controls on the distribution of these taxa occurring in the modern plant communities in the southern South Island. Species of the genus *Metrosideros* produce pollen grains that have limited dispersal capability (Allen et al., 2002; Randall, 1991); its under-representation in modern pollen rain may be explained by its ornithophilous and entomophilous (bees) pollination strategy (Allen et al., 2002; Godley, 1979). Thus, the presence of pollen from these species in the Lake Von pollen record, even in very low or trace abundances, is indicative of local occurrence. In particular the broadleaved *Metrosideros umbellata* (southern rata) is a drought-intolerant cold-resistant angiosperm tree, commonly found in montane and sub-alpine environments with high humid conditions in western sectors of the South Island (Wardle, 1971; Wilmshurst et al., 2007). Tree-ferns of the genus *Cyathea* produce abundant small spores that are readily dispersed by wind and water (Large and Braggins, 1990), thus, its presence in the pollen record may represent local and/or extra-local signals. *Cyathea smithii* is a cold-resistant water-consuming species that commonly grows under tall podocarp, beech, kānuka and broadleaved forest, occurring from lowland up to sub-alpine environments mostly west of the main divide (Brownsey and Perrie, 2014). Given these characteristics, the prominence of *Metrosideros* and *Cyathea* between ~16.7 and ~14.8 ka suggests their local presence which, in the context of pollen assemblages, indicate a transition from an open alpine landscape toward a more highly vegetated landscape dominated by shrubs likely from sub-alpine environments with isolated patches of subalpine-montane vegetation. The increase in woody vegetation, notably *Metrosideros* along with tree ferns, suggest a rise in the tree line.

The palynology of Lake Von records a modest increase in Poaceae at the expense of *Coprosma* between ~14.8 and 12.6 ka. This was concurrent with a slight decline in *Myrsine*, a minor increase in the *Blechnum*, increases in Asteraceae Asteroideae and the water-demanding but cold resistant tree *Metrosideros* (*Metrosideros umbellata*) which achieved their maximum

abundances coeval with *Cyathea* (*Cyathea smithii* type) in a ~2% plateau and stabilization of organic matter content (Figures 4.2 and 4.9). These data suggest a reversal of pre-existing trends towards a relatively more open landscape and the spread of sub-alpine/alpine cold-tolerant trees, shrubs, herbs and understory ferns near Lake Von. This period was followed by a recovery in *Coprosma* between ~12.6 and 10.8 ka, contemporaneous with gradual declines in Poaceae and *Blechnum*, major increases in the tree-fern *Cyathea* and the tree-shrub *Myrsine*, abrupt drops in Asteraceae Asteroideae, *Metrosideros* and in the rest of ferns (*Hypolepis*, *Asplenium*, *Histiopteris* type, *Lycopodium* type) and the resumption of the deglacial rising trend in organic matter content (Figures 4.3 and 4.9). These results indicate the return of a more extensive and likely closed canopy vegetation cover dominated by *Coprosma*, accompanied by other small trees and shrubs, and declines of the subalpine-montane trees *Metrosideros* and cold-tolerant alpine shrubs.

An abrupt increase in arboreal pollen started at ~10.8 ka with a prominent rise in the pollen percentages of the conifer shrub-tree *Halocarpus* (probably *Halocarpus bidwillii*, as it is found in the region today), accompanied by slight increases in the tall warm-temperate conifers *Podocarpus*, *Prumnopitys taxifolia*, *Prumnopitys ferruginea* and *Dacrycarpus*. This was contemporaneous with abrupt declines in the small-shrub *Coprosma* and the tree-fern *Cyathea*, the virtual disappearance of the cold-resistant and drought-intolerant *Metrosideros*, the understory water-demanding *Blechnum* and most other ferns and herbs (Figure 4.9). This was followed by a rapid and prominent rise in the conifer tree *Phyllocladus* (probably *Phyllocladus alpinus*, as it is currently found growing close to the site) at ~10.1 ka at the expense of *Halocarpus,* continuing as the dominant taxon until ~7.2 ka and accompanied by low abundance in *Halocarpus* and the tall conifers *Podocarpus*, *Prumnopitys taxifolia*, *Prumnopitys ferruginea* and *Dacrycarpus*, and contemporaneous with an increase in macroscopic CHAR (Figure 4.6). Thus, these data indicate a sudden species turnover from a landscape dominated by small shrubs and herbs toward a conifer-dominated landscape, with increased fire activity at the beginning of the Holocene. A clue to interpreting this conifer-dominated interval involves the autecology of these taxa occurring in this sector of the South Island. On the one hand, conifer species produce large quantities of bisaccate (*Halocarpus*, *Phyllocladus*, *Podocarpus*, *Prumnopitys taxifolia*, *Prumnopitys ferruginea*) and trisaccate (*Dacrycarpus*) pollen grains which are generally susceptible to long-distance transport, hence,

the abundance of these species during this period might represent a combination of signals derived from local and extra local populations. On the other hand, the highly cold-tolerant *Halocarpus* (*Halocarpus bidwillii*) and *Phyllocladus* (*Phyllocladus alpinus*) trees occur in upper montane environments up to the treeline and in eastern sectors of the main divide of the Southern Alps with low precipitation levels (Sakai and Wardle, 1978; Wardle, 1991). In contrast, the more temperate *Podocarpus*, *Prumnopitys taxifolia*, *Prumnopitys ferruginea* and *Dacrycarpus* trees commonly are found in lower sectors along the western slopes of the Southern Alps (Wardle, 1991). Thus, high percentages of *Halocarpus* and *Phyllocladus* in the pollen record between ~10.8 and ~7.2 ka may represent a local signal originating from local subalpine woody communities combined with population located in the eastern slopes of the Southern Alps, with temperate conifers developing and expanding likely in lower sectors distal to Lake Von suggesting a regional upward shift in the tree-line at this latitude of the Southern Alps.

I observe a sustained increase in the cool-temperate silver beech *Lophozonia menziesii* between ~7.2 and ~3.7 ka along with the evergreen drought-intolerant conifer *Dacrydium cupressinum*, and contemporaneous with a decline in *Phyllocladus*, relatively low abundance in *Halocarpus*, persistence and high variability of the tall warm-temperate conifers *Podocarpus*, *Prumnopitys taxifolia*, *Prumnopitys ferruginea* and *Dacrycarpus* and low-magnitude macroscopic CHAR (Figures 4.6 and 4.9). These results indicate a shift from a conifer-dominated subalpine landscape toward a more complexly- vegetated landscape with small and tall conifers and expansion of beech tree species with relatively low fire activity. *Lophozonia menziesii* occurs from sea level to the timberline, but frequently is found in high elevation close to the modern treeline on the wetter western slopes of the Southern Alps (Stewart et al., 1996), therefore its presence in the pollen record may represent an upward expansion. Hence, I posit that *Halocarpus* and *Phyllocladus* were confined in the highest sectors of the Southern Alps, while cool-temperate beech trees developed in mid-elevation sectors and warm-temperate podocarps species dominated in lower sectors along the west coast of the southwestern South Island.

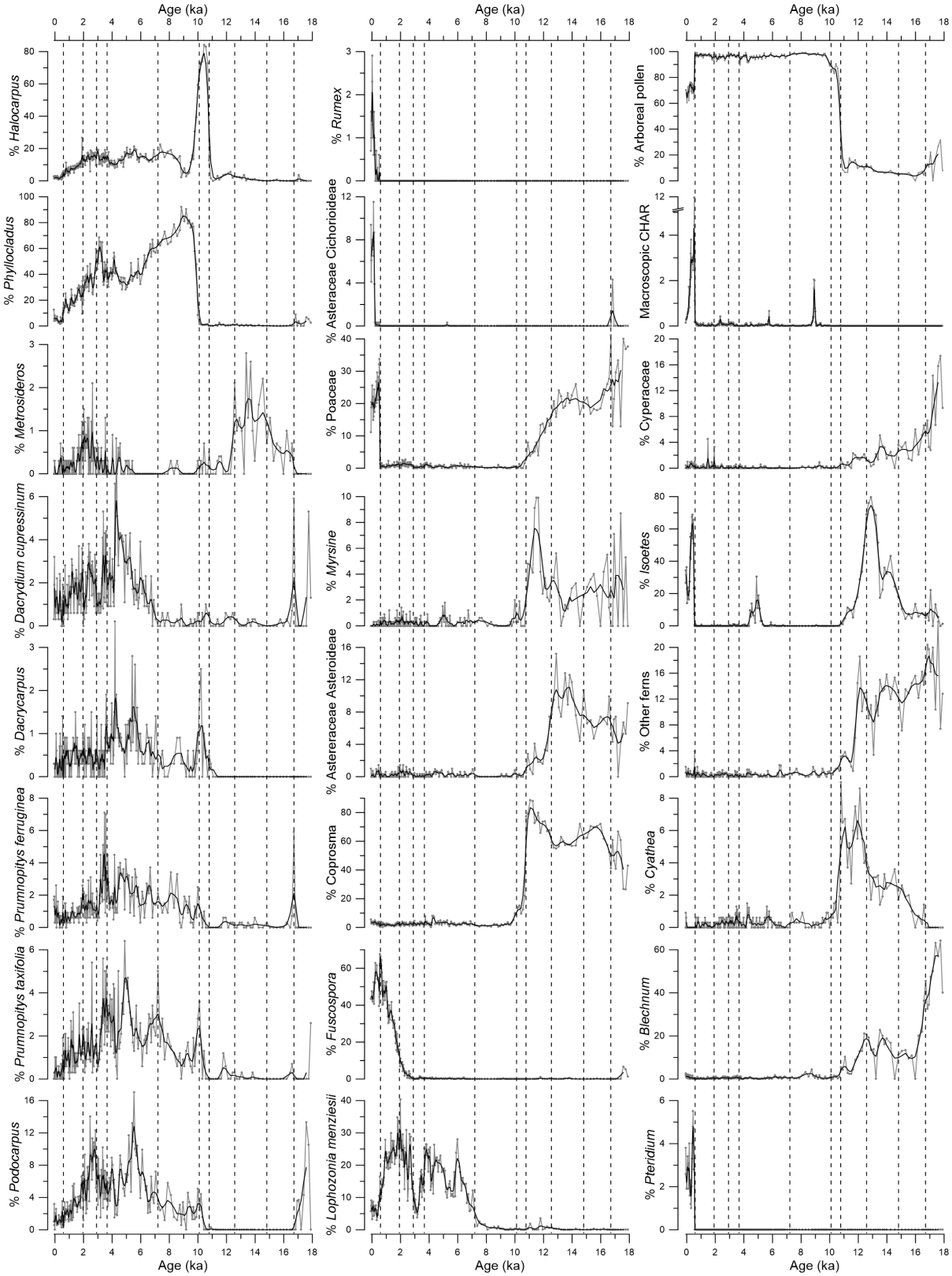

Figure 4.9. Selected pollen taxa form the Lake Von record expressed on an age scale. I calculated a weighted moving average (black lines) from the raw percentage data (light gray lines). The dashed vertical lines indicate major changes in the pollen stratigraphy described and discussed in the main text.

The pollen record shows a prominent decline in the cool-temperate silver beech *Lophozonia menziesii* between ~3.7 and ~2.9 ka, contemporaneous with a conspicuous rise in *Phyllocladus*, relatively low abundance in the cold-resistant and drought-intolerant *Metrosideros*, a marked decline in *Dacrydium cupressinum* and variability in the tall conifer trees *Prumnopitys ferruginea*, *Prumnopitys taxifolia*, *Dacrycarpus* and *Podocarpus*. This was followed by a rapid increase in *Lophozonia menziesii* between ~2.9 and ~1.9 ka, along with a slight increase in the other beech trees *Fuscospora* (in this locality, most likely mountain beech) and accompanied by rises in *Dacrydium cupressinum* and *Metrosideros*, a decline in *Phyllocladus* and relatively low abundance in tall conifers. I also note peak fire activity between ~3.3 and ~2.4 ka (two statistically significant events) (Figure 4.6). Thus, these findings indicate a short-lived increase in subalpine conifers between ~3.7 and ~2.9 ka, followed by the expansion of cool-temperate silver beech forests between ~2.9 and ~1.9 ka.

A sustained increase in *Fuscospora* (probably mostly mountain beech) between ~1.9 and ~0.56 ka, was concurrent with a decline in the silver beech *Lophozonia menziesii*, a decrease in the drought-intolerant and cold-resistant *Metrosideros*, declines in small and tall conifers and lack of macroscopic CHAR (Figures 4.6 and 4.9). As alluded earlier, the palynomorph *Fuscospora* probably represents the species *Fuscospora solandri* var. *cliffortioides* (mountain beech) because other *Fuscospora*-type species such as *Fuscospora solandri* var. *solandri*, *Fuscospora fusca* and *Fuscospora truncata* are either absent or are limited to small populations in southernmost South Island (Wardle, 1991). *Fuscospora solandri* var. *cliffortioides* is widely distributed in a range of climatic regimes associated with high altitude and thus cooler temperatures and relatively pure forests of this species dominate in the drier eastern slopes of the Southern Alps (Stewart et al., 1996). Therefore, I interpret this pollen assemblage as a shift from a landscape co-dominated by cool-temperate silver beech and small and tall conifers toward a landscape dominated by mountain and silver beech forests. Because Lake Von is located ~55 km east of the Alps divide, I posit that the species *Fuscospora solandri* var. *cliffortioides* probably occurred on the eastern flanks of the Southern Alps near the study site.

Finally, I observe an abrupt increase in Poaceae at ~0.56 ka along with the herbs *Rumex* and the opportunist ferns *Pteridium esculentum*, and concurrent with an abrupt decline in arboreal pollen but with the prevalence and dominance of the mountain beech *Fuscospora*

and peak macroscopic CHAR (three statistically significant events) (Figures 4.6 and 4.9). These findings indicate a forest opening and increased fire activity associated with large-scale landscape clearance attributable to human disturbance (early Polynesian), leading to the increase and expansion of opportunist species near to Lake Von during the last millennial.

4.5.2. Paleohydrologic balance

The Lake Von pollen record shows conspicuous changes in the abundance of the aquatic lycopsid *Isoetes* (likely *Isoetes alpina* given its modern distribution) (Figure 4.10). Species of the genus *Isoetes* (quillwort), in particular *Isoetes alpina* , forms a distinctive vegetation zone at the deepest edge of the turf communities in South Island lakes, usually growing in water between 1 to 4 m depth, although in exceptionally clear New Zealand lakes quillwort has been recorded to depths of up to 12 m (Hawes et al., 2003). Hence, shifts in the abundance of *Isoetes* in the palynological record of Lake Von can be representative of variations in the extent and/or proximity of relatively shallow environments to the coring site which, in this study, correspond to the deepest part of the lake. The pollen record shows relatively low abundance of *Isoetes* between ~18.0 and ~14.8 ka, followed by its sustained increase toward maximum abundance between ~14.8 and ~12.6 ka. A subsequent decline in *Isoetes* between ~12.6 and ~10.8 ka culminated in its virtual disappearance between ~10.8 and ~0.54 ka with a short-lived rise between ~5.3 and ~4.4 ka. I observe an abrupt and prominent increase in *Isoetes* between ~0.54 and ~0.24 ka, followed by a rapid, low-magnitude decline between ~0.24 and ~0.03 ka, and a final modest increase during the last ~30 years (Figure 4.10).

As illustrated in Figure 4.7 the modern abundance of *Isoetes* spores obtained from sediment-water interface samples shows a positive relationship with water depth. From these results, together with the observed depth range and habitat of *Isoetes alpina*, I suggest that the abundance of the species *Isoetes* in the pollen record of Lake Von can be invoked as a qualitative proxy for lake level fluctuations over time at this site. On this basis, I interpret these results as relatively low lake levels between ~18.0 and ~14.8 ka, relatively high lake levels between ~14.8 and ~12.6 ka, decreased lake levels between ~12.6 and ~10.8 ka, major decline in lake levels between ~10.8 and ~0.54 ka with a short-lived interval of increasing lake levels between ~5.3 and ~4.4 ka, a rapid lake level rising at ~0.54 ka persisting with little

variations until the present. From this discussion I propose that high lake levels led to the inundation of extensive flatlands in the periphery of Lake Von, generating suitable habitat for the establishment and expansion of *Isoetes*. On the contrary, a lake level lowering led to the aerial exposure and reduction of extensive low-lying marginal areas where *Isoetes* can grow.

I note the inferred lake level rising at ~0.54 ka was synchronous with increases in Poaceae values, the opportunist fern *Pteridium* and the herbs *Rumex*, and a decline in arboreal pollen and fire activity (Figures 4.6 and 4.9) indicative of anthropogenic disturbance, consistent with evidence of regional Polynesian and European settlement (McWethy et al., 2010; Ogden et al., 1998; Perry et al., 2014). I posit that deforestation may have affected the hydrology of Lake Von, thus, the increase in lake levels at ~0.54 ka may have been induced by human disturbance rather than climate influence.

4.5.3. Paleoclimate inferences

The Lake Von records reveal past hydrological and climatic changes from centennial to multi-millennial timescales in the southwestern South Island during the last ~18,000 years. The pollen record shows the rapid establishment of alpine vegetation dominated by cold-tolerant shrubs, herbs and ferns between ~18.0 and ~16.7 ka. This was followed by a gradual transition toward *Coprosma*-dominated subalpine vegetation with local occurrence of the subalpine/montane cold-resistant and drought-intolerant tree *Metrosideros* and the cold-tolerant hygrophilous tree fern *Cyathea* between ~16.7 and ~14.8 ka (Figure 4.9), in the context of relatively low lake levels (Figure 4.10). Therefore, these data suggest an initial phase with cool temperature under relatively humid conditions between ~18.0 and ~16.7 ka, followed by cold-temperate conditions and a modest increase in precipitation between ~16.7 and ~14.8 ka that maintained relatively low lake levels or below threshold levels for the expansion of *Isoetes*. Furthermore, the reconstructed SmT shows a rising trend starting at ~18.0 ka (Figure 4.8), which, in conjunction with the vegetation-inferred temperature trend, I interpret as warm summer temperatures and less severe winter following the onset of T1.

Between ~14.8 and ~12.6 ka, I observe an increase in vegetation indicative of alpine environments (Poaceae, Asteraceae Asteroideae, ferns) at the expense of *Coprosma* (Figure 4.9), suggesting a modest lowering in the treeline in response to a decline in temperature.

Because this interval also shows a major increase in the cold-tolerant hygrophilous *Metrosideros* and a rapid rise in lake levels (Figure 4.10), I interpret enhanced precipitation during this cooler interval. I note a contrast between vegetation-inferred overall temperature decline and chironomid-based summer temperature during this interval (Figure 4.8). I posit that increased seasonality (warmer summer and colder winter) established at ~14.8 ka, suggesting that changes in dryland vegetation may be reflecting shifts in winter temperature coupled with enhanced precipitation between ~14.8 and ~12.6 ka.

The increase and dominance of *Coprosma* between ~12.6 and ~10.8 ka, along with a major decline in vegetation characteristic of alpine environments (Poaceae, Asteraceae Asteroideae, ferns) mark the resumption of deglacial warming. This interval also shows a rapid decline in the cold-tolerant drought-tolerant *Metrosideros* and lower lake-levels (Figures 4.9 and 4.10), interpreted as a decline in precipitation. The SmT shows a marked decline during this interval (Figure 4.8), suggesting that declines in cold-resistant vegetation were driven by competition from species that benefit from milder winter temperatures, or from reduced precipitation, or both.

The palynology of Lake Von indicates conspicuous increases of the subalpine cold-tolerant conifers *Halocarpus* and *Phyllocladus* at ~10.8 and ~10.1 ka, respectively (Figures 4.9). Because the warm-temperate tall conifers *Podocarpus*, *Prumnopitys taxifolia*, *Prumnopitys ferruginea* and *Dacrycarpus* also rose during this interval, I interpret a warming, which led to the upward expansion of *Halocarpus* and *Phyllocladus* remaining as the dominant local species and confined probably in cool subalpine environments close to Lake Von. Concurrently, tall temperate podocarp species (*Podocarpus*, *Prumnopitys taxifolia*, *Prumnopitys ferruginea*, *Dacrycarpus*) likely expanded in lowlands in the eastern slopes of the Southern Alps distal to Lake Von. The rise of the drought-tolerant *Prumnopitys taxifolia* during this interval, along with the virtual disappearance of the cold-tolerant and drought-intolerant *Metrosideros* and lower lake levels than during the previous interval (Figure 4.10), suggest a major decline in precipitation at the beginning of the Holocene. Because *Phyllocladus* is less tolerant of low temperature than *Halocarpus* (Sakai and Wardle, 1978), I posit that an upward shift in the tree-line occurred in response to a multimillennial-scale rise in temperature at ~10.8 ka with a two-phase warming event that lasted until ~7.2 ka. Its initial phase, during the *Halocarpus* increase between ~10.8 and ~10.1 ka, features warm and reduced precipitation.

The second phase, during the *Phyllocladus* rise between ~10.1 and ~7.2 ka, shows a major increase in temperature and persistence of reduced precipitation. Within this interval I also note the highest reconstructed SmT values (Figure 4.8), suggesting that the establishment of very warm summers led to the expansion of temperate tall conifers at this latitude of the Southern Alps, albeit probably at lower elevations than at Lake Von, judging by the low pollen percentages.

I observe that macroscopic CHAR rose slightly between ~10.0 and ~9.1 ka, followed by an abrupt increase between ~9.1 and ~8.7 ka (two statistically significant events) (Figure 4.6). Previously, macroscopic CHAR had been absent between ~18.0 and ~10.0 ka. At this time the pollen assemblages were dominated primarily by small shrubs and herbs and with low arboreal pollen abundance between ~18.0 and ~10.8 ka under persistent precipitation. This period was followed by interval dominated by the small-trees *Halocarpus* between ~10.8 and ~10.1 ka (Figure 4.9) under inferred reduced precipitation. Increased fire activity in Lake Von was concurrent with *Phyllocladus*-dominated interval established by ~10.1 ka, coeval with a reduction in precipitation, warm conditions and the highest SmT values. Hence, these results indicate a correspondence between increases in the magnitude and frequency of local fires, woody fuel, precipitation and temperature. The combination of warm, dry summers and woody vegetation prone to desiccation provided ideal conditions for the increased prevalence of wildfire observed at the beginning of the Holocene.

The cool-temperate silver beech *Lophozonia menziesii* rose to prominence between ~7.2 and ~3.7 ka, along with the hygrophilous conifer *Dacrydium cupressinum* and relatively low abundance but with high variability presence of pollen from the warm-temperate tall conifers (*Podocarpus*, *Prumnopitys taxifolia*, *Prumnopitys ferruginea*, *Dacrycarpus*) (Figure 4.9). *Dacrydium cupressinum* occurs frequently from sea level to ~300-400 m.a.s.l. in the southern South Island over a very wide climatic range but is restricted to moist sites in areas with low rainfall (Franklin, 1968). Given the fact that *Lophozonia menziesii* and *Dacrydium cupressinum* grow in humid environments along the western slopes of the Southern Alps (Franklin, 1968; Norton et al., 1988), local or not, I interpret their increases between ~7.2 and ~3.7 ka as shift toward increased precipitation under relatively cold conditions; *Lophozonia*, locally and *Dacrydium* at lower elevations. Within this multi-millennial-scale interval, I detect low-magnitude centennial-scale declines in *Lophozonia menziesii* and *Dacrydium cupressinum*

between ~6.0 and ~5.2 and ~4.4 and ~4.1 ka, concurrent with increases in the drought-tolerant *Prumnopitys taxifolia* (Figure 4.9). Thus, superimposed upon this multi-millennial interval of increased precipitation, I suggest low-magnitude events with reduced precipitation between ~6.0 and ~5.2 and ~4.4 and ~4.1 ka, alternating with periods of increased precipitation between ~7.2 and ~6.0 ka, ~5.2 and ~4.4 ka, concurrent with a short-lived lake level rise between ~4.1 and ~3.7 ka. Considering these changes occurred in a context of low lake levels between ~7.2 and ~3.7 ka, I suggest that precipitation changes were insufficient in magnitude to trigger palynologically discernible changes in *Isoetes* indicative of lake levels variability. I also note low frequency and magnitude of local fires coeval with these centennial-scale intervals mentioned above (Figure 4.10), suggesting that high variability in precipitation drove wildfires near Lake Von. This interval also features a declining trend in the reconstructed SmT values (Figure 4.8), suggesting that colder summers may have promoted the establishment and expansion of cool-temperate silver beech trees.

Lophozonia menziesii shows a conspicuous decline between ~3.7 and ~2.9 ka, coeval with a decrease in the hygrophilous tree *Dacrydium cupressinum* and a rapid increase in the subalpine conifer *Phyllocladus* probably expanding over eastern drier sectors of the Southern Alps. This was followed by a sustained increase in *Lophozonia menziesii* between ~2.9 and ~1.9 ka, accompanied by rises in the drought-intolerant *Metrosideros* and the hygrophilous *Dacrydium cupressinum*, contemporaneous with a decline in *Phyllocladus*. I interpret these findings as a decline in precipitation between ~3.7 and ~2.9 ka and likely warmer conditions than the previous interval, followed by a modest increase in precipitation and cooler conditions and persistent low lake levels between ~2.9 and ~1.9 ka. These vegetation changes were concurrent with a slight increase in summer temperature (Figure 4.8) and the occurrence of two local fires (two statistically significant events) (Figure 4.7), suggesting that warmer summers may have promoted the generation of fires in the vicinity of Lake Von even under humid conditions.

The Lake Von pollen record shows a rapid and prominent increase in *Fuscospora* between ~1.9 and ~0.56 ka at the expense of small and tall conifers and the drought-intolerant *Metrosideros*, contemporaneous with a slight decline in silver beech *Lophozonia menziesii*. Because the palynomorph *Fuscospora* probably represents the species *Fuscospora solandri* var. *cliffortioides*, trees that are frequently found in the eastern flanks of the Southern Alps

with low rainfall (Stewart et al., 1996), I Interpret these changes primarily as a decline in precipitation.

4.5.4. Regional and hemispheric paleoclimate implications

The Lake Von area was covered by the South Von glacier lobe during the LGM (Barrell, 2011). Local ice-free conditions have prevailed in this sector of the southern South Island since at least ~18.0 ka. Between ~18.0 and ~16.7 ka, the Lake Von record indicates rapid colonization and expansion of alpine vegetation and relatively low lake levels under cold and relatively humid conditions. I interpret these results as indicating a relatively low precipitation regime during the early portion of T1, suggesting moderate SWW influence in the Lake Von area and/or a southward shift of the SWW from their equatorward-displaced position during the LGM. This SWW shift was contemporaneous with the onset of deglacial warming and atmospheric CO_2 rise (Monnin et al., 2001) (Figure 4.10), lending support to the hypothesized role of the SWW as a driver of atmospheric CO_2 variations by modulating upwelling of CO_2-rich deep water in the Southern Ocean (Anderson et al., 2009; Toggweiler, 2009; Toggweiler et al., 2006).

Following the onset of T1, the Lake Von record indicates warmer conditions, a rise in summer temperatures and a slight increase in precipitation between ~16.7 and ~14.8 ka, revealed by an increase in *Metrosideros*, a shift from alpine to subalpine vegetation, higher SmT values and relatively low lake levels. I interpret these results as a modest increase in SWW influence, probably reflecting a northward shift or strengthening of the SWW over southern New Zealand. Recently, Anderson et al. (2018) reported stratigraphic and geochemical evidence for paleohydrologic changes from the same site studied in this thesis (Lake Von) spanning since ~16.0 ka. Unlike this thesis, Anderson et al. (2018) analyzed sediments cores collected from intermediate water depths in Lake Von (~5-m water depth vs ~15-m water depth for this study). These authors found three discontinuities in sediment accumulation at ~15.1, ~12.8 and ~12.2 ka (Figure 4.10), interpreted as relatively low lake levels. The first discontinuity in the Anderson's et al., (2018) record is contemporaneous with relatively low lake levels inferred in this thesis from the abundance of *Isoetes* between ~16.7 and ~14.8 ka (Figure 4.10), but concurrent with an inferred modest rise in precipitation. Thus, I posit that lake

levels were relatively dynamic, induced by higher temperature, especially during summer-time and under slightly more SWW influence. Such shifts were contemporaneous with a rise in temperature reported from records from New Zealand (Newnham et al., 2012; Vandergoes et al., 2008) and CO_2 rise (Monnin et al., 2001).

Increased precipitation, cooler conditions and increased seasonality in the Lake Von record between ~14.8 and ~12.8 ka, inferred from a rise in *Metrosideros*, expansion of alpine vegetation, and higher lake levels and SmT values, suggest an enhanced SWW influence equivalent in timing to the ACR. These results are in agreement with reconstructed-SWW influence and cooling inferred from terrestrial records from the South Island (Anderson et al., 2018; Hinojosa et al., 2019; McGlone et al., 2004; Vandergoes et al., 2008), contemporaneous with glacial readvances in the Southern Alps of New Zealand (Kaplan et al., 2013; Putnam et al., 2010; Sikes et al., 2013) and Western Patagonia (Moreno et al., 2009b; Moreno et al., 2012; Sagredo et al., 2011), and a halt in the deglacial CO_2 rise reported from Antarctic records (Monnin et al., 2001) (Figure 4.10). Hence, I posit that a strengthening and northward shift in the SWW might have diminished the stress on the surface of the Southern Ocean, reducing upwelling of CO_2-rich water, and, consequently, lowering of atmospheric CO_2 concentration.

This interval on enhanced SWW corresponding broadly to the ACR was followed by reduced precipitation, warmer conditions, probably less seasonality and a lowering of lake levels between ~12.8 and ~10.8 ka. Combined, these factors suggest a decrease in SWW influence. This was coeval with two disconformities detected in sediment cores obtained from shallower sectors of Lake Von indicative of low lake levels (Anderson et al., 2018) implying a reduction of the SWW influence in the southwestern of the South Island (Anderson et al., 2018; Hinojosa et al., 2019), and contemporaneous with glacial recession in the Southern Alps of New Zealand (Kaplan et al., 2010) and Western Patagonia (Moreno et al., 2009b; Moreno et al., 2012; Sagredo et al., 2011; Strelin et al., 2011), renewed Antarctic warming and resumption of the atmospheric CO_2 (Monnin et al., 2001). From this discussion, I suggest a poleward shift of the SWW that may have invigorated upwelling and release of the CO_2 to the atmosphere.

The transition from shrubs/grass-dominated landscape toward a landscape dominated by conifer broadleaf forest dominated by *Halocarpus* and *Phyllocladus* between ~10.8 and ~7.2 ka, along with lower lake levels, higher SmT and increased fire activity, suggest a major warming and more reduced SWW influence marking the beginning of the Holocene in Lake

Von. I note correspondence in timing and composition of vegetation changes with other palynological sites located in drier sectors east of the main topographic divide in the southern South Island (McGlone et al., 1995; McGlone and Moar, 1998; Vandergoes et al., 2008). In contrast, pollen records from sites located in wetter sectors south and west of Lake Von are dominated by tall warm-temperate podocarp forest characterized by *Prumnopitys taxifolia*, *Prumnopitys ferruginea*, *Dacrycarpus dacrydioides* and *Dacrydium cupressinum* (McGlone and Bathgate, 1983; Vandergoes et al., 1997; Wilmshurst et al., 2002). Differences in the composition of plan communities among sites, illustrate the marked rain shadow effect in the southern South Island of New Zealand, which was exacerbated by the warmer conditions, especially during summer, and less precipitation during the early Holocene. Warm and dry conditions have also been reported from other terrestrial records from the South Island (Anderson et al., 2018; Hinojosa et al., 2019; Vandergoes et al., 1997), concurrent with peak fire activity at global and sub-continental scale (Power et al., 2008; Whitlock et al., 2007). Similar results from other mid-latitude landmasses show reduced SWW influence throughout the southern mid-latitudes (e.g. Anderson et al., 2018; McGlone et al., 2019), suggesting a multi-millennial zonally symmetric decline in SWW strength at the commencement of the Holocene (Fletcher and Moreno, 2012).

The Lake Von record then shows a sustained decline in temperature, in particular during summer, and increase in precipitation between ~7.2 and ~3.7 ka, suggesting an increase in the SWW influence. Superimposed upon, and following, this multi-millennial climate trend I detect alternating dry and wet oscillations of millennial- and centennial-scale with low precipitation between ~6.0 and ~5.2, ~4.4 and ~4.1, ~3.7 and ~2.9, and ~1.9 and ~0.56 ka implying diminished SWW influence (Figure 4.10). Wet periods in the intervening intervals suggest increased SWW influence. Similar findings have been reported from Lago Cipreses in southwestern Patagonia in southern South America (Moreno et al., 2018b). They suggest changes in the amount of precipitation driven by centennial-scale SWW, indicating discrete decline in SWW influence at ~7.4 (CC10), ~6.0 (CC9), ~4.8 (CC8), ~4.1 (CC7), ~3.4 (CC6), ~3.1 (CC5), ~2.4 (CC4), ~1.6 (CC3), ~1.1 (CC2) ka and ~0.2 ka (CC1). I observe that five of these events (CC9, CC7, CC5, CC3 and CC2) overlap in timing with centennial-scale phases of reduced precipitation from the Lake Von record (Figure 4.10). Moreno et al. (2018b) attributed these changes to Southern Annular Mode (SAM)-like shifts at centennial timescale.

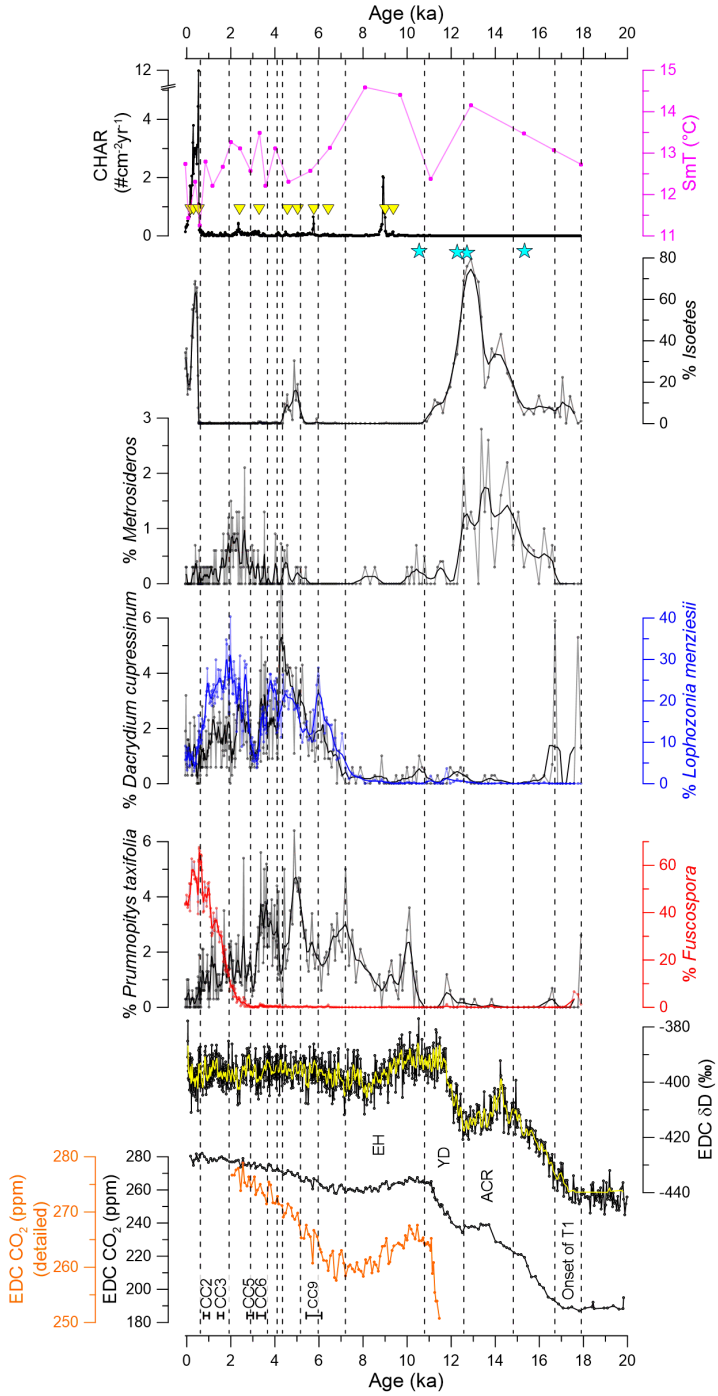

Figure 4.10. Comparison of selected terrestrial taxa (%*Fuscospora*, %*Prumnopitys taxifolia*, %*Lophozonia menziesii*, %*Dacrydium cupressinum* and %*Metrosideros*) and aquatic plants (%*Isoetes*), along with macroscopic CHAR, statistically significant charcoal peaks (yellow triangles) and SmT from Lake Von. Also shown are ice data from Antarctica over the last ~20,000 years (Jouzel and Masson-Delmotte, 2007; Monnin et al., 2001) and the timing of Cipreses cycles (CC-n, bars bellow the bottommost curve) (Moreno et al., 2018b). The dashed vertical lines constrain the timing of the main inferred climate changes from the Lake Von record, indicating the onset of the T1, Antarctic Cold Reversal (ACR), Younger Dryas chron (YD) and the early Holocene (EH). The light blue start indicate the timing of discontinuities detected in shallow sectors of Lake Von reported by Anderson et al. (2018).

Considering that SAM is the source of climate variability in western Patagonia (>~46°S) and southern South Island (Chapter 2, subsection 2.2.2), I postulate that precipitation variability in these sectors may represent a trans-Pacific response to centennial shifts in the SWW influence in the southern mid-latitudes during the Holocene.

4.6. Conclusions

1. Ice-free conditions emerged at Lake Von no later than ~18.0 ka, leading to the rapid colonization, establishment and expansion of shrubs, herbs and ferns characteristic of alpine vegetation under relatively cold and humid conditions between ~18.0 and ~16.7 ka. These developments suggest moderate SWW influence at the Lake Von area and/or a southward shift of the SWW.
2. The appearance of the drought-intolerant *Metrosideros* between ~16.7 and ~14.8 ka, along with rises in subalpine vegetation and SmT, suggest a rise in temperature and a modest increase in precipitation. I interpret these data as a modest increase in SWW influence, as a result of a northward shift or strengthening of the SWW following the onset of T1.
3. An increase in hygrophilous species, expansion of subalpine/alpine vegetation, and high SmT values and lake levels between ~14.8 and ~12.8 ka indicates a reversal to cold conditions with seasonality of temperature and an increase in precipitation. These changes suggest enhanced SWW influence, likely reflecting a northward shift of the SWW during the Antarctic Cold Reversal.
4. I detect warmer and drier conditions between ~12.8 and ~10.8 ka with milder winter, revealed by high abundance of subalpine vegetation, a decrease in *Metrosideros* and declines in lake levels and SmT. I interpret these findings as reduction in SWW influence as a result of a southward shift of the SWW during the Younger Dryas chron.
5. A further warming pulse and reduced precipitation occurred between ~10.8 and ~7.2 ka, revealed by a prominent rise in conifer broadleaf forests dominated by *Halocarpus* and *Phyllocladus*, the increase in the drought-tolerant *Prumnopitys taxifolia*, high fire activity and SmT, and lower lake levels. These results suggest a decline in SWW influence marking the commencement of the Holocene.
6. I detect alternating dry and wet oscillations of millennial- and centennial-scale with low precipitation between ~6.0 and ~5.2, ~4.4 and ~4.1, ~3.7 and ~2.9, and ~1.9 and

~0.56 ka implying diminished SWW influence at these times. Wet oscillations in the intervening interval suggest increased precipitation, interpreted as enhanced SWW influence.

7. Rapid deforestation and expansion of invasive and opportunist species, accompanied by fire activity at ~0.54 ka, marked the time of Polynesian settlement at the Lake Von area.

Chapter 5

Vegetation, fire and climate history in southwestern Patagonia (52°S) during the last 17,000 years

5.1. Abstract

I present a detailed pollen and charcoal record from Lago Pintito, Última Esperanza region, southwestern Patagonia, to examine the vegetation, fire, and climate evolution since the Last Glacial Termination (T1). I detect dominance of high Andean herbs and shrubs along with limited fire activity between ~17.0 and ~14.2 ka. A rapid increase of *Nothofagus* trees at ~14.2 ka led to the establishment and dominance of forests at ~12.8 ka. A subsequent increasing trend in *Nothofagus* is coeval with a rise in fire between ~12.5 and ~6.8 ka. A further distinctive increase of *Nothofagus* at ~6.8 ka led to closed-canopy forests that have remained extraordinarily resilient until the present, despite climate shifts and natural and human disturbances. Comparison between multiple paleovegetation reconstructions from Última Esperanza area reveals spatial variability in the development of *Nothofagus* forests during T1 that might have been forced by local megafaunal pressure until the beginning of the Holocene. I detect cold and dry conditions between ~17.0 and ~16.4 ka, followed by ameliorated temperatures and increased precipitation between ~16.4 and ~14.2 ka, and relatively wet conditions between ~14.2 and ~12.5 ka. Enhanced precipitation seasonality and/or variability between ~12.5 and ~11.4 ka, was followed by a prominent decline in precipitation between ~11.4 and ~6.8 ka. Centennial-scale alternating dry and wet phases starting at ~6.8 ka, comprise four dry intervals between ~5.8 and ~5.2, ~4.6 and ~3.7, ~3.3 and ~3.0, and ~1.0 and ~0.4 ka, and wet conditions in the intervening intervals. I posit variations in the influence of the Southern Westerly Winds (SWW) in southwestern Patagonia to explain these hydroclimatic changes. Millennial-scale shifts dominate the earlier part of the record, with diminished SWW between ~17.0 and ~16.4 ka, increased SWW between ~16.4 and ~14.2 ka, minor decline between ~14.2 and ~12.5 ka, enhanced SWW between ~12.5 and ~11.4 ka, major decline between ~11.4 and ~6.8 ka, and centennial scale SWW shifts during the last ~6800 years. Covariation in paleoclimate trends inferred from Lago Pintito record with western Patagonian records and Antarctic records since the beginning of T1 suggest a strong teleconnection between mid- and high-latitudes in the Southern Hemisphere.

5.2. Introduction

As discussed in Chapter 2 (subsection 2.2.1), the Southern Westerly Winds (SWW) are an important component of the atmospheric circulation of the middle latitudes of the Southern Hemisphere that directly interact with atmospheric pressures from subtropical and high-latitude regions (Sturman and Tapper, 2006). The SWW dominate the climate of continental landmasses between 30°S and 60°S, primarily through their effect on regional hydrology (Garreaud, 2007). Paleoclimate research over the last few decades has stressed the importance of the SWW in the generation of climate changes at different geographic and temporal scales (e.g. Moreno, 2004). Modelling and empirical studies have proposed that shifts in the SWW drove changes in global-deep water circulation and upwelling of CO_2-enriched deep waters in the Southern Ocean during glacial-interglacial transitions (Anderson et al., 2009; Denton et al., 2010; Toggweiler, 2009; Toggweiler et al., 2006) and the Holocene (last ~11.700 years) (Fletcher and Moreno, 2011; Moreno et al., 2010). Unfortunately, the paucity and ambiguity of available data for constraining past SWW activity in mid- and high-latitudes sectors of the Southern Hemisphere, limits our understanding of the behaviour of the SWW and their paleoclimate effects at hemispheric and global scales during and since the Last Glacial Termination (Termination 1=T1, ~18-11.7 ka; ka= 1000 calendar years before present; present= AD 1950).

Southwestern Patagonia (50-53°S; Figure 5.1), in southern South America (40-55°S), is a key region for deciphering past climate and SWW changes in the southern mid-latitudes, including their impact on vegetation, hydrology and fire occurrence. This region has witnessed repeated expansion and retreat of massive Andean glaciers originating from the Patagonian Ice Sheet (PIS) throughout the Quaternary. This glacial activity affected the landscape directly, promoting changes in the structure, composition and dynamics of the regional vegetation on ice-free sectors (Fesq-Martin et al., 2004; Heusser, 1995; Moreno et al., 2018b; Villa-Martínez and Moreno, 2007). Paleovegetation studies report a broadly coherent vegetation and fire history on both the western and eastern sides of the Andes Cordillera following ice recession during T1. These records indicate an initial phase with cold-tolerant herbs (Poaceae, *Acaena*, Asteraceae) and heath (*Empetrum rubrum*, Ericaceae), along with a low abundance of arboreal taxa (Markgraf and Huber, 2010). Subsequent increases in *Nothofagus* at various times (Figure 5.2, Table 5.1) led to woodland and forests which have persisted with little

variation until the present (Fesq-Martin et al., 2004; Fontana and Bennett, 2012; Huber et al., 2004; Markgraf and Huber, 2010; Moreno et al., 2018b; Villa-Martínez and Moreno, 2007; Wille et al., 2007). Whilst these vegetation trends during T1 and the Holocene are broadly consistent throughout the region, less coherence is evident in the timing, millennial-scale structure and climatic interpretations of these vegetation changes, highlighting heterogeneities in stratigraphic and chronologic control, time span, sampling resolution and variations in depositional settings within and among study sites (Table 5.1). The majority of these records are based on material collected from bogs or shallow lakes that have undergone terrestrialization, an aspect that affects their environmental sensitivity through time (Table 5.1). These depositional environments typically feature significant variations in sedimentation rates, alternation of subaqueous and subaerial deposition, and over-representation of local vegetation growing on the site surface, skewing the paleovegetation signal toward an extremely local record (Moreno et al., 2009a).

The few records not affected by these challenging depositional settings in southern Patagonia reveal our limited knowledge and understanding of past variations of the SWW from multi-millennial to centennial timescales. These studies identify SWW shifts during "critical" climatic states through T1, including stronger-than-present SWW influence coeval with regional glacial readvances during the Antarctic Cold Reversal (ACR: 14.6-12.9 ka) (Moreno et al., 2009b; Moreno et al., 2012; Strelin et al., 2011), and a further increase of the SWW during the Younger Dryas chron (YD: 12.9-11.5 ka) (Moreno et al., 2012). More problematic is the interpretation of SWW behaviour during the early Holocene (11.5-7.5 ka), with opposite views for either minimum (Moreno et al., 2010; Moreno et al., 2018b) or maximum (Lamy et al., 2010) SWW influence during this interval. According to Moreno et al., (2018) a subsequent increase in SWW influence started at ~7.5 ka followed by centennial-scale variations since ~5.5 ka. It is important to point out, however, that there are no continuous records from constant lacustrine depositional environments in continental sectors of Southwestern Patagonia that document paleovegetation and paleoclimate change spanning from the onset of T1 until the present.

Another poorly understood subject is the spatiotemporal dynamics of deciduous *Nothofagus* forests throughout Patagonia during and following T1. Their timing and pattern of spread along the eastern slopes of the Patagonian Andes has been of particular interest (Henríquez

et al., 2017; Moreno et al., 2019; Villa-Martínez et al., 2012), along with the sensitivity of forest communities to climate and varying disturbance regimes (fire, volcanic event, human) (Henríquez et al., 2015; Jara and Moreno, 2014). Compared with Central Patagonia (Moreno et al., 2019) and Tierra del Fuego (Mansilla et al., 2016, 2018; McGlone et al., 2010), where considerable advances in these issues have been forthcoming, the southwestern Patagonian sectors have not been satisfactorily addressed in the palynological literature. Additional high-precision palynological records from this region are fundamental for deciphering the timing and pattern of colonization, expansion and establishment of deciduous *Nothofagus* forests, and their resilience to climate changes and disturbance regimes, whether natural or anthropogenic.

Here I present detailed and continuous pollen, charcoal and stratigraphic records from sediment cores from Lago Pintito (52°2'39.82''S, 72°22'46.73''W, 170 m.a.s.l.), a small closed-basin lake located in the Última Esperanza area along the eastern slope of the Andean Cordillera of Chilean southwestern Patagonia (Figure 5.1). These data allow me to examine the vegetation, fire, and climate history of the region since 17 ka, and to consider important questions in relation to the issues raised above. In terms of climate: what was the timing and structure of climate change through T1?; is there evidence for climate reversals or accelerations at millennial timescales?; did the SWW exert a maximum or minimum influence during the early Holocene in Southwestern Patagonia?; did the SWW vary at millennial/centennial timescales during the Holocene? In terms of vegetation: when did the *Nothofagus* forests establish in Última Esperanza area?; what was the source of these species?; how did the forest communities respond to climate change and disturbance regimes during and since T1? To provide context for these particular questions, the next section reviews the study area and published palynological evidence for the postglacial history of *Nothofagus* in southern Patagonia.

5.2.1. Study area

Southwestern Patagonia (50-53°) features numerous channels, fjords, islands and archipelagos along the Pacific margin as a result of the tectonic subsidence of southern Patagonian Andes. This region also includes the Southern Volcanic Zone, featuring a number of active volcanoes with documented late-Quaternary and historical activity, such as Reclus, Burney and Aguilera (Stern et al., 2015; Stern, 2008). The southern Andes harbour numerous

glaciers and the southern Patagonia ice field (SPI) (Figure 5.1). These ice lobes have expanded and coalesced multiples times to form the SPI during the Quaternary glaciations, which extended for 1700 km over the Andes (38°-55°S) during the LGM (Glasser et al., 2008).

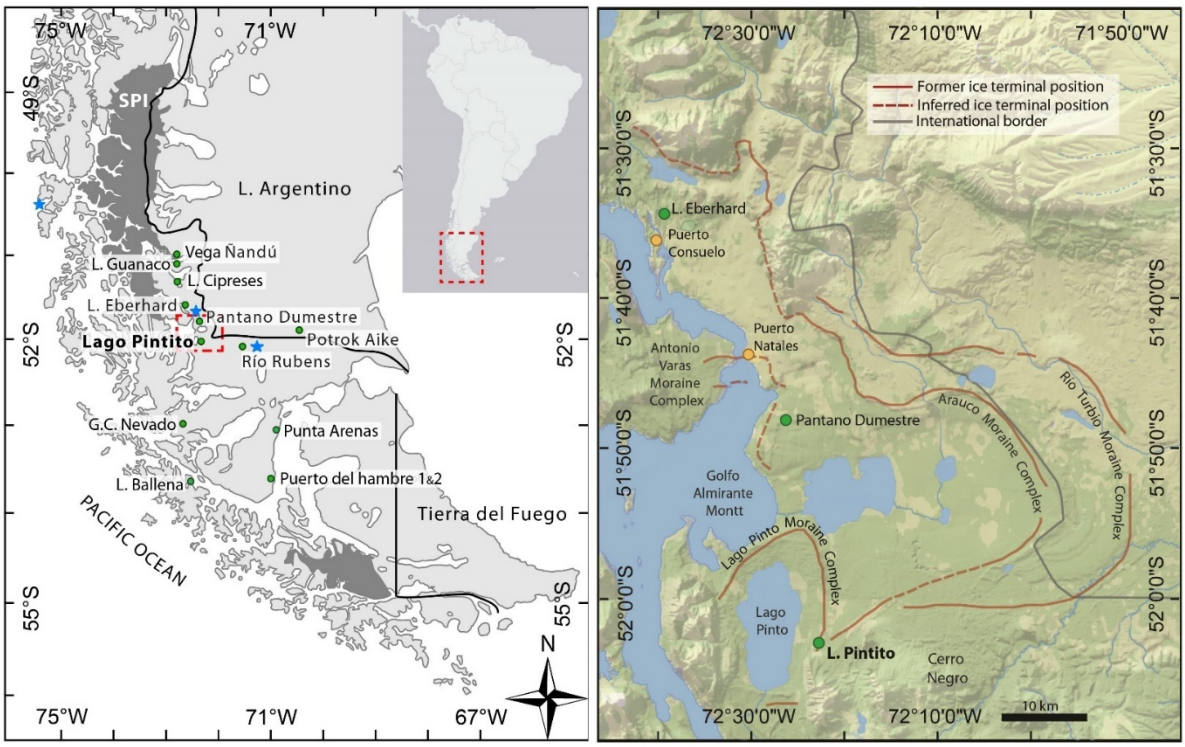

Figure 5.1. Left panel: Map of southwestern Patagonia showing the location of Lago Pintito, other sites mentioned in the text (green dots) and weather stations (blue stars; from east to west: Isla Guarello, Puerto Natales and Morro Chico stations). Right panel: Detail of the sector of Última Esperanza area indicating as a red line the position of terminal moraines based on Sagredo et al. (2011).

This study focuses on the site Lago Pintito, a small and shallow (1.5 m max. depth) closed-basin lake with a simple bathymetry, located in the Última Esperanza area. Stratigraphic, geomorphologic and geochronologic studies provide constraints on the timing and extent of outlet glacier lobes of the PIS through the LGM and T1 in the Última Esperanza area. These studies show at least two major glacial advances culminating at ~48.0 ka and ~33.9 ka, forming the Río Turbio moraines and the Arauco moraines, respectively (García et al., 2018a) (Figure 5.1). The Última Esperanza lobe remained in this position likely until ~17.0 ka, then thinned and abandoned the Arauco moraines leading to the formation of proglacial lake Puerto Consuelo (Sagredo et al., 2011). In its early stage, this proglacial lake reached elevations ranging between 150 and 125 m.a.s.l. and drained eastward through the Frontera meltwater

channels. During this stage the Lago Pinto ice lobe, which was a tributary of the Última Esperanza lobe during the LGM, stabilized and formed a medial/frontal moraine complex (Sagredo et al., 2011) (Figure 5.1). Lago Pintito is situated in an intermorainal depression of the Pinto moraine complex adjacent to Lago Pinto (Figure 5.1) in the Última Esperanza area. The surrounding vegetation consists of deciduous *Nothofagus* forests dominated by the species *N. pumilio* and *N. antarctica*, accompanied by understory herbs, shrubs and ferns (e.g. *Acaena* spp, *Berberis* spp, *Blechnum penna-marina*) and the European herbs *Rumex acetosella*.

Southwestern Patagonia constitutes the southernmost continental landmasses in the Southern Hemisphere capable of monitoring past changes in the SWW using terrestrial paleoenvironmental archives. Its climate is under the permanent influence of the SWW. Local precipitation shows a strong positive correlation with zonal wind speeds on the windward side of the Andes Cordillera (Garreaud, 2007), a relationship that even persists in sectors as far as 50-70 km to the east of the Andean divide (Moreno et al., 2018b). This relationship underpins my rationale to use palynological proxies to infer past changes in the amount and distribution of precipitation in southern Patagonia as a method for reconstructing SWW behaviour through time. The climate of the Última Esperanza area is transitional between the hyperhumid oceanic climates on the western coast and the semiarid, strongly continental climates east of the Andes. Meteorological records from the Pacific coast show an annual precipitation of 9000 mm (Isla Guarello, 50°23’S, 75°15’W), which significantly declines to 360 mm in the Morro Chico weather station (52°03’S, 71°25’W) (Figure 5.1). Local to Lago Pintito, meteorological records from Puerto Natales show a mean annual temperature between 6-7°C with an annual range of 9 to 10°C, and mean annual precipitation of 513 mm, achieving maximum amounts during March, April, August and November (Climatic explorer CR2, http://explorador.cr2.cl/).

These climate patterns are reflected in distinctive patterns of vegetation communities distributed along latitudinal, longitudinal and altitudinal transects throughout the region. The composition and distribution of the main vegetation units along a west-east transect are briefly described here, based on Roig et al. (1985): (i) Magellanic Evergreen Forest: This unit occurs mainly along temperate sectors of the archipelagos of central and southern Patagonia where annual precipitation ranges from 2000 to 6000 mm (<100 m.a.s.l). It is characterised

by the dominance of *Nothofagus betuloides*, along with the conifer *Pilgerodendron uviferum* and other trees such as *Raukaua laetevirens* (Araliaceae), *Drimys winteri* (Winteracae), and *Tepualia stipularis* (Myrtaceae). The shrubs *Desfontainia fulgens* (Desfontainiaceae) and *Embothrium coccineum* (Proteaceae) dominate near the forest edges, and the forest interior is dominated by *Berberis ilicifolia* (Berberidaceae), *Escallonia serrata* (Escalloniaceae), *Lebetanthus myrsinites* (Epacridaceae), *Phylesia magellanica* (Phylesiaceae), *Luzuriaga marginata* (Luzuriagaceae), and *Chilliotrichum diffusum* (Asteraceae), along with ferns *Blechnum penna-marina* (Blechnaceae), *Gleichenia quadripartite* (Gleicheniaceae), *Asplenium dareoides* (Aspleniaceae), *Hymenophyllum spp.* (Hymenophyllaceae) and *Grammitis magellanica* (Grammitidaceae). (ii) Magellanic Deciduous Forest: This forest community is distributed in cold sectors between 50 and 900 m.a.s.l. where annual precipitation is ~750 mm. It is dominated almost exclusively by the winter-deciduous *Nothofagus antarctica* and *Nothofagus pumilio*, the latter forming mixed forest with the evergreen tree *Nothofagus betuloides* in humid sectors. The species-poor shrub stratum develops only near the forest periphery, and includes *Berberis ilicifolia* (Berberidaceae), *Ribes magellanicus* (Grossulariaceae), *Chiliotrichum diffusum* (Asteraceae), *Escallonia serrata*, *Empetrum rubrum* (Ericaceae), *Maytenus disticha* (Celastraceae) and *Embothrium coccineum* (Proteaceae). The herbaceous understory is dominated by *Acaena ovalifolia* (Rosaceae), *Ozmorhiza depauperate* (Apiaceae), *Cardamine glacialis* (Brassicaeae), and the fern *Blechnum penna-marina* (Blechnaceae). (iii) Patagonian steppe: This unit is found in sectors with heightened continentality, where the mean annual precipitation is <400 mm. It is dominated by the species *Festuca gracillima*, accompanied by *Festuca magallanica*, *Stipa brevipes*, *Bromus unioloides* (Poaceae), *Acaena argentea*, *A. intergerrima*, *A. pinnatifida* (Rosaceae), *Adesmia pumila* (Papilionaceae), and *Arjona patagonica* (Santalaceae), along with common shrubs such as *Adesmia boronoides*, *Berberis buxifolia*, *Berberis empetrifolia*, *C. diffusum*, *Baccharis magallanica* (Asteraceae), *Mulinum spinosum* (Apiaceae), and *Verbena tridens* (Verbenaceae). (iv) Andean desert: This unit occurs above the *Nothofagus* forest under colder conditions (>1000 m.a.s.l.). It includes small patches of *Nothofagus pumilio* and dwarf shrubs such as *Escallonia rubra* and *Ribes cuccullatum*. The herbaceous cover is dominated by *Acaena magallanica*, *Pernettya pumilia* (Ericaceae), *Empetrum rubrum* (Empetraceae), *Senecio skottbergii* (Asteraceae), *Leuceria leonthopodioides* (Asteraceae), *Perezia megalantha*

(Asteraceae), *Nassauvia lagascae* (Asteraceae), *Agrostis canina* (Poaceae) and *Festuca pyrogea*.

5.2.2. Regional vegetation history

Palynological records published during the last few decades in southern Patagonia report varying ages for the presence, appearance and expansion of *Nothofagus* (southern beech) forests along the southern Patagonian Andes during T1 (Table 5.1). Leaving aside depositional and chronological differences between records, an early phase of herb and shrub dominance with low levels of *Nothofagus* (mean <10%) is evident in eastern sectors of the Andes Cordillera, but with different timing between sites: between ~12.6 and ~10.7 ka at Vega Ñandú (Villa-Martínez and Moreno, 2007), ~15.4 and ~12 ka at Lago Guanaco (Moreno et al., 2010), ~14.6 and ~12.1 ka at Lago Cipreses (Moreno et al., 2018b), ~12.7 and ~11.2 ka at Lago Eberhard (Moreno et al., 2012), ~14.6 and ~11.1 ka at Pantano Dumestre (Moreno et al., 2012), ~17.0 and~7.0 ka at Río Rubens (Huber et al., 2004) and ~16.0 and ~8.6 ka at Potrok Aike (Wille et al., 2007). *Nothofagus* pollen is completely absent at the northern sector sites of Rio Rubens between ~17.0 and ~15.9 ka and Potrok Aike between ~16.0 and ~15.5 ka. Similar assemblages are found in two sites located in the southern sector, with low abundance in *Nothofagus* (mean: <10%) before ~10.5 ka at Puerto del Hambre-1 (Clapperton et al., 1995) and ~12.5 ka at Puerto del Hambre-2 (Heusser, 1995). An exception to this pattern is the Punta Arenas pollen record which shows dominance of *Nothofagus* forests (>60%) between ~17.2 and ~16.6 ka, followed by its rapid decline and persistence in low abundance until ~10.3 ka (Heusser, 1995). The early high abundance of *Nothofagus* at Punta Arenas site, along with Puerto del Hambre-1 (~30% at ~17.8 ka) and Puerto del Hambre-2 (~30% at ~17.2 ka) sites, represent the oldest presence of *Nothofagus* woodland and forests along this region during T1.

Within the non-arboreal dominated period, there are unsustained ~20% increments in *Nothofagus* abundance between ~13.8 and ~13.2 ka at Pantano Dumestre, ~13.6 and ~13.3 ka at Río Rubens, ~13.6 and ~13.2 ka at Punta Arenas, ~12.3 and ~12.0 ka at Lago Guanaco, ~10.9 and ~10.7 ka at Vega Ñandú and ~8.6 and ~8.5 ka at Potrok Aike. Sustained ~20% rises in *Nothofagus* are evident between ~12.8 and ~12.1 ka at Lago Cipreses, ~11.3 and ~11.2 ka at Lago Eberhard, ~11.3 and ~11.1 ka at Pantano Dumestre, ~11.5 and ~11.0 ka at Río Rubens, ~11.7 and ~10.9 ka at Puerto del Hambre-1, ~12.8 and ~12.5 ka at Puerto del Hambre-2 and

~10.6 and ~10.3 ka at Punta Arenas. These phases in *Nothofagus* expansion eventually led to the permanent or intermittent establishment of *Nothofagus* woodland and forests (60-65% *Nothofagus* pollen) at ~11.5 ka at Lago Cipreses, at ~10.9 ka at Lago Eberhard, at ~10.5 ka at Pantano Dumestre, at ~6.8 ka at Río Rubens, at ~10.5 ka at Puerto Hambre-1, at ~9.0 ka at Puerto Hambre-2 and at ~5.8 ka at Punta Arenas (Figure 5.2, Table 5.1).

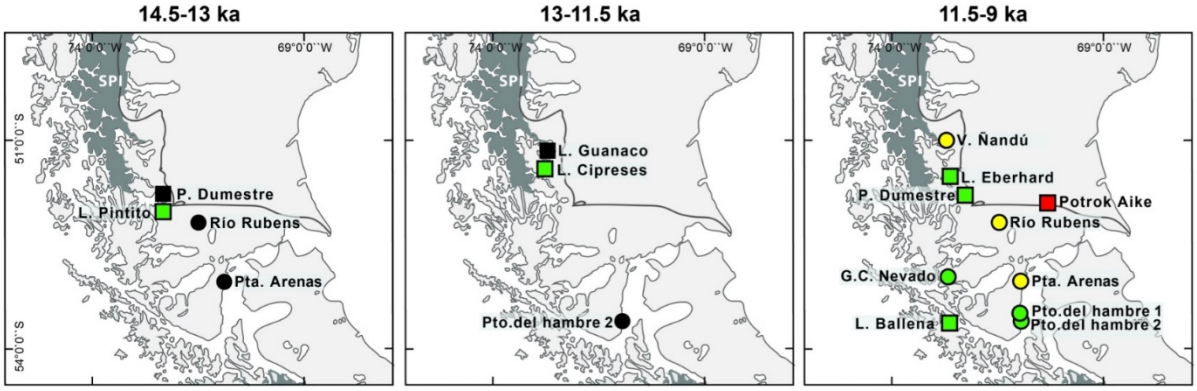

Figure 5.2. Geographic distribution of the establishment of *Nothofagus* forests preceded by an initial *Nothofagus* rise (~20% increment) during T1 and the early Holocene throughout Southwestern Patagonia. Also indicating the site type (lake: square, bog: circle), and the timing for the establishment of *Nothofagus* forests (green), the initial ~20% increase (black), the entrenchment of *Nothofagus* forests <9 ka (yellow) and forest-free sites (red).

Unlike the eastern sector of the southern Patagonian Andes, the western sector has only two palynological records to date. The pollen record from Gran Campo Nevado indicates low abundance of *Nothofagus* before ~10.9 ka (Fesq-Martin et al., 2004). The Lago Ballena pollen record shows the absence of *Nothofagus* between ~16.7 and ~14.5 ka (Fontana and Bennett, 2012), followed by its increase in the context of a landscape dominated by herbs and shrubs between ~14.5 and ~10.3 ka. There are sustained ~20% increases in *Nothofagus* between ~11.2 and ~10.9 ka at Gran Campo Nevado and ~11.1 and ~10.4 ka at Lago Ballena, followed by the establishment of *Nothofagus* woodland and forests (60-65%) at ~10.4 ka and ~10.0 ka, respectively (Figure 5.2).

To summarise, pollen records from eastern and western sectors of the southern Patagonian Andes suggest that the spread of *Nothofagus* might have occurred from *Nothofagus* forests located in the south-eastern sector of the Andes between ~17.8 and ~17.2 ka (Punta Arenas, Puerto del Hambre-1 and 2), expanding towards north-eastern sectors after ~15.9 and ~15.5

ka, and finally south-western sectors after ~14.5 ka. Nevertheless, there are significant heterogeneities between the sites in the timing and geography for the establishment of *Nothofagus* woodland and forests in Southwestern Patagonia during T1 and the beginning of the Holocene as well as its continuity until the present, subjects that remain unaddressed in the Patagonian literature.

Table 5.1. Synthesis of palynological sites located in Southwestern Patagonia, indicating site name, location, elevation, record type, number of radiocarbon dates, age rage of the pollen stratigraphy, the interpolated age for the establishment of *Nothofagus* forests (>60%), and the robustness of the chronologic control.

Site name	Location	Elevation (m)	Record Type	N° ^{14}C	Age Range (ka)	>60% ka	Chronologic control
Vega Ñandú (Villa-Martínez et al., 2012)	50°55'58.08''S, 72°46'03.72''W	200	bog sediment	12	0-12.6	2.4	Precise
Lago Guanaco (Moreno et al., 2009a; Moreno et al., 2009b)	50°59'53.16''S, 72°41'48.84''W	190	lake sediment	19	0-15.4	0.4	Precise
Lago Cipreses (Moreno et al., 2018b)	51°17'06.09''S, 72°51'12.58''W	110	lake sediment	23	0-14.6	11.5	Precise
Lago Eberhard (Moreno et al., 2012)	51°34'36.98''S, 72°40'4.27''W	70	lake sediment	12	10.4-12.7	10.9	Precise
Pantano Dumestre (Moreno et al., 2012)	51°48'13.83''S, 72°26'9.15''W	80	lake sediment (modern bog)	8	9-14.6	10.5	Broad
Lago Pintito (This study)	52°2'39.82''S, 72°22'46.73''W	170	lake sediment	16	0-17.0	13.0	Precise
Potrok Aike (Wille et al., 2007)	51°57'50.15''S, 70°22'27.64''W	112	lake sediment	17	0-16.0	No	Precise
Río Rubens (Huber et al., 2004)	52°4'39.95''S, 71°31'8.52''W	220	Bog sediment	19	0-17.0	6.8	Precise
Gran Campo Nevado (Fesq-Martin et al., 2004)	52°52'47.20''S, 72°55'38.15''W	70	Bog sediment	7	0-14.0	10.4	Broad
Punta Arenas (Heusser, 1995)	53°10'31.50''S, 70°56'35.43''W	75	bog sedimet	6	0-16.5	5.8	Broad
Puerto Hambre: 1 (Clapperton et al., 1995)	53°37'00.12''S, 70°52'00.12''W	5	bog sediment	7	0-18.0	10.5	Broad
Lago Ballena (Fontana and Bennett, 2012)	53°38'32.89''S, 72°26'40.88''W	70	lake sediment	8	0-16.7	10.0	Broad
Puerto Hambre: 2 (Heusser, 1995)	53°38'54.59''S, 70°57'55.18''W	5	bog sediment	6	0-18.0	9.0	Broad

5.3. Material and methods

Multiple overlapping sediment cores were obtained from the deepest sector of Lago Pintito (1.5 m water depth). I sampled and processed 1-cc and 2-cc sediment samples along continuous contiguous 1-cm thick sections for pollen and macroscopic charcoal analyses, respectively. The chronology of the records is constrained by 16 AMS radiocarbon dates of

bulk sediment sample (Table 5.2), because no macrofossils could be found. All procedures involved in the extraction and sampling of sediment cores, the development of the age model, the processing of pollen and charcoal samples, the calculation of the rates of change parameter (ROC) are described in chapter 2.

5.4. Results

5.4.1. Stratigraphy and chronology

The composite sedimentary record from Lago Pintito is 440 cm in length and comprises sections from the core series PS0606C (segment 1 to 3), PS0606D (segment 1), PS0606F (segments 1 to 2), and the water-sediment interface core PS1702SC1 (Figure 5.3). The lowermost portion consists of a basal unit of sands and gravel between 440 and 416 cm, followed by organic silts between 416 and 263 cm, a clastic layer between 262 and 259 cm, and organic-rich lake mud (gyttja) from 263 cm to the top of the record (Figure 5.3). The radiocarbon age-depth model (Table 5.2 and Figure 5.4), along with the sediment stratigraphy, suggest continuous sedimentation in a constant lacustrine environment over the last ~17,000 years. I found 4 tephra throughout the record: at 335-334 cm, 248-247 cm, 223-222 cm, and 148-147 cm composite depth, with interpolated ages of 4.4, 7.5, 8.9 and 14.7 ka, respectively, suggesting aerial fallout deposit from explosive events originating from V. Reclus (R1), V. Mt. Burney (MB1), V. Hudson (H1) and V. Mt. Burney (MB2) based on tephrochronostratigraphic correlation (Stern et al., 2015; Stern, 2008) and trace-element compositions for R1 (Sagredo et al., 2011).

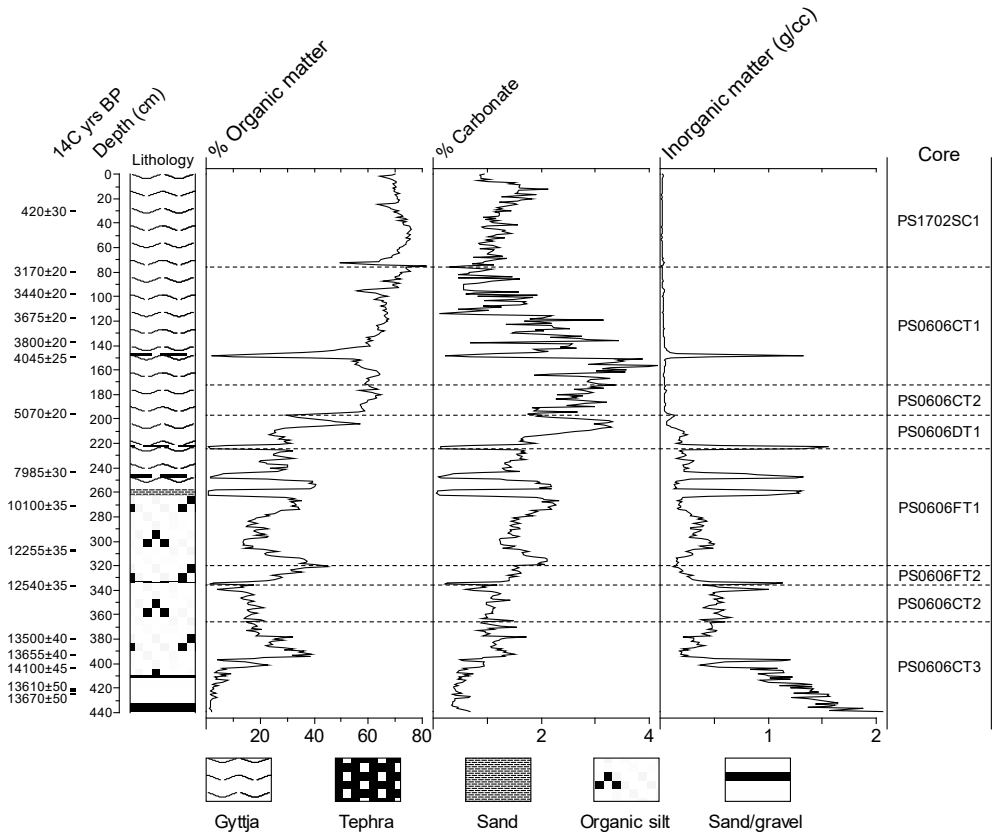

Figure 5.3. Radiocarbon dates, stratigraphic column, loss-on-ignition selected parameters and identity of the cores from the Lago Pintito record. Dashed horizontal lines represent core boundaries.

Table 5.2. Radiocarbon dates and calibrated ages of the Lago Pintito record. The calibration of the radiocarbon dates was made using the southern hemisphere datasets included in CALIB7.0.1.

Laboratory code	Core code	Depth (cm)	14C yr BP	±1 σ error	2σ range cal yr BP	Median probability cal yr BP
179763	PS1701SC1	30	420	30	326-503	457
171473	PS0606CT1	79	3170	20	3247-3442	3352
171474	PS0606CT1	97	3440	20	3570-3709	3642
171475	PS0606CT1	117	3675	20	3857-4078	3944
171476	PS0606CT1	137	3800	20	3991-4234	4120
171477	PS0606CT1	149	4045	25	4413-4567	4478
171478	PS0606CT2	194	5070	20	5662-5893	5809
179760	PS0606FT1	243	7985	30	8642-8980	8800
179761	PS0606FT1	270	10,100	35	11,347-11,795	11,579
179762	PS0606FT1	307	12,255	35	13,972-14,245	14,105
171481	PS0606CT2	326	12,540	35	14,344-15,051	14,734
171482	PS0606CT3	369	13,500	40	16,001-16,379	16,192
171483	PS0606CT3	382	13,655	40	16,213-16,624	16,400
171484	PS0606CT3	393	14,100	45	16,859-17,347	17,086
128981	PS0606CT3	411	13,610	50	16,145-16,579	16,343
128980	PS0606CT3	414	13,670	50	16,213-16,661	16,422

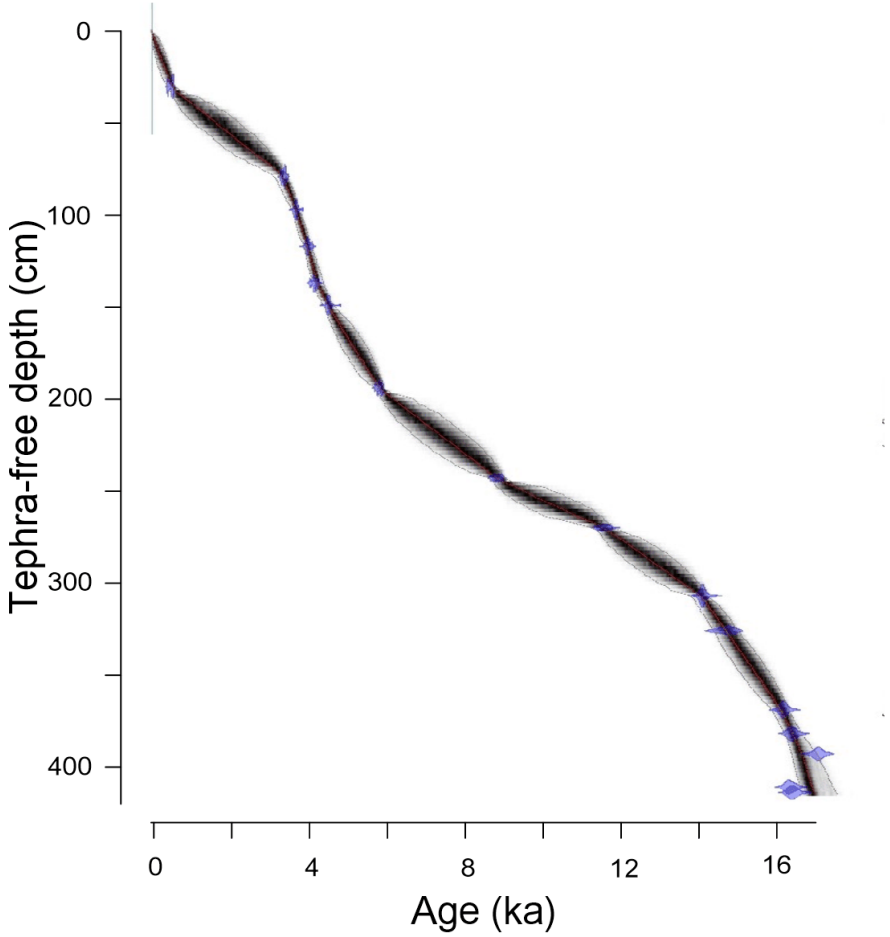

Figure 5.4. Age model of Lago Pintito record developed using Bacon. The probability distribution of each calibrated radiocarbon date is shown in blue, and the 95% confidence interval of the Bayesian age model is represented in grey.

5.4.2. Pollen record

The pollen record comprises 394 samples with a median time resolution of 33 years between adjacent samples (Figure 5.5). I was able to identify most of the palynomorphs to family or genus level, and in some cases to species level (*Empetrum rubrum*, *Gunnera magellanica*, *Lycopodium magellanicum*). The palynomorph *Nothofagus dombeyi* type includes several other *Nothofagus* species present in Southwestern Patagonia, i.e. *N. betuloides*, *N. pumilio* and *N. antarctica*. In the following paragraphs, I describe the most notable changes in each pollen zone, highlighting the three most abundant taxa and their mean abundances in parenthesis.

Zone PIN-1 (405-382 cm, ~17.0-16.4 ka) is characterized by the assemblage *Empetrum* (45%)-Poaceae (39%)-Asteraceae subf. Asteroideae (6%). This zone starts with a prominent decrease in Poaceae (from ~75% to 20%) and a conspicuous increase in *Empetrum* (from 10% to 70%) reaching its highest abundance of the entire record at ~16.7 ka. The herbs Asteraceae subfamily Asteroideae and *Acaena* show a downward trend, while *Gunnera* and *Lycopodium* exhibit a discrete increase near the end of this zone. The aquatic *Myriophyllum* (41%) and the micro alga *Pediastrum* (50%) decline with fluctuations through this zone.

Zone PIN-2 (382-331 cm, 16.4-14.9 ka) features the assemblage Poaceae (56%)-*Gunnera* (16%)-*Empetrum* (15%). Poaceae exhibits a sustained increase through this zone, *Empetrum* shows a rapid decline at the beginning and then remains relatively invariant (plateau ~10%), while *Gunnera* increases abruptly (from ~10 to 30%). Asteraceae subfamily Asteroideae (7.5%) and *Acaena* (3.5%) exhibit increasing trends, along with a gradual rise in *Blechnum* (5%) and a sustained decrease in *Lycopodium* (3.4%). *Myriophyllum* decreases at the beginning of this zone (from 13% to 3%) and persists in trace abundance (mean <1%), while *Pediastrum* (63%) shows a prominent rise from 35% to 80%.

Zone PIN-3 (331-312 cm, 14.9-14.3 ka) is dominated by Poaceae (54%)-*Empetrum* (23%)-Asteraceae subfamily Asteroideae (12%) with a decreasing trend in Poaceae, increments in *Empetrum* and Asteraceae subfamily Asteroideae, along with a major rise in *Blechnum* (35%) which reaches its maximum abundance of the record (max. ~48%) near the end of this zone, coeval with rapid declines in *Gunnera* and *Pediastrum* (55%) (from 12% to 5% and from 70% to 16%, respectively). *Myriophyllum* (<0.5%) virtually disappears from the record during this interval. Arboreal pollen exhibits a slight increase by the end of this zone (from mean 2% to mean 4%) driven by a minor increase in *Nothofagus dombeyi* type (<2%) along with its hemiparasitic mistletoe *Misodendrum* (<1%).

Zone PIN-4 (312-293 cm, 14.3-13.1 ka) is characterized by the assemblage Poaceae (35%)-*Empetrum* (31%)-*Nothofagus dombeyi* type (19%). *Nothofagus dombeyi* type exhibits a prominent increase from 5% to 60%, accompanied by traces of *Misodendrum* (<1%). Poaceae declines abruptly at the beginning and end of this zone, while *Empetrum* shows a steady decline, along with a decrease in Asteraceae subfamily Asteroideae, a significant decrease in *Blechnum* (from 36% to 6%, mean: 19%) and a rapid rise in *Pediastrum* (from 33% to 72%, mean: 55%) which falls by the end of this interval.

Zone PIN-5 (293-268 cm, 13.1-11.4 ka) is dominated by the assemblage *Nothofagus dombeyi* type (68%)-Poaceae (17%)-*Empetrum* (6%). This zone shows a steady rise in *Nothofagus dombeyi* type and a significant increase in *Misodendrum* (from 1% to 8%; mean: 2%) near the end of this zone. *Empetrum* features an abrupt decline, Poaceae exhibits a slight increase followed by a rapid decline by the end of this zone, coeval with a decreasing trend in Asteraceae subfamily Asteroideae and a rapid rise in *Blechnum* (14%). *Pediastrum* exhibits an abrupt increase and reaches its maximum abundance of the record (max. 89%; mean: 60%) at ~12.3 ka, followed by its rapid decline until the end of this zone.

Zone PIN-6 (268-209 cm, 11.4-6.7 ka) features dominance of *Nothofagus dombeyi* type (79%)-Poaceae (11%)-*Misodendrum* (3%). *Nothofagus dombeyi* type continues its increasing trend from the previous zone, Poaceae abundance remains stable, while *Misodendrum* shows a conspicuous increase near the end of this zone. The rest of the shrubs and herbs remain in low abundance (mean <3%). *Pediastrum* shows a prominent decline at the beginning of this zone, while the macrophyte *Isoetes* (68%) exhibits an abrupt increase from 1% to 90% reaching its maximum (95%) abundance of the entire record at 10.3 ka.

Zone PIN-7 (209-26 cm, 6.7-0.4 ka) is dominated by *Nothofagus dombeyi* type (96%)-*Misodendrum* (1.5%)-Poaceae (1%). *Nothofagus dombeyi* type dominates this zone, with little variation, while the rest of the terrestrial taxa exhibit trace abundance (<1%). *Isoetes* (23%) persists over the entire zone with large- and short-magnitude fluctuations (mean: 10% to 40%) and *Pediastrum* (1.5%) shows low abundance through this zone with two discrete increases centred at 4 and 3 ka.

Zone PIN-8 (26-0 cm, 0.4 ka-present) is characterized by the assemblage *Nothofagus dombeyi* type (93%)-Poaceae (2%)-*Misodendrum* (2%). *Nothofagus dombeyi* type dominates with a decline through this zone, concurrent with an increase in non-arboreal taxa, chiefly Poaceae and *Rumex* (<1%). The macrophyte *Isoetes* (18%) presents a decreasing trend until the end of this zone.

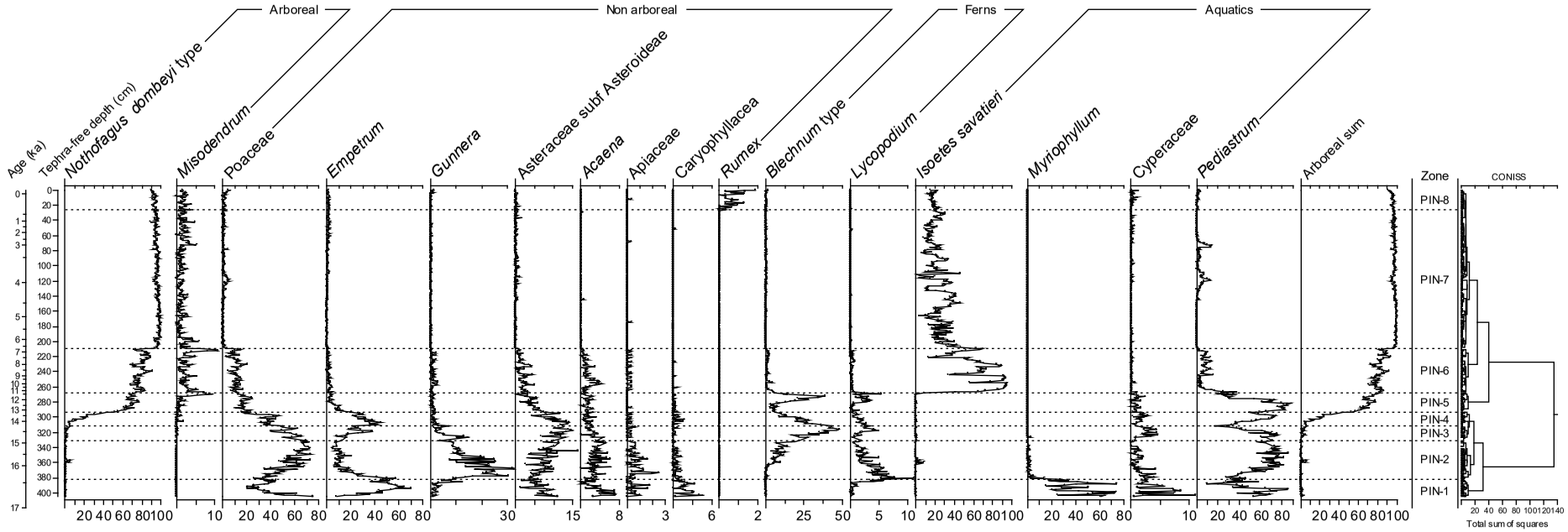

Figure 5.5. Pollen percentage diagrams of the Lago Pintito record. The primary Y axis represents the depth without tephra and the secondary Y axis the age model. The dashed horizontal lines demark the boundaries of the pollen assemblage zones, informed by CONNIS.

5.4.3. Macroscopic charcoal record

The macroscopic Charcoal Accumulation Rates (CHAR) record from Lago Pintito shows virtual absence of particles between ~17.0 and ~12.5 ka, followed by a prominent increase between ~12.5 and ~6.9 ka, relatively low accumulation between ~6.9 and ~0.4 ka and a rise after ~0.4 ka (Figure 5.6). Timeseries analysis of the macroscopic charcoal record revealed 14 statistically significant peaks over the last 17,000 years, interpreted as local fire events. I note a multi-millennial-scale structure in the fire frequency parameter, with maxima between ~12.5 and ~11.7 and ~9 and ~6.9 ka. Large-magnitude fire events occurred during the highest fire frequency intervals at ~12.1, ~12, ~9.6 and ~7.7 ka (Figure 5.6).

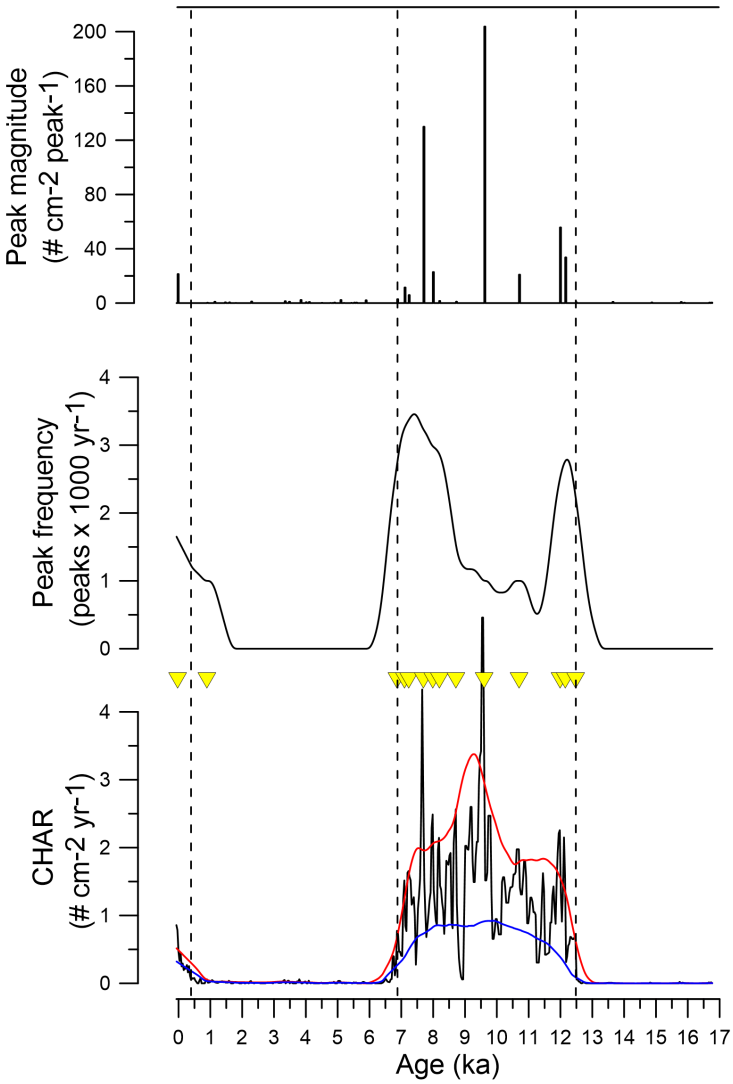

Figure 5.6. Macroscopic charcoal record from Lago Pintito and time series analysis performed with the program CharAnalysis indicating the calculated background (blue line) using a lowess robust to outliers, the local defined threshold (red line), and the statistically significant charcoal peaks (yellow triangles). Also shown are the fire frequency curve and the magnitude bars. The dashed lines demark the intervals with fire activity.

5.5. Discussion

5.5.1. Vegetation, fire and climate history

The pollen and macroscopic charcoal records from Lago Pintito enable the assessment of vegetation, fire regime and climate changes over the last ~17,000 years in the Última Esperanza sector of Southwestern Patagonia. Between ~17.0 and ~14.2 ka, the pollen record shows an open landscape dominated by herbs and shrubs (Poaceae, Asteraceae subfamily Asteroideae, *Acaena* and Caryophyllaceae, *Empetrum*) commonly found in the Patagonian steppe and High Andean sectors along with very low arboreal pollen (<2%) and high abundance of the planktonic alga *Pediastrum* (Figure 5.5). Because this pollen assemblage also includes *Gunnera*, *Blechnum* type, and *Lycopodium magellanicum*, currently absent from the Patagonian Steppe but present in humid sectors of the western Andes, I interpret this dominance of alpine vegetation in the lowlands of the Última Esperanza region during the initial phases of T1 as indicating cold and relatively humid conditions. Within this treeless interval I note that *Empetrum* and the littoral macrophytes *Myriophyllum* and Cyperaceae attained their highest abundance in the entire Lago Pintito record between ~17.0 and ~16.4 ka. The pre-eminence of *Empetrum*, along with scarce presence of mesic herbs, suggests an alpine environment under likely intense cold and relatively dry conditions during the initial portion of T1. On the other hand, peak abundance of *Myriophyllum* and Cyperaceae at the coring site suggests their littoral habitat occurred closer to core site at the deepest portion of the lake, which I interpret as a low lake level stand. These percentage maxima ended abruptly at ~16.4 ka and plummeted to low abundance (*Empetrum* ~10%, *Myriophyllum* <4%, Cyperaceae <2%) contemporaneous with abrupt increases in the hygrophilous herbs *Gunnera* and *Lycopodium magellanicum* between ~16.4 and ~15.9 ka followed, in turn, by rapid rises in Poaceae, Asteraceae subfamily Asteroideae, *Acaena* and the water-demanding fern *Blechnum* type between ~15.9 and ~14.2 ka (Figure 5.5). I interpret intense cold and dry conditions between ~17.0 and ~16.4 ka, judging from an absence of hygrophilous and mesic herbs and the inference of low lake levels, followed by less severe cold conditions and increased humidity between ~16.4 and ~14.2 ka that drove increases in hygrophilous and mesic herbs, along with a lake level rise.

Empetrum rose abruptly from ~15% to ~40% and returned to ~10% between ~14.2 and ~12.6 ka, coeval with declines in *Lycopodium magellanicum* from ~4% to ~1% and *Blechnum* type

from ~44% to ~6%. These changes are preceded by a slight increase in *Nothofagus* and its mistletoe *Misodendrum* at ~14.6, which led to a rapid increase in *Nothofagus* from <2% to 60% at 14.2 ka and the establishment of an open forest at ~12.8 ka. I note subsequent increments in *Lycopodium magellanicum* and *Blechnum* type between ~12.6 and ~11.4 ka, contemporaneous with a rise in macroscopic CHAR and a halt in the rising trend of *Nothofagus* between ~12.5 and ~11.4 ka (Figures 5.5 and 5.6). The latter resumed its rise, indicating wider forest expansion between ~11.4 and ~7.0 ka, with low-magnitude millennial-scale fluctuations. This early Holocene interval also features prominent multi-millennial-scale maxima in the macrophyte *Isoetes* and macroscopic CHAR (Figures 5.5 and 5.6). Similar to *Myriophyllum* and Cyperaceae during the earliest T1 phase, I interpret increases in the macrophyte *Isoetes savatieri* as centripetal expansion of littoral environments toward the deepest part of the lake, where the coring site is located, implying a regressive lake-level phase between ~11.4 and ~6.8 ka. The macroscopic CHAR increase after ~13.0 ka suggests heightened fire activity in the context of *Nothofagus* woodlands/forests. Modern studies show that wildfire occurrence in western Patagonia is limited by ignition source and desiccation, considering that abundant biomass is not a limiting factor in these forested environments (Holz and Veblen, 2012). I interpret these changes as a response of the local vegetation to moderate cold and wet conditions between ~14.2 and ~12.6 ka, increased rainfall seasonality/variability between ~12.6 and ~11.4 ka, and a major decline in precipitation between ~11.4 and ~6.8 ka.

A steep increase in *Nothofagus dombeyi* type at ~6.8 ka led to its maximum abundance in the Lago Pintito record (mean: 98%) which has persisted with little variations until the present (Figure 5.5). This change in terrestrial vegetation was contemporaneous with the virtual disappearance of charcoal and a prominent decline in *Isoetes savatieri*. The latter lingered until the present with a series of fluctuations (Figure 5.5) that include oscillations below 45% abundance, i.e. approximately half the magnitude of the early Holocene rise, between ~5.8 and ~5.2, ~4.6 and ~3.7, ~3.3 and ~3.0, and ~1.0 and ~0.4 ka (Figure 5.5). These results suggest establishment of closed-canopy *Nothofagus* forests, absence of fires and a lake level rise overprinted with fluctuations over the last ~6800 years (Figures 5.5 and 5.6). The exotic herb *Rumex*, a key palynological indicator for European settlement in the region, appears in the Lago Pintito record at ~0.38 ka (2σ range: 0.24-0.47 ka; 1570 AD). The interpolated age for

the first *Rumex* pollen in the record might be an overestimation considering that historical records define the arrival and the onset of European settlement of the area of Southwestern Patagonia in the year 1891 AD (Martinic, 1974). Nevertheless, the coeval rise of *Rumex* and charcoal, along with a slight decline in *Nothofagus* (from 95 to 87%) (Figures 5.5 and 5.6), suggest limited perturbation of the *Nothofagus* forests surrounding Lago Pintito to low-magnitude human disturbance.

5.5.2. Regional paleoclimate implications

The Lago Pintito record suggests cold conditions and low lake levels between ~17.0 and ~16.4 ka, followed by a lake level rise at ~16.4 ka. These results suggest low SWW influence at ~52°S brought about by poleward-shifted SWW at the beginning of T1, followed by a marked increase at ~16.4 ka that I attribute to a northward shift of the SWW. I note that these climate interpretations were coeval with similar paleoclimate inferences from terrestrial records from northwestern (Moreno et al., 2018a; Pesce and Moreno, 2014) and central-western Patagonia (Vilanova et al., 2019), providing a coherent picture for SWW changes at the onset of T1 and supporting the postulate role of the SWW as a trigger of upwelling of CO_2 enriched deep water in the Southern Ocean during T1 (Anderson et al., 2009).

High lake levels initiated at ~16.4 ka at Lago Pintito led to a multi-millennial phase of high lake levels that lasted until ~11.4 ka, suggesting a persistent SWW influence at ~52°S with a millennial-scale structure. Within this interval, I detect increased SWW-derived precipitation between ~16.4 and ~14.2 ka, and ~12.6 and ~11.4 ka with high rainfall seasonality/variability coeval with the YD chron of the Northern Hemisphere. I observe that high SWW influence persisted between ~14.2 and ~12.6 ka during the ACR, but lower in magnitude than the 16.4-14.2 ka interval (Figure 5.7). A recent study from central-western Patagonia detected in-phase positive SWW anomalies between the Central Patagonian Andes and southwestern Patagonia during the ACR and YD chron and out-of-phase positive anomalies with northwestern Patagonia (Vilanova et al., 2019). The results from the Lago Pintito record are in agreement with these findings. Hence, my inferred SWW shifts from Lago Pintito record, in conjunction with published SWW variability from northwestern (Moreno et al., 2018a; Pesce and Moreno, 2014), central-western (Vilanova et al., 2019) and southwestern Patagonia (Moreno et al.,

2012), suggest expansion and strengthening of the SWW in western Patagonia between ~16.4 and ~14.2 ka, equatorward shift of the maximum zone of SWW influence focusing on northwestern Patagonia during the ACR, and polewards shift of the maximum zone of SWW influence affecting central-western and southwestern Patagonia during the YD chron.

A prominent decrease in lake levels between ~11.4 and ~6.8 ka and increased fire activity mark the beginning of the Holocene in the Última Esperanza area. These changes are concurrent with peak fire activity in southern South America (>30°S) (Power et al., 2008; Whitlock et al., 2007) and negative precipitation anomalies reported from terrestrial records from northwestern (Abarzúa et al., 2004; Henríquez et al., 2015; Moreno, 2004; Moreno and Videla, 2016; Moreno et al., 2018a; Pesce and Moreno, 2014), central-western (Van Daele et al., 2016; Vilanova et al., 2019; Villa-Martínez et al., 2012) and southwestern Patagonia (Moreno et al., 2010; Moreno et al., 2018b; Moreno et al., 2012), suggesting to me a generalized decline in SWW influence in western sectors of southern South America. These findings do not concur with the results and interpretations reported by Lamy et al. (2010), which indicate a positive anomaly in SWW influence during the early Holocene. My conclusions, however, are consistent with similar paleo SWW reconstructions from other mid-latitude landmasses in the Southern Hemisphere (southern New Zealand, Anderson et al., 2018; southern Australia, Fitzsimmons and Barrows, 2010; southern Africa, Meadows and Baxter, 1999; southern South America, Moreno et al., 2018a), suggesting a multi-millennial zonally symmetric decline in SWW strength in the Southern Hemisphere during the early Holocene (Fletcher and Moreno, 2012).

The results from Lago Pintito suggest an increase in precipitation at ~6.8 ka inferred from a rapid decline in *Isoetes* (Figure 5.7), followed by the onset of alternating periods of dry and wet conditions attributable to changes in the intensity and/or latitudinal position of the SWW at centennial timescales. Positive anomalies in *Isoetes* between ~5.8 and ~5.2, ~4.6 and ~3.7, ~3.3 and ~3.0, and ~1.0 and ~0.4 ka (Figure 5.7) suggest lower lake levels in response to a decline in precipitation associated with weak SWW influence. A recent study from Lago Cipreses in southwestern Patagonia (Moreno et al., 2018b) identified low-magnitude centennial-scale variations in the cover of evergreen-deciduous *Nothofagus* forest, diversification of the forest understorey, decline in lake levels and paleofire activity following

Figure 5.7. Comparison of macroscopic charcoal and selected terrestrial taxa (%*Gunnera*, %hygrophilous ferns and lycophytes [%*Blechnum* type and %*Lycopodium magellanicum*]) and Macrophytes (%*Isoetes* and %*Myriophyllum*) from Lago Pintito record, along with the δ deuterium (Jouzel and Masson-Delmotte, 2007) and atmospheric CO_2 records from Antarctic ice cores (Monnin et al., 2001). The coloured rectangles represent the interpreted climate conditions from the Lago Pintito record (dark red: dry conditions, slight red: relative dry conditions, dark sky blue: wetter conditions, light sky blue: relative wet conditions). The bars below the bottommost curve represent the timing of Cipreses cycles (CC-n) (Moreno et al., 2018b), and the acronyms refer to ACR: Antarctic Cold Reversal; YD chron: Younger Dryas chronozone; EH: Early Holocene.

the early Holocene. The authors interpreted these results as changes in the amount of precipitation driven by shifts in the SWW influence, indicating discrete declining pulses at ~7.4 (CC10), ~6.0 (CC9), ~4.8 (CC8), ~4.1 (CC7), ~3.4 (CC6), ~3.1 (CC5), ~2.4 (CC4), ~1.6 (CC3), ~1.1 (CC2) ka and ~0.2 ka (CC1). Six of these events (CC9, CC8, CC7 CC6, CC5 and CC2) overlap in timing with centennial-scale phases of diminished precipitation from the Lago Pintito record (Figure 5.7). This correspondence in timing and direction of paleoclimate change between Lago Pintito and Lago Cipreses raises the possibility that centennial-scale climate events affected a broad sector of southwestern Patagonia over the last ~7000 years. Centennial-scale intervals of diminished precipitation initiated at ~7.0 ka in southwestern Patagonia were contemporaneous with centennial-scale climate changes reported from northwestern (Moreno and Videla, 2016; Moreno et al., 2018a) and west-central (Simi et al., 2017) Patagonia that commenced at ~6.5 and ~3.2 ka, respectively, suggesting that high-frequency variability in climate and SWW influence across western Patagonia might have started following the multi-millennial-scale extreme dry/warm early Holocene.

5.5.3. Regional biogeographic implications

The results from Lago Pintito show similar pollen assemblages and temporal patterns to other sites located along the eastern sectors of the southern Patagonian Andes during the early stage of T1. The Lago Pintito record features dominance of herbs and shrubs with the virtual absence of arboreal pollen between ~17 and ~14.6 ka, followed by the onset of the increase of *Nothofagus* trees that started at ~14.2 ka. Further east, this signal is also documented in palynological records from Potrok Aike and Río Rubens (Huber et al., 2004; Wille et al., 2007), indicating the rise of *Nothofagus* abundance at ~15.5 and ~15.9 ka, respectively. The Punta Arenas pollen record (Heusser, 1995), on the other hand, shows dominance of *Nothofagus* forests in the south-eastern sector of the southern Patagonian Andes between the interpolated ages ~17.2 and ~16.9 ka, followed by its sustained decline through T1. I note that the chronology for the early presence of *Nothofagus* woodland and forests at the Punta Arenas site is only constrained by one radiocarbon date (~16.1 ka; 2σ:16.5-15.7 ka) located 50 cm above the bottom of the pollen stratigraphy, indicating the limited chronologic control of the pollen record during this interval. The findings from Lago Pintito, in conjunction with the pollen records from Río Rubens, Potrok Aike and Punta Arenas, suggest to me a northward

afforestation of the eastern sector of the southern Andes from refugia located in the south-eastern margin of the Andes in southwestern Patagonia during T1. An alternative scenario for the spread of *Nothofagus* trees proposed by Moreno et al. (2019), is the existence of multiple-refugia along the eastern sectors of the Central Patagonian Andes outside the influence of the PIS during the LGM and T1, although these ideas need to be tested with more detailed pollen records from southernmost Patagonian sectors.

I observe important differences in the spatial/temporal expansion and establishment of *Nothofagus* forests in the Lago Pintito record and sites from western and eastern sectors of the southern Patagonian Andes during the T1/Holocene transition. The large, rapid, uninterrupted single rise in *Nothofagus* at Lago Pintito between~14.2 ka and ~12.8 ka equivalent in timing with the ACR, led to the establishment of *Nothofagus* forests (>60%) close to Lago Pintito. These changes were contemporaneous with discrete and much lower magnitude increases in *Nothofagus* abundance (~20%) in three sites located north (Pantano Dumestre) (Moreno et al., 2012) and south (Río Rubens, Punta Arenas) (Heusser, 1995; Huber et al., 2004) of Lago Pintito along the eastern sector of the southern Patagonian Andes (Figure 5.2). I point out that a similar vegetation pattern occurs later (~20% increase), between ~13.0 and ~11.5 ka coeval with the YD chron at three sites (Lago Guanaco, Lago Cipreses and Pto. del Hambre 2) (Heusser, 1995; Moreno et al., 2018b; Moreno et al., 2012), although *Nothofagus* forests only became established at Lago Cipreses (Moreno et al., 2018b) (Figure 5.2). I also note increasing trends in *Nothofagus* abundance at nine sites between ~11.5 and ~9.0 ka within the early Holocene, leading to the establishment of *Nothofagus* forests in most sites located in western sectors (G.C. Nevado, Lago Ballena) (Fesq-Martin et al., 2004; Fontana and Bennett, 2012) and in the proximity of the eastern slopes of the southern Andes Cordillera (Lago Eberhard, Pantano Dumestre, Pto. del Hambre 1 and 2) (Clapperton et al., 1995; Heusser, 1995; Moreno et al., 2012). Further east, three sites show established *Nothofagus* forests after ~9.0 ka (Vega Ñandú, Río Rubens, Punta Arenas) (Huber et al., 2004; Villa-Martínez et al., 2012) and one site located furthest east (Potrok Aike) (Wille et al., 2007) did not develop *Nothofagus* forests during the Holocene (Figure 5.2). These regional heterogeneities in *Nothofagus* forest history might reflect the combination of local site factors and regional climate trends, which include i) the persistence of ice lobes adjacent to the eastern and western slope of the Andes, controlling the spread of *Nothofagus* trees along

the southern Patagonian Andes during T1, ii) a west to east precipitation gradient along this region and iii) suppression of *Nothofagus* forest establishment driven by local pressures (discussed in the following paragraph).

In addition to these inter-regional differences in the timing of deciduous *Nothofagus* spread, I also observe major divergences among sites located within the Última Esperanza area of southwestern Patagonia, including Lago Pintito, Lago Eberhard and Pantano Dumestre (Figure 5.1). At Pantano Dumestre and Lago Eberhard, located at ~27 km and ~55 km northwest of Lago Pintito respectively, the transition from a landscape dominated by cold-resistant shrubs/herbs to *Nothofagus*-dominated forest/woodlands took place between ~11.4 and ~10.0 ka (Moreno et al., 2012), ~3000 years later than in Lago Pintito (Figure 5.8). These differences are surprising considering the proximity of the sites and the fact that species of the genus *Nothofagus* produce large quantities of pollen that can be transported long distances (Heusser, 1989). Moreno et al. (2012) interpreted the transition from shrubs/herbs to *Nothofagus* forests recorded at Lago Eberhard and Pantano Dumestre records as a tree line rise driven by a warming phase, but this explanation is not applicable to the Lago Pintito record where *Nothofagus* expansion took place between ~14.2 and ~12.8 ka under regional cold conditions (Sagredo et al., 2018) and coeval with the ACR.

I suggest that the resolution of this biogeographic puzzle requires more information and better understanding of the chronology of terrestrial biota and glacial history of Última Esperanza through T1. Archaeological evidence from Cueva del Medio (51°34’S, 72°36’W) and Cueva Lago Sofia 1 (51°32’S, 72°34’W), located ~53 and ~57 km northwest of Lago Pintito, respectively, indicate the presence of megafauna in the Última Esperanza area since the retreat of the Última Esperanza lobe at the beginning of T1 (Metcalf et al., 2016; Villavicencio et al., 2016). An ice-dammed proglacial lake developed following the deglacial process and covered Pantano Dumestre and Lago Eberhard until ~15.2 and ~12.8 ka (Sagredo et al., 2011), respectively. I speculate that megafauna would have inhabited proglacial lake-free sectors close to Lago Pintito during this proglacial lake phase and migrated toward Pantano Dumestre and Lago Eberhard areas once glacial lake levels dropped. I posit that this megafaunal migration marked the end of megafaunal occupation that had previously suppressed forest expansion and thus promoted the conversion of a landscape dominated by cold-resistant shrubs/herbs into *Nothofagus*-dominated forests in the vicinity of Lago Pintito between ~14.2

and ~12.8 ka. At the same time, the locus of megafaunal grazing pressure, including the trampling, and felling of trees or carving pathways, was transferred to sectors near to Pantano Dumestre and Lago Eberhard, suppressing the rise of *Nothofagus* forests there for ~3000 years (Figure 5.8). An alternative explanation for the rapid rise of *Nothofagus* in the Última Esperanza area might involve an increase in the advection of pollen grains attributable to log-distance transport from *Nothofagus* forests located along the Pacific coast. I rule out this alternative scenario because Pantano Dumestre and Lago Eberhard pollen records continued with background levels of *Nothofagus* (~20% and ~10%) until ~11.4 ka. Although here I provide a means of resolving the conundrum of different timings for forests expansion in Última Esperanza that is compatible with the existing pollen records and archaeological evidence from this region, additional palynological evidences from Última Esperanza area are needed to test this postulated explanation.

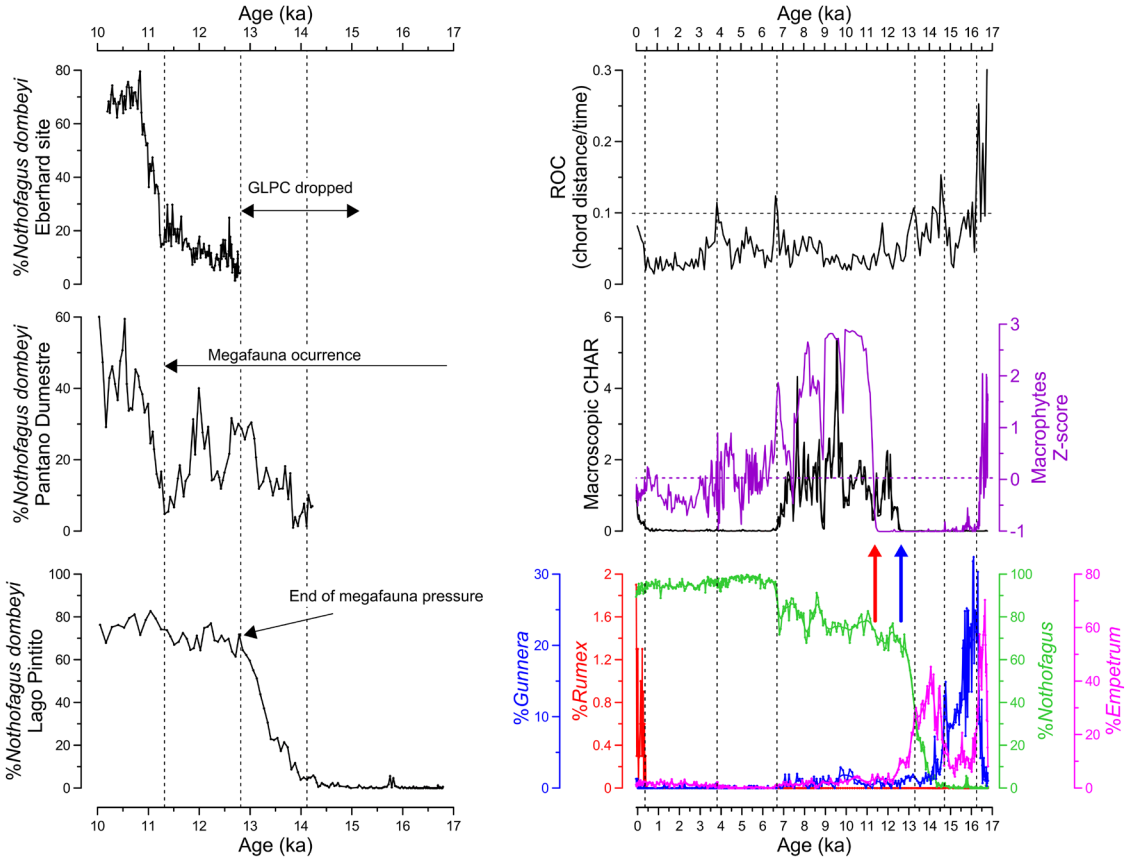

Figure 5.8. Left panel: Comparison of Lago Pintito *Nothofagus dombeyi* with Pantano Dumestre and Eberhard site (Moreno et al., 2012), indicating the end of megafauna pressure at Lago Pintito and the interval of megafauna occurrence at Lago Dumestre and Eberhard site. GLPC: Glacial Lake Puerto Consuelo. Right panel: The upper curve represents the rates of change parameter (ROC), the middle curves show CHAR and

macrophytes (z-score), and the bottom curves show terrestrial taxa (%*Rumex*, %*Gunnera*% *Nothofagus* and %*Empetrum*). The blue and red arrows indicate transitions toward increased rainfall seasonality/variability and dry conditions, respectively. The dashed vertical lines mark periods of prominent/rapid changes in terrestrial taxa.

The results from Lago Pintito suggest the extraordinary persistence of *Nothofagus* forests during the last ~12.8 ka, preceded by conspicuous vegetation changes following the commencement of T1. The rates of change parameter (ROC), a measurement of the magnitude and rapidity of change in the terrestrial vegetation (Grimm and Jacobson, 1992), reveals two prominent vegetation changes associated with i) the *Gunnera* rise by ~16.4 ka following the beginning of T1, and ii) the *Empetrum* increase by ~14.6 ka at the beginning of the ACR, in the context of dominance of non-arboreal pollen. ROC also shows three minor changes related to i) the decline of *Empetrum* and the increase of *Nothofagus* forests by ~13.2 ka at the end of ACR, ii) the onset of closed-canopy *Nothofagus* woodland and forests by ~6.8 ka, and iii) a low-magnitude decline of *Nothofagus* by ~4.0 ka (from ~97 to ~94 %) (Figure 5.8). I observe that the seasonality of precipitation increases between ~12.6 and ~11.4 ka, followed by a major decline in precipitation during the early Holocene and contemporaneous with high accumulation rates of macroscopic charcoal. These climate changes along with high fire activity did not alter the constancy of *Nothofagus* forests during this period. *Nothofagus* forests persisted and became even more prominent when dense closed-canopy *Nothofagus* forests stablished in the vicinity of Lago Pintito at~6.8 ka, coeval with enhanced precipitation variability and a period of muted fire activity, continuing with little variation throughout the Holocene. I note a discrete signal in ROC during the last ~300 years, which I attribute to a minor decline in *Nothofagus* abundance set by Chilean/European deforestation and the spread of the exotic invasive herb *Rumex acetosella* along with increased fire activity (Figure 5.8). A recent study from Lago Cipreses (Moreno et al., 2018b), located in southwestern Patagonia ~90 km northwest of Lago Pintito, detected millennial to centennial-scale variations of *Nothofagus* abundance (between ~50 and ~90%) interpreted as varying degrees of openness of the closed-canopy Magellanic forests established at ~11.0 ka. Unlike the Lago Cipreses record and other sites from the eastern (Gran Campo Nevado, Lago Ballena) and western (Lago Guanaco, Lago Eberhard, Pantano Dumestre, Río Rubes, Potrok Aike, Punta Arenas, Puerto del Hambre 1-2) sectors of the southern Andes, the palynology of Lago Pintito suggests that *Nothofagus* forests have been notably resilient since their establishment close

to Lago Pintito in the Última Esperanza area at ~12.8 ka, despite the conspicuous climate states at the end of T1, high fire activity during the early Holocene, increased climate variability started at ~6.8 ka, and human activity during the last few centuries.

5.6. Conclusions

Stratigraphic and chronologic data indicate a constant depositional setting and uninterrupted sedimentary record in the Lago Pintito basin in the Última Esperanza region spanning from the onset of the local T1 until the present. This exceptional scenario has enabled the reconstruction of past changes in terrestrial and aquatic environments and, in turn, climate conditions from centennial to multi-millennial timescales in southwestern Patagonia during the last ~17,000 years. The main conclusions are:

1. Cold-resistant and hygrophilous shrubs and herbs colonized recent ice-free sectors close to Lago Pintito at ~17.0 ka. This assemblage dominated the landscape and persisted as the dominant vegetation until ~14.2 ka, followed by a rapid and interrupted rise in *Nothofagus dombeyi* which lasted until ~12.8 ka and marked a major vegetation change from scrubland/grasslands to Magellanic *Nothofagus* forests in the Última Esperanza area.
2. *Nothofagus* forests established close to Lago Pintito at ~12.8 ka, followed by their wider expansion and development of dense closed-canopy *Nothofagus* forests from ~6.8 ka. Dense *Nothofagus* forest has persisted as the dominant vegetation with little variation despite natural and human disturbances, indicating their strong resilience to environmental change and disturbance regimes.
3. Heterogeneity of forest expansion in the Última Esperanza area during T1 poses a paleovegetation puzzle. I hypothesize that the presence of megafauna in this sub-region might have affected the spread of arboreal vegetation near Lago Pintito. I posit that megafauna abandoned the surrounding area of Lago Pintito between ~14.2 and ~12.8 ka, enabling the expansion and establishment of local *Nothofagus* forests. Megafaunal grazing pressure was transferred to sectors near to Pantano Dumestre,

suppressing the rise of *Nothofagus* forests in these sectors until megafaunal extinctions at the beginning of the Holocene.

4. Variability in terrestrial and aquatic vegetation along with charcoal data indicates changes in the amount of precipitation at multi-millennial, millennial, and centennial timescales during the last ~17,000 years. Considering the positive correlation between zonal wind speeds and local precipitation, I infer reduced SWW influence in southwestern Patagonia (52°S) between ~17.0 and ~16.4 ka, increased SSW influence between ~16.4 and ~14.2 ka and ~12.5 and ~11.4 ka and persistent SWW influence but lower in magnitude between ~14.2 and ~12.5 ka.
5. I detect a prominent lake level lowering in Lago Pintito between ~11.7 and ~6.8 ka, interpreted as reduced SWW influence in southwestern Patagonia during the early Holocene.
6. Centennial-scale changes in precipitation in Lago Pintito started at ~6.8 ka, and I infer that the SWW influence was reduced between ~5.8 and ~5.2, ~4.6 and ~3.7, ~3.3 and ~3.0, and ~1.0 and ~0.4 ka, with increased influence in the intervening intervals.
7. Overall, these paleoclimate trends revealed by Lago Pintito over the last ~17,000 years, in conjunction with previous paleoclimate reconstructions from Patagonian and Antarctic records, suggest a strong teleconnection between mid- and high-latitudes in the Southern Hemisphere.

Chapter 6

Synthesis and Conclusions

This thesis has presented detailed fossil pollen and charcoal records from sediment cores from two small closed-basin lakes located in Western Patagonia in southern South America, along with detailed fossil pollen and charcoal records and an exploratory chironomid record from sediment cores obtained from a closed-basin lake from southern South Island of New Zealand. These records have enabled me to address the thesis objectives (Chapter 1, subsection 1.2) by providing reconstructions of vegetation, fire regime and climate change at these sites, as well as the behaviour of the Southern Westerly Winds (SWW) since the Last Glacial Maximum (LGM) in Western Patagonia in southern South America and southern South Island of New Zealand.

This concluding chapter summarises these multiproxy-based reconstructions and presents a synthesis of the major climate shifts that can be inferred from these records. This chapter also discusses and addresses the research hypotheses stated in the introductory chapter 1.

6.1. Vegetation, fire and climate change synthesis

6.1.1. The Last Glacial Maximum (LGM, ~24.0-17.5 ka)

The LGM period is only covered by pollen and macroscopic charcoal records from Lago Emerenciana (Chapter 3). The pollen record shows scattered woodlands featuring high-elevation species-poor *Nothofagus*-dominated Subantarctic and High-Andean vegetation between ~24.0 and ~17.5 ka, and lack of fires (Figure 6.1). Within this interval I observe a sustained increase in cold-resistant herbs of the Apiaceae family and the water-demanding fern *Blechnum* that started at ~22.8 ka, showing peak abundance between ~19.7 and ~17.5 ka (Figure 6.1). These findings suggest an initial phase with relatively cold conditions and persistent precipitation between ~24.0 and ~22.8 ka, followed by a decline in temperature and a marked increase in precipitation between ~19.7 and ~17.5 ka.

6.1.2. The Last Glacial Termination (T1, ~17.5-11.2 ka)

The Last Glacial termination period is covered by all three records presented in this thesis. The Lago Emerenciana record shows an increase in Myrtaceae that started ~17.5 ka, at the expense of vegetation indicative of Subantarctic forests and High-Andean environments, coeval with an increase in fire activity (Figures 6.1 and 6.2). This floristic turnover suggests a transition from glacial cold and high precipitation toward temperate conditions and less precipitation at the onset of T1. Cold-temperate conditions with strong desiccating summer winds and increased precipitation seasonality ensued between ~16.3 and ~14.5 ka, revealed by rises in *Fitzroya/Pilgerodendron* and *Tepualia*+*Raukaua*. A subsequent increase in the cold-tolerant hygrophilous conifer *Podocarpus nubigena* between ~14.5 and ~12.5 ka along with a decline in *Tepualia*+*Raukaua* indicate colder conditions and increased precipitation (Figure 6.1). This was followed by a decline in *Podocarpus nubigena* and an increase in *Tepualia*+*Raukaua* between ~12.5 and ~11.1 ka, suggesting persistence of cold conditions and reduced precipitation.

The Lago Pintito record shows the pre-eminence of *Empetrum* between ~17.0 and ~16.4 ka in a context of low lake levels, suggesting intense cold conditions and low local precipitation. This was followed by less severe cold conditions and increased precipitation between ~16.4 and ~14.2 ka, revealed by rises in mesic herbs (Poaceae, Asteraceae subfamily Asteroideae, *Acaena*), hygrophilous species (*Gunnera*, *Lycopodium magellanicum* and *Blechnum*) and lake levels. Subsequently, *Empetrum* rose abruptly and continued with relatively high values between ~14.2 and ~12.6 ka, coeval with declines in the hygrophilous *Lycopodium magellanicum* and *Blechnum*, followed by their rises in *Lycopodium magellanicum*, *Blechnum*, arboreal pollen and fire activity between ~12.6 and ~11.4 ka (Figure 6.1). These changes suggest moderate cold and precipitation levels between ~14.2 and ~12.6 ka, and enhanced precipitation seasonality/variability between ~12.6 and ~11.4 ka.

The Lake Von record indicates dominance of alpine vegetation with cold-tolerant shrubs, herbs and ferns (*Coprosma*, Poaceae, *Blechnum*) between ~18.0 and ~16.7 ka, followed by a gradual transition toward *Coprosma*-dominated subalpine vegetation with the local presence of subalpine/montane hygrophilous trees (*Metrosideros*) between ~16.7 and ~14.8 ka with a rise in SmT (Figure 6.1). These data suggest an early stage with cold and relatively wet conditions between ~18.0 and ~16.7 ka, followed by cold-temperate conditions with warmer

summer and a slight increase in precipitation between ~16.7 and ~14.8 ka. I observe a rise in vegetation characteristic of alpine environments (Poaceae, Asteraceae Asteroideae, ferns) between ~14.8 and ~12.6 ka at the expense of *Coprosma*, accompanied by increases in the cold-tolerant hygrophilous *Metrosideros* and lake levels. This was followed by the increase and dominance of *Coprosma* between ~12.6 and ~10.8 ka, along with decline in alpine vegetation (Poaceae, Asteraceae Asteroideae, ferns), cold-tolerant hygrophilous trees (*Metrosideros*), lake levels and SmT. I interpret these data as indicating a decline in temperatures with high seasonality and enhanced precipitation between ~14.8 and ~12.6 ka, followed by warming with likely milder winter temperatures and reduced precipitation between ~12.6 and ~10.8 ka.

6.1.3. Early Holocene (~11.2-7.2 ka)

The palynology of Lago Emerenciana shows the disappearance of the cold-tolerant *Podocarpus nubigena* at ~11.1 ka, contemporaneous with major increases in Myrtaceae and *Tepualia*+*Raukaua*, a rising trend in *Nothofagus*, the appearance of the thermophilous summer-drought resistant trees *Eucryphia*/*Caldcluvia*, major openness of the landscape revealed by a rise in *Weinmannia trichosperma* and local fires between ~11.1 and ~7.6 ka (Figure 6.1). I interpret these results as a warming phase with a reduced precipitation regime.

The Lago Pintito record indicates the virtual disappearance of water-demanding ferns at ~11.7 ka, in the context of a landscape dominated by *Nothofagus* forests, large-magnitude fire events and a prominent lake level lowering that lasted until ~6.8 ka revealed by a conspicuous increase in the aquatic *Isoetes* (Figure 6.1), suggesting a major reduction in precipitation.

The Lake Von record indicates conspicuous increases of the subalpine cold-tolerant conifers *Halocarpus* and *Phyllocladus* at ~10.8 and ~10.1 ka, respectively, dominating the landscape until ~7.2 ka. This was contemporaneous with an increase in tall conifers (*Podocarpus*, *Prumnopitys taxifolia*, *Prumnopitys ferruginea* and *Dacrycarpus*), and the highest SmT (Figures 6.1). Considering that *Prumnopitys taxifolia* is a drought-resistant conifer, and hygrophilous taxa disappeared, fire activity increased, and lake levels declined during this interval, these data suggest a further warming pulse and reduced precipitation.

6.1.4. Mid- to late Holocene (~7.2-0.6 ka)

The Lago Emerenciana pollen record shows a prominent increase in *Eucryphia*/*Caldcluvia* at ~7.6 ka that led to its highest abundance between ~6.2 and ~4.4 ka with centennial-scale variations, followed by decline between ~4.4 and ~2.4 ka. These vegetational changes were concurrent with a decline in *Tepualia*+*Raukaua* between ~7.6 and ~4.4 ka, followed by its increase between ~4.4 and ~2.4 ka, interpreted as high and low lake level, respectively (Figure 6.1). These findings suggest high SWW influence between ~7.6 and ~4.4 ka, followed by weak SWW between ~4.4 and ~2.4 ka, with probably high climate variability and seasonality in precipitation.

The palynology of Lago Pintito indicates the establishment of closed-canopy *Nothofagus* forests at ~6.8 ka, along with a lake level rise overprinted with fluctuations over the last ~6800 years revealed by shifts in the aquatic *Isoetes*. I detect a series of fluctuations that include oscillations in *Isoetes* below 45% abundance, i.e. approximately half the magnitude of the early Holocene rise, between ~5.8 and ~5.2, ~4.6 and ~3.7, ~3.3 and ~3.0, and ~1.0 and ~0.4 ka (Figure 6.1). These findings suggest an increase in precipitation at ~6.8 ka, overprinted with centennial-scale changes in precipitation with reduced levels between ~5.8 and ~5.2, ~4.6 and ~3.7, ~3.3 and ~3.0, and ~1.0 and ~0.4 ka, with increased precipitation in the intervening intervals.

The pollen record from Lake Von shows an increase in the cool-temperate silver beech (*Lophozonia menziesii*) between ~7.2 and ~3.7 ka, along with the hygrophilous conifer *Dacrydium cupressinum*, relatively low abundance but with high variability in the warm-temperate tall conifers and a declining trend in SmT (Figure 6.1). Within this multi-millennial-scale interval, I detect low-magnitude centennial-scale decline in *Lophozonia menziesii* and *Dacrydium cupressinum* between ~6.0 and ~5.2 ka and ~4.4 and ~4.1 ka, concurrent with increase in the drought-tolerant *Prumnopitys taxifolia*. These changes were followed by decline in *Lophozonia menziesii* and *Dacrydium cupressinum* between ~3.7 and ~2.9 ka, sustained increase in *Lophozonia menziesii*, *Dacrydium cupressinum* and the drought-intolerant *Metrosideros* between ~2.9 and ~1.9 ka, and a rapid and prominent rise in *Fuscospora* between ~1.9 and ~0.56 ka (Figure 6.1). I interpret these data as a decline in temperature, especially during summer, and a sustained rise in precipitation between ~7.2 and ~3.7 ka. Superimposed upon, and following this multi-millennial climate trend, I detect

alternating dry and wet oscillations of millennial- and centennial-scale with low precipitation between ~6.0 and ~5.2, ~4.4 and ~4.1, ~3.7 and ~2.9, and ~1.9 and ~0.56 ka, and wet periods in the intervening intervals suggesting increased precipitation.

6.1.5. Summary of inter-site comparisons

The Lago Emerenciana, Lago Pintito and Lake Von records indicate:

i) Dominance of vegetation indicative of humid conditions and lack of fire activity, with persistent precipitation in northwestern Patagonia at ~43°S between ~ 24.0 and ~17.5 ka (Figure 6.1).

ii) An increase/dominance in vegetation indicative of relatively low humid conditions, and depressed precipitation regime in all sites between ~17.5 and ~16.5 ka (Figure 6.1)

iii) A rise in vegetation indicative of relatively more humid conditions and increased precipitation in all sites between ~16.5 and ~14.5 ka (Figure 6.1).

iv) An increase in hygrophilous vegetation and an inferred stronger precipitation regime in northwestern Patagonia and southwestern South Island of New Zealand between ~14.5 and ~12.6 ka, and a decline in hygrophilous vegetation and relatively lower precipitation in southwestern Patagonia (Figure 6.1).

v) A decline in hygrophilous vegetation and lower precipitation regime in northwestern Patagonia and southwestern South Island of New Zealand between ~12.6 and ~11.2 ka, and a rise in hygrophilous vegetation and higher precipitation regime in southwestern Patagonia (Figure 6.1).

vi) An increase (decline) in drought-tolerant (intolerant) vegetation, higher fire activity, and a decline in precipitation in all sites between ~11.2 and ~7.2 ka (Figure 6.1).

vii) An increase in vegetation indicative of humid conditions and increased precipitation in all sites at ~7.2 ka, overprinted with millennial- and/or centennial-scale changes in vegetation and precipitation with lack/intermittent fire activity between ~7.2 and ~0.5 ka (Figure 6.1).

viii) The Lago Pintito and Lake Von records show increased fire activity during the last ~600 years, coeval with a decline in arboreal pollen and rise in vegetation indicative of human disturbance (Chilean, Māori, European). I observe that the Lago Emerenciana record shows similar changes, with an increase in macroscopic CHAR coeval with exotic herbs in the uppermost assemblages.

Table 6.1. Summary of inferred precipitation regime between the three study sites, Lago Emerenciana, Lake Von and Lago Pintito.

Site / Timing	Lago Emerenciana (43°S, 74°W)	Lake Von (45°S, 168°E)	Lago Pintito (52°S, 72°W)
~24.0 and ~17.5 ka	major		
~17.5 and ~16.5 ka	diminished	diminished	diminished
~16.5 and ~14.5 ka	minor	minor	major
~14.5 and ~12.6 ka	major	major	minor
~12.6 and ~11.2 ka	minor	minor	major
~11.2 and ~7.2 ka	diminished	diminished	diminished
Last ~7200 years	major and high variability	major and high variability	major and high variability

6.2. Discussion

6.2.1. Regional and hemispheric implications

When comparing past changes in vegetation, fire activity and inferred precipitation regimes across sites with very different physiographic, regional and hemispheric settings, major differences are to be expected. In particular, local hydrologic and physiographic setting and other site factors are likely to have a varying influence on vegetation developments that at times may over-ride the visibility in these datasets of broader scale trends or patterns at any given site. It is hardly surprising therefore that I have detected similarities as well as differences in timing and direction of past vegetation changes and the major inferred climate developments at multi-millennial, millennial and centennial timescales. Notwithstanding these complexities, the following sections examine the extent of intra-regional coherency in inferred climate shifts.

The preceding section has described the climate history of northwestern Patagonia, southwestern Patagonia and southwestern South Island of New Zealand with a particular

emphasis on precipitation variability. Because local precipitation in all three regions exhibits a strong positive correlation with zonal wind strength (Figure 2.2), this relationship provides a means for inferring changes in past SWW strength for the duration of these records The latitudinal range the study sites also provides an opportunity to evaluate latitudinal shift in the SWW in the middle latitudes of the Southern Hemisphere.

In this section I examine the timing and direction of precipitation regimes inferred from these three records and their implications for SWW variability in the mid and high latitudes of Southern Hemisphere during and since the LGM. I acknowledge that only the Lago Emerenciana record extents into the LGM interval.

6.2.2. The SWW during the LGM (~24-17.5 ka)

The Lago Emerenciana record suggests that glacial cold conditions were accompanied by a high precipitation regime between ~24.0 and ~17.5 ka in northwestern Patagonia (41°-43°S) at ~43°S with maximum precipitation between ~22.8 and ~17.5 ka. These results replicate pollen-based hydrological reconstructions from northwestern Patagonia in southern South America, suggesting a strong and permanent influence of the SWW during the LGM that increased to a maximum between ~22.8 and ~17.5 ka (Heusser, 1995; Heusser et al., 1999; Moreno et al., 2015; Moreno et al., 1999; Moreno et al., 2018a). A recent synthesis and analysis of paleoenvironmental data from New Zealand also indicate strengthening of the southern westerly winds during the LGM, (Lorrey and Bostock, 2017; Lorrey et al., 2012), and when taken together with the southern South America data suggests a zonally symmetric trans-Pacific SWW shift equatorwards. In contrast, some paleoclimate reconstructions from western Patagonia and New Zealand indicate relatively drier conditions than present during the LGM (Drost et al., 2007; Markgraf et al., 2007; Whittaker et al., 2011; Williams et al., 2005), implying weak SWW across the southern Pacific. This divergence can be attributed to two possible scenarios: i) strong/equatorward shift of the SWW or ii) weak/poleward shift of the SWW. As stated in chapter 1, recent studies have proposed that latitudinal shifts and intensity variations of the SWW played a crucial role in driving glacial-interglacial changes in the global oceans' heat and carbon cycling during and since the LGM (Anderson et al., 2009; Denton et al., 2010; Fletcher and Moreno, 2011; Moreno et al., 2010; Toggweiler et al., 2006). These authors hypothesize that reduced SWW stress in the surface of the Southern Ocean result in increased ocean stratification, reduction of upwelling in the Southern Ocean and

ventilation CO_2-enriched deep water and, consequently, lowering of atmospheric CO_2, and vice versa. I note that strong SWW influence in northwestern Patagonia during the LGM reported in this thesis was concurrent with low atmospheric CO_2 concentration revealed by Antarctic ice core records (Monnin et al., 2001) (Figure 6.1). Thus, I posit that the SWW shifted equatorward during the LGM (scenario i), giving empirical support to the hypothesized role of the SWW mentioned above.

6.2.3. The SWW during T1 (~17.5-11.2 ka)

I interpret a decline in precipitation in all sites (Lago Emerenciana, Lago Pintito and Lake Von) between ~17.5 and ~16.5 ka as indicative of less SWW influence in northwestern and southwestern Patagonia (at ~43°S and ~55°S) and southern South Island of New Zealand (at ~45°S) as a result of a southward shift of the SWW at the commencement of T1 (Figure 6.1). This was contemporaneous with the establishment of warmer conditions and reduced precipitation in northwestern Patagonia (Moreno et al., 2015; Moreno et al., 2018a; Pesce and Moreno, 2014) and New Zealand (Newnham et al., 2003), a warming detected from pollen records in New Zealand (Newnham et al., 2003; Vandergoes et al., 2013), extensive glacier recession throughout Patagonia and the central Southern Alps in New Zealand (Barrell, 2011; Moreno et al., 2015; Putnam et al., 2013; Sagredo et al., 2011) and a sustained increase in temperature and atmospheric CO_2 concentration recorded from Antarctic ice cores (Monnin et al., 2001). A poleward shift of the SWW at the beginning of T1 may have increased wind stress on the surface of the Southern Ocean, invigorated upwelling of CO_2-enriched deep water and release of CO_2 to the atmosphere, leading to a positive feedback on deglacial warming (Anderson et al., 2009).

I observe relatively warmer conditions and precipitation in all sites between ~16.5 and ~14.5 ka, probably reflecting a northward shift or strengthening of the SWW over northwestern and southwestern Patagonia and southern New Zealand. These changes are in agreement with paleoclimate inferences from records from northwestern (Moreno, 2020; Moreno et al., 2015; Moreno et al., 2018a; Pesce and Moreno, 2014) and central-west Patagonia (Henríquez et al., 2017; Vilanova et al., 2019), southern South Island of New Zealand (Anderson et al., 2018; Newnham et al., 2012; Vandergoes et al., 2008), and contemporaneous with CO_2 rise recorded in Antarctic ice core records (Monnin et al., 2001) (Figure 6.1).

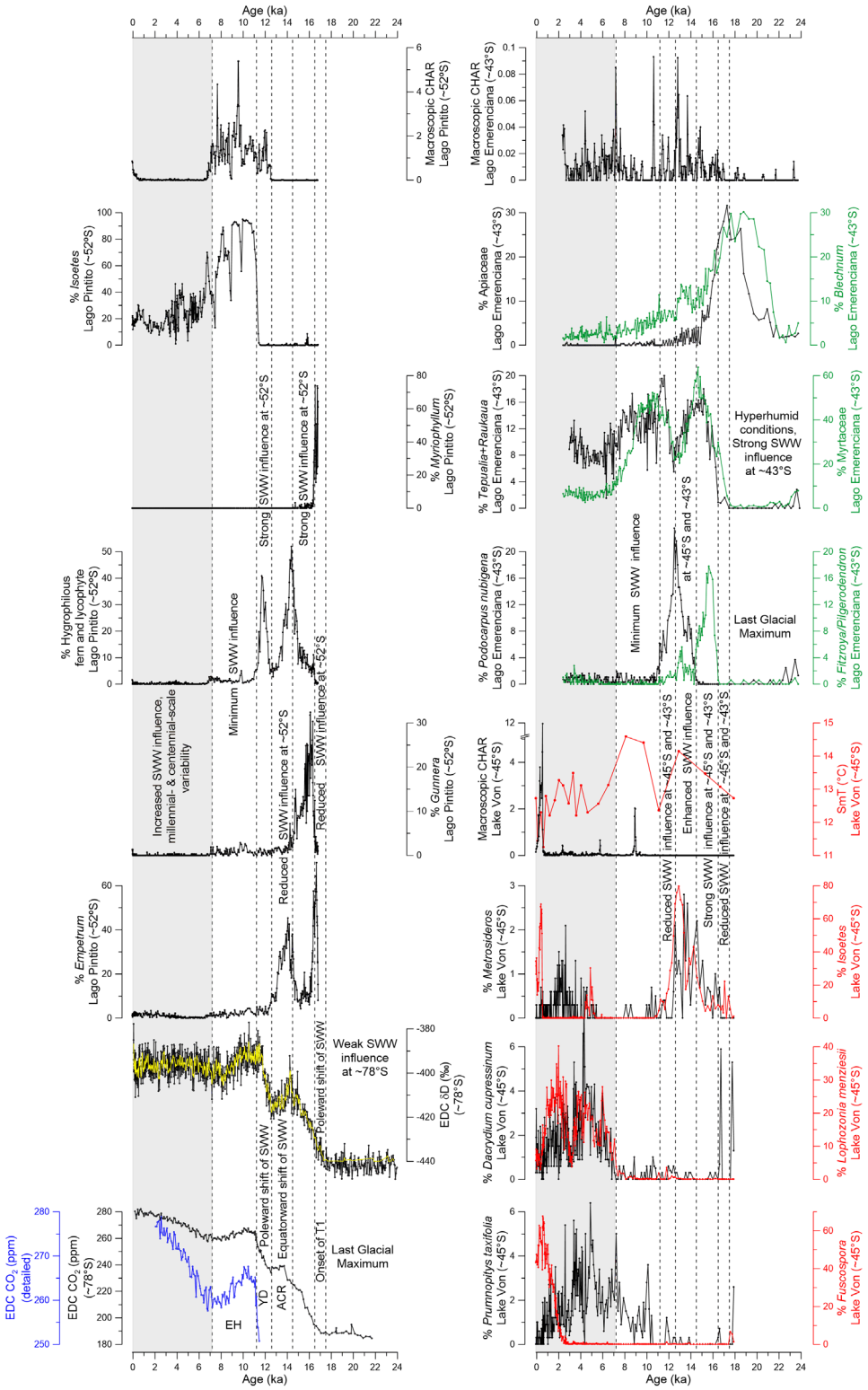

Figure 6.1. Comparison of selected pollen taxa and macroscopic charcoal records from Lago Emerenciana, Lake Von and Lago Pintito records, with reconstructed summer temperature (SmT) from Lake Von and ice data from Antarctic records (Monnin et al., 2001). The vertical dashed lines constrain the timing of the main inferred climate changes, indicating the Last Glacial Maximum (LGM), Antarctic Cold Reversal (ACR), Younger Dryas chron (YD) and the early Holocene (EH). The left vertical gray rectangles highlight an interval with increased SWW influence with millennial- and centennial-scale variability over the last ~7000 years.

I detect a coherent cooling and heterogeneities in precipitation among sites between ~14.5 and ~12.6 ka. I observe enhanced precipitation in Lago Emerenciana and Lake Von during this period, interpreted as stronger SWW influence over northwestern Patagonia (at ~43°S) and southern New Zealand (at ~45°S) during the Antarctic Cold Reversal (ACR). The Lago Pintito record, on the other hand, indicates high precipitation but lower in magnitude than the previous interval, suggesting permanent but less SWW influence in southwestern Patagonia (at ~52°S). I interpret these results as an equatorward shift of the SWW with the zone of maximum SWW influence over northwestern Patagonia and southern New Zealand and the southern margins of the SWW over southwestern Patagonia (Figure 6.1). Recently, Vilanova et al. (2019) detected in-phase positive SWW anomalies between the Central Patagonian Andes (45° and 49°S) and southwestern Patagonia during the ACR and out-of-phase positive anomalies with northwestern Patagonia. My results presented in this thesis are in agreement with Vilanova et al. (2019) findings, suggesting a northward shift of the SWW during the ACR. These findings are consistent with reconstructed-SWW influence and cooling detected in southern New Zealand (Anderson et al., 2018; Hinojosa et al., 2019; McGlone et al., 2004; Vandergoes et al., 2008; Vandergoes and Fitzsimons, 2003), and contemporaneous with glacial readvances in the Southern Alps of New Zealand (Kaplan et al., 2013; Putnam et al., 2010; Sikes et al., 2013) and Western Patagonia (Moreno et al., 2009b; Sagredo et al., 2018; Sagredo et al., 2011), and a halt in the deglacial CO_2 rise (Monnin et al., 2001).

Lago Emerenciana and Lake Von records indicate a decline in precipitation between ~12.6 and ~11.2 ka, suggesting a reduction of the SWW in northwestern Patagonia and southern New Zealand, contemporaneous with Younger Dryas chron (YD). In Lago Pintito record, on the other hand, I detect an increase in precipitation during the same interval, suggesting enhanced SWW influence in southwestern Patagonia (Figure 6.1). Combined, I interpret these data as a poleward shift of the SWW during the YD chron, with the zone of maximum SWW influence over southwestern Patagonia, and the northern margins of the SWW affecting over northwestern Patagonia and southern New Zealand. These results are consistent with diminished SWW influence inferred from paleoclimate records from northwestern Patagonia (Moreno et al., 2018a; Pesce and Moreno, 2014) and southern New Zealand (Anderson et al., 2018; Hinojosa et al., 2019), and increased SWW influence detected in central-western (Henríquez et al., 2017; Vilanova et al., 2019) and southwestern Patagonia (Moreno et al.,

2012). These changes were contemporaneous with glacial recession in southwestern Patagonia (García et al., 2018b; Mendelova et al., 2017; Moreno et al., 2009b; Sagredo et al., 2011) and in the southern Alps (Kaplan et al., 2010) and renewed Antarctic warming and resumption of the atmospheric CO_2 (Monnin et al., 2001).

6.2.4. The SWW during the early to late Holocene (~11.2-0.6 ka)

Large-scale warming and major reduction in precipitation in all sites between ~11.2 and ~7.2 ka suggest reduced SWW influence in northwestern and southwestern Patagonia and southern New Zealand at the beginning of the Holocene (Figure 6.1). I note correspondence in timing with weak SWW reported from other records from Western Patagonia (Abarzúa et al., 2004; Moreno, 2004, 2020; Moreno et al., 2015; Moreno and Videla, 2016; Moreno et al., 2018a; Moreno et al., 2018c; Moreno et al., 2012; Pesce and Moreno, 2014; Van Daele et al., 2016; Villa-Martínez et al., 2012) and southern New Zealand (Anderson et al., 2018; Hinojosa et al., 2019; Vandergoes et al., 1997), and diminished SWW influence throughout other Southern Hemisphere landmasses, suggesting a zonally symmetric decline in the SWW strength during the early Holocene (Fletcher and Moreno, 2012). I posit that diminished wind stress on the surface of the Southern Ocean at the commencement of the Holocene, resulted in reduction of deep upwelling and CO_2 ventilation and, consequently, a conspicuous lowering of atmospheric CO_2 concentration (Monnin et al., 2001) (Figure 6.1). An alternative scenario involves a poleward contraction of the SWW during the early Holocene (Lamy et al., 2010), which would imply an increase in upwelling and CO_2 ventilation and rising in atmospheric CO_2 rather than the observed decrease in Antarctic ice core records (Monnin et al., 2001).

Increased precipitation in all sites at ~7.2 ka suggests a strengthening of the SWW in nothwestern and southwestern Patagonia and southern New Zealand (Figure 6.1). Stronger SWW influence at southern mid-latitudes is concurrent with a sustained rise in atmospheric CO_2 reported from Antarctic records (Monnin et al., 2001), suggesting major SWW influence over the Southern Ocean and, therefore, enhanced ventilation CO_2-enriched deep water. Millennial- and centennial-scale changes in precipitation are superimposed upon, and following this increasing trend started at ~7.2 ka and lasted until ~0.6 ka, indicating high variability of the SWW. Other paleoclimate records from mid- and high- latitude in the

Southern Hemisphere also show millennial- and centennial-scale shifts in the SWW (Hinojosa et al., 2017; Knudson et al., 2011; Koffman et al., 2014; Moreno et al., 2018b; Moy et al., 2008; Turney et al., 2016), explained by the establishment of stronger regional climate modes such as ENSO (El Niño-Southern Oscillation) and/or SAM (Southern Annular Mode) (Hinojosa et al., 2017; Moreno et al., 2018c).

6.2.5. Fire regime

Macroscopic charcoal records from Lago Emerenciana, Lago Pintito and Lake Von allowed the examination of local fire occurrence in Western Patagonia and southern New Zealand during and since the LGM, with important variations in timing, frequency and magnitude of events (Figure 6.2). The Lago Emerenciana, Lago Pintito and Lake Von records shows lack of fire activity between ~24.0 and ~17.5 ka, ~17.0 and ~12.6 ka, and ~18.0 and ~10.0 ka, respectively, in a context of a landscape dominate by herbs and shrubs with humid/hyperhumid conditions. Fire activity started at ~17.0, ~12.6 and ~10.0 ka in Lago Emerenciana, Lago Pintito and Lake Von, respectively, contemporaneous with rising/high abundance of arboreal vegetation and less humid/dry conditions, with large-magnitude fire events in all sites between ~11.1 and ~7.2 ka under drier conditions. This was followed by either lack or low fire activity in all sites with low-magnitude events between ~7.2 and ~0.6 ka (Figure 6.2). Altogether, these data indicate a close correspondence between woodland/forest establishment and increases in the magnitude and frequency of charcoal peaks (Figure 6.2), raising the possibility that a climate-induced accumulation of woody fuel, combined with climate-induced desiccation of coarse, were necessary for the occurrence of fire in these sectors. I observe that broad-scale syntheses of charcoal records also show high fire activity during the early Holocene in southern South America (Power et al., 2008; Whitlock et al., 2007), followed by a generalized decline between ~9.5 and ~6.0 ka, and intensification during the last ~3,000 years. These authors postulated that this fire activity was driven primary by climate changes related to shifts in the SWW. However, Power et al. (2008) found heterogeneity in the paleofire signals between other Southern Hemisphere landmasses, suggesting that Native American populations may have generated ignition of biomass since ~13.0 ka (Borrero et al., 2009; Power et al., 2008). Unlike southern South America, New Zealand records the first arrival of Polynesians (Māori) during the last millennium (at ~0.7 ka) (Wilmshurst et al., 2008), thus the

occurrence of paleofires beyond ~0.7 ka cannot be attributed to human activity. Hence, I posit that generation of paleofires in all sites were driven mainly by a high seasonality in precipitation and/or decline in precipitation driven by a hemisphere-wide reduction in the SWW influence at the beginning of the Holocene.

I observe that sites located in northwestern and southwestern Patagonia show onset of Chile/European disturbance during the last millennium, revealed by deforestation and spread of exotic herbs (*Rumex*) and increased fire activity (Figure 6.2). In Lake Von I observe the commencement of human (Māori) disturbance at ~0.56 ka, with a decline in arboreal pollen and rises in herbs and fern species that, in a context of a prominent rise in fire activity, are indicative of human disturbance (*Pteridium*, *Rumex* and Asteraceae Cichorioideae).

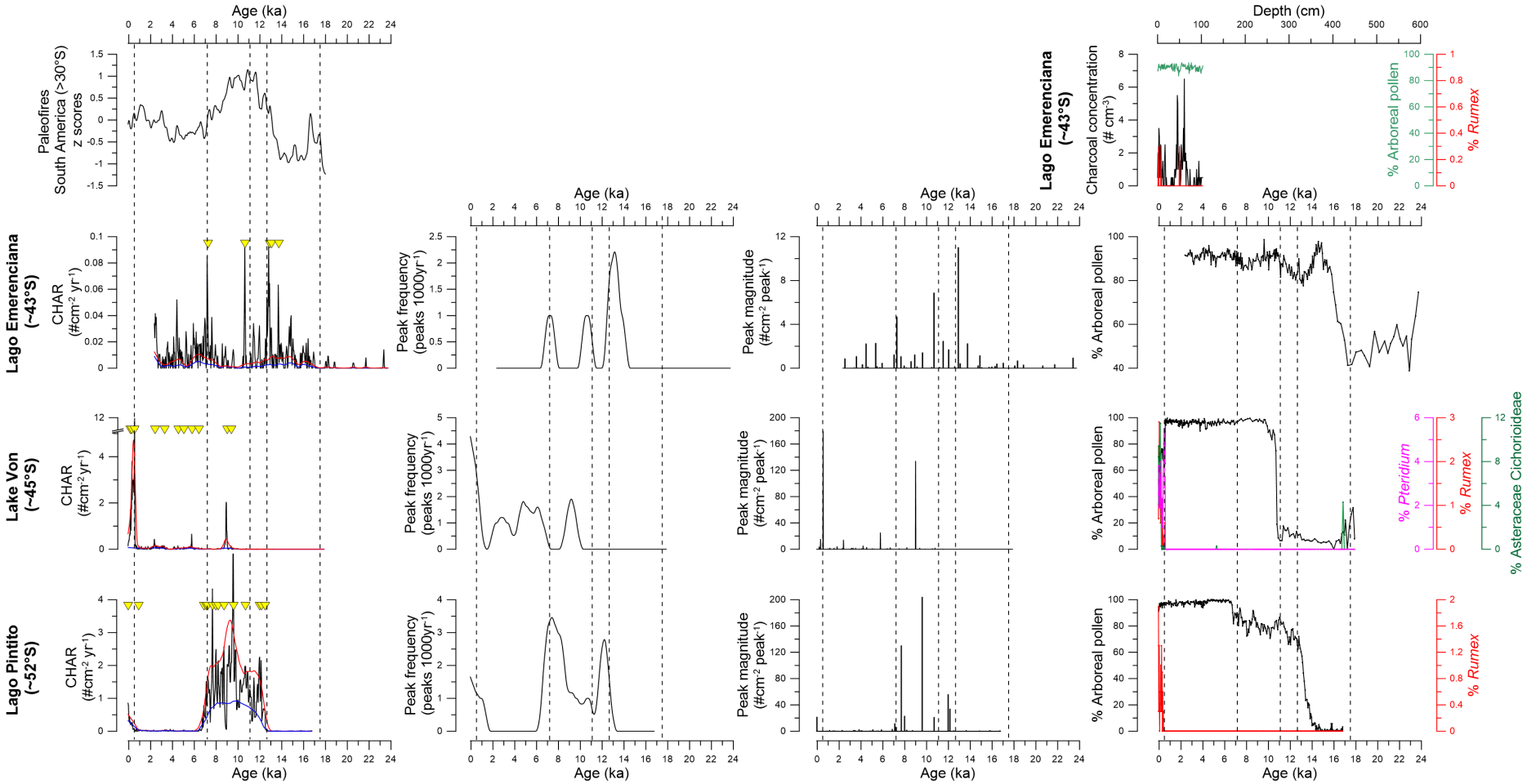

Figure 6.2. Comparison of macroscopic charcoal records and results of CharAnalysis from Lago Emerenciana, Lake Von and Lago Pintito, along with arboreal pollen and species indicative of disturbances (*Rumex* and *Pteridium*). Also shown are the charcoal synthesis curve from southern South America (Power et al., 2008) and charcoal concentration from Lago Emerenciana from the water-sediment interface core. The vertical dashed lines indicate important changes in the records. In left panels are shown the calculated background (blue lines), locally defined threshold values (red lines), and statistically significant charcoal peaks (yellow rectangles).

6.3. Research hypothesis

The findings from Lago Emerenciana, Lago Pintito and Lake Von aided me to test the following hypotheses:

i) Climate variability

Hypothesis 1: If hemisphere-wide climate changes have been the main drivers of terrestrial environmental transformations in landmasses across the southern mid-latitudes during and since the LGM, then fossil pollen and macroscopic charcoal records from Western Patagonia (at 43° and at 52°S) and New Zealand's southern South Island (at 46°S) should show:

a) Coherence in the timing and direction of vegetation change;
b) Coherence in the timing and direction of fire-regime change.

Hypothesis 2: If sub-continental climatic and/or non-climatic (human activity) regimes have been the main drivers of terrestrial environmental transformations in landmasses across the southern mid-latitudes during and since the LGM, then fossil pollen and macroscopic charcoal records from Western Patagonia (at 43°S and at 52°S) and New Zealand's southern South Island (at 46°S) should show:

a) Divergence in the timing and direction of vegetation change;
b) Divergence in the timing and direction of fire-regime change.

Based on the results discussed in section 6.2, I observe that the Lago Emerenciana and Lake Von records reveal coherence in timing and direction of vegetation and fire regime at millennial and multi-millennial scales between ~18.0 and ~4.0 ka. I note that Lago Pintito record also shows coherence in timing of vegetation and fire regime with Lago Emerenciana and Lake Von between ~17.5 and ~7.0 ka, but exhibits divergence in direction of vegetation and fire between ~14.5 and ~11.2 ka. These results suggest that hemisphere-wide climate change, particularly latitudinal shifts in the SWW may have modulated terrestrial environmental transformation in Western Patagonia and southern South Island of New Zealand. Divergence in the timing and direction of vegetation and fire regime between sites

started at ~7.0 ka, attributed to heterogeneities at sub-continental levels caused by climate modes such as ENSO and SAM. All records show decline in arboreal cover driven by human disturbance during the last few centuries through the use of fire, leading to deforestation and expansion of invasive/opportunistic species.

ii) SWW and atmospheric CO_2 co-variability

Hypothesis 1: If shifts in the position and/or strength of the SWW modulated the atmospheric CO_2 concentration through wind-driven upwelling of CO_2-rich deep waters in the high southern latitudes during and since the LGM, then inferred SWW changes from paleoecological records from Western Patagonia and New Zealand's southern South Island should show:

a) Poleward shifts and/or enhanced SWW influence concurrent with increases in atmospheric CO_2 concentration;
b) Equatorward shifts and/or reduced SWW influence concurrent with declining atmospheric CO_2 concentration.

Hypothesis 2: If shifts in the position and/or strength of the SWW do not modulated the atmospheric CO_2 concentration through wind-driven upwelling of CO_2-rich deep waters in the high southern latitudes during and since the LGM, then inferred SWW changes from paleoecological records from Western Patagonia and New Zealand's southern South Island should show:

a) Poleward shifts and/or enhanced SWW influence concurrent with declining in atmospheric CO_2 concentration;
b) Equatorward shifts and/or reduced SWW influence concurrent with increases atmospheric CO_2 concentration.

Based on the results discussed in section 6.2, I note that suggested poleward shifts of the SWW and/or enhanced SWW influence over the southernmost site (Lago Pintito, ~52°S) were concurrent with increases in atmospheric CO_2 concentration, while suggested equatorward shifts and/or reduced SWW influence over the southernmost site (Lago Pintito) were

concurrent with decline in atmospheric CO_2 concentration. Therefore, I posit that hemisphere-wide changes in the position and/or strength of the SWW have modulated the atmospheric CO_2 concentration through wind-driven upwelling of CO_2-rich deep waters in the high southern latitudes during and since the LGM.

6.4. Future research directions

6.4.1. Develop more paleoclimate records from southern mid-latitudes

Although the results from all three records presented in this thesis provide multi-millennial and sub-millennial hemisphere-wide trends in climate and SWW in the southern mid-latitudes, I acknowledge that additional paleoclimate studies are needed to better understand latitudinal changes in the SWW. I suggest that further studies should be focused on sectors north (<~45°S) and south (>~45°S) of Lake Von in New Zealand, as well as in central-west Patagonia (~45-49°S) in southern South America.

6.4.2. Developing and improvement of Chironomid records

The exploratory chironomid record from Lake Von provides valuable insights into summer temperature in southwestern New Zealand at multi-millennial timescales. However, I note that the low resolution of this record impedes the visualization of sub-millennial changes, and the relationship with millennial and centennial-scales shifts in terrestrial ecosystems. Improved resolution and the development of new chironomid records from both New Zealand and Western Patagonia will contribute to elucidating climate patterns in the southern mid-latitudes.

References

Abarzúa, A. M., Moreno, P. I. (2008). Changing fire regimes in the temperate rainforest region of southern Chile over the last 16,000 yr. *Quaternary Research, 69*(1), 62-71. doi:https://doi.org/10.1016/j.yqres.2007.09.004

Abarzúa, A. M., Villagrán, C., Moreno, P. I. (2004). Deglacial and postglacial climate history in east-central Isla Grande de Chiloé, southern Chile (43°S). *Quaternary Research, 62*(1), 49-59. doi:https://doi.org/10.1016/j.yqres.2004.04.005

Allen, R., Stewart, G. H., Rogers, G. (2002). Maintenance of key tree species.

Alley, R. B., Clark, P. U., Keigwin, L. D., Webb, R. S. (1999). Making Sense of Millennial-Scale Climate Change. In *Mechanisms of Global Climate Change at Millennial Time Scales* (pp. 385-394).

Anderson, H. J., Moy, C. M., Vandergoes, M. J., Nichols, J. E., Riesselman, C. R., Van Hale, R. (2018). Southern Hemisphere westerly wind influence on southern New Zealand hydrology during the Lateglacial and Holocene. *Journal of Quaternary Science, 33*(6), 689-701. doi:10.1002/jqs.3045

Anderson, R. F., Ali, S., Bradtmiller, L. I., Nielsen, S. H. H., Fleisher, M. Q., Anderson, B. E., Burckle, L. H. (2009). Wind-Driven Upwelling in the Southern Ocean and the Deglacial Rise in Atmospheric CO₂. *Science, 323*(5920), 1443-1448. doi:10.1126/science.1167441

Armitage, P. D., Pinder, L., Cranston, P. (2012). *The Chironomidae: biology and ecology of non-biting midges*: Springer Science & Business Media.

Barrell, D. (2011). Quaternary glaciers of New Zealand. In *Developments in Quaternary Sciences* (Vol. 15, pp. 1047-1064): Elsevier.

Barrell, D. J. A., Almond, P. C., Vandergoes, M. J., Lowe, D. J., Newnham, R. M. (2013). A composite pollen-based stratotype for inter-regional evaluation of climatic events in New Zealand over the past 30,000 years (NZ-INTIMATE project). *Quaternary Science Reviews, 74*, 4-20. doi:https://doi.org/10.1016/j.quascirev.2013.04.002

Birks, H. j. b., Braak, C. j. f. T., Line, J. M., Juggins, S., Stevenson, A. C., Battarbee, R. W., Mason, B. J., Renberg, I., Talling, J. F. (1990). Diatoms and pH reconstruction. *Philosophical Transactions of the Royal Society of London. B, Biological Sciences, 327*(1240), 263-278. doi:doi:10.1098/rstb.1990.0062

Blaauw, M., Christen, J. A. (2011). Flexible paleoclimate age-depth models using an autoregressive gamma process. *Bayesian Anal., 6*(3), 457-474. doi:10.1214/11-BA618

Borrero, L. A., Barberena, R., Franco, N. V., Charlin, J., Tykot, R. H. (2009). Isotopes and rocks: geographical organisation of southern Patagonian hunter-gatherers. *International Journal of Osteoarchaeology, 19*(2), 309-327. doi:10.1002/oa.1036

Bracegirdle, T. J. (2019). "The Climate Data Guide: Southern Hemisphere westerly jet strength and position." *National Center for Atmospheric Research Staff (Eds).*

Bradley, R. S. (2015). Chapter 9 - Lake Sediments. In R. S. Bradley (Ed.), *Paleoclimatology (Third Edition)* (pp. 319-343). San Diego: Academic Press.

Brodersen, K. P., Lindegaard, C. (1999). Classification, assessment and trophic reconstruction of Danish lakes using chironomids. *Freshwater Biology, 42*(1), 143-157. doi:10.1046/j.1365-2427.1999.00457.x

Brodersen, K. P., Quinlan, R. (2006). Midges as palaeoindicators of lake productivity, eutrophication and hypolimnetic oxygen. *Quaternary Science Reviews, 25*(15), 1995-2012. doi:https://doi.org/10.1016/j.quascirev.2005.03.020

Broecker, W. S. (1998). Paleocean circulation during the Last Deglaciation: A bipolar seesaw? *Paleoceanography, 13*(2), 119-121. doi:10.1029/97pa03707

Brooks, S. J., Langdon, P. G., Heiri, O., Association, Q. R. (2007). *The Identification and Use of Palaearctic Chironomidae Larvae in Palaeoecology*: Quaternary Research Association.

Brownsey, P., Perrie, L. (2014). Flora of New Zealand Ferns and Lycophytes. *Breitwieser, I. Heenan, Wilton, AD Flora of New Zealand*.

Buizert, C., Adrian, B., Ahn, J., Albert, M., Alley, R. B., Baggenstos, D., Bauska, T. K., Bay, R. C., Bencivengo, B. B., Bentley, C. R., Brook, E. J., Chellman, N. J., Clow, G. D., Cole-Dai, J., Conway, H., Cravens, E., Cuffey, K. M., Dunbar, N. W., Edwards, J. S., Fegyveresi, J. M., Ferris, D. G., Fitzpatrick, J. J., Fudge, T. J., Gibson, C. J., Gkinis, V., Goetz, J. J., Gregory, S., Hargreaves, G. M., Iverson, N., Johnson, J. A., Jones, T. R., Kalk, M. L., Kippenhan, M. J., Koffman, B. G., Kreutz, K., Kuhl, T. W., Lebar, D. A., Lee, J. E., Marcott, S. A., Markle, B. R., Maselli, O. J., McConnell, J. R., McGwire, K. C., Mitchell, L. E., Mortensen, N. B., Neff, P. D., Nishiizumi, K., Nunn, R. M., Orsi, A. J., Pasteris, D. R., Pedro, J. B., Pettit, E. C., Buford Price, P., Priscu, J. C., Rhodes, R. H., Rosen, J. L., Schauer, A. J., Schoenemann, S. W., Sendelbach, P. J., Severinghaus, J. P., Shturmakov, A. J., Sigl, M., Slawny, K. R., Souney, J. M., Sowers, T. A., Spencer, M. K., Steig, E. J., Taylor, K. C., Twickler, M. S., Vaughn, B. H., Voigt, D. E., Waddington, E. D., Welten, K. C., Wendricks, A. W., White, J. W. C., Winstrup, M., Wong, G. J., Woodruff, T. E., Members, W. D. P. (2015). Precise interpolar phasing of abrupt climate change during the last ice age. *Nature, 520*(7549), 661-665. doi:10.1038/nature14401

Campbell, J. F. E., Fletcher, W. J., Hughes, P. D., Shuttleworth, E. L. (2016). A comparison of pollen extraction methods confirms dense-media separation as a reliable method of pollen preparation. *Journal of Quaternary Science, 31*(6), 631-640. doi:10.1002/jqs.2886

Chandler, C., Cheney, P., Thomas, P., Trabaud, L., Williams, D. (1983). *Fire in forestry. Volume 1. Forest fire behavior and effects. Volume 2. Forest fire management and organization*: John Wiley & Sons, Inc.

Chapman, M. R., Shackleton, N. J., Duplessy, J.-C. (2000). Sea surface temperature variability during the last glacial–interglacial cycle: assessing the magnitude and pattern of climate change in the North Atlantic. *Palaeogeography, Palaeoclimatology, Palaeoecology, 157*(1), 1-25. doi:https://doi.org/10.1016/S0031-0182(99)00168-6

Clapperton, C. M., Sugden, D. E., Kaufman, D. S., McCulloch, R. D. (1995). The Last Glaciation in Central Magellan Strait, Southernmost Chile. *Quaternary Research, 44*(2). doi:https://doi.org/10.1006/qres.1995.1058

Cumberland, K. B. (1971). Climatic Change or Cultural Interference? New Zealand in Moahunter Times. In S. R. Eyre (Ed.), *World Vegetation Types* (pp. 216-226). London: Palgrave Macmillan UK.

Davies, B. J., Darvill, C. M., Lovell, H., Bendle, J. M., Dowdeswell, J. A., Fabel, D., García, J.-L., Geiger, A., Glasser, N. F., Gheorghiu, D. M., Harrison, S., Hein, A. S., Kaplan, M. R., Martin, J. R. V., Mendelova, M., Palmer, A., Pelto, M., Rodés, Á., Sagredo, E. A., Smedley, R. K., Smellie, J. L., Thorndycraft, V. R. (2020). The evolution of the

Patagonian Ice Sheet from 35 ka to the present day (PATICE). *Earth-Science Reviews, 204*, 103152. doi:https://doi.org/10.1016/j.earscirev.2020.103152

Dean, W. E. (1974). Determination of carbonate and organic matter in calcareous sediments and sedimentary rocks by loss on ignition; comparison with other methods. *Journal of Sedimentary Research, 44*(1), 242-248. doi:10.1306/74d729d2-2b21-11d7-8648000102c1865d

Denton, G. H., Anderson, R. F., Toggweiler, J. R., Edwards, R. L., Schaefer, J. M., Putnam, A. E. (2010). The Last Glacial Termination. *Science, 328*(5986), 1652-1656. doi:10.1126/science.1184119

Denton, G. H., Lowell, T. V., Heusser, C. J., Schlüchter, C., Andersen, B. G., Heusser, L. E., Moreno, P. I., Marchant, D. R. (1999). Geomorphology, Stratigraphy, and Radiocarbon Chronology of LlanquihueDrift in the Area of the Southern Lake District, Seno Reloncaví, and Isla Grande de Chiloé, Chile. *Geografiska Annaler: Series A, Physical Geography, 81*(2), 167-229. doi:10.1111/1468-0459.00057

Diaz, H. F., Hoerling, M. P., Eischeid, J. K. (2001). ENSO variability, teleconnections and climate change. *International Journal of Climatology, 21*(15), 1845-1862. doi:https://doi.org/10.1002/joc.631

Dieffenbacher-Krall, A. C., Vandergoes, M. J., Denton, G. H. (2007). An inference model for mean summer air temperatures in the Southern Alps, New Zealand, using subfossil chironomids. *Quaternary Science Reviews, 26*(19), 2487-2504. doi:https://doi.org/10.1016/j.quascirev.2007.06.016

Dieffenbacher-Krall, A. C., Vandergoes, M. J., Woodward, C. A., Boothroyd, I. K. (2008). Guide to identification and ecology of New Zealand subfossil chironomids found in lake sediment. *Climate Change Institute, University of Maine, Orono, 11*.

Dillehay, T. D., Ocampo, C., Saavedra, J., Sawakuchi, A. O., Vega, R. M., Pino, M., Collins, M. B., Scott Cummings, L., Arregui, I., Villagran, X. S., Hartmann, G. A., Mella, M., González, A., Dix, G. (2015). New Archaeological Evidence for an Early Human Presence at Monte Verde, Chile. *PLOS ONE, 10*(11), e0141923. doi:10.1371/journal.pone.0141923

Dodson, J. R. (1998). Timing and response of vegetation change to Milankovitch forcing in temperate Australia and New Zealand. *Global and Planetary Change, 18*(3), 161-174. doi:https://doi.org/10.1016/S0921-8181(98)00018-6

Drost, F., Renwick, J., Bhaskaran, B., Oliver, H., McGregor, J. (2007). A simulation of New Zealand's climate during the Last Glacial Maximum. *Quaternary Science Reviews, 26*(19), 2505-2525. doi:https://doi.org/10.1016/j.quascirev.2007.06.005

Eggermont, H., Heiri, O., Russell, J., Vuille, M., Audenaert, L., Klaassen, G., Verschuren, D. (2008). *Fossil Chironomidae (Insecta: Diptera) as Paleothermometers in the African Tropics*. Paper presented at the AGU Fall Meeting Abstracts. https://ui.adsabs.harvard.edu/abs/2008AGUFMGC21A0715E

Faegri, K., Kaland, P. E., Krzywinski, K. (1989). *Textbook of pollen analysis*: John Wiley & Sons Ltd.

Fenner, N., Freeman, C. (2011). Drought-induced carbon loss in peatlands. *Nature Geoscience, 4*(12), 895-900. doi:10.1038/ngeo1323

Fercovic, E. I. (2020). Evolución de la vegetación, regímenes de fuego y clima en el extremo suroriental de Isla Grande de Chiloé desde el término de la última glaciación. *Departamento de Ciencias Ecol ógicas. Universidad de Chile, Santiago*.

Fesq-Martin, M., Friedmann, A., Peters, M., Behrmann, J., Kilian, R. (2004). Late-glacial and Holocene vegetation history of the Magellanic rain forest in southwestern Patagonia, Chile. *Vegetation History and Archaeobotany, 13*(4), 249-255. doi:10.1007/s00334-004-0047-6

Figueroa, J. A., Lusk, C. H. (2001). Germination requirements and seedling shade tolerance are not correlated in a Chilean temperate rain forest. *New Phytologist, 152*(3), 483-489. doi:10.1046/j.0028-646X.2001.00282.x

Fitzsimmons, K. E., Barrows, T. T. (2010). Holocene hydrologic variability in temperate southeastern Australia: An example from Lake George, New South Wales. *The Holocene, 20*(4), 585-597. doi:10.1177/0959683609356589

Fitzsimons, S. J. (1997). Late-glacial and early Holocene glacier activity in the Southern Alps, New Zealand. *Quaternary International, 38-39*, 69-76. doi:https://doi.org/10.1016/S1040-6182(96)00022-5

Fletcher, M.-S., Moreno, P. I. (2011). Zonally symmetric changes in the strength and position of the Southern Westerlies drove atmospheric CO2 variations over the past 14 k.y. *Geology, 39*(5), 419-422. doi:10.1130/g31807.1

Fletcher, M.-S., Moreno, P. I. (2012). Have the Southern Westerlies changed in a zonally symmetric manner over the last 14,000 years? A hemisphere-wide take on a controversial problem. *Quaternary International, 253*, 32-46. doi:https://doi.org/10.1016/j.quaint.2011.04.042

Fontana, S. L., Bennett, K. (2012). Postglacial vegetation dynamics of western Tierra del Fuego. *The Holocene, 22*(11), 1337-1350. doi:10.1177/0959683612444144

Franklin, D. A. (1968). Biological flora of New Zealand. *New Zealand Journal of Botany, 6*(4), 493-513. doi:10.1080/0028825X.1968.10428587

García, J.-L., Hein, A. S., Binnie, S. A., Gómez, G. A., González, M. A., Dunai, T. J. (2018a). The MIS 3 maximum of the Torres del Paine and Última Esperanza ice lobes in Patagonia and the pacing of southern mountain glaciation. *Quaternary Science Reviews, 185*, 9-26. doi:https://doi.org/10.1016/j.quascirev.2018.01.013

García, J.-L., Maldonado, A., de Porras, M. E., Nuevo Delaunay, A., Reyes, O., Ebensperger, C. A., Binnie, S. A., Lüthgens, C., Méndez, C. (2018b). Early deglaciation and paleolake history of Río Cisnes Glacier, Patagonian Ice Sheet (44°S). *Quaternary Research, 91*(1), 194-217. doi:10.1017/qua.2018.93

Garreaud, R. D. (2007). Precipitation and Circulation Covariability in the Extratropics. *Journal of Climate, 20*(18), 4789-4797. doi:10.1175/jcli4257.1

Glasser, N. F., Jansson, K. N., Harrison, S., Kleman, J. (2008). The glacial geomorphology and Pleistocene history of South America between 38°S and 56°S. *Quaternary Science Reviews, 27*(3), 365-390. doi:https://doi.org/10.1016/j.quascirev.2007.11.011

Godley, E. J. (1979). Flower biology in New Zealand. *New Zealand Journal of Botany, 17*(4), 441-466. doi:10.1080/0028825X.1979.10432564

Godley, E. J., Moar, N. T. (1973). Vegetation and Pollen Analysis of Two Bogs on Chiloé. *New Zealand Journal of Botany, 11*(2), 255-268. doi:10.1080/0028825X.1973.10430278

Gonzalorena, L. (2015). Historia postglacial de la vegetación de Lago Tarumán en la zona centro-occidental de Isla Grande de Chiloé: inferencias paleoambientales a partir de un registro palinológico de alta resolución. *Departamento de Ciencias Ecol ógicas. Universidad de Chile, Santiago*.

Grimm, E. C. (1987). CONISS: a FORTRAN 77 program for stratigraphically constrained cluster analysis by the method of incremental sum of squares. *Computers & Geosciences, 13*(1), 13-35. doi:https://doi.org/10.1016/0098-3004(87)90022-7

Grimm, E. C., Jacobson, G. L. (1992). Fossil-pollen evidence for abrupt climate changes during the past 18 000 years in eastern North America. *Climate Dynamics, 6*(3), 179-184. doi:10.1007/BF00193530

Hawes, I., Riis, T., Sutherland, D., Flanagan, M. (2003). Physical constraints to aquatic plant growth in New Zealand lakes. *Journal of Aquatic Plant Management, 41*, 44-52.

Heiri, O., Lotter, A. F. (2001). Effect of low count sums on quantitative environmental reconstructions: an example using subfossil chironomids. *Journal of Paleolimnology, 26*(3), 343-350. doi:10.1023/A:1017568913302

Heiri, O., Lotter, A. F., Lemcke, G. (2001). Loss on ignition as a method for estimating organic and carbonate content in sediments: reproducibility and comparability of results. *Journal of Paleolimnology, 25*(1), 101-110. doi:10.1023/a:1008119611481

Henrichs, M. L., Walker, I. R., Mathewes, R. W. (2001). Chironomid-based paleosalinity records in southern British Columbia, Canada: a comparison of transfer functions. *Journal of Paleolimnology, 26*(2), 147-159. doi:10.1023/A:1011180810493

Henríquez, W. I., Moreno, P. I., Alloway, B. V., Villarosa, G. (2015). Vegetation and climate change, fire-regime shifts and volcanic disturbance in Chiloé Continental (43°S) during the last 10,000 years. *Quaternary Science Reviews, 123*, 158-167. doi:https://doi.org/10.1016/j.quascirev.2015.06.017

Henríquez, W. I., Villa-Martínez, R., Vilanova, I., De Pol-Holz, R., Moreno, P. I. (2017). The last glacial termination on the eastern flank of the central Patagonian Andes (47 ° S). *Climate of the Past, 13*, 879.

Heusser, C. (1994). Paleoindians and fire during the late Quaternary in southern South America. *Revista Chilena de Historia Natural, 67*(4), 435-443.

Heusser, C. J. (1971). *Pollen and spores of Chile*: University of Arizona Press.

Heusser, C. J. (1989). Late Quaternary vegetation and climate of southern Tierra del Fuego. *Quaternary Research, 31*(3), 396-406. doi:https://doi.org/10.1016/0033-5894(89)90047-1

Heusser, C. J. (1990a). Chilotan piedmont glacier in the southern Andes during the last glacial maximum. *Andean Geology, 17*(1), 3-18.

Heusser, C. J. (1990b). Ice age vegetation and climate of subtropical Chile. *Palaeogeography, Palaeoclimatology, Palaeoecology, 80*(2), 107-127. doi:https://doi.org/10.1016/0031-0182(90)90124-P

Heusser, C. J. (1995). Three Late Quaternary pollen diagrams from Southern Patagonia and their palaeoecological implications. *Palaeogeography, Palaeoclimatology, Palaeoecology, 118*(1), 1-24. doi:https://doi.org/10.1016/0031-0182(94)00138-X

Heusser, C. J. (2003). *Ice Age Southern Andes: A Chronicle of Palaeoecological Events*: Elsevier Science.

Heusser, C. J., Denton, G. H., Hauser, A., Andersen, B. G., Lowell, T. V. (1995). Quaternary pollen records from the Archipiélago de Chiloé in the context of glaciation and climate. *Andean Geology, 22*(1), 25-46.

Heusser, C. J., Flint, R. F. (1977). Quaternary glaciations and environments of northern Isla Chiloé, Chile. *Geology, 5*(5), 305-308. doi:10.1130/0091-7613(1977)5<305:qgaeon>2.0.co;2

Heusser, C. J., Heusser, L. E. (2006). Submillennial palynology and palaeoecology of the last glaciation at Taiquemó (~50,000calyr, MIS 2–4) in southern Chile. *Quaternary Science Reviews, 25*(5), 446-454. doi:https://doi.org/10.1016/j.quascirev.2005.04.008

Heusser, C. J., Heusser, L. E., Lowell, T. V. (1999). Paleoecology of The Southern Chilean Lake District-Isla Grande de Chiloé During Middle–late Llanquihue Glaciation and Deglaciation. *Geografiska Annaler: Series A, Physical Geography, 81*(2), 231-284. doi:10.1111/1468-0459.00058

Heusser, C. J., Streeter, S. S., Stuiver, M. (1981). Temperature and precipitation record in southern Chile extended to ~43,000 yr ago. *Nature, 294*(5836), 65-67. doi:10.1038/294065a0

Higuera, P. E., Brubaker, L. B., Anderson, P. M., Hu, F. S., Brown, T. A. (2009). Vegetation mediated the impacts of postglacial climate change on fire regimes in the south-central Brooks Range, Alaska. *Ecological Monographs, 79*(2), 201-219. doi:10.1890/07-2019.1

Hill, M. (1973). Diversity and Evenness: A Unifying Notation and Its Consequences. *Ecology, 54*, 427-432. doi:10.2307/1934352

Hinojosa, J. L., Moy, C. M., Stirling, C. H., Wilson, G. S., Eglinton, T. I. (2017). A New Zealand perspective on centennial-scale Southern Hemisphere westerly wind shifts during the last two millennia. *Quaternary Science Reviews, 172*, 32-43. doi:https://doi.org/10.1016/j.quascirev.2017.07.016

Hinojosa, J. L., Moy, C. M., Vandergoes, M., Feakins, S. J., Sessions, A. L. (2019). Hydrologic Change in New Zealand During the Last Deglaciation Linked to Reorganization of the Southern Hemisphere Westerly Winds. *Paleoceanography and Paleoclimatology, 34*(12), 2158-2170. doi:https://doi.org/10.1029/2019PA003656

Hogg, A. G., Heaton, T. J., Hua, Q., Palmer, J. G., Turney, C. S., Southon, J., Bayliss, A., Blackwell, P. G., Boswijk, G., Ramsey, C. B. (2020). SHCal20 Southern Hemisphere calibration, 0–55,000 years cal BP. *Radiocarbon, 62*(4), 759-778.

Hogg, A. G., Hua, Q., Blackwell, P. G., Niu, M., Buck, C. E., Guilderson, T. P., Heaton, T. J., Palmer, J. G., Reimer, P. J., Reimer, R. W., Turney, C. S. M., Zimmerman, S. R. H. (2013). SHCal13 Southern Hemisphere calibration, 0–50,000 years cal BP. *Radiocarbon, 55*(2), 1-15. doi:DOI:10.2458/azu_js_rc.55.16783

Hollin, J. T., Schilling, D. H. (1981). Late Wisconsin-Weichselian mountain glaciers and small ice caps. In: Denton, G.H., Hughes, T. J. (Eds.), The Last Great Ice Sheets. Wiley Interscience. 179-206.

Holloway, J. T. (1954). Forest and climates in the South Island, New Zealand. *Transactions of the Royal Society of New Zealand, 82: 329-410*.

Holz, A., Veblen, T. T. (2012). Wildfire activity in rainforests in western Patagonia linked to the Southern Annular Mode. *International Journal of Wildland Fire, 21*(2), 114-126. doi:https://doi.org/10.1071/WF10121

Huber, U. M., Markgraf, V., Schäbitz, F. (2004). Geographical and temporal trends in Late Quaternary fire histories of Fuego-Patagonia, South America. *Quaternary Science Reviews, 23*(9), 1079-1097. doi:https://doi.org/10.1016/j.quascirev.2003.11.002

Jara, I. A., Moreno, P. I. (2012). Temperate rainforest response to climate change and disturbance agents in northwestern Patagonia (41°S) over the last 2600years. *Quaternary Research, 77*(2), 235-244. doi:https://doi.org/10.1016/j.yqres.2011.11.011

Jara, I. A., Moreno, P. I. (2014). Climatic and disturbance influences on the temperate rainforests of northwestern Patagonia (40 °S) sinceB<14,500 cal yr BP. *Quaternary Science Reviews, 90*, 217-228.

Jara, I. A., Newnham, R. M., Alloway, B. V., Wilmshurst, J. M., Rees, A. B. (2017). Pollen-based temperature and precipitation records of the past 14,600 years in northern New Zealand (37°S) and their linkages with the Southern Hemisphere atmospheric circulation. *The Holocene, 27*(11), 1756-1768. doi:10.1177/0959683617708444

Jouzel, J., Masson-Delmotte, V. (2007). EPICA Dome C Ice Core 800KYr deuterium data and temperature estimates. In *Supplement to: Jouzel, Jean; Masson-Delmotte, Valerie; Cattani, Olivier; Dreyfus, Gabrielle; Falourd, Sonia; Hoffmann, G; Minster, B; Nouet, J; Barnola, Jean-Marc; Chappellaz, Jérôme A; Fischer, Hubertus; Gallet, J C; Johnsen, Sigfus J; Leuenberger, Markus C; Loulergue, Laetitia; Luethi, D; Oerter, Hans; Parrenin, Frédéric; Raisbeck, Grant M; Raynaud, Dominique; Schilt, Adrian; Schwander, Jakob; Selmo, Enrico; Souchez, Roland; Spahni, Renato; Stauffer, Bernhard; Steffensen, Jørgen Peder; Stenni, Barbara; Stocker, Thomas F; Tison, Jean-Louis; Werner, Martin; Wolff, Eric W (2007): Orbital and millennial Antarctic climate variability over the past 800,000 years. Science, 317(5839), 793-797, https://doi.org/10.1126/science.1141038*: PANGAEA.

Kaplan, M. R., Schaefer, J. M., Denton, G. H., Barrell, D. J. A., Chinn, T. J. H., Putnam, A. E., Andersen, B. G., Finkel, R. C., Schwartz, R., Doughty, A. M. (2010). Glacier retreat in New Zealand during the Younger Dryas stadial. *Nature, 467*(7312), 194-197. doi:10.1038/nature09313

Kaplan, M. R., Schaefer, J. M., Denton, G. H., Doughty, A. M., Barrell, D. J. A., Chinn, T. J. H., Putnam, A. E., Andersen, B. G., Mackintosh, A., Finkel, R. C., Schwartz, R., Anderson, B. (2013). The anatomy of long-term warming since 15 ka in New Zealand based on net glacier snowline rise. *Geology, 41*(8), 887-890. doi:10.1130/g34288.1

Karoly, D. J., Vincent, D. G., Schrage, J. M. (1998). General Circulation. In D. J. Karoly & D. G. Vincent (Eds.), *Meteorology of the Southern Hemisphere* (pp. 47-85). Boston, MA: American Meteorological Society.

Kidson, J. W., Renwick, J. A. (2002). Patterns of convection in the tropical pacific and their influence on New Zealand weather. *International Journal of Climatology, 22*(2), 151-174. doi:10.1002/joc.737

Knudson, K. P., Hendy, I. L., Neil, H. L. (2011). Re-examining Southern Hemisphere westerly wind behavior: insights from a late Holocene precipitation reconstruction using New Zealand fjord sediments. *Quaternary Science Reviews, 30*(21), 3124-3138. doi:https://doi.org/10.1016/j.quascirev.2011.07.017

Knutti, R., Flückiger, J., Stocker, T. F., Timmermann, A. (2004). Strong hemispheric coupling of glacial climate through freshwater discharge and ocean circulation. *Nature, 430*(7002), 851-856. doi:10.1038/nature02786

Koffman, B. G., Kreutz, K. J., Breton, D. J., Kane, E. J., Winski, D. A., Birkel, S. D., Kurbatov, A. V., Handley, M. J. (2014). Centennial-scale variability of the Southern Hemisphere westerly wind belt in the eastern Pacific over the past two millennia. *Clim. Past, 10*(3), 1125-1144. doi:10.5194/cp-10-1125-2014

Krawchuk, M. A., Moritz, M. A., Parisien, M.-A., Van Dorn, J., Hayhoe, K. (2009). Global Pyrogeography: the Current and Future Distribution of Wildfire. *PLOS ONE, 4*(4), e5102. doi:10.1371/journal.pone.0005102

Lamy, F., Hebbeln, D., Wefer, G. (1999). High-Resolution Marine Record of Climatic Change in Mid-latitude Chile during the Last 28,000 Years Based on Terrigenous Sediment Parameters. *Quaternary Research, 51*(1), 83-93. doi:https://doi.org/10.1006/qres.1998.2010

Lamy, F., Kilian, R., Arz, H. W., Francois, J.-P., Kaiser, J., Prange, M., Steinke, T. (2010). Holocene changes in the position and intensity of the southern westerly wind belt. *Nature Geoscience, 3*(10), 695-699. doi:10.1038/ngeo959

Langgut, D., Almogi-Labin, A., Bar-Matthews, M., Weinstein-Evron, M. (2011). Vegetation and climate changes in the South Eastern Mediterranean during the Last Glacial-Interglacial cycle (86 ka): new marine pollen record. *Quaternary Science Reviews, 30*(27), 3960-3972. doi:https://doi.org/10.1016/j.quascirev.2011.10.016

Large, M. F., Braggins, J. E. (1990). Effect of different treatments on the morphology and size of fern spores. *Review of Palaeobotany and Palynology, 64*(1), 213-221. doi:https://doi.org/10.1016/0034-6667(90)90135-6

Letréguilly, A., Reeh, N., Huybrechts, P. (1991). The Greenland ice sheet through the last glacial-interglacial cycle. *Palaeogeography, Palaeoclimatology, Palaeoecology, 90*(4), 385-394. doi:https://doi.org/10.1016/S0031-0182(12)80037-X

Ljung, K., Björck, S. (2007). Holocene climate and vegetation dynamics on Nightingale Island, South Atlantic—an apparent interglacial bipolar seesaw in action? *Quaternary Science Reviews, 26*(25), 3150-3166. doi:https://doi.org/10.1016/j.quascirev.2007.08.003

Lorrey, A., Williams, P., Salinger, J., Martin, T., Palmer, J., Fowler, A., Zhao, J.-x., Neil, H. (2008). Speleothem stable isotope records interpreted within a multi-proxy framework and implications for New Zealand palaeoclimate reconstruction. *Quaternary International, 187*(1), 52-75. doi:https://doi.org/10.1016/j.quaint.2007.09.039

Lorrey, A. M., Bostock, H. (2017). The Climate of New Zealand Through the Quaternary. In J. Shulmeister (Ed.), *Landscape and Quaternary Environmental Change in New Zealand* (pp. 67-139). Paris: Atlantis Press.

Lorrey, A. M., Bostock, H. C. (2014). Australasia: An Overview of Modern Climate and Paleoclimate during the Last Glacial Maximum. In J. Beattie, E. O'Gorman, & M. Henry (Eds.), *Climate, Science, and Colonization: Histories from Australia and New Zealand* (pp. 19-42). New York: Palgrave Macmillan US.

Lorrey, A. M., Vandergoes, M., Almond, P., Renwick, J., Stephens, T., Bostock, H., Mackintosh, A., Newnham, R., Williams, P. W., Ackerley, D., Neil, H., Fowler, A. M. (2012). Palaeocirculation across New Zealand during the last glacial maximum at ~21 ka. *Quaternary Science Reviews, 36*, 189-213. doi:https://doi.org/10.1016/j.quascirev.2011.09.025

Macara, G. R. (2014). *The climate and weather of Southland*: NIWA.

Mansilla, C. A., McCulloch, R. D., Morello, F. (2016). Palaeoenvironmental change in Southern Patagonia during the Lateglacial and Holocene: Implications for forest refugia and climate reconstructions. *Palaeogeography, Palaeoclimatology, Palaeoecology, 447*, 1-11. doi:https://doi.org/10.1016/j.palaeo.2016.01.041

Mansilla, C. A., McCulloch, R. D., Morello, F. (2018). The vulnerability of the Nothofagus forest-steppe ecotone to climate change: Palaeoecological evidence from Tierra del Fuego (~53°S). *Palaeogeography, Palaeoclimatology, Palaeoecology, 508*, 59-70. doi:https://doi.org/10.1016/j.palaeo.2018.07.014

Mark, A. F., Bliss, L. C. (1970). The high-alpine vegetation of Central Otago, New Zealand. *New Zealand Journal of Botany, 8*(4), 381-451. doi:10.1080/0028825X.1970.10430156

Mark, A. F., McLennan, B. (2005). The conservation status of New Zealand's indigenous grasslands. *New Zealand Journal of Botany, 43*(1), 245-270.

Markgraf, V. (1993). Climatic History of Central and South America since 18,000 yr B.P

Comparison of Pollen Records and Model Simulations. In H. E. Wright, J. E. Kutzbach, T. Webb, W. F. Ruddiman, F. A. Street-Perrott, & P. J. Bartlein (Eds.), *Global Climates since the Last Glacial Maximum* (NED - New edition ed., pp. 357-385): University of Minnesota Press.

Markgraf, V., Huber, U. M. (2010). Late and postglacial vegetation and fire history in Southern Patagonia and Tierra del Fuego. *Palaeogeography, Palaeoclimatology, Palaeoecology, 297*(2), 351-366. doi:https://doi.org/10.1016/j.palaeo.2010.08.013

Markgraf, V., Whitlock, C., Haberle, S. (2007). Vegetation and fire history during the last 18,000 cal yr B.P. in Southern Patagonia: Mallín Pollux, Coyhaique, Province Aisén (45°41'30" S, 71°50'30" W, 640 m elevation). *Palaeogeography Palaeoclimatology Palaeoecology, 254*, 492-507.

Martinic, M. (1974). Reconocimiento geogra´fico y colonizacio´n de Ultima Esperanza. *Anales del Instituto de la Patagonia, 5*, 5–53.

Maslin, M. A., Smart, C. W. (2010). Holocene bipolar climate seesaw: possible subtle evidence from the deep North East Atlantic Ocean? *Journal of Quaternary Science, 25*(3), 237-242. doi:10.1002/jqs.1344

Massaferro, J., Larocque-Tobler, I. (2013). Using a newly developed chironomid transfer function for reconstructing mean annual air temperature at Lake Potrok Aike, Patagonia, Argentina. *Ecological Indicators, 24*, 201-210. doi:https://doi.org/10.1016/j.ecolind.2012.06.017

Massaferro, J., Larocque-Tobler, I., Brooks, S. J., Vandergoes, M., Dieffenbacher-Krall, A., Moreno, P. (2014). Quantifying climate change in Huelmo mire (Chile, Northwestern Patagonia) during the Last Glacial Termination using a newly developed chironomid-based temperature model. *Palaeogeography, Palaeoclimatology, Palaeoecology, 399*, 214-224. doi:https://doi.org/10.1016/j.palaeo.2014.01.013

McGlone, M., Wilmshurst, J. (1999). Dating initial Maori environmental impact in New Zealand. *Quaternary International, 59*, 5-16.

McGlone, M. S. (1983). Polynesian Deforestation of New Zealand: A Preliminary Synthesis. *Archaeology in Oceania, 18*(1), 11-25.

McGlone, M. S., Bathgate, J. L. (1983). Vegetation and climate history of the Longwood Range, South Island, New Zealand, 12 000 B. P. to the present. *New Zealand Journal of Botany, 21*(3), 293-315. doi:10.1080/0028825X.1983.10428560

McGlone, M. S., Mark, A. F., Bell, D. (1995). Late Pleistocene and Holocene vegetation history, Central Otago, South Island, New Zealand. *Journal of the Royal Society of New Zealand, 25*(1), 1-22. doi:10.1080/03014223.1995.9517480

McGlone, M. S., Moar, N. (1998). Dryland Holocene vegetation history, Central Otago and the Mackenzie Basin, South Island, New Zealand. *New Zealand Journal of Botany, 36*, 91-111.

McGlone, M. S., Richardson, S. J., Burge, O. R., Perry, G. L. W., Wilmshurst, J. M. (2017). Palynology and the Ecology of the New Zealand Conifers. *Frontiers in Earth Science, 5*(94). doi:10.3389/feart.2017.00094

McGlone, M. S., Salinger, M. J., Moar, N. T. (1993). Paleovegetation Studies of New Zealand's Climate since the Last Glacial Maximum. In H. E. Wright, J. E. Kutzbach, T. Webb, W. F. Ruddiman, F. A. Street-Perrott, & P. J. Bartlein (Eds.), *Global Climates since the Last Glacial Maximum* (NED - New edition ed., pp. 294-317): University of Minnesota Press.

McGlone, M. S., Turney, C. S. M., Wilmshurst, J. M. (2004). Late-glacial and Holocene vegetation and climatic history of the Cass Basin, central South Island, New Zealand. *Quaternary Research, 62*(3), 267-279. doi:https://doi.org/10.1016/j.yqres.2004.09.003

McGlone, M. S., Turney, C. S. M., Wilmshurst, J. M., Renwick, J., Pahnke, K. (2010). Divergent trends in land and ocean temperature in the Southern Ocean over the past 18,000 years. *Nature Geoscience, 3*(9), 622-626. doi:10.1038/ngeo931

McGlone, M. S., Wilmshurst, J. M., Richardson, S. J., Turney, C. S. M., Wood, J. R. (2019). Temperature, Wind, Cloud, and the Postglacial Tree Line History of Sub-Antarctic Campbell Island. *Forests, 10*(11), 998.

McGlone, M. S., Wilmshurst, J. M., Wiser, S. K. (2000). Lateglacial and Holocene vegetation and climatic change on Auckland Island, Subantarctic New Zealand. *The Holocene, 10*(6), 719-728. doi:10.1191/09596830094962

McWethy, D. B., Whitlock, C., Wilmshurst, J. M., McGlone, M. S., Fromont, M., Li, X., Dieffenbacher-Krall, A., Hobbs, W. O., Fritz, S. C., Cook, E. R. (2010). Rapid landscape transformation in South Island, New Zealand, following initial Polynesian settlement. *Proceedings of the National Academy of Sciences, 107*(50), 21343-21348. doi:10.1073/pnas.1011801107

Meadows, M. E., Baxter, A. J. (1999). Late Quaternary Palaeoenvironments of the southwestern Cape, South Africa: a regional synthesis. *Quaternary International, 57-58*, 193-206. doi:https://doi.org/10.1016/S1040-6182(98)00060-3

Mendelova, M., Hein, A. S., McCulloch, R., Davies, B. (2017). The Last Glacial Maximum and deglaciation in central Patagonia, 44°S–49°S. *2017, 43*(2), 32. doi:10.18172/cig.3263

Mercer, J. H. (1965). Glacier Variations in Southern Patagonia. *Geographical Review, 55*(3), 390-413. doi:10.2307/213136

Metcalf, J. L., Turney, C., Barnett, R., Martin, F., Bray, S. C., Vilstrup, J. T., Orlando, L., Salas-Gismondi, R., Loponte, D., Medina, M., De Nigris, M., Civalero, T., Fernández, P. M., Gasco, A., Duran, V., Seymour, K. L., Otaola, C., Gil, A., Paunero, R., Prevosti, F. J., Bradshaw, C. J. A., Wheeler, J. C., Borrero, L., Austin, J. J., Cooper, A. (2016). Synergistic roles of climate warming and human occupation in Patagonian megafaunal extinctions during the Last Deglaciation. *Science Advances, 2*(6), e1501682. doi:10.1126/sciadv.1501682

Meurk, C. D. (1984). BIOCLIMATIC ZONES FOR THE ANTIPODES — AND BEYOND? *New Zealand Journal of Ecology, 7*, 175-181.

Moar, N. T. (1993). Pollen grains of New Zealand dicotyledonous plants. *Pollen grains of New Zealand dicotyledonous plants.*

Monnin, E., Indermühle, A., Dällenbach, A., Flückiger, J., Stauffer, B., Stocker, T. F., Raynaud, D., Barnola, J.-M. (2001). Atmospheric CO₂ Concentrations over the Last Glacial Termination. *Science, 291*(5501), 112-114. doi:10.1126/science.291.5501.112

Montecinos, A., Aceituno, P. (2003). Seasonality of the ENSO-Related Rainfall Variability in Central Chile and Associated Circulation Anomalies. *Journal of Climate, 16*(2), 281-296. doi:10.1175/1520-0442(2003)016<0281:soterr>2.0.co;2

Moreno, P. I. (2004). Millennial-scale climate variability in northwest Patagonia over the last 15 000 yr. *Journal of Quaternary Science, 19*(1), 35-47. doi:10.1002/jqs.813

Moreno, P. I. (2020). Timing and structure of vegetation, fire, and climate changes on the Pacific slope of northwestern Patagonia since the last glacial termination. *Quaternary Science Reviews, 238*, 106328. doi:https://doi.org/10.1016/j.quascirev.2020.106328

Moreno, P. I., Denton, G. H., Moreno, H., Lowell, T. V., Putnam, A. E., Kaplan, M. R. (2015). Radiocarbon chronology of the last glacial maximum and its termination in northwestern Patagonia. *Quaternary Science Reviews, 122*, 233-249. doi:https://doi.org/10.1016/j.quascirev.2015.05.027

Moreno, P. I., Francois, J. P., Moy, C. M., Villa-Martínez, R. (2010). Covariability of the Southern Westerlies and atmospheric CO2 during the Holocene. *Geology, 38*(8), 727-730. doi:10.1130/g30962.1

Moreno, P. I., François, J. P., Villa-Martínez, R. P., Moy, C. M. (2009a). Millennial-scale variability in Southern Hemisphere westerly wind activity over the last 5000 years in SW Patagonia. *Quaternary Science Reviews, 28*(1), 25-38. doi:https://doi.org/10.1016/j.quascirev.2008.10.009

Moreno, P. I., Kaplan, M. R., François, J. P., Villa-Martínez, R., Moy, C. M., Stern, C. R., Kubik, P. W. (2009b). Renewed glacial activity during the Antarctic cold reversal and persistence of cold conditions until 11.5 ka in southwestern Patagonia. *Geology, 37*(4), 375-378. doi:10.1130/g25399a.1

Moreno, P. I., Lowell, T. V., Jacobson Jr, G. L., Denton, G. H. (1999). Abrupt Vegetation and Climate Changes During the Last Glacial Maximumand Last Termination in The Chilean Lake District: A Case Study from Canal De La Puntilla (41°S). *Geografiska Annaler: Series A, Physical Geography, 81*(2), 285-311. doi:10.1111/1468-0459.00059

Moreno, P. I., Simi, E., Villa-Martínez, R. P., Vilanova, I. (2019). Early arboreal colonization, postglacial resilience of deciduous Nothofagus forests, and the Southern Westerly Wind influence in central-east Andean Patagonia. *Quaternary Science Reviews, 218*, 61-74. doi:https://doi.org/10.1016/j.quascirev.2019.06.004

Moreno, P. I., Videla, J. (2016). Centennial and millennial-scale hydroclimate changes in northwestern Patagonia since 16,000 yr BP. *Quaternary Science Reviews, 149*, 326-337. doi:https://doi.org/10.1016/j.quascirev.2016.08.008

Moreno, P. I., Videla, J., Valero-Garcés, B., Alloway, B. V., Heusser, L. E. (2018a). A continuous record of vegetation, fire-regime and climatic changes in northwestern Patagonia spanning the last 25,000 years. *Quaternary Science Reviews, 198*, 15-36. doi:https://doi.org/10.1016/j.quascirev.2018.08.013

Moreno, P. I., Vilanova, I., Villa-Martínez, R., Dunbar, R. B., Mucciarone, D. A., Kaplan, M. R., Garreaud, R. D., Rojas, M., Moy, C. M., De Pol-Holz, R., Lambert, F. (2018b). Onset and Evolution of Southern Annular Mode-Like Changes at Centennial Timescale. *Scientific Reports, 8*(1), 3458. doi:10.1038/s41598-018-21836-6

Moreno, P. I., Vilanova, I., Villa-Martínez, R., Garreaud, R. D., Rojas, M., De Pol-Holz, R. (2014). Southern Annular Mode-like changes in southwestern Patagonia at centennial timescales over the last three millennia. *Nature Communications, 5*(1), 4375. doi:10.1038/ncomms5375

Moreno, P. I., Vilanova, I., Villa-Martínez, R. P., Francois, J. P. (2018c). Modulation of Fire Regimes by Vegetation and Site Type in Southwestern Patagonia Since 13 ka. *Frontiers in Ecology and Evolution, 6*(34). doi:10.3389/fevo.2018.00034

Moreno, P. I., Villa-Martínez, R., Cárdenas, M. L., Sagredo, E. A. (2012). Deglacial changes of the southern margin of the southern westerly winds revealed by terrestrial records from SW Patagonia (52°S). *Quaternary Science Reviews, 41*, 1-21. doi:https://doi.org/10.1016/j.quascirev.2012.02.002

Moros, M., De Deckker, P., Jansen, E., Perner, K., Telford, R. J. (2009). Holocene climate variability in the Southern Ocean recorded in a deep-sea sediment core off South Australia. *Quaternary Science Reviews, 28*(19), 1932-1940. doi:https://doi.org/10.1016/j.quascirev.2009.04.007

Moy, C. M., Dunbar, R. B., Moreno, P. I., Francois, J.-P., Villa-Martínez, R., Mucciarone, D. M., Guilderson, T. P., Garreaud, R. D. (2008). Isotopic evidence for hydrologic change related to the westerlies in SW Patagonia, Chile, during the last millennium. *Quaternary Science Reviews, 27*(13), 1335-1349. doi:https://doi.org/10.1016/j.quascirev.2008.03.006

Muzzarelli, R. A. A. (2011). Chitin Nanostructures in Living Organisms. In N. S. Gupta (Ed.), *Chitin: Formation and Diagenesis* (pp. 1-34). Dordrecht: Springer Netherlands.

Newnham, R. M., Eden, D. N., Lowe, D. J., Hendy, C. H. (2003). Rerewhakaaitu Tephra, a land–sea marker for the Last Termination in New Zealand, with implications for global climate change. *Quaternary Science Reviews, 22*(2), 289-308. doi:https://doi.org/10.1016/S0277-3791(02)00137-3

Newnham, R. M., Vandergoes, M. J., Sikes, E., Carter, L., Wilmshurst, J. M., Lowe, D. J., McGlone, M. S., Sandiford, A. (2012). Does the bipolar seesaw extend to the terrestrial southern mid-latitudes? *Quaternary Science Reviews, 36*, 214-222. doi:https://doi.org/10.1016/j.quascirev.2011.04.013

Noble, A., Palmer, S. M., Glaves, D. J., Crowle, A., Brown, L. E., Holden, J. (2018). Prescribed burning, atmospheric pollution and grazing effects on peatland vegetation composition. *Journal of Applied Ecology, 55*(2), 559-569. doi:10.1111/1365-2664.12994

Norton, D. A., Herbert, J. W., Beveridge, A. E. (1988). The ecology of Dacrydium cupressinum: A review. *New Zealand Journal of Botany, 26*(1), 37-62. doi:10.1080/0028825X.1988.10410098

Ogden, J., Basher, L. E. S., McGlone, M. (1998). Fire, Forest Regeneration and Links with Early Human Habitation: Evidence from New Zealand. *Annals of Botany, 81*(6), 687-696.

Paez, M. M., Villagran, C., Carillo, R. (1994). *Modelo de la dispersion polinica actual en la region templada chileno - argentina de Sudamerica y su relacion con el clima y la vegetacion* (Vol. 67). Revista Chilena de Historia Natural.

Parry, L. E., Holden, J., Chapman, P. J. (2014). Restoration of blanket peatlands. *J Environ Manage, 133*, 193-205. doi:10.1016/j.jenvman.2013.11.033

Perry, G. L. W., Wilmshurst, J. M., McGlone, M. S. (2014). Ecology and long-term history of fire in New Zealand. *New Zealand Journal of Ecology, 38*(2), 157-176.

Pesce, O. H., Moreno, P. I. (2014). Vegetation, fire and climate change in central-east Isla Grande de Chiloé (43°S) since the Last Glacial Maximum, northwestern Patagonia. *Quaternary Science Reviews, 90*, 143-157. doi:https://doi.org/10.1016/j.quascirev.2014.02.021

Philander, S. G. H. (1983). El Niño Southern Oscillation phenomena. *Nature, 302*(5906), 295-301. doi:10.1038/302295a0

Pichon, J.-J., Labeyrie, L. D., Bareille, G., Labracherie, M., Duprat, J., Jouzel, J. (1992). Surface water temperature changes in the high latitudes of the southern hemisphere over the Last Glacial-Interglacial Cycle. *Paleoceanography, 7*(3), 289-318. doi:10.1029/92pa00709

Pillans, B., Naish, T. (2004). Defining the Quaternary. *Quaternary Science Reviews, 23*(23), 2271-2282. doi:https://doi.org/10.1016/j.quascirev.2004.07.006

Power, M. J., Marlon, J., Ortiz, N., Bartlein, P. J., Harrison, S. P., Mayle, F. E., Ballouche, A., Bradshaw, R. H. W., Carcaillet, C., Cordova, C., Mooney, S., Moreno, P. I., Prentice, I. C., Thonicke, K., Tinner, W., Whitlock, C., Zhang, Y., Zhao, Y., Ali, A. A., Anderson, R. S., Beer, R., Behling, H., Briles, C., Brown, K. J., Brunelle, A., Bush, M., Camill, P., Chu, G. Q., Clark, J., Colombaroli, D., Connor, S., Daniau, A.-L., Daniels, M., Dodson, J., Doughty, E., Edwards, M. E., Finsinger, W., Foster, D., Frechette, J., Gaillard, M.-J., Gavin, D. G., Gobet, E., Haberle, S., Hallett, D. J., Higuera, P., Hope, G., Horn, S., Inoue, J., Kaltenrieder, P., Kennedy, L., Kong, Z. C., Larsen, C., Long, C. J., Lynch, J., Lynch, E. A., McGlone, M., Meeks, S., Mensing, S., Meyer, G., Minckley, T., Mohr, J., Nelson, D. M., New, J., Newnham, R., Noti, R., Oswald, W., Pierce, J., Richard, P. J. H., Rowe, C., Sanchez Goñi, M. F., Shuman, B. N., Takahara, H., Toney, J., Turney, C., Urrego-Sanchez, D. H., Umbanhowar, C., Vandergoes, M., Vanniere, B., Vescovi, E., Walsh, M., Wang, X., Williams, N., Wilmshurst, J., Zhang, J. H. (2008). Changes in fire regimes since the Last Glacial Maximum: an assessment based on a global synthesis and analysis of charcoal data. *Climate Dynamics, 30*(7), 887-907. doi:10.1007/s00382-007-0334-x

Punt, W., Hoen, P. P., Blackmore, S., Nilsson, S., Le Thomas, A. (2007). Glossary of pollen and spore terminology. *Review of Palaeobotany and Palynology, 143*(1), 1-81. doi:https://doi.org/10.1016/j.revpalbo.2006.06.008

Putnam, A., Denton, G., Schaefer, J., Barrell, D., Andersen, G., Finkel, R., Schwartz, R., Doughty, A., Kaplan, M., Christian. (2010). Glacier advance in southern middle-latitudes during the Antarctic Cold Reversal. *Nature Geoscience, 3*, 700-704. doi:10.1038/ngeo962

Putnam, A. E., Schaefer, J. M., Denton, G. H., Barrell, D. J. A., Andersen, B. G., Koffman, T. N. B., Rowan, A. V., Finkel, R. C., Rood, D. H., Schwartz, R., Vandergoes, M. J., Plummer, M. A., Brocklehurst, S. H., Kelley, S. E., Ladig, K. L. (2013). Warming and glacier recession in the Rakaia valley, Southern Alps of New Zealand, during Heinrich Stadial 1. *Earth and Planetary Science Letters, 382*, 98-110. doi:https://doi.org/10.1016/j.epsl.2013.09.005

Quintana, J. M., Aceituno, P. (2012). Changes in the rainfall regime along the extratropical west coast of South America (Chile): 30-43º S. *Atmósfera, 25*, 1-22.

Randall, P. M. (1991). A one-year pollen trapping study in Westland and Canterbury, South Island, New Zealand. *Journal of the Royal Society of New Zealand, 21*(2), 201-218. doi:10.1080/03036758.1991.10431407

Rees, A. B. H., Cwynar, L. C. (2010a). Evidence for early postglacial warming in Mount Field National Park, Tasmania. *Quaternary Science Reviews, 29*(3), 443-454. doi:https://doi.org/10.1016/j.quascirev.2009.10.003

Rees, A. B. H., Cwynar, L. C. (2010b). A test of Tyler's Line – response of chironomids to a pH gradient in Tasmania and their potential as a proxy to infer past changes in pH. *Freshwater Biology, 55*(12), 2521-2540. doi:10.1111/j.1365-2427.2010.02482.x

Rees, A. B. H., Cwynar, L. C., Cranston, P. S. (2008). Midges (Chironomidae, Ceratopogonidae, Chaoboridae) as a temperature proxy: a training set from Tasmania, Australia. *Journal of Paleolimnology, 40*(4), 1159-1178. doi:10.1007/s10933-008-9222-6

Reimer, P. J., Bard, E., Bayliss, A., Beck, J. W., Blackwell, P. G., Bronk Ramsey, C., Buck, C. E., Cheng, H., Edwards, R. L., Friedrich, M., Grootes, P. M., Guilderson, T. P., Haflidason, H., Hajdas, I., Hatté, C., Heaton, T. J., Hoffmann, D. L., Hogg, A. G., Hughen, K. A., Kaiser, K. F., Kromer, B., Manning, S. W., Niu, M., Reimer, R. W., Richards, D. A., Scott, E. M., Southon, J. R., Staff, R. A., Turney, C. S. M., van der Plicht, J. (2013). IntCal13 and Marine13 radiocarbon age calibration curves 0-50,000 years cal BP. *Radiocarbon, 55*(4), 1869-1887. doi:DOI:10.2458/azu_js_rc.55.16947

Roberts, R. G., Flannery, T. F., Ayliffe, L. K., Yoshida, H., Olley, J. M., Prideaux, G. J., Laslett, G. M., Baynes, A., Smith, M. A., Jones, R., Smith, B. L. (2001). New Ages for the Last Australian Megafauna: Continent-Wide Extinction About 46,000 Years Ago. *Science, 292*(5523), 1888-1892. doi:10.1126/science.1060264

Rojas, M., Moreno, P., Kageyama, M., Crucifix, M., Hewitt, C., Abe-Ouchi, A., Ohgaito, R., Brady, E. C., Hope, P. (2009). The Southern Westerlies during the last glacial maximum in PMIP2 simulations. *Climate Dynamics, 32*(4), 525-548. doi:10.1007/s00382-008-0421-7

Rossaro, B. (1991). Chironomids and water temperature. *Aquatic Insects, 13*(2), 87-98. doi:10.1080/01650429109361428

Sagredo, E. A., Kaplan, M. R., Araya, P. S., Lowell, T. V., Aravena, J. C., Moreno, P. I., Kelly, M. A., Schaefer, J. M. (2018). Trans-pacific glacial response to the Antarctic Cold Reversal in the southern mid-latitudes. *Quaternary Science Reviews, 188*, 160-166. doi:https://doi.org/10.1016/j.quascirev.2018.01.011

Sagredo, E. A., Moreno, P. I., Villa-Martínez, R., Kaplan, M. R., Kubik, P. W., Stern, C. R. (2011). Fluctuations of the Última Esperanza ice lobe (52°S), Chilean Patagonia, during the last glacial maximum and termination 1. *Geomorphology, 125*(1), 92-108. doi:https://doi.org/10.1016/j.geomorph.2010.09.007

Sakai, A., Wardle, P. (1978). FREEZING RESISTANCE OF NEW ZEALAND TREES AND SHRUBS. *New Zealand Journal of Ecology, 1*, 51-61.

Schmithusen, J. (1956). Die raumliche Ordnung der chilenischen Vegetation. *Bonner Geogr. Abh., 17*.

Seager, R., Battisti, D. S. (2005). *Challenges to our understanding of the general circulation: abrupt climate change*.

Shulmeister, J., Goodwin, I., Renwick, J., Harle, K., Armand, L., McGlone, M. S., Cook, E., Dodson, J., Hesse, P. P., Mayewski, P., Curran, M. (2004). The Southern Hemisphere westerlies in the Australasian sector over the last glacial cycle: a synthesis. *Quaternary International, 118-119*, 23-53. doi:https://doi.org/10.1016/S1040-6182(03)00129-0

Sikes, E. L., Medeiros, P. M., Augustinus, P., Wilmshurst, J. M., Freeman, K. R. (2013). Seasonal variations in aridity and temperature characterize changing climate during the last deglaciation in New Zealand. *Quaternary Science Reviews, 74*, 245-256. doi:https://doi.org/10.1016/j.quascirev.2013.01.031

Simi, E., Moreno, P. I., Villa-Martínez, R., Vilanova, I., de Pol-Holz, R. (2017). Climate change and resilience of deciduous Nothofagus forests in central–east Chilean Patagonia

over the last 3200 years. *Journal of Quaternary Science, 32*(6), 845-856. doi:10.1002/jqs.2948

Simpson, G. (2007). Analogue Methods in Palaeoecology: Using the analogue Package. *Journal of Statistical Software, 22*. doi:10.18637/jss.v022.i02

Sinclair, M. R., Wratt, D. S., Henderson, R. D., Gray, W. R. (1997). Factors Affecting the Distribution and Spillover of Precipitation in the Southern Alps of New Zealand—A Case Study. *Journal of Applied Meteorology, 36*(5), 428-442. doi:10.1175/1520-0450(1997)036<0428:Fatdas>2.0.Co;2

Stern, C., Moreno, P., Henríquez, W., Villa-Martínez, R., Sagredo, E., Aravena, J., de Pol-Holz, R. (2015). Holocene tephrochronology around Cochrane (~47° S), southern Chile. *Andean Geology, 43*(1), 1-19. doi:[doi:http://dx.doi.org/10.5027/andgeoV43n1-a01]

Stern, C. R. (2008). Holocene tephrochronology record of large explosive eruptions in the southernmost Patagonian Andes. *Bulletin of Volcanology, 70*(4), 435-454. doi:10.1007/s00445-007-0148-z

Stewart, G., Ogden, J., Allen, R. (1996). Ecology of New Zealand Nothofagus forests. In (pp. 25-82).

Stocker, T. F. (1998). The Seesaw Effect. *Science, 282*(5386), 61-62. doi:10.1126/science.282.5386.61

Stockmarr, J. (1971). 1971: Tablets with spores used in absolute pollen analysis. Pollen et Spores 13, 615-621.

Strelin, J. A., Denton, G. H., Vandergoes, M. J., Ninnemann, U. S., Putnam, A. E. (2011). Radiocarbon chronology of the late-glacial Puerto Bandera moraines, Southern Patagonian Icefield, Argentina. *Quaternary Science Reviews, 30*(19), 2551-2569. doi:https://doi.org/10.1016/j.quascirev.2011.05.004

Sturman, A. P., Tapper, N. J. (2006). *The Weather and Climate of Australia and New Zealand.* (2nd ed.). *Melbourne VIC Australia: Oxford University Press*.

Sutherland, J. L., Carrivick, J. L., Evans, D. J. A., Shulmeister, J., Quincey, D. J. (2019). The Tekapo Glacier, New Zealand, during the Last Glacial Maximum: An active temperate glacier influenced by intermittent surge activity. *Geomorphology, 343*, 183-210. doi:https://doi.org/10.1016/j.geomorph.2019.07.008

Thompson, D. W. J., Wallace, J. M. (2000). Annular Modes in the Extratropical Circulation. Part I: Month-to-Month Variability*. *Journal of Climate, 13*(5), 1000-1016. doi:10.1175/1520-0442(2000)013<1000:amitec>2.0.co;2

Timmermann, A., Gildor, H., Schulz, M., Tziperman, E. (2003). Coherent Resonant Millennial-Scale Climate Oscillations Triggered by Massive Meltwater Pulses. *Journal of Climate, 16*(15), 2569-2585. doi:10.1175/1520-0442(2003)016<2569:crmcot>2.0.co;2

Toggweiler, J. R. (2005). Climate change from below. *Quaternary Science Reviews, 24*(5), 511-512. doi:https://doi.org/10.1016/j.quascirev.2005.01.002

Toggweiler, J. R. (2009). Shifting Westerlies. *Science, 323*(5920), 1434-1435. doi:10.1126/science.1169823

Toggweiler, J. R., Russell, J. L., Carson, S. R. (2006). Midlatitude westerlies, atmospheric CO2, and climate change during the ice ages. *Paleoceanography, 21*(2). doi:10.1029/2005pa001154

Turney, C. S. M., Jones, R. T., Fogwill, C., Hatton, J., Williams, A. N., Hogg, A., Thomas, Z. A., Palmer, J., Mooney, S., Reimer, R. W. (2016). A 250-year periodicity in Southern Hemisphere westerly winds over the last 2600 years. *Clim. Past, 12*(2), 189-200. doi:10.5194/cp-12-189-2016

Turney, C. S. M., McGlone, M. S., Wilmshurst, J. M. (2003). Asynchronous climate change between New Zealand and the North Atlantic during the last deglaciation. *Geology, 31*(3), 223-226. doi:10.1130/0091-7613(2003)031<0223:accbnz>2.0.co;2

Turney, C. S. M., Wilmshurst, J. M., Jones, R. T., Wood, J. R., Palmer, J. G., Hogg, A. G., Fenwick, P., Crowley, S. F., Privat, K., Thomas, Z. (2017). Reconstructing atmospheric circulation over southern New Zealand: Establishment of modern westerly airflow 5500 years ago and implications for Southern Hemisphere Holocene climate change. *Quaternary Science Reviews, 159*, 77-87. doi:https://doi.org/10.1016/j.quascirev.2016.12.017

Ugalde, P. I. (2016). Variaciones climáticas y vegetacionales durante la Última terminación Glacial en el pantano Pindal, Isla Lemuy, Archipiélago de Chiloé. *Pontificia Universidad Católica de Chile*.

Ummenhofer, C. C., England, M. H. (2007). Interannual Extremes in New Zealand Precipitation Linked to Modes of Southern Hemisphere Climate Variability. *Journal of Climate, 20*(21), 5418-5440. doi:10.1175/2007jcli1430.1

Van Daele, M., Bertrand, S., Meyer, I., Moernaut, J., Vandoorne, W., Siani, G., Tanghe, N., Ghazoui, Z., Pino, M., Urrutia, R., De Batist, M. (2016). Late Quaternary evolution of Lago Castor (Chile, 45.6°S): Timing of the deglaciation in northern Patagonia and evolution of the southern westerlies during the last 17 kyr. *Quaternary Science Reviews, 133*, 130-146. doi:https://doi.org/10.1016/j.quascirev.2015.12.021

van den Bos, V., Rees, A., Newnham, R., Vandergoes, M., Wilmshurst, J., Augustinus, P. (2018). Holocene temperature, humidity and seasonality in northern New Zealand linked to Southern Hemisphere summer insolation. *Quaternary Science Reviews, 201*, 77-88. doi:https://doi.org/10.1016/j.quascirev.2018.10.008

Vandergoes, M. J., Dieffenbacher-Krall, A. C., Newnham, R. M., Denton, G. H., Blaauw, M. (2008). Cooling and changing seasonality in the Southern Alps, New Zealand during the Antarctic Cold Reversal. *Quaternary Science Reviews, 27*(5), 589-601. doi:https://doi.org/10.1016/j.quascirev.2007.11.015

Vandergoes, M. J., Fitzsimons, S. J. (2003). The Last Glacial–Interglacial Transition (LGIT) in south Westland, New Zealand: paleoecological insight into mid-latitude Southern Hemisphere climate change. *Quaternary Science Reviews, 22*(14), 1461-1476. doi:https://doi.org/10.1016/S0277-3791(03)00074-X

Vandergoes, M. J., Fitzsimons, S. J., Newnham, R. M. (1997). Late glacial to Holocene vegetation and climate change in the eastern Takitimu Mountains, western Southland, New Zealand. *Journal of the Royal Society of New Zealand, 27*(1), 53-66. doi:10.1080/03014223.1997.9517527

Vandergoes, M. J., Newnham, R. M., Denton, G. H., Blaauw, M., Barrell, D. J. A. (2013). The anatomy of Last Glacial Maximum climate variations in south Westland, New Zealand, derived from pollen records. *Quaternary Science Reviews, 74*, 215-229. doi:https://doi.org/10.1016/j.quascirev.2013.04.015

Vandergoes, M. J., Newnham, R. M., Preusser, F., Hendy, C. H., Lowell, T. V., Fitzsimons, S. J., Hogg, A. G., Kasper, H. U., Schlüchter, C. (2005). Regional insolation forcing of late Quaternary climate change in the Southern Hemisphere. *Nature, 436*(7048), 242-245. doi:10.1038/nature03826

Vilanova, I., Moreno, P. I., Miranda, C. G., Villa-Martínez, R. P. (2019). The last glacial termination in the Coyhaique sector of central Patagonia. *Quaternary Science Reviews, 224*, 105976. doi:https://doi.org/10.1016/j.quascirev.2019.105976

Villa-Martínez, R., Moreno, P. I. (2007). Pollen evidence for variations in the southern margin of the westerly winds in SW Patagonia over the last 12,600 years. *Quaternary Research, 68*(3), 400-409. doi:https://doi.org/10.1016/j.yqres.2007.07.003

Villa-Martínez, R., Moreno, P. I., Valenzuela, M. A. (2012). Deglacial and postglacial vegetation changes on the eastern slopes of the central Patagonian Andes (47°S). *Quaternary Science Reviews, 32*, 86-99. doi:https://doi.org/10.1016/j.quascirev.2011.11.008

Villagran, C. (2001). Un modelo de la historia de la vegetación de la Cordillera de La Costa de Chile central-sur: la hipótesis glacial de Darwin. *Revista chilena de historia natural, 74*(4), 793-803.

Villagrán, C. (1980). Vegetationsgeschichtliche und pflanzensoziologische Untersuchungen im Vicente Perez Rosales National park (Chile). *Diss. Bot., 54*, 1-165.

Villagrán, C. (1985). *Analisis palinologico de los cambios vegetacionales durante el tardiglacial y postglacial en chiloe, chile*.

Villagrán, C. (1988a). Expansion of Magellanic Moorland during the late Pleistocene: Palynological evidence from northern Isla de Chiloé, Chile. *Quaternary Research, 30*(3), 304-314. doi:https://doi.org/10.1016/0033-5894(88)90006-3

Villagrán, C. (1988b). Late quaternary vegetation of southern Isla Grande de Chiloé, Chile. *Quaternary Research, 29*(3), 294-306. doi:https://doi.org/10.1016/0033-5894(88)90037-3

Villalba, R., Lara, A., Masiokas, M. H., Urrutia, R., Luckman, B. H., Marshall, G. J., Mundo, I. A., Christie, D. A., Cook, E. R., Neukom, R., Allen, K., Fenwick, P., Boninsegna, J. A., Srur, A. M., Morales, M. S., Araneo, D., Palmer, J. G., Cuq, E., Aravena, J. C., Holz, A., LeQuesne, C. (2012). Unusual Southern Hemisphere tree growth patterns induced by changes in the Southern Annular Mode. *Nature Geoscience, 5*(11), 793-798. doi:10.1038/ngeo1613

Villavicencio, N. A., Lindsey, E. L., Martin, F. M., Borrero, L. A., Moreno, P. I., Marshall, C. R., Barnosky, A. D. (2016). Combination of humans, climate, and vegetation change triggered Late Quaternary megafauna extinction in the Última Esperanza region, southern Patagonia, Chile. *Ecography, 39*(2), 125-140. doi:10.1111/ecog.01606

Walker, I. R. (1987). Chironomidae (Diptera) in paleoecology. *Quaternary Science Reviews, 6*(1), 29-40. doi:https://doi.org/10.1016/0277-3791(87)90014-X

Walker, I. R. (2001). Midges: Chironomidae and Related Diptera. In J. P. Smol, H. J. B. Birks, & W. M. Last (Eds.), *Tracking Environmental Change Using Lake Sediments: Volume 4: Zoological Indicators* (pp. 43-66). Dordrecht: Springer Netherlands.

Walker, I. R., Smol, J. P., Engstrom, D. R., Birks, H. J. B. (1991). An Assessment of Chironomidae as Quantitative Indicators of Past Climatic Change. *Canadian Journal of Fisheries and Aquatic Sciences, 48*(6), 975-987. doi:10.1139/f91-114

Wardle, J. A. (1984). *The New Zealand Beeches: Ecology, Utilisation, and Management*: New Zealand Forest Service.

Wardle, P. (1964). Facets of the distribution of forest vegetation in New Zealand. *New Zealand Journal of Botany, 2*(4), 352-366. doi:10.1080/0028825X.1964.10428748

Wardle, P. (1971). Biological flora of New Zealand 6. Metrosideros umbellata Cav. [Syn. M. lucida (Forst.f.) A. Rich.] (Myrtaceae) Southern rata. *New Zealand Journal of Botany, 9*(4), 645-671. doi:10.1080/0028825X.1971.10430227

Wardle, P. (1991). *Vegetation of New Zealand*: Cambridge University Press.

Whitlock, C., Larsen, C. (2001). Charcoal as a Fire Proxy. In J. P. Smol, H. J. B. Birks, W. M. Last, R. S. Bradley, & K. Alverson (Eds.), *Tracking Environmental Change Using Lake Sediments: Terrestrial, Algal, and Siliceous Indicators* (pp. 75-97). Dordrecht: Springer Netherlands.

Whitlock, C., Moreno, P. I., Bartlein, P. (2007). Climatic controls of Holocene fire patterns in southern South America. *Quaternary Research, 68*(1), 28-36. doi:https://doi.org/10.1016/j.yqres.2007.01.012

Whittaker, T. E., Hendy, C. H., Hellstrom, J. C. (2011). Abrupt millennial-scale changes in intensity of Southern Hemisphere westerly winds during marine isotope stages 2–4. *Geology, 39*(5), 455-458. doi:DOI:10.1130/G31827.1

Wille, M., Maidana, N. I., Schäbitz, F., Fey, M., Haberzettl, T., Janssen, S., Lücke, A., Mayr, C., Ohlendorf, C., Schleser, G. H., Zolitschka, B. (2007). Vegetation and climate dynamics in southern South America: The microfossil record of Laguna Potrok Aike, Santa Cruz, Argentina. *Review of Palaeobotany and Palynology, 146*(1), 234-246. doi:https://doi.org/10.1016/j.revpalbo.2007.05.001

Williams, P. W., King, D., Zhao, J., Collerson, K. (2005). Late Pleistocene to Holocene composite speleothem 18O and 13C chronologies from South Island, New Zealand, did a global Younger Dryas really exist? *Earth and Planetary Science Letters, 230*, 301-317.

Wilmshurst, J. M., Anderson, A. J., Higham, T. F. G., Worthy, T. H. (2008). Dating the late prehistoric dispersal of Polynesians to New Zealand using the commensal Pacific rat. *Proceedings of the National Academy of Sciences, 105*(22), 7676-7680. doi:10.1073/pnas.0801507105

Wilmshurst, J. M., McGlone, M. S., Charman, D. J. (2002). Holocene vegetation and climate change in southern New Zealand: linkages between forest composition and quantitative surface moisture reconstructions from an ombrogenous bog. *Journal of Quaternary Science, 17*(7), 653-666. doi:https://doi.org/10.1002/jqs.689

Wilmshurst, J. M., McGlone, M. S., Leathwick, J. R., Newnham, R. M. (2007). A pre-deforestation pollen-climate calibration model for New Zealand and quantitative temperature reconstructions for the past 18 000 years BP. *Journal of Quaternary Science, 22*(5), 535-547. doi:https://doi.org/10.1002/jqs.1135

Zetzsche, F., Kalt, P., Liechti, J., Ziegler, E. (1937). Zur Konstitution des Lycopodium-Sporonins, des Tasmanins und des Lange-Sporonins. XI. Mitteilung über die Membran der Sporen und Pollen. *Journal für Praktische Chemie, 148*(9-10), 267-286. doi:10.1002/prac.19371480903

Appendix 1

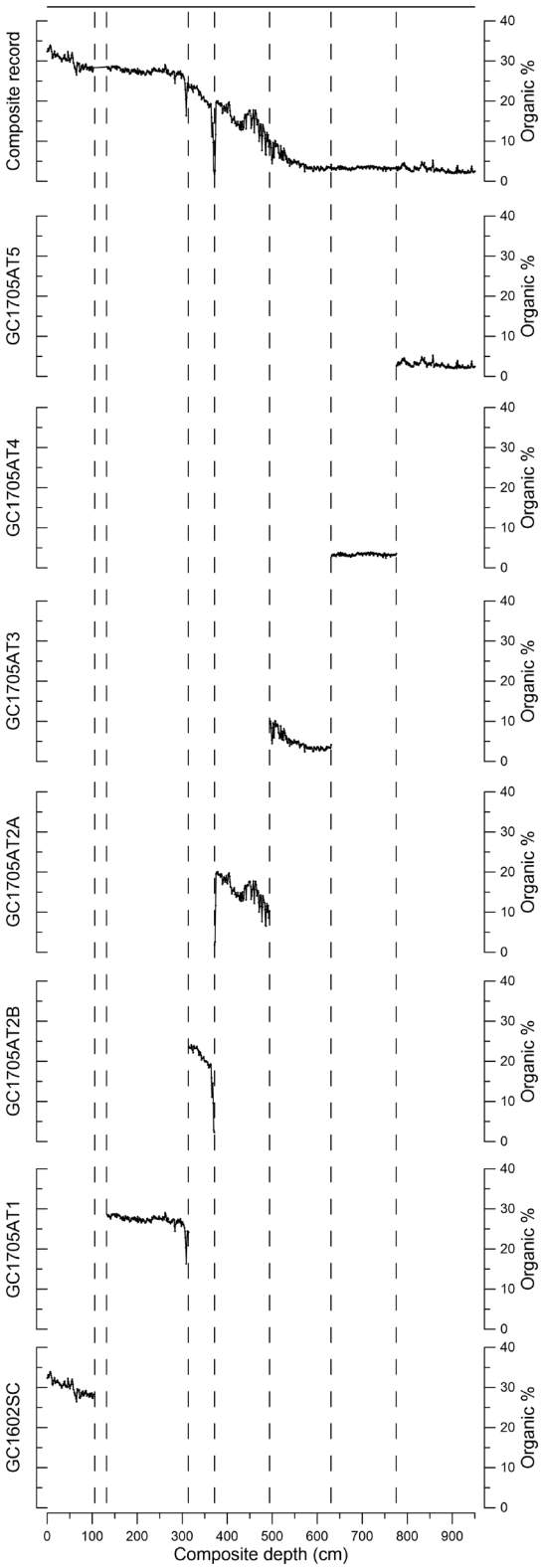

Figure A1.1. Organic matter (%) of sediment cores (as determined by loss-on-ignition [LOI]) from Lago Emerenciana, indicating the identity of each cores. These stratigraphies were compiled to make a composite record (upper most curve). The vertical dashed lines indicate tie points.

Appendix 2

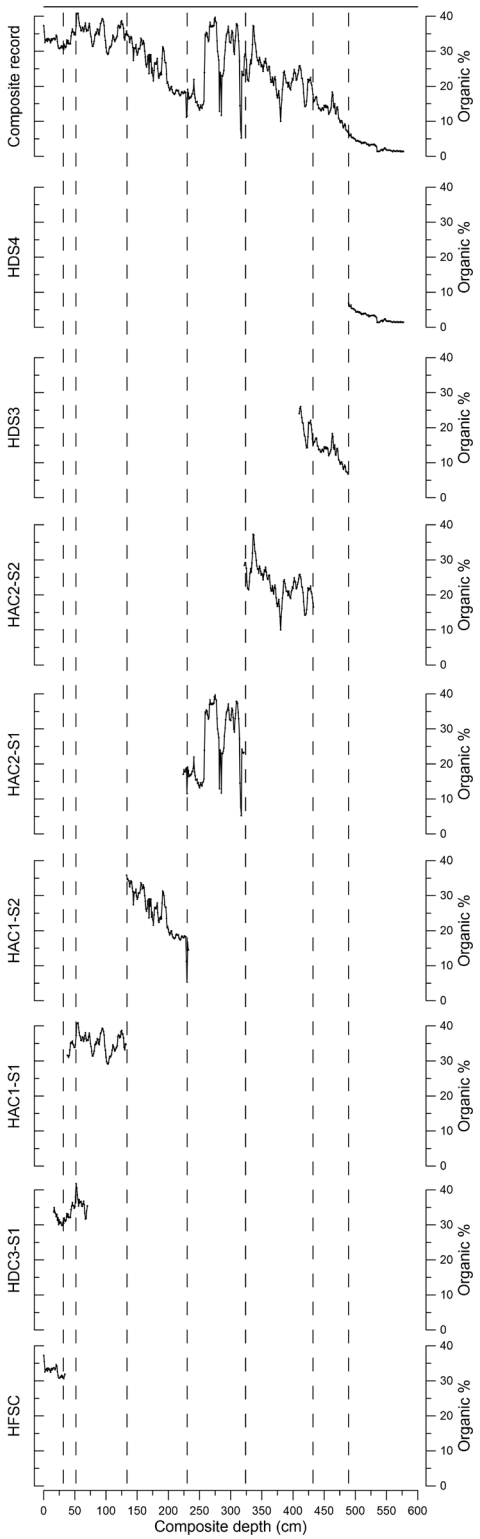

Figure A2.1. Organic matter (%) of sediment cores (as determined by loss-on-ignition [LOI]) from Lake Von, indicating the identity of each cores. These stratigraphies were compiled to make a composite record (upper most curve). The vertical dashed lines indicate tie points.

Table A2.1. Southwest-northeast (SW-NE) and northwest-southeast (NW-SE) transects where sediment-water interface samples were collected from Lake Von, indicating the location and water depth of each sampling point.

Transect	Code sample	Location	Water depth (m)
1) SW-NE	25	45°14’34.89’’S 168°17’51.96’’E	1.1
	27	45°14’34.02’’S 168°17’52.98’’E	3.4
	29	45°14’30.98’’S 168°17’55.87’’E	12.9
	31	45°14’29.92’’S 168°17’57.18’’E	14.6
	32	45°14’28.48’’S 168°17’58.13’’E	10.3
	33	45°14’28.28’’S 168°17’59.49’’E	8.4
	35	45°14’26.79’’S 168°18’02.07’’E	4.9
	36	45°14’25.66’’S 168°18’03.76’’E	2.9
2) NW-SE	42	45°14’27.77’’S 168°17’51.54’’E	5.6
	43	45°14’28.35’’S 168°17’52.79’’E	10
	44	45°14’29.56’’S 168°17’55.03’’E	14.4
	45	45°14’31.14’’S 168°17’57.81’’E	10.8
	46	45°14’31.51’’S 168°17’58.07’’E	8.1

Figure A2.2. Percentage (upper diagram) and concentration (lower diagram) pollen records from sediment-water interface samples collected through transect 1 in Lake Von.

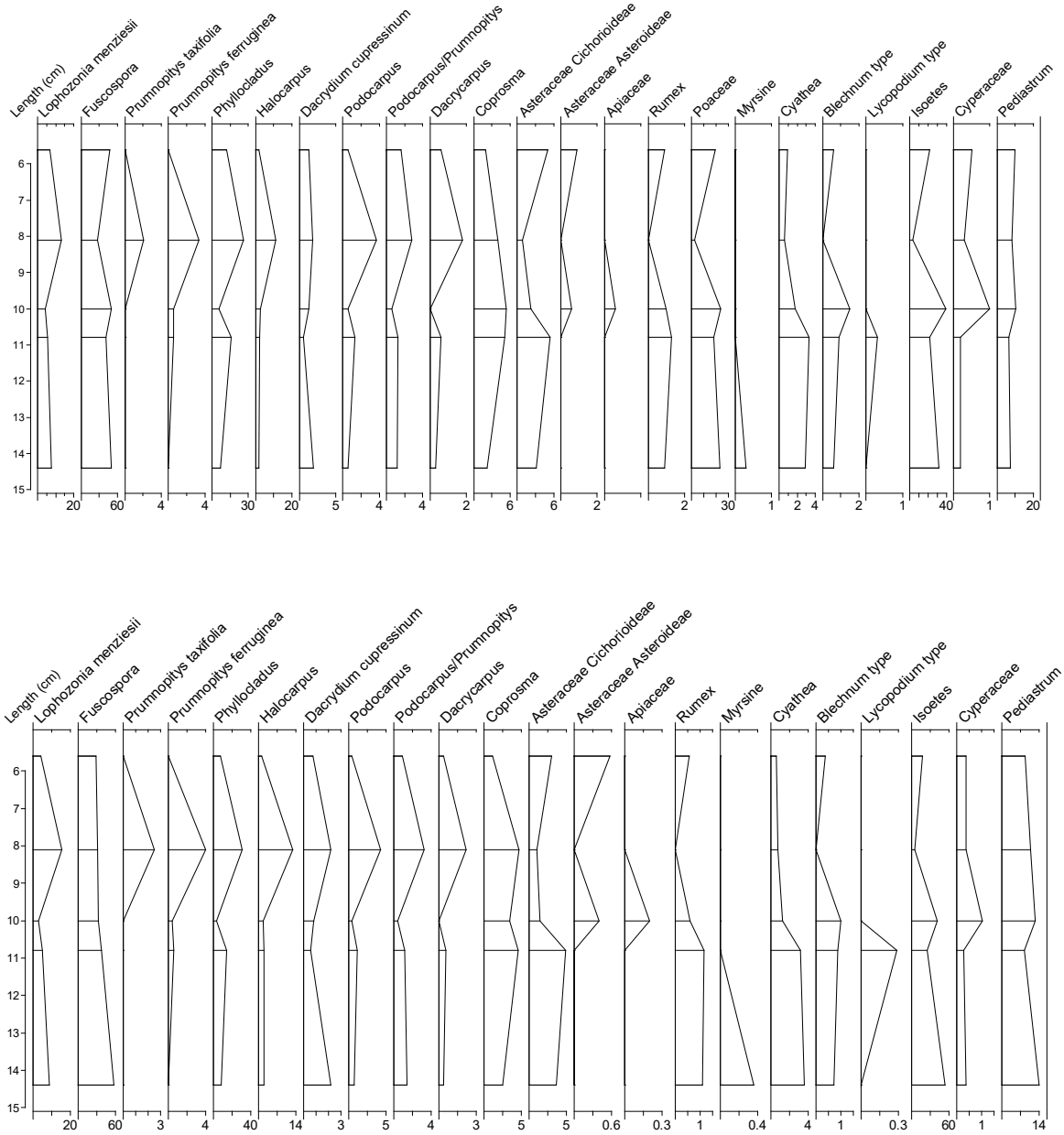

Figure A2.3. Percentage (upper diagram) and concentration (lower diagram) pollen records from sediment-water interface samples collected through transect 2 in Lake Von.

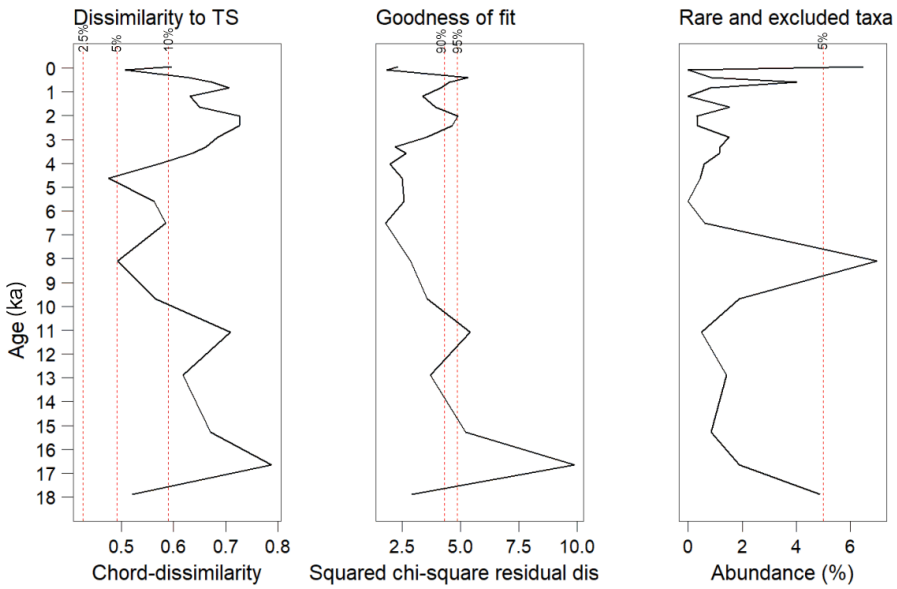

Figure A3.4. Reconstruction diagnostics for Lake Von fossil chironomid samples. Left panel shows the distance of sample to closest modern analogue in the training set indicating with red dashed lines 2.5th, 5th and 10th percentiles of dissimilarities within the training set. Middle panel shows the fit of fossil samples, indicating with red dashed lines the 90th and 95th percentiles of residual distances of training set samples. Right panel shows the abundance of rare taxa and taxa excluded from modelling in the fossil assemblage, indicating with a red dashed line the boundary above which the abundance of rare and excluded taxa is considered high (5%).

Appendix 3

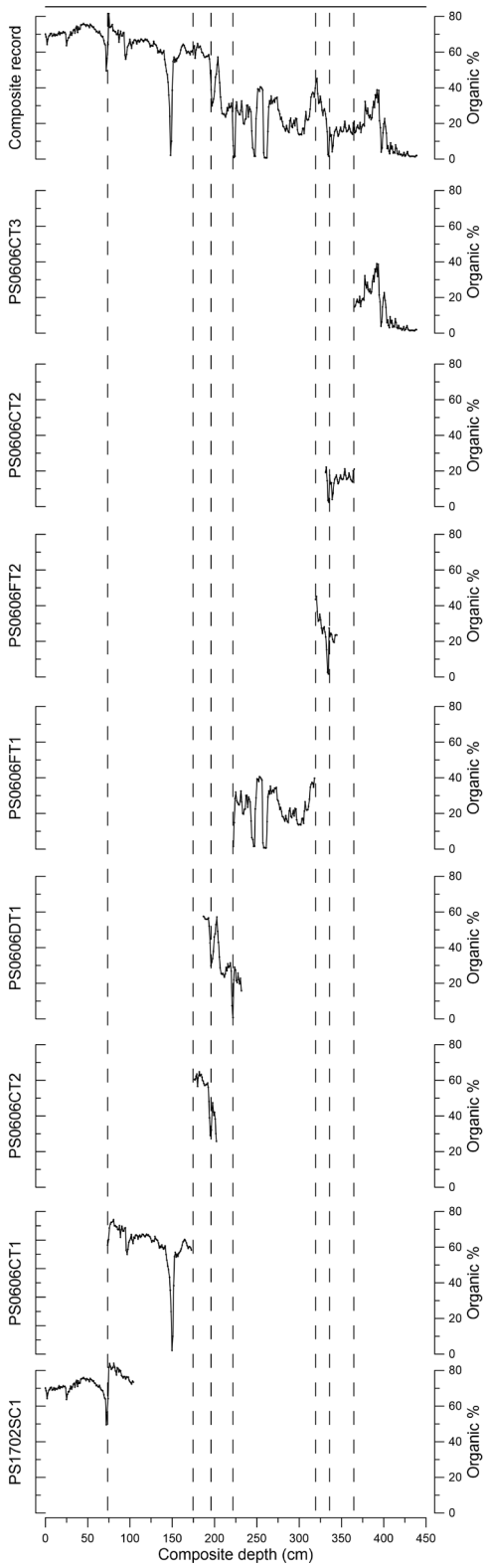

Figure A3.1. Organic matter (%) of sediment cores (as determined by loss-on-ignition [LOI]) from Lago Pintito, indicating the identity of each cores. These stratigraphies were compiled to make a composite record (upper most curve). The vertical dashed lines indicate tie points.